Using *in vitro* and *ex vivo* models of lung injury as a platform to identify and study mechanisms driving lung repair

A thesis submitted for the degree of Doctor of Philosophy
Imperial College London

Esther Bankole

2025

Cardio Respiratory Interface
National Heart and Lung Institute
Faculty of Medicine
Imperial College London

Statement of Originality and Copyright Declaration

I hereby declare that this thesis, and all of the work presented is my original work. Any ideas or quotations from the work of other people, published or otherwise, or from my own previous work are fully acknowledged in accordance with the standard referencing practices of the discipline.

Acknowledgments

First and foremost, I thank God for guiding me through this PhD journey. It has been a true challenge, but his strength and grace has sustained me every step of the way. “I can do all things through Christ who strengthens me” (Philippians 4:13).

I would like to express my gratitude to my supervisors, Dr Charlotte Dean and Professor Terry Tetley for giving me the opportunity to undertake this PhD, for their continuous guidance, encouragement and invaluable support. Your support has been instrumental throughout this journey. Thank you for taking the time to read this thesis and for offering advice and guidance. To Dr Charlotte Dean, my primary supervisor, thank you for your support, thank you for believing in me and for everything that you have taught me about experimental design and research. I have learnt so much under your guidance, lessons that have profoundly shaped my career as a scientist and that I will carry with me throughout my career. To Professor Terry Tetley, my secondary supervisor, thank you for encouraging me to think outside of the box and for sharing your wealth of research experience. Your anecdotes and motivating stories have not only enriched my understanding of scientific research but have also inspired me throughout this journey. Thank you to the patients that donated tissue samples, and to the amazing Biobank coordinators and staff at RBH.

I had the privilege of meeting many incredible friends and colleagues at Imperial, to whom I am deeply grateful for their support, for all the laughs and the encouragement along the way. It meant a lot to have people to share and discuss this journey with. Dr Sally Kim, Dr Sek-Shir Cheong and Rebecca Chen, thank you for your help and support in the lab.

Thank you to my friends outside of academia for all the love, support and for showing genuine curiosity about my research. Thank you to my family for their unwavering support and love throughout this PhD journey Mum and Dad, thank you for always encouraging me to pursue my dreams and for instilling in me the resilience to keep going. Your pep talks and words of wisdom have meant more than I can express. Michael, my brother thanks for always offering me the best advice and thank you for being such a great role model, you have truly inspired me.

Abstract

Current treatments for respiratory diseases, including chronic obstructive pulmonary disease (COPD), idiopathic pulmonary fibrosis (IPF) and asthma are not curative, highlighting an unmet need for novel therapies. Our limited understanding of signalling pathways involved in lung repair, and lack of advanced models replicating the complexity of the human lung poses a challenge. Developmental signalling pathways are reactivated during lung repair; modulating these pathways offers potential for regenerative therapeutics. This PhD tested the hypothesis that pathways essential for lung development play critical roles in alveolar repair and/or regeneration.

WNT, retinoic acid (RA), and Sonic Hedgehog (SHH) pathways were screened using *in vitro* wound healing assays to investigate their effects on epithelial and endothelial cell migration during repair. Based on these assays, SHH was selected for further investigation. SHH is critical for lung development, particularly branching morphogenesis and fibroblast expansion in the adult lung, however, its role in repair remains poorly understood. I demonstrated that SHH modulates fibroblasts, SHH treatment increased migration in human lung fibroblasts (HLFs) while co-culture of HLF with alveolar epithelial cells (A549) increased migration of both cell types. Using the *ex vivo* Acid injury and repair (AIR) model, SHH increased vimentin^{+} fibroblasts in acid-injured regions of AIR-PCLS and was associated with myofibroblast (α- SMA) and lipofibroblasts (ADRP) expression. The human model (hAIR) was established as part of this thesis, SHH treatment similarly increased ADRP^{+} cells in hAIR-PCLS.

To explore whether SHH signalling contributes to disease pathology, I analysed a cohort of emphysematous tissue samples and observed upregulation of *SHH* and downregulation of *HHIP*, suggesting changes in pathway activation. These findings were supported by COPD Cell Atlas data, showing consistent changes in SHH pathway activity across multiple cell populations. Collectively, these findings support a role for SHH in lung repair and highlights its potential as a regenerative therapeutic target.

Table of Contents

List of Figures

List of Tables

Abbreviations

ACM – Alveolar capillary membrane

ADH – Alcohol dehydrogenase

ADRP – Adipose differentiation related protein

AIR model – Acid Injury and Repair Model

ALDH1A1 - Aldehyde dehydrogenase 1

ALI – Acute Lung Injury

ALI culture model – Air-liquid interface culture model

ARDS – acute respiratory distress syndrome

ATI – Alveolar Type 1 Cells

ATII – Alveolar Type 2 Cells

α-SMA – Alpha smooth muscle actin

AQP5 – Aquaporin 5

A549 cells – Human alveolar adenocarcinoma epithelial cells

BASCs – Bronchioalveolar stem cells

BADJ – Bronchioalveolar-duct junction

BCs – Basal cells

BSA – Bovine Serum Albumin

β-ME – Beta-mercaptoethanol

BMP – Bone morphogenetic protein

BPD – Bronchopulmonary dysplasia

B2M - Beta-2 microglobulin

CaCl – Calcium Chloride

CAV1 – Caveolin 1

cDNA – Complementary deoxyribonucleic acid

CKO – Conditional knockout

COPD – Chronic Obstructive Pulmonary Disease

Ct – Cycle threshold

CYP2F2 – Cytochrome P450 2F2

DEAB – 4-diethylaminobenzaldehyde

Dhh – Desert hedgehog

DMEM – Dulbecco Modified Eagle Medium

DMSO – Dimethyl sulfoxide

Dll – Delta-like canonical Notch Ligands

E – Embryonic Day i.e. E1

EC – Endothelial Cell

ECM – Extracellular matrix

ED_{50} – The median effective dose

EGM – Endothelial Growth Media

EGM- MV – Endothelial Growth Media - Microvascular

EMT – Epithelial- mesenchymal transition

ERG – ETS related gene

EtOH – Ethanol

EthD-1 – Ethidium homodimer-1

FACs – Fluorescence-Activated Cell Sorting

FBS – Foetal Bovine Serum

FCS – Foetal calf serum

FEV1 – Forced expiratory volume in 1 second

FGF – Fibroblast Growth Factor

FGFR – Fibroblast Growth Factor Receptor

FVC – Forced vital capacity

FZD – Frizzled

GAPDH – glyceraldehyde 3-phosphate dehydrogenase

Gli – Glioblastoma

GUSB – Glucuronidase beta

GWAS – Genome wide association studies

hAIR model – Human AIR model

HBBS – Hanks Balanced Salt Solution

HGF – Human Growth Factor

HUVECs – Human Umbilical Vein Endothelial Cells

HPMVECs – Human Pulmonary Microvascular Endothelial Cells

HCl – Hydrochloric acid

Hh – Hedgehog

Hhip – Hedgehog interacting protein

HLF – Human lung fibroblasts

HOPX – Homeodomain-only protein

hPCLS – Human Precision Cut Lung Slices

hPSCs – Induced human pluripotent stem cells

HTII-280 – Human alveolar type two cells

H&E staining – Haematoxylin and eosin staining

Ihh – Indian hedgehog

IPF – Idiopathic pulmonary fibrosis

iPSCs – Induced pluripotent stem cells

KRT – Keratin

MRI – Magnetic resonance imaging

MTT – 3-(4, 5-dimethylthiazol-2-yl)-2, 5-diphenyl tetrazolium bromide

n – Biological replicate

NAMs – New approach methodologies

NATs – Non-animal technologies

$NaC_6H_7O_6$ – Sodium Alginate

NCID – Notch intracellular domain

NEBs – Neuroendocrine bodies

NGFR – Nerve Growth Factor Receptor

NG2 – proteoglycan neural/glial antigen 2

NKX2-1 – NK2 Homeobox-1

NO_2 – Nitrogen dioxide

P – Postnatal day i.e. P1

PAH – Pulmonary arterial hypertension

PBS – Phosphate Buffered Saline

PCLS – Precision Cut Lung Slices

PCP – Planar Cell Polarity

Pcw – Post conception week

PDGF – Platelet derived growth factor

PDGFR-α – Platelet derived growth factor receptor- alpha

Pdpn – Podoplanin

PFA – Paraformaldehyde

PNEC – Pulmonary neuroendocrine cells

PRISMA - Preferred Reporting Items for Systematic reviews and Meta-Analyses

proSP-C – Pro surfactant protein C

Ptch – Patched

qPCR – Quantitative real-time polymerase chain reaction

RA – Retinoic Acid

RAGE – Receptor for advanced glycation end products

RALDH – Retinaldehyde dehydrogenase

RAR – Retinoic Acid Receptor

RARE – Retinoic acid response element

RBP – Retinol binding protein

RIN – RNA integrity number

RNA – ribonucleic acid

ROI – Region of interest

RXR – Retinoid x receptors

SAHM-1 – Stapled α-helical peptide derived from mastermind- like 1

scRNA-seq – Single-cell RNA sequencing

SEM – Standard Error of Mean

SF – Serum Free

SFTPC – Surfactant protein C

SNP – Single nucleotide polymorphism

Shh – Sonic Hedgehog

Smo – Smoothened

SNP – Single nucleotide polymorphism

SOX protein – Sex determining region Y-box protein

SO_2 – Sulphur dioxide

SP – Surfactant protein

SUFU – Suppressor of Fused

TEAD – TEA-domain

TGF- β - Transforming Growth Factor β

TM4SF1 – Transmembrane 4 L Six Family Member 1

TRP63 – Transformation-related protein 63

VEGF – Vascular endothelial growth factor

VEGFR – Vascular endothelial growth factor receptor

Wls – Wntless

Wnt – Wingless-related Integration Site

WT – Wildtype

YAP/TAZ – Yes associated protein/ transcriptional co-activator with PDZ binding motif

2D – two dimensional

3D – three dimensional

RPMI - Roswell Park Memorial Institute medium

<u>Nomenclature to clarify use of genes and proteins:</u>

SHH - SHH protein

SHH – human gene

shh – mouse gene

*Sonic hedgehog is used as an example here but the same rules of nomenclature are used for all proteins and genes mentioned in this thesis.

Chapter 1

Introduction

Introduction

The global burden of respiratory diseases continues to rise, over 1 billion individuals worldwide suffer from an acute or chronic respiratory disease(1). In healthy individuals, the lungs possess a remarkable capacity for intrinsic repair following injury(2, 3). However, individuals with respiratory disease are often unable to mount a successful repair response, indicating disruption of intrinsic repair mechanisms(2, 4). Current treatments for respiratory diseases that involve dysregulated repair, including chronic obstructive pulmonary disease (COPD), idiopathic pulmonary fibrosis (IPF) and asthma are not curative and do not reverse disease pathology(2-5). In cases of severe lung damage, lung transplantation is often the only viable option(2-5). However, it has been reported that long term survival for individuals with lung transplants is limited, 54 % at 5 years and only 32 % at 10 years post-transplant (6). Additionally, there is a scarcity of suitable donor lungs available for transplantation(7). Therefore, there is an unmet need for novel therapies that promote lung repair and/or regeneration and the development of such therapies requires knowledge of the mechanisms that underpin lung repair and regeneration and the signalling pathways involved in these processes. Signalling pathways involved in lung development have been identified and studied (8-14). Importantly, many of these signalling pathways, are known to be re-activated during repair (11, 13), raising the possibility that harnessing signalling pathways required for lung development might be an effective route to repair and/or regenerate damaged lung tissue (11, 13).

This thesis focuses on investigating the potential role of key lung developmental signalling pathways in the repair and regeneration of damaged lung tissue. To investigate this overarching hypothesis, I combined existing published data about the roles these pathways play during lung development, with mouse and human *in vitro* and *ex vivo* models lung models. Following initial experiments, I focused the remainder of the thesis on assessing the therapeutic potential of the SHH pathway in repairing damaged lung tissue.

1.1 Lung development

Lung development is a complex and highly coordinated process which begins during gestation and ends postnatally (12, 14-16). The process is divided into five distinct but overlapping stages (Figure. 1.1); embryonic, pseudoglandular, canalicular, saccular and alveolar(12, 14-17) (Figure. 1.1). Despite the difficulties of accessing and visualising human lung tissue, because the lungs lie deep inside the thoracic cavity, recent studies have begun to characterise morphological changes that occur at stages of human lung development(12, 18). Additionally, mouse models have enhanced our understanding of the different stages of lung development, particularly at the molecular level, despite there being some notable differences between mouse and human lung development, discussed in section 1.2.1-1.2.2(12, 14). Understanding each of the stages that contribute to the development of the lungs is crucial in the context of repair and regeneration because studies have shown that molecular mechanisms and signals involved in development are reactivated during repair in response to lung injury (11-13, 19).

1.1.1 Embryonic stage

The embryonic stage marks the onset of lung development (16, 19, 22, 37, 41) and occurs between 4-7 post conception weeks (pcw) in humans (Figure. 1.1), which corresponds to embryonic days 9-12 (E9-12) in mice (16, 19). During this stage, the primary epithelial lung bud emerges from the ventral anterior foregut endoderm, which is surrounded by mesenchyme derived from splanchnic mesoderm (16, 19, 22, 37). By the end of pcw 4 the respiratory bud separates distally to form two primordial buds (primary left and right lung buds) (16, 19, 22, 37). Subsequently, the buds begin to branch (Figure. 1.1) and by the end of pcw 5, the primary lobes of the lung are established (16, 19, 25). This process is tightly regulated by interplay between transcription factors and signalling pathways (16, 19, 34)

Specifically, the transcription factor, NK2 Homeobox-1 (NKX2-1) is the first transcription factor expressed in the ventral anterior foregut endoderm and is critical for driving specification of early respiratory progenitors and initiating the formation of the primary lung buds (34, 42-44). In addition to this, sex determining Y- box (SOX) proteins 2 and 9 are responsible for driving epithelial specification and early branching which establishes the primary lobes by pcw 5 (16,

22, 34, 43). During this stage, in humans both SOX2 and SOX9 are expressed at the distal tips of lung buds while notably in mice only SOX9 is expressed during the embryonic stage (19).

1.1.2 Pseudoglandular stage

The pseudoglandular stage of lung development occurs between 5 to 17 pcw in humans, which corresponds to E12-16 in mice (12, 14-16, 20). During this stage, branching morphogenesis takes place where the endodermal epithelium undergoes successive rounds of branching to form the characteristic respiratory tree (Figure. 1.1) (12, 14-16, 21). This process is driven by reciprocal signalling interactions between the epithelium and mesenchyme (12, 14-16, 21). In parallel, lung tissue differentiation also begins during this stage; cartilage, smooth muscle cells, goblet and basal cells begin to appear (9, 12, 14-16). Simultaneously, vascularisation occurs alongside branching morphogenesis and differentiation, blood vessels start developing adjacent to the airways (9, 12, 14-16).

At around 10 pcw foetal breathing movements have also been observed and are thought to contribute to lung development and growth through stretching and expansion of the lungs (14, 16, 22, 23). By the end of the pseudoglandular stage (pcw 17) the terminal bronchioles have developed, the future acini (fundamental gas exchange units) are observed and the complete structure of the human airway tree is established(8, 15, 16, 20).

1.1.3 Canicular stage

During the canalicular stage, at 16-26 pcw (E15-17), further epithelial branching occurs, leading to the expansion of the respiratory tree (Figure. 1.1) and thinning of the surrounding mesenchyme(12, 14-16). Division of terminal bronchioles leads to the formation of the primary acinus, comprising the respiratory bronchioles and alveolar ducts (8, 12, 15, 16). The alveolar epithelium begins to differentiate, cuboidal cells are observed in the proximal airways and peripheral squamous cells begin to emerge (8, 12, 15, 16). Vascularisation and angiogenesis occur along the airways, the number of capillaries surrounding the acinus

increases leading to the formation of a capillary network, marking the beginning of formation of the blood-air barrier(15, 16, 24).

1.1.4 Saccular stage

The saccular stage is the penultimate stage of lung development, which occurs at 26-36 pcw in humans and E17-P5 in mice (Figure. 1.1). This stage of lung development is characterised by the formation of thin- walled sacculi that appear in clusters at the ends of the terminal airways (8, 12, 15, 16, 24). During this stage, branching morphogenesis comes to an end and the respiratory airways begin to widen, whilst interstitial tissue decreases in volume(10-12, 18). Primitive alveolar saccules, separated by septa increase in size and become surrounded by a capillary bilayer which forms within the intersaccular septa(8, 15, 16, 24). This contributes to the beginning of the formation of the alveolar capillary membrane (ACM). Differentiation of the epithelium continues; alveolar type 1 and type 2 (ATI and ATII) cells can be morphologically distinguished(12, 15, 16). Pulmonary surfactant synthesis from ATII cells is also initiated and lamellar bodies can be seen(8, 12, 15, 16). Towards the end of the saccular stage, elastin bundles begin to deposit at the base of saccules in preparation for alveolarisation (8, 14, 21).

1.1.5 Alveolar development

The alveolar stage is the final stage of lung development and is defined by the septation of saccule walls, which leads to the formation and maturation of alveoli. This process is known as alveolarisation or alveologenesis (Figure. 1.1-1.2). This expands the lung surface area required for gas exchange and the process is orchestrated by interactions between epithelial cells, endothelial cells and mesenchymal cells including myofibroblasts, which deposit elastin to support septation (8, 14). Angiogenesis and microvascular maturation coincide with alveolar maturation; the capillary bilayer formed in earlier stages of lung development fuses to form a singular capillary system. Capillaries surround gas exchange surfaces(12, 16, 21).

Alveolarisation in humans, begins *in utero* and is often separated into phases; bulk (from 36 pcw to ~ 3 years) and continued alveolarisation(8, 14, 16, 21). Studies using imaging techniques have demonstrated that the number of alveoli continues to increase up until early adulthood (~21 years)(12, 14, 16, 21). In addition to alveolar septation, recent imaging studies have provided more insight into the mechanisms through which alveoli form and it is now understood that additional morphogenetic processes occur including clustering of epithelial cells and formation of mesenchymal rings. Further highlighting the importance of advanced imaging techniques(25, 26).

Due to limited access to human tissue at later stages of lung development, much of what is known about alveolarisation is based on studies conducted in mice(12, 14, 27). However, alveolarisation begins postnatally in mice (P5-P20) (8, 12, 14-16) and some critical differences between mouse and human lung tissue exist at this stage(26, 27). At birth, the murine lung is able to support efficient gas exchange despite being in the saccular stage, in contrast, lungs of pre-term infants born at this stage are not competent for efficient gas exchange(27). This highlights a difference in the functionality of the tissue and is an important caveat to consider, since term murine lung tissue is used as a model for pre-term human lungs and is used to study regenerative therapies(27).

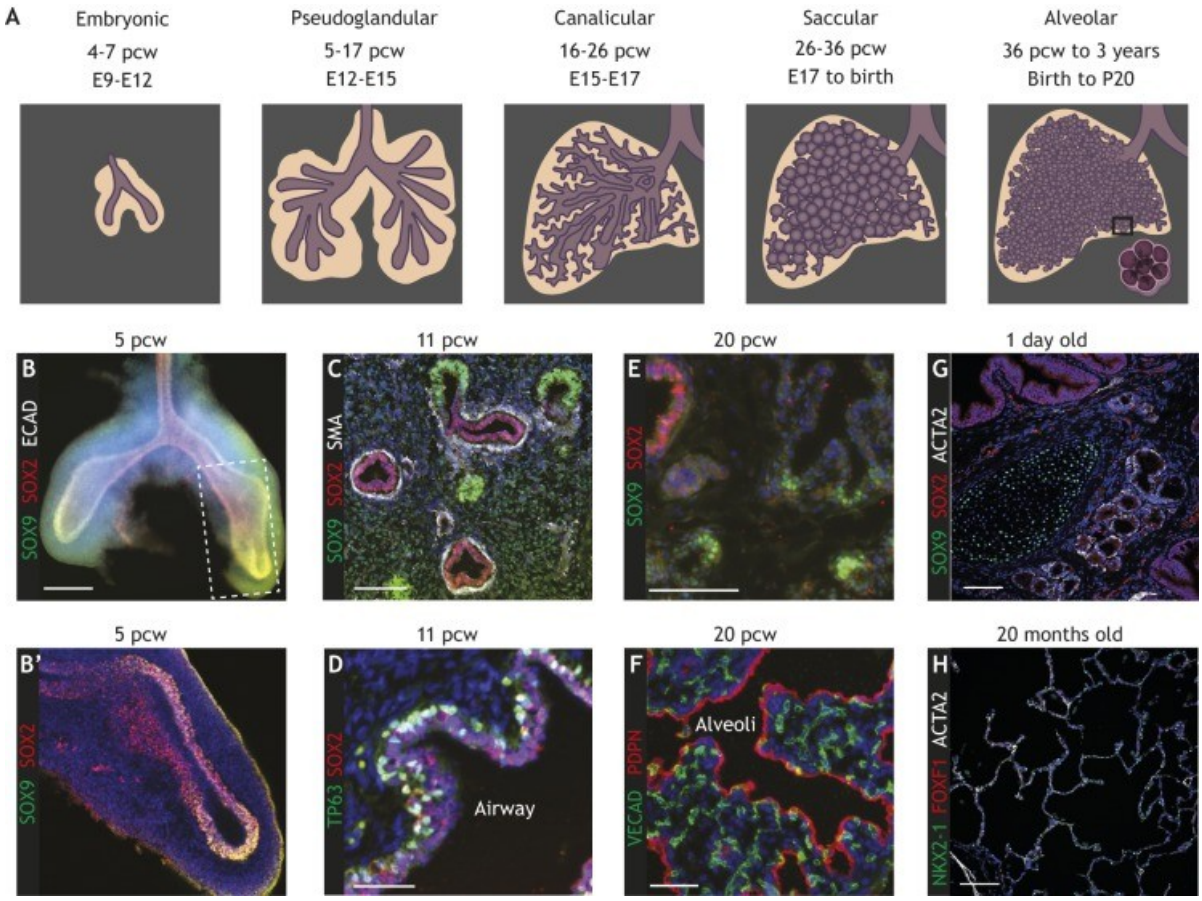

Figure 1.1. Stages of lung development.

(A) Schematic diagram summarising the morphological changes that occur over the five distinct stages of lung development, the time periods in which each stage occurs is indicated in post conception weeks (pcw) for humans and embryonic days (E) and postnatal days (P) for mice. (B) Cryosection of an embryonic stage lung showing primary branching and co-expression of SOX2/SOX9 at the distal tips. (B') Magnified view of the boxed region shown in (B), further highlights SOX2/SOX9 co-expression at distal tips. (C-D) Cryosections of pseudoglandular stage lungs, showing continued SOX2/SO9 co-expression at distal tips and early airway differentiation. In (C) smooth muscle actin shown in white (SMA) marks smooth muscle cells, while in (D) TP63 shown in green marks differentiating basal cells. (E-F) Cryosections of canalicular stage lungs, showing SOX9+/SOX2- expression at the distal tips and early alveolar differentiation, which is marked by widening of distal airspaces shown in E. Increasing proximity between developing vasculature marked by VE-cadherin (VECAD-CHD) shown in green and the developing alveolar epithelium marked by podoplanin (PDPN) shown in red are depicted in F. (G-H) Cryosections of postnatal lungs during the alveolar stage. In (G) SOX9 (green) marks cartilage, SOX2 (red) marks airway epithelium and ACTA2 (white) marks smooth muscle, while in (H) NKX2-1 (green) marks lung epithelium, FOX1 (red) marks the mesenchyme and ACTA2 (white) marks smooth muscle, alveolar maturation and septal formation are shown. Scale bars shown: 200 mm (B); 50 mm (C, D, F); 100 mm (E, G, H). Adapted from Nikolić MZ, Sun D, Rawlins EL. Human lung development: recent progress and new challenges. Development. 2018 Aug 15;145(16): dev163485.(12).

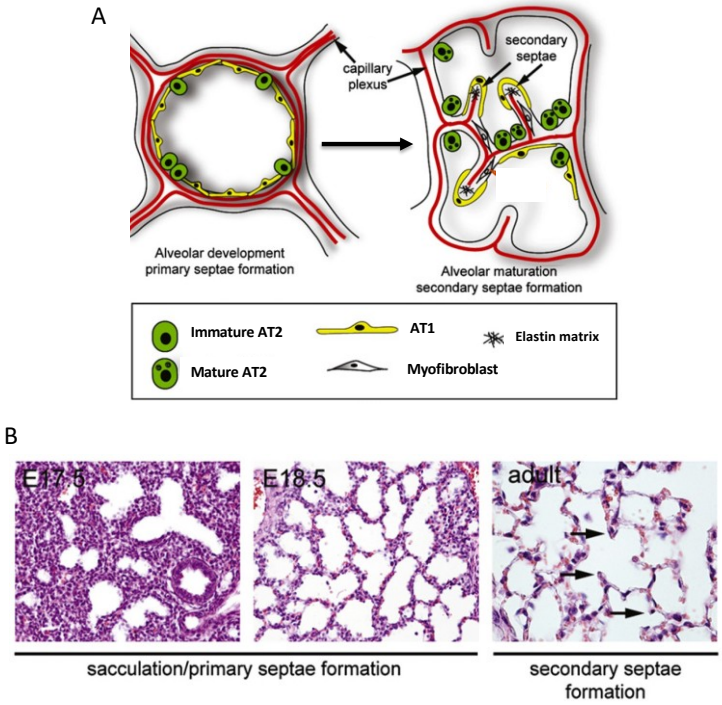

***Figure 1.2. Alveolarisation of the lungs from saccule to alveoli*.**

(A) Summary of changes that occur from alveolar development to alveolar maturation, the epithelium within saccules begins to differentiate into alveolar type 1 (ATI) and alveolar type 2 (ATII) cells. The change from the primary septae to secondary septae is driven by interaction between epithelium, myofibroblasts and the vascular endothelium. The change from a capillary bilayer to a single capillary network is also shown. (B) Histological sections (Haematoxylin and eosin stain- H & E) of mouse lung tissue showing changes in lung morphology from the saccular stage to alveolar maturation (when secondary septae are formed). Adapted from Morrisey EE, Hogan BL. Preparing for the first breath: genetic and cellular mechanisms in lung development. Dev Cell. 2010 Jan 19;18(1):8-23. (28).

1.2 The adult lung and repair

As previously highlighted, many of the key signalling pathways involved in lung development are reactivated during repair (11, 13). To investigate the role that these pathways may have in repair and regeneration, it is essential to understand the structural organisation and cellular composition of the lung, as well as the mechanisms that regulate cell turnover and homeostasis. Particularly, understanding the spatial organisation of cells and how they interact with each other under normal physiological conditions provides important insight into how the lung may become dysregulated post-injury, and how these cells could be targeted to promote repair and regeneration.

1.2.1 The anatomy of the adult lung

The adult lung is composed of a branched network of airways (Figure. 1.3) and blood vessels, divided into distinct anatomical zones that vary in structure and function(17, 29-31). Airway branching begins at the trachea and continues through successive branching generations up until the alveolar sacs. In humans, the lung has approximately 23 branching generations, which can be subdivided into functional zones; the conducting airways (generations 0-16) which is responsible for transporting inhaled air to terminal airway units (alveoli) and the respiratory airways (generations 17-23), where gas exchange takes place (Figure. 1.3) (17, 29-31). The conducting airways are composed of the trachea, bronchi, bronchioles, pulmonary arteries and veins and the respiratory airways are composed of respiratory bronchioles, alveolar ducts, alveoli and ACM. A notable distinction between the mouse and human lungs is a reduction in branching generations, the mouse lung has fewer branching generations (approximately 17), it is likely that this is due to differences in lung size (14, 32, 33).

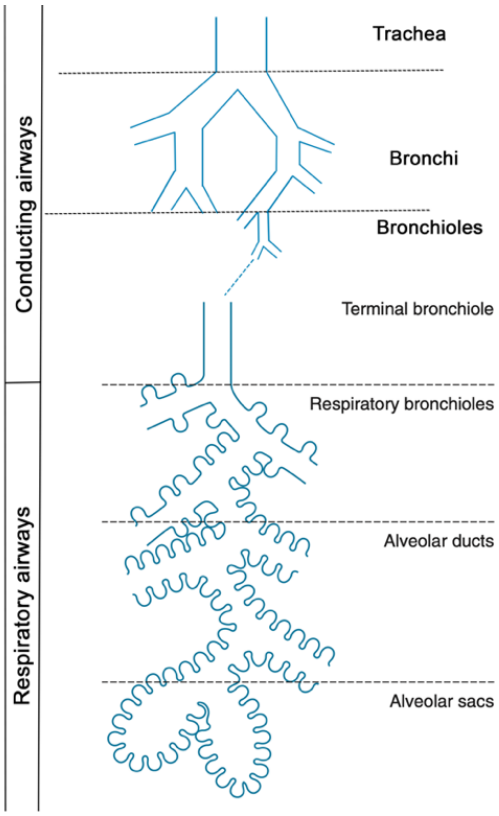

Figure 1.3. The anatomical structure of lung branching network.

Schematic diagram outlining the distinction between conducting airways and respiratory airways in the human lung. Adapted from Lumb AB. Functional Anatomy of the Respiratory Tract. In: Lumb AB, editor. Nunn's Applied Respiratory Physiology. 8th ed. Elsevier; 2017. p. 3-16.e11. (29) and Schittny JC. Development of the lung. Cell Tissue Res. 2017 Sep;367(3):427-44. (16).

1.2.2 Cellular composition of the lung

The lungs contain over 40 distinct cell populations including ATI and ATII, secretory cells (goblet and club), ciliated cells and basal cells (34-37). These cell sub-types are organised in tissue compartments (epithelium, vascular endothelium, stroma) based on their function; the cellular composition is also species specific (Figure. 1.4)(35). Disruption of the organisation of cells a hallmark of many respiratory diseases(4, 35, 38).

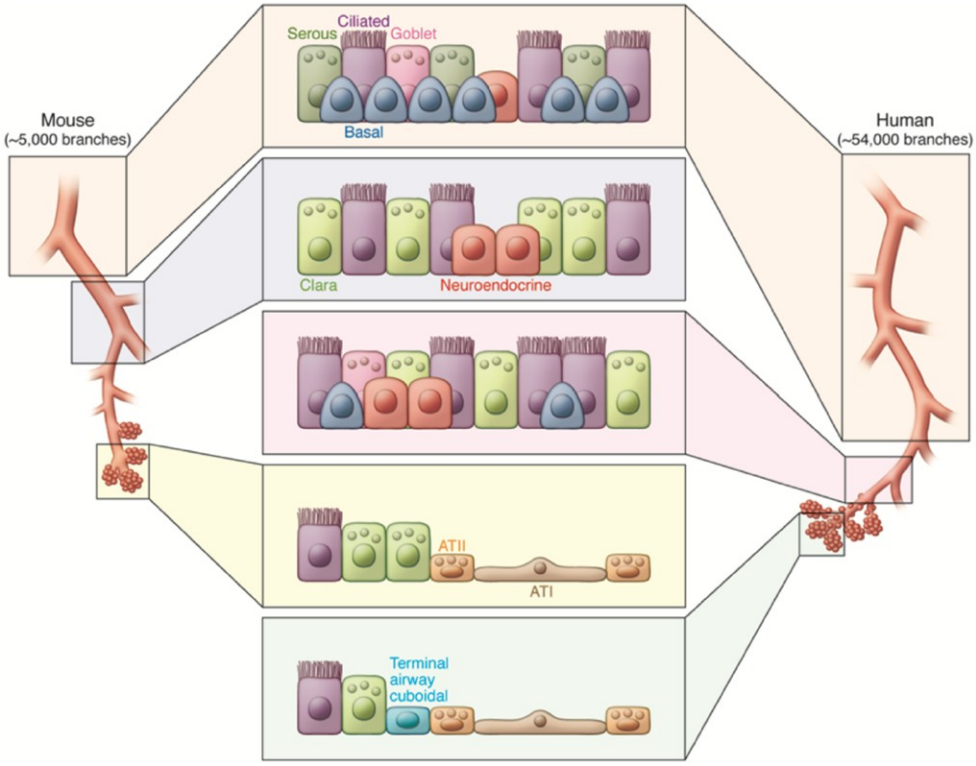

Figure 1.4**. **Regional differences in epithelial cell composition along the proximal-distal axis of the human and mouse lung. The cellular composition of the lung epithelium varies across the proximal-distal axis of the lung and differs between humans and mice. In humans and mice the tracheobronchial region is lined by pseudostratified epithelium, which is composed of basal cells (BCs), ciliated cells, club cells, goblet cells. However, there are more goblet cells present in humans than mice and BCs are also present distally in the terminal bronchioles of humans while they are confined to the trachea and primary bronchi of mice. The murine bronchioles are lined by a simple columnar epithelium which is primarily composed of ciliated and club cells only. In human's respiratory bronchioles are lined by a cuboidal epithelium leading to the alveolar compartment which is composed of ATI and ATII cells. Adapted from Rackley CR, Stripp BR. Building and maintaining the epithelium of the lung. J Clin Invest. 2012 Aug;122(8):2724-30. (10).

1.2.2.1 Airway Epithelium (proximal lung)

The structure, function and type of epithelial cells present varies between the conducting airways (proximal lung) and the respiratory airways (distal lung) (Figure. 1.4)(10, 39).

Conducting airways

As previously outlined, the conducting airways are composed of the trachea, bronchi and bronchioles. This region of the lung is lined by pseudostratified epithelium, which is composed of several specialised cells including basal cells, secretory cells, ciliated cells and neuroendocrine cells (Figure. 1.4) (10, 12, 29-31, 35, 39).

Basal cells

Basal cells (BC) are located in the basal layer of the proximal airway epithelium, where they function as key epithelial progenitors. In humans, BCs are present throughout the conducting airways, whereas in mice they are confined to the trachea and primary bronchi (Figure. 1.4) (10, 40, 41). BCs are capable of both self-renewal and differentiation into secretory and ciliated cells(33, 35, 39, 42, 43). Therefore, BCs play an important role in the maintenance of the epithelial cell population during homeostasis and repair (33, 35, 39, 42, 43).

Secretory cells

The two main types of secretory cells present in the airway epithelium are goblet cells and club cells (previously known as Clara cells) (Figure. 1.4).

Goblet cells are responsible for the secretion of mucins, primarily MUC5A and MUC5B which can also be used to mark the presence of goblet cells(10, 39, 44). Mucins are the main structural components of mucus, which forms a protective barrier to trap inhaled particles, allergens and pathogens (10, 39, 44, 45). Therefore, goblet cells play an essential role in the innate immune response(39, 45, 46). Goblet cells increase in response to chronic inflammation and goblet cell hyperplasia is a hallmark of respiratory diseases such as COPD and asthma(3, 33, 39, 47). Goblet cells are more abundant in the airway epithelium of humans than in mice (Figure. 1.4)(10, 12, 34).

Club cells can be easily distinguished from goblet cells by their dome shape and smooth apical surface which extends into the lumen(3, 35, 40, 41). In humans, club

cells are predominantly confined to the bronchioles, but in mice they are distributed throughout the epithelium (3, 35, 48, 49). Club cells play a role in epithelial maintenance during homeostasis and repair; however mouse studies have revealed that their function is dependent on their anatomical location(35, 42, 50). Club cells located in the trachea of mice, where basal cells are also present, exhibit limited capacity for self-renewal and are considered to be a transiently amplifying population, that can differentiate into ciliated cells(35, 42, 51). In contrast, in the bronchioles of mice, where basal cells are absent, club cells are capable of both self-renewal and differentiation into ciliated cells(35, 42).

Ciliated cells

Ciliated cells present in the airway epithelium arise during development or through differentiation of basal cells or secretory cells during repair, as previously outlined(29, 39, 52). Ciliated cells are characterised by the presence of motile cilia on their apical surface, each ciliated cell has roughly 300 cilia(29, 39, 53). Co-ordinated beating of cilia drives mucociliary clearance, enabling the removal of inhaled particles, pathogens and allergens trapped in mucus produced by goblet cells (10, 39, 44, 45, 53). Therefore, playing an important role in the innate immune response(53, 54). Ciliated cells are not capable of differentiation into other cell types, they are terminally differentiated (39, 52, 53).

Neuroendocrine cells

Pulmonary neuroendocrine cells (PNECs) also referred to as neuroendocrine bodies (NEBs) when found in clusters are rare epithelial cells which are usually found located at the airway branch points (3, 29, 39, 55, 56). While PNECs are more abundant in developing lung, the number of PNECs is reduced in the adult lung (29, 39, 55, 56) Despite this, PNECs play an important sensory role in the airways, they respond to changes in the airway microenvironment such as allergens, noxious stimuli, mechanical stretch and secretion of peptides and neurotransmitters(39, 56-58). Interestingly, recent evidence from mouse studies has shown that NEBs contain a

population of naphthalene resistant variant club cells which are able to self-renew(39, 56-58).

1.2.2.2 Alveolar region (distal lung)

The alveolus

The alveolus is the site of gas exchange in the lung(10, 29, 59) and comprises 90 % of the total lung volume(60). Each alveolus is composed of two continuous cellular layers; the alveolar epithelium and the endothelium which together form the alveolar capillary membrane (ACM) (Figure. 1.5-1.6)(29-31, 59). The epithelial and endothelial basement membranes may be closely fused in some regions or separated by a thin interstitial space, which varies in thickness and composition (29-31, 59, 61). In addition to this, the alveolar niche also encompasses interstitial fibroblasts and immune cell populations (Figure. 1.5)(29-31, 59).

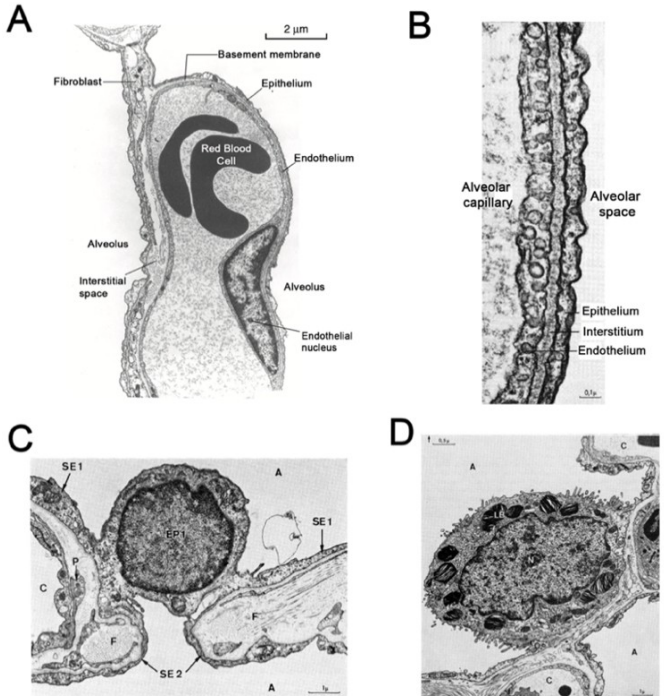

Figure 1.5. Alveolus cells.

Electron micrographs of (A) Cross-section of an alveolar capillary with cell surrounding cell types labelled (B) ACM of a dog lung showing alveolar cellular layers (epithelium and endothelium) and the interstitium. (C) Type 1 alveolar epithelial cell from monkey lung showing squamous structure and elongation of cell. (D) Type 2 alveolar epithelial cell showing presence of lamellar bodies and microvilli on apical surface. (A) Adapted from Lumb AB. Functional Anatomy of the Respiratory Tract. In: Lumb AB, editor. Nunn's Applied Respiratory Physiology. 8th ed. Elsevier; 2017. p. 3-16. e11. (11) (B-D) Adapted from Weibel ER. Morphological basis of alveolar-capillary gas exchange. Physiol Rev. 1973 Apr;53(2):419-95. (30).

Alveolar epithelial cells

The alveolar epithelium is composed of ATI and ATII cells(10, 29, 39, 62).ATI cells are flat squamous epithelial cells that cover ~ 95 % of the alveolar surface area (Figure. 1.5C, Figure. 1.6)(29, 39, 61-66). Electron microscopy has shown that ATI cells are very thin (< 0.1 μm) except in regions expanded to accommodate nuclei (29, 39, 63-65). They form a continuous epithelial sheet and are joined by tight junctions, which are ~ 1 nm(29, 67). The highly extensive and flattened morphology of ATI cells facilitates efficient gas exchange across the ACM(12, 29, 30, 64, 68). In addition to the role that ATI cells play in gas exchange, studies suggest that ATI cells can contribute to homeostasis and repair by de-differentiating into ATII cells, however this remains disputed among researchers(29, 65, 69-71).

ATII cells comprise approximately 60 % of the total alveolar epithelial cell population, but cover only 5 % of the alveolar surface are due to their compact, cuboidal shape (Figure. 1.5D, Figure. 1.6)(3, 10, 61, 62, 72, 73). The primary function of ATII cells is the synthesis and secretion of pulmonary surfactant (3, 10, 29, 62, 73). Pulmonary surfactant is a biological film primarily composed of complex lipids and proteins (SP-A, SP-B, SP-C, SP-D), which have immunomodulatory functions(60, 74-77). Surfactants also function to reduce surface tension and this prevents the alveoli from collapsing during exhalation(10, 60, 75-77). ATII cells can be distinguished from ATI cells by their shape as well as the presence of lamellar bodies and apical microvilli in ATII cells (Figure. 1.5C-D)(29, 39, 73, 78). In addition to the production of surfactants, ATII cells act as facultative progenitor cells within the alveoli and are capable of self-renewal and differentiation into ATI cells in response to alveolar injury(71, 78-80). While ATII cells play a very important role in surfactant production within the alveolar epithelium, and are exclusively responsible for producing SP-C, they are not the sole producers of other surfactant proteins. Club cells have also been shown to secrete SP-A, SP-B and SP-D(76).

In addition to differences in their morphology (Figure. 1.5-1.6), ATI and ATII cells can be identified by immunolabelling different proteins present in either ATI or ATII only (78, 81). Cell-type specific proteins present in ATI include podoplanin (Pdpn also referred to a T1α), aquaporin 5 (AQP5), receptor for advanced glycation end products (RAGE, also referred to as AGER), and caveolin 1 (CAV1) (78, 81).Surfactant protein C (SFTPC) or its precursor, pro surfactant protein C (proSP-C) are used as ATII specific markers, this is the most appropriate marker because SFTPC is the only surfactant protein that is found restricted in ATII cells(78).Furthermore, ATII progenitor cells can only be identified by proSP-C (78, 82)

Endothelial cells

The alveolar endothelium lines the capillaries which form part of the ACM (Figure. 1.5A-B, Figure. 1.6) and plays an important role in gas exchange, vascular homeostasis and immune regulation(16, 30, 83, 84). Alveolar endothelial cells (ECs) form a mesh-like network that envelops the alveoli maximising the surface area available to facilitate efficient gas exchange with the adjacent alveolar epithelium (16, 30, 61, 83, 85). The alveolar endothelium and epithelium are separated by a thin interstitial space and there are some regions where the cellular compartments are also fused together at the basement membrane. This also contributes to efficient gas exchange (30, 83, 85).

The interstitium

The alveolar interstitium is the space that lies between the epithelial and endothelial basement membranes of the ACM(30, 59, 60, 86). The interstitial space contains interstitial fluid, which supports the structure of the alveolar capillary interface and facilitates molecular exchange between alveolar epithelial cells and capillary endothelial cells(60, 87). The interstitium is composed of various ECM components, including elastin and collagen, which support the elasticity and tensile strength of the lungs(29, 59, 60, 88). Additionally, embedded within the interstitium are a population of heterogeneous mesenchymal cells, which are spatially and functionally distinct (30,

60, 87, 89). These cells include fibroblasts (myofibroblasts and lipofibroblasts), pericytes, smooth muscle cells and lymphatic cells(59, 60, 87).

Pericytes

Pericytes are a subpopulation of mesenchymal stromal cells, which are located adjacent to blood vessels and alveolar capillaries (86, 90, 91). Pericytes contribute to vascular stability, blood vessel maturation and intercellular signalling (31, 86, 90, 91). Structurally, pericytes have elongated processes, which extend and envelope the endothelium and connect to capillary ECs via junction proteins (31, 86, 90-92). Pericytes can be distinguished from smooth muscle cells and fibroblasts and by the expression of proteoglycan neural/glial antigen 2 (NG2)(86, 93). Some studies have also shown that pericytes exhibit mesenchymal progenitor cell properties and have the capacity to differentiate into fibroblasts and smooth muscle cells(86, 93).

Fibroblasts

Fibroblasts are the most abundant cell type located in the interstitium are also responsible for the production of ECM(60, 66, 94). Interstitial fibroblasts are known to maintain alveolar compliance and support the structure of the alveolus, some fibroblast sub-populations exist in the interstitium (60, 66, 94, 95).

Myofibroblasts

Myofibroblasts drive the production of elastin, which is responsible for the contractile motion of the alveoli during inhalation (66, 89, 95-97). Myofibroblasts are typically quiescent but have been reported to be more abundant in a number of disease states, for example in fibrosis, where myofibroblasts have been associated with excessive ECM deposition(95, 98-100). Myofibroblasts express alpha smooth muscle actin (α-SMA) (95, 96).

Lipofibroblasts

Lipofibroblasts are found adjacent to ATII cells (101-103)(Figure. 1.6). Lipofibroblasts contain lipid droplets which are required for the production of lung surfactant(94, 95, 101, 103). Lipofibroblasts express adipose differentiation-related protein (ADRP) and platelet derived growth factor receptor- alpha (PDGFR-α-)(79, 103-105). In addition to supporting surfactant synthesis, this subset of fibroblasts has also been found to play an important role in supporting and directing the differentiation of ATII cells into ATI cells(94, 95, 101, 103).

Alveolar Immune cells

The lung is host to diverse populations of immune cells distributed across the airways and the alveolar region(39, 106, 107). In the airways, immune cells include lymphoid cells, natural killer cells, and dendritic cells (39, 106, 107). These immune cell populations are critical for maintaining pulmonary homeostasis while providing rapid responses to injury and infection(39, 106, 107). In the alveoli, alveolar macrophages (Figure. 1.6) are the most predominant population of immune cells(39, 106, 108). They play a critical role in surfactant turnover and phagocytosis of foreign inhaled particles, allergens and pathogens(39, 106, 109). Alveolar macrophages are tissue-resident cells, derived from foetal monocytes during development, although some monocyte-derived macrophages can be recruited from the circulation during inflammation or in response to injury(107-110). There are also macrophages located in the interstitium, Interstitial macrophages, which have distinct phenotypes and functions to alveolar macrophages. Interstitial macrophages contribute to tissue homeostasis and immune regulation(39, 106-108).

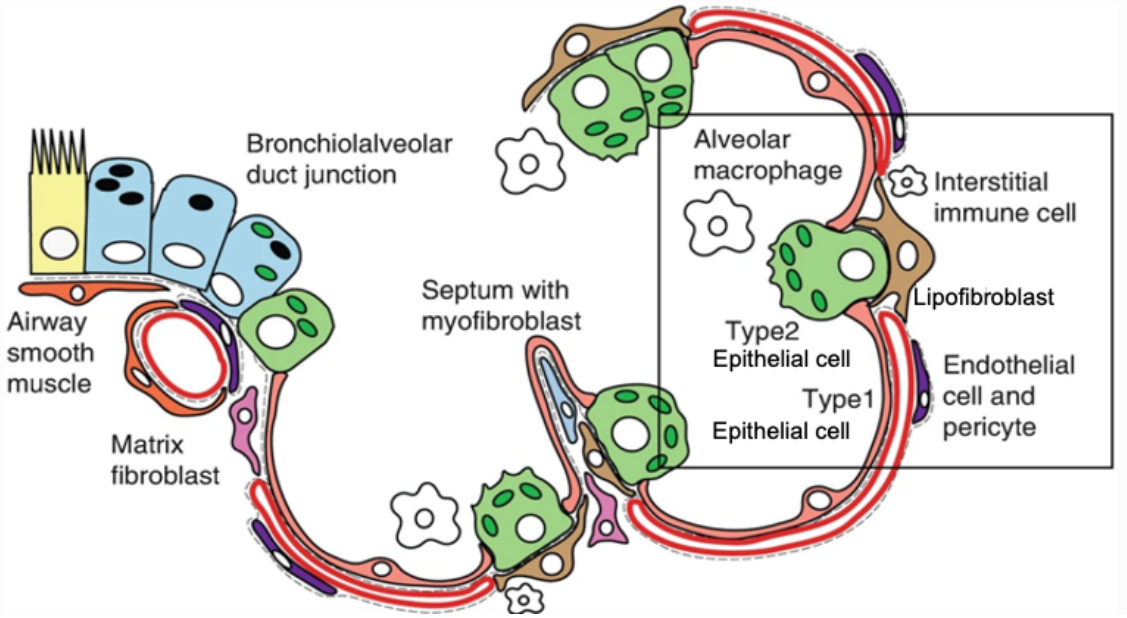

Figure 1.6. Cellular composition of the alveolar niche.

Schematic diagram illustrating the key cell types that the alveolar niche is comprised of, including ATI, ATII, endothelial cells, fibroblast cells and immune cells. Adapted from Hogan BLM, editor. The Alveolar Stem Cell Niche of the Mammalian Lung. Singapore: Springer Singapore; 2020. (102).

1.2.3 Homeostasis in the adult lung

Cellular turnover is essential for the maintenance of tissue structure and function. The epithelial cells that line the proximal-distal lung axis are continuously exposed to environmental insults such as pathogens, hypoxia, environmental toxins, particulate matter and physical trauma(111-113). Therefore, they need to be able to respond efficiently to environmental triggers to restore damaged tissue and retain tissue integrity(111-113). In the adult lung, homeostasis is partly maintained by tissue resident progenitor and stem cell populations. Researchers have identified several progenitor cell populations at different anatomical locations in the lungs (2, 3, 80, 111-113). Many of these cells function as facultative stem cell populations, meaning that they have specialised functions within the tissue under normal conditions but can also serve as stem cells in response to injury(2, 3, 69, 111, 113). Progenitor cell populations are partially differentiated cells that are committed to specific cellular lineages and are capable of self-renewal and can differentiate into distinct subtypes of cells(12, 112-114). As opposed to pluripotent stem cells which are less differentiated and are not committed to specific cellular lineages(12, 112, 114). During homeostasis, the number of these facultative/progenitor cells is relatively low, however in

response to injury, these cells can become activated progenitor cell populations that aid tissue repair and regeneration (2, 3, 38, 69).Furthermore, some of these cells also exhibit plasticity and are capable of de-differentiation into a less specialised multipotent state before re-differentiating to aid restoral of damaged tissue(2, 3, 69, 113, 115). For example cell ablation studies in the mouse trachea have demonstrated that can club cells have the potential to differentiate into basal cells following injury (116, 117). It has also recently been shown that ATII like cells can replicate and differentiate into ATI like cells following pneumonectomy (71).

Although there are some differences in the epithelial cell composition along the proximal-distal axis between the human and mouse lung (section 1.2.2, Figure. 1.4), mouse studies have provided important information about the localisation and function of resident progenitor cell populations(10, 112, 113). Key epithelial progenitor cell populations that have been identified in the lungs include Basal cells (BCs), club cells, bronchioalveolar stem cells (BASCs) and Alveolar Type 2 (ATII) cells (Figure. 1.7).

Basal cells (BC)

As previously outlined BCs and club cells are located within the airways(10, 33, 118-121). Studies have shown that BCs play a central role in maintaining and replenishing the airway epithelium(2, 118, 122-124). They are capable of self-renewal as well as differentiation into different cell types including secretory cells and ciliated cells (Figure. 1.7)(51, 118, 122, 125). BCs function as stem cells along most of the proximal-distal airway axis in humans, but are absent from the respiratory bronchioles and alveoli. Whereas, in mice, BCs only function as stem cells in the trachea (122-124). BCs can be distinguished and sorted using specific marker genes (2, 118). For example, BCs have been observed to positively express different cell specific markers including *transformation-related protein 63 (TRP63*), keratin 5 (krt5) and 14 (krt14), *nerve growth factor receptor (ngfr)* and Pdpn using both genetic models and Fluorescence-Activated Cell Sorting (FACs) (2, 118, 122-124).

A range of different techniques have been employed to investigate BCs. Notably, a technique known as Pulse-seq, which is a combination of lineage tracing and single-cell RNA sequencing (scRNA-seq), has been used to investigate the dynamics of BC differentiation(118, 126). This

has provided insight into BC differentiation and has confirmed the role of BCs in replenishing secretory and ciliated cell populations, as well as PNECs, ionocytes and tuft cells which are less abundant(51, 122, 125-127). However, our understanding of mechanisms which underlie BC self-renewal and differentiation is still incomplete(118). Studies show that intracellular signalling plays a significant role in the determination of BC fate(118). It has been demonstrated, using loss of function studies, that Notch signalling promotes and is required for the differentiation of BCs(2, 128-130). Furthermore, genetic activation studies showed that Notch signalling promotes a secretory cell fate i.e. differentiation into club cells, whilst it does not appear that notch signalling has an impact on BC self-renewal(2, 118, 130, 131). BC proliferation and differentiation occurs at low levels during homeostasis but increases during repair(118, 130). Experiments in mice exposed to sulphur dioxide (SO_2) or naphthalene to specifically induce damage to the airway epithelium has demonstrated that BCs were a source of stem cells in the airways following injury, specifically following damage of club cells (103, 123).

Club cells

Another stem cell population that has been identified in the airways is the club cell population (Figure. 1.7). These cells predominantly maintain the bronchiolar epithelium during homeostasis and during repair in response to injury(2, 121, 132, 133). Club cells are facultative stem cells that exhibit plasticity in response to epithelial damage and are capable of both self-renewal and differentiation and de-differentiation (121, 133). Club cells can be identified by their expression of secretoglobin family 1A member 1 (*Scgb1a1*) and Cytochrome P450 2F2 (*cyp2f2*)(2). Lineage tracing studies have shown that club cells can differentiate into ciliated and de-differentiate into basal cells(42, 116, 121). Interestingly, in a murine model where basal cells were ablated from the airway epithelium using diphtheria toxin, club cells were shown to repopulate the epithelium by proliferating and de-differentiating into TRP63/KRT5$^+$ basal-like cells (116).

Variant Club Cells

Furthermore, a subset of club cells, referred to as variant club cells have been identified and are characterised by the expression of *Scgb1a1* and the lack of *cyp2f2 e*xpression(2, 121). In

murine models, exposure to naphthalene leads to the ablation of *cyp2f2*$^{+}$ club cells, whilst variant *cyp2f2*$^{-}$ club cells are resistant to naphthalene induced injury(121, 134). In response to injury, variant club cells repopulate the damaged airways by self-renewal and differentiation(2, 50, 121). Typically, these variant club cells are found in two niches, adjacent to NEBs in the pseudostratified epithelium and at bronchioloalveolar junctions (BADJs) in the distal airways(50, 121, 135, 136). Although our understanding of club cells is largely informed by murine models, the proliferative capacity of club cells has been examined and demonstrated in humans through analysis of histological samples obtained from human lung tissue(40).

Bronchoalveolar duct junction cells (BADJ)

The BADJ is the region that lies between the bronchiolar region and the alveolar region of the lungs, key stem cell populations have been identified in this region(137, 138). In addition to club cells, BASCs (Figure. 1.7) have been identified at the BADJ and this population of stem cells contributes to bronchiolar and alveolar repair (2, 133, 135, 137, 138). BASCs are *Scg1ab1*$^{+}$ and *sftpc*$^{+}$ (the gene encoding SP-C), this reflects the ability for this population to differentiate into club cells and ATII cells(133, 138). Importantly BASCs can be distinguished from progenitor cell populations in the proximal and distal epithelium. Notably, variant club cells at neuroendocrine bodies (NEBS) which express s*cg1ab1* also express *uropankin 3A* (Upk3a) (139, 140) which is not expressed by BASCs. Additionally ATII cells in the alveoli only express *sftpc* and are *scg1ab1*$^{-}$.

ATII cells

In the alveolar region, ATII cells are the primary facultative stem cell population(78-80, 141). (Figure. 1.7) In response to injury, facultative stem cells become activated from the ATII cell population, increase and can differentiate into ATI and ATII cells and to restore functional alveoli (2, 28, 38, 141). The regenerative capacity of ATII cells was initially demonstrated using tritiated thymidine pulse/chase experiments in rodents(142-144). In rat models of nitrogen dioxide (NO_2) induced oxidative injury, there was an initial increase in the number of ATII cells followed by an increase in the number of ATI cells over time(142, 144). These investigations

provided evidence that ATII cells can differentiate into ATI cells, a correlation was established between the increase in ATI cells and earlier proliferation of ATII cells following injury(142, 144). The findings from these investigations were supported by experiments conducted with monkeys (145). Monkeys were exposed to a hypoxic environment and histological analysis of samples using haematoxylin and eosin (H&E) staining confirmed an increase in ATI cells in comparison to ATII cells in monkeys during recovery (145). The progenitor potential of ATII cells was also demonstrated using early *in vitro* experiments, where primary ATII cells were cultured and were observed to transition into ATI-like cells. The shape of these cells changed and they expressed markers for ATI cells(146, 147).

Recent studies using lineage tracing have corroborated the role of ATII cells as the facultative stem cells in the alveolar region(79, 80, 148). Lineage-labelled ATII cells have been shown to self-renew under homeostatic conditions, therefore maintaining the alveolar epithelium. Following injury induced by bleomycin or ablation using diphtheria toxin, lineage-labelled ATII cells have been demonstrated to proliferate and differentiate into ATI cells(79). Additionally, when ATII cells were selectively ablated using diphtheria toxin, clonal expansion or remaining cells occurred and clusters of both ATII and ATI were observed, further highlighting the capacity of ATII cells to self-renew and differentiate(79). Interestingly, injury induced by diphtheria toxin led to a significantly lower rate of differentiation when compared to bleomycin induced injury(79). This indicates that the regenerative capacity of ATII cells is dependent on the insult. Building on this, organoid culture investigations have demonstrated that factors and signals from the alveolar niche support the regenerative capacity of alveolar progenitor cells(79, 141). It was demonstrated that platelet derived growth factor receptor-alpha^{+} (PDGFRA^{+})stromal cells, which included lipofibroblasts, enhanced the growth and differentiation of organoids derived from alveolar progenitors(79). In the alveolar niche lipofibroblasts are located adjacent to ATII cells (101-103). In addition to this, lipofibroblasts have been shown to support alveolar development (94) and during homeostasis contribute to the production of surfactant by transferring lipids to ATII cells (94, 149). Furthermore, PDGFRA^{+} fibroblasts have been identified as a source of secreted Wnts(150, 151), which play a role in the maintenance of ATII stemness. This highlights the importance of understanding

how key signalling pathways modulate homeostasis in the alveolar niche, as well as repair and regeneration.

In contrast to ATII cells, ATI cells have a limited proliferative capacity and were previously believed to be terminally differentiated(3, 71, 121), however, emerging studies have demonstrated that a subset of ATI cells exhibit some plasticity(65, 71). Lineage tracing studies have shown that *Hopx*$^{+}$ ATI cells can dedifferentiate into ATII cells following pneumonectomy in mice (71). Additionally, the same study showed that organoids derived from *Hopx*$^{+}$ ATI cells gave rise to sftpc^{+} ATII cells(71). In support of these findings another study showed that although ATI cells in lung tissue from rats do not express *sftpc*, a marker for ATII cells or cc10 a marker for club cells, the expression of these markers could be induced(152).

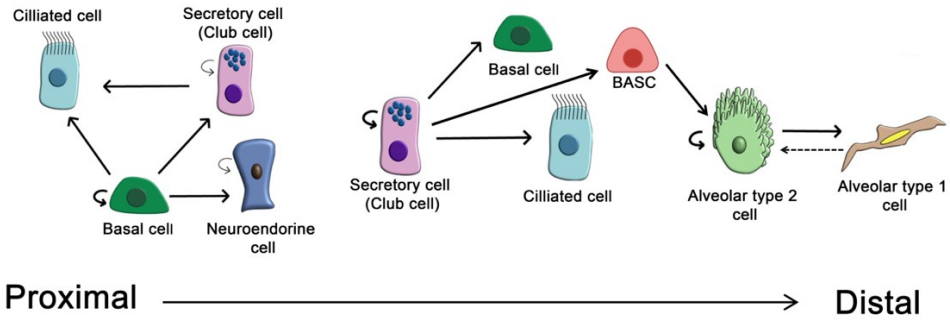

Figure 1.7. Progenitor cells along proximal distal axis of lungs.

Schematic outlining the progenitor cells that line the airways and their differentiation repertoire. Curved lines demonstrate self-renewal of cells, while. Dotted lines demonstrate limited capacity. Figure adapted from Tata PR, Rajagopal J. Plasticity in the lung: making and breaking cell identity. Development. 2017 Mar 1;144(5):755-66.(117).

1.2.4 Repair and regeneration of the lungs

It was previously believed that the lungs had a limited capacity to repair following injury(2, 37). However, increasing studies have shown that the lungs have a remarkable capacity for repair and regeneration and that the lungs are more dynamic than was previously understood(2, 37). Additionally, imaging studies showing that alveologenesis continues till ~ 21 years(12, 14, 16, 21), as well as the identification of several progenitor cell populations (2, 3, 80, 111-113) (outlined in section 1.2.3) further highlight the plasticity and regenerative

potential of the lungs. Although the processes are closely related, repair and regeneration describe two different responses to tissue damage; when tissue is repaired a scar is produced during the process and the full function of the tissue is not restored, whereas regeneration is used to describe the complete replacement of damaged tissue with new functional tissue(37, 111, 153).

Animal models have provided insightful information and have demonstrated the capacity of the lungs to regenerate under certain conditions. A study in rats showed thar animals fed a restricted calorie diet of one fifth of their usual daily consumption for 10 days (154) led to alveolar damage and a reduction in lung surface as well as enlarged airspaces, resembling emphysema. Remarkably, restoration of normal daily calorie intake reversed these morphological changes(154). A similar study conducted with mice showed alveolar destruction when calories were restricted, however after 15 days of calorie restriction, mice were refed their normal daily calorie intake and this led to alveolar regeneration(155). Interestingly, adult humans with anorexia nervosa also exhibit emphysema-like morphological changes to their lungs, however studies investigating potential alveolar regeneration following an increase in calories have not been conducted in humans(156, 157).

In 2012, a medical case study reported compensatory lung growth in a 33-year-old woman, 15 years after pneumonectomy (Figure. 1.8)(158). Additionally, her lung function, increased markedly, she had a 51 % increase in forced expiratory volume in 1 second (FEV_1) and a 35 % increase in forced vital capacity (FVC), after 15 years(158). Further to this, an increase in her lung volume was observed and using hyperpolarized helium-3 gas magnetic resonance imaging (MRI), a 64 % increase in the number of alveoli was observed(158). Therefore, this indicates that neo-alveolarisation or the generation of new alveoli occurred in the years following the pneumonectomy(103).

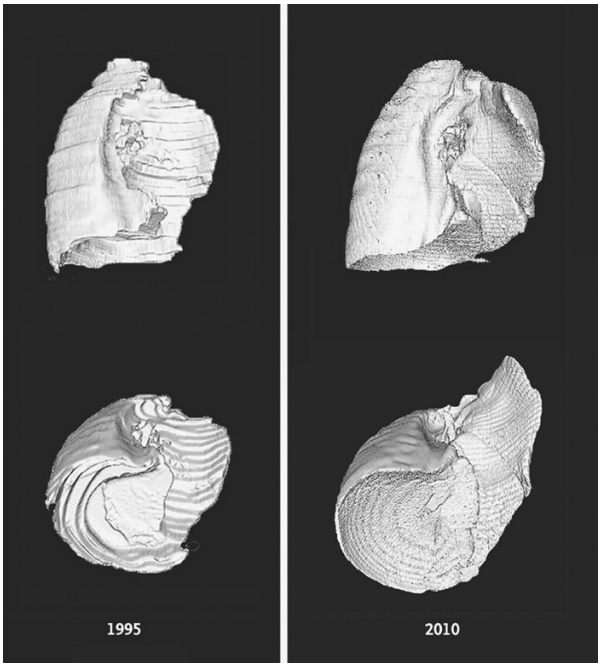

Figure 1.8. Regeneration of adult lung following pneumonectomy.

3D reconstruction of axial CT images of left lung, following a right-sided pneumonectomy in 1995 and 15 years later in 2010. An increase in lung volume is evident in images from 2010 demonstrating the lung growth. Adapted from Butler JP, Loring SH, Patz S, Tsuda A, Yablonskiy DA, Mentzer SJ. Evidence for adult lung growth in humans. N Engl J Med. 2012 Jul 19;367(3):244-7. (158).

Lung growth has also been observed in mice that have undergone pneumonectomy(159, 160), ATII cell proliferation was also observed 3 days post pneumonectomy in mice and differentiation into ATI cells was observed from around day 7 post pneumonectomy (159, 160).

As outlined, the lungs possess a remarkable capacity for repair. However, emerging studies suggest that the extent of repair and regeneration can vary(37, 38). Following injury, the lung epithelium can initiate repair and regenerate through the activation of progenitor cells (outlined in section1.2.3) and signalling pathways (explored in more detail in section 1.3) which drive repopulation of the epithelium. However, in most lung diseases aberrant remodelling and differentiation of cells occurs(37, 38). These is a spectrum of aberrant repair leading to disease for example, excessive repair can lead to fibrotic disease while insufficient lung repair is a hallmark of COPD(37, 38). Furthermore repair, regeneration and remodelling are all influenced by both intrinsic factors such as genetics and ageing and extrinsic factors including exposure to cigarette smoke, particulate matter, infection and drugs (Figure. 1.9)

(37, 38). Highlighting the need for further studies to investigate the mechanisms and signals that govern repair and cell fate post injury, in order to maintain a balance between 'good' repair and regeneration whilst preventing aberrant remodelling (37, 38).

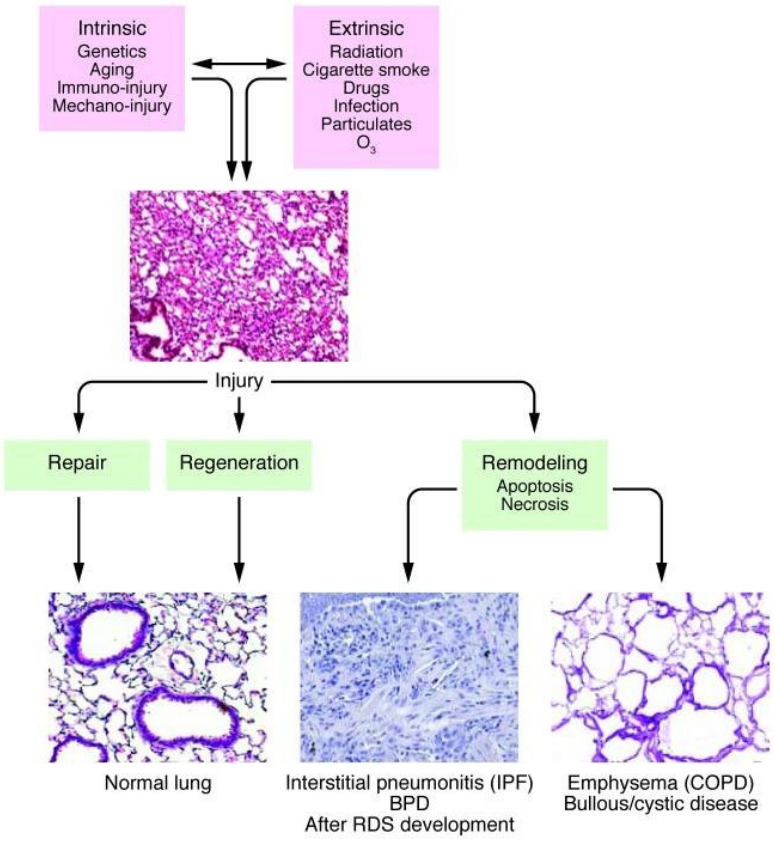

Figure 1.9. The balance between normal repair, regeneration and aberrant remodelling.

Schematic outlining the cellular response of the lungs to intrinsic and extrinsic sources of injury and how this may lead to normal repair and regeneration of aberrant remodelling. Adapted from Beers MF, Morrisey EE. The three R's of lung health and disease: repair, remodeling, and regeneration. J Clin Invest. 2011 Jun;121(6):2065-73.(37).

1.3 Key signalling pathways for lung development and repair

Using mouse models, the role of numerous signalling pathways has been studied across all stages of development from the embryonic stage to alveolarisation (Figure. 1.10)(8, 10, 11, 14). In addition to their roles in development, several of these signalling pathways have been shown to be reactivated in lung repair following injury, offering potential for regenerative therapeutics (11-13, 19).

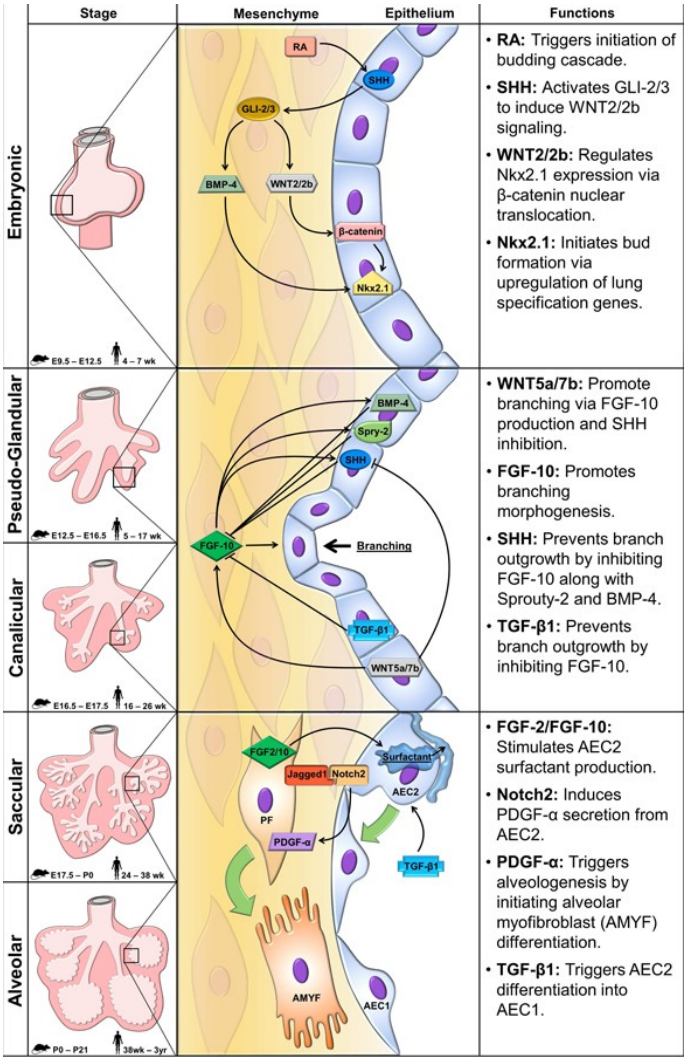

Figure 1.10. Signalling pathways driving lung development from the embryonic stage to alveolar stage.

Schematic diagram outlining the key signalling pathways that regulate mammalian lung development, based on mouse studies. Lung development begins on E 9.5 in mice with lung bud formation, initiated by a cascade driven by retinoic acid (RA) that activates Shh → Wnt2/2b/β-catenin →Nkx2.1 During the pseudoglandular stage, branching morphogenesis is driven by FGF-10 which is induced by Wnt5a/7b and inhibited by Shh, Bone Morphogenic Protein-4 (BMP-4) and Sprouty-2 (SPRY-2). In the canalicular stage further branching is inhibited by Shh, TGF-β and BMP-4 inhibition of FGF-10. In the saccular stage early alveolar development occurs, this is regulated by FGF-2/FGF-10. During the alveolar stage TGF-β and Notch signalling regulate the differentiation of ATII cells. Green arrows on diagram indicate points of progenitor cell differentiation. Adapted from Chanda D, Otoupalova E, Smith SR, Volckaert T, De Langhe SP, Thannickal VJ. Developmental pathways in the pathogenesis of lung fibrosis. Mol Aspects Med. 2019 Apr; 65:56-69. (13).

1.3.1 Fibroblast growth factor (FGF) signalling pathway

FGF signalling is required throughout lung development. There are 22 FGF ligands, divided into 7 subfamilies based on their function and sequence homology(13, 161, 162). Canonical FGFs interact with FGF receptors leading to the activation of downstream intracellular

signalling cascades including Ras/MAPK, PI3K/AKT, PLCγ, or JAK/STAT (Figure. 1.11)(13, 161, 162). (13, 162). In early lung development, FGF plays an important role in mediating branching morphogenesis, specifically FGF10 expressed in the mesoderm/mesenchyme directs domain branching (where new branches arise) by acting on epithelial cells that express the ligand receptor. (9, 28, 161). Furthermore, lack of lung development (agenesis) has been observed in FGF10$^{-/-}$mice(161). In alveolarisation, FGF7 signalling is important for alveolar maturation and mediating distal growth of alveoli, FGF8 signalling has also been detected at later stages of alveolarisation(161, 162). In the adult lung, FGF signalling regulates cell proliferation, turnover and differentiation, specifically FGF2 maintains cellular homeostasis and quiescence(13, 161, 162). Studies have also demonstrated elevated expression of FGF2 in IPF(13), however, this has been associated with epithelial repair(163).In response to injury, FGF10 initiates differentiation of alveolar progenitor cells into epithelial cells and a reduction in FGF10 has been linked to the progression of pulmonary fibrosis (13, 161, 162).

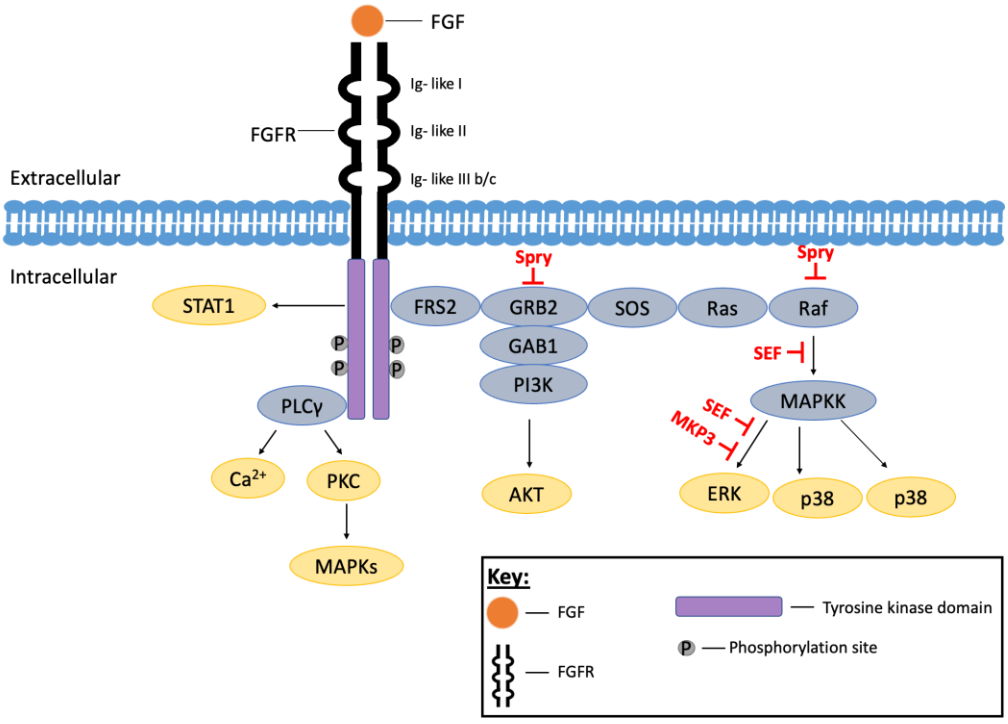

Figure 1.11. FGF Signalling pathway.
Binding of FGFS to FGFRs triggers dimerisation and activation of FGFRs. Activated FGFRs phosphorylate FRS2α which binds to GRB2 activating downstream effectors which include SOS, GAB1 and CBL. This activates signalling through multiple pathways: Ras/MAPK, PI3K/AKT, STAT or PLCγ pathways. Negative pathway regulators include SPRY (inhibits GRB2 and Raf), SEF (inhibits ERK phosphorylation), MKP3 (dephosphorylates ERK) Adapted from Xie Y, Su N, Yang J, Tan Q, Huang S, Jin M, et al. FGF/FGFR signaling in health and disease. Signal Transduct Target Ther. 2020 Dec 18;5(1):181. (164).

1.3.2 Transforming growth factor-β signalling pathway

The transforming growth factor β (TGF-β) superfamily is a family of polypeptide growth factors including TGFs (TGF-β1, TGF-β2 and TGF-β3), Bone morphogenetic proteins (BMP-1 – BMP-20) and activins(8, 13). TGF-β signalling occurs when ligands bind to cell surface receptors leading to the activation of SMAD proteins, once activated SMAD proteins translocate to the nucleus and regulate gene expression (Figure. 1.12)(8, 13). TGF-β ligand isoforms and BMP ligands are expressed at different stages during lung development(8, 13, 165). During the pseudoglandular stage of lung development TGF-β1 is highly expressed and along with other key signalling pathways is responsible for regulating branching morphogenesis(8, 13, 165). TGF-β1 expression has been shown to prevent aberrant branching and outgrowths(8, 13, 165). Supporting this, overexpression of TGF-β1 in mouse lung buds was shown to inhibit branching morphogenesis(8, 13, 165). Conversely, BMP-4 expression in the pseudoglandular stage of lung development stimulates branching(8, 13), this has been demonstrated by overexpression of BMP-4 in developing mouse lungs(8, 166, 167). Paracrine sonic hedgehog (Shh) signalling has been shown to induce expression of BMP-4 during this stage(13). Further to this, TGF-β signalling has been found to play a key role in alveolarisation, particularly studies have shown that TGF-β1 signalling is important for the differentiation of alveolar type 2 cells to mature alveolar type 1 cells(8, 13). Interestingly, it has been demonstrated that TGF- β signalling is upregulated during lung disease, particularly in pulmonary fibrosis (13, 168-170). TGF- β drives myofibroblast differentiation and stimulates excessive ECM deposition (13, 168). Additionally, some research suggests that TGF- β also supresses the production of anti-fibrotic factors including hepatocyte growth factor and prostaglandin E2 further contributing to IPF disease pathology(13, 168).

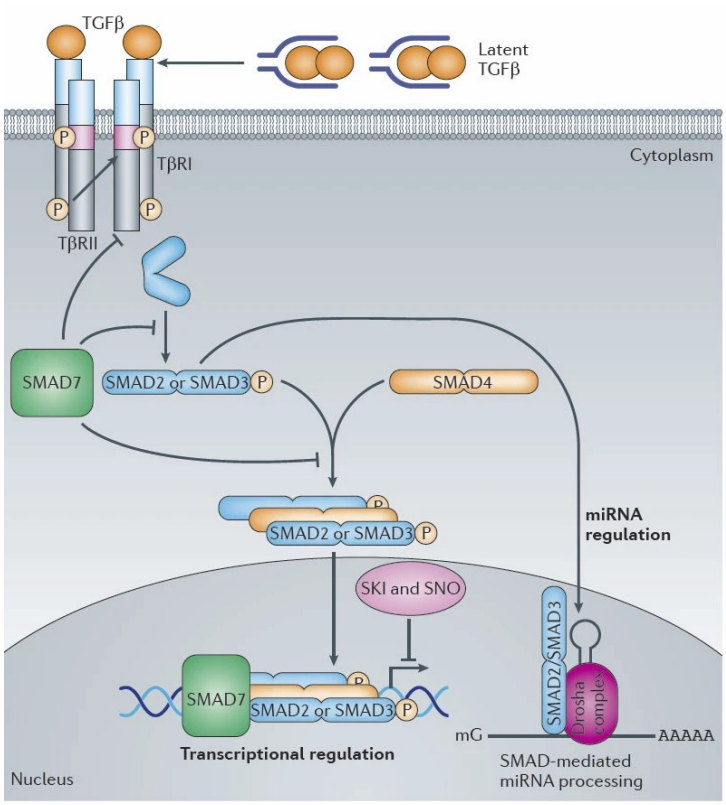

Figure 1.12. Canonical TGF-β signalling.
TGF-β ligands form a complex with latency-associated peptide (LAP) and latent TGF-β-binding protein (LTBP) and become activated. Then they bind to TGF-β receptors (TβRI and TBRII) which drives phosphorylation and activation of SMAD proteins (SMAD2/3). SMADs form a complex with co-SMAD (SMAD4) and the SMAD complex translocates into the nucleus, where it binds to transcription factors and regulates gene expression. Adapted from Akhurst RJ, Hata A. Targeting the TGFβ signalling pathway in disease. Nat Rev Drug Discov. 2012 Oct;11(10):790-811. (169).

1.3.3 Hedgehog signalling pathway

In mammals three conserved Hedgehog (Hh) ligands have been identified; Sonic Hh (Shh), Desert Hh (Dhh) and Indian Hh (Ihh)(171, 172). Canonical Hh signalling (Figure. 1.13) is dependent on the binding of Hh ligands to the receptor Patched (Ptch), resulting in a cascade that activates and regulates the Glioblastoma (Gli) transcription factors (171, 173, 174).

Shh is synthesised as a 45 kDa precursor protein and subsequently undergoes autocatalytic cleavage forming two Shh peptides: 26 kDa carboxy terminal segment, SHH-C and a 19 kDa amino-terminal segment, SHH-N (172, 174-176). SHH-N functions as the biologically active form of the protein that initiates the signalling cascade(172, 177). Although SHH-C does not directly participate in signal transduction, it is believed to facilitate the autoproteolytic

cleavage process that results in cholesterol binding to SHH-N(172). Following cholesterol modification, SHH-N is secreted from the producing cell via a transport protein(178). In *Drosophila*, this transporter has been identified as Dispatched (Dsp), and a homologous protein with a similar function exists in mammals(172, 178, 179). In the absence of the Shh ligand (SHH-N), the receptor Ptch inhibits the activity of the transmembrane protein Smoothened (Smo) (171-174). Binding of SHH-N to Ptch relieves this inhibition, enabling Smo to activate downstream signalling events that promote the activation of Gli transcription factors(171-174). Activated Gli proteins translocate to the nucleus, where they regulate gene expression (171-174).

Current research shows that canonical SHH signalling is essential in lung development(11, 13, 180, 181). In early lung development SHH signalling plays a role in the regulation of branching morphogenesis and co-ordination of epithelial-mesenchymal interactions (11, 13, 180, 181) . SHH signalling in particular is required for branching morphogenesis, Shh expression is elevated at tips of the bronchial branches where it mediates mesenchymal differentiation and proliferation, starting during the pseudoglandular stage(13, 180, 181). This gives rise to bronchial smooth muscle cells(180-182). Investigations with Shh conditional knockout (CKO) mice, demonstrated that an absence of Shh during the pseudoglandular stage leads to aberrant branching morphogenesis(180-182). Furthermore, histological analysis of Shh null mutants revealed improper separation of tracheal tubes after the formation of the primary lung buds (183). In early alveolarisation, $Gli1^{+}$ cells are detected in the mesenchyme, but gradually reduce during alveolar maturation. Therefore, studies suggest that SHH signalling plays an important role in the initial epithelial-mesenchymal interactions that drive primary septation (180, 181, 184). It has also been demonstrated that inhibition of Shh at this stage disrupts septation(185). Studies have also begun to decipher the role of SHH signalling in the adult lung where Shh has been shown to maintain quiescence of mesenchymal and progenitor cell populations (9, 11, 13, 181). SHH, which is expressed by epithelial cells signals to adjacent mesenchymal cells to maintain quiescence and prevent excessive proliferation(181, 185, 186). Gli1, a downstream transcription factor in the canonical SHH signalling pathway is expressed in the mesenchyme and is therefore a marker of pathway activation(181, 185-187). Using conditional, tamoxifen-inducible knockout mice, it has been demonstrated that conditional

deletion of SHH in epithelial cells or Smo (the pathway signal transducer) in mesenchymal cells, can result in mesenchymal expansion(186). Evidence also suggests that SHH signalling induces fibroblast expansion during repair (13, 181). A study showed that SHH signalling is transiently downregulated following injury, and this leads mesenchymal cells to proliferate and drive repair, this was demonstrated by tracking Gli1^{+} cells using Gli1^nlacZ reporter mice (187). The same study reported that subsequent pathway reactivation restored quiescence(187). It has also been demonstrated that SHH signalling regulates myofibroblast activation (13, 181, 185) through crosstalk with the Wnt/β-catenin signalling pathway(188), specifically by interacting with Wnt10. This also highlights coordination of homeostasis and repair across pathways. However dysregulation or excessive myofibroblast activation can lead to fibrotic remodelling and elevated SHH levels have been observed in IPF lung tissue(13, 181, 189, 190). Highlighting the importance of pathway regulation.

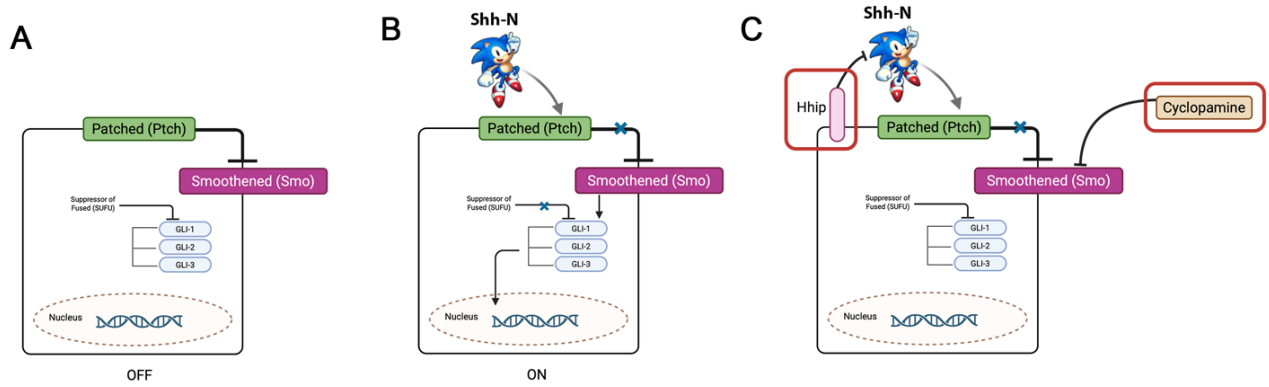

Figure 1.13. Sonic Hedgehog signalling pathway.

(A) In the inactive pathway the absence of the Shh ligand allows Patched (Ptch) to inhibit Smoothened (Smo), which prevents downstream signalling (B) In the active state, the Shh precursor undergoes autoproteolytic cleavage forming the active SHH-N ligand which is transported to the target cell by dispatched. SHH-N binds to Ptch and Inhibits the activity of Ptch. The signalling cascade is triggered and Smoothened (Smo) is activated. Smo releases an intracellular signal, activating Gli proteins. Gli proteins dissociate from Suppressor of Fused (SUFU), allowing nuclear translocation of Gli proteins and gene expression. (C) Inhibition of SHH signalling. Hedgehog-interacting protein (Hhip) binds to SHH-N and alters its conformations, preventing SHH-N from binding to Ptch. Cyclopamine inhibits Smo, which blocks Gli activation. Adapted from Villavicencio EH, Walterhouse DO, Iannaccone PM. The sonic hedgehog-patched-gli pathway in human development and disease. Am J Hum Genet. 2000 Nov;67(5):1047-54.(174). Figure generated using Biorender.

1.3.4 Hippo signalling

The Hippo signalling pathway is a highly conserved pathway (Figure. 1.14) that is known to play an important role in the regulation of cell proliferation, tissue development and homeostasis, organ size, tumorigenesis, apoptosis and regeneration(13, 191-193).

The pathway is activated by upstream stimuli such as an increase in cell density and/or an increase in cell-cell contact(13, 191-193). Upon activation, a phosphorylation cascade occurs which leads to the phosphorylation and inactivation of Yes associated proteins/transcriptional co-activator with PDZ binding motif (YAP/TAZ) (Figure. 1.)(13, 191, 192). However, when the pathway is inactivated, YAP/TAZ is not phosphorylated and translocates into the nucleus where it binds to TEA- domain (TEAD) transcription factors leading to the expression of genes associated with cell proliferation, differentiation and the inhibition of apoptosis(13, 191, 192). Activation of the Hippo signalling effectors YAP/TAZ has been found to play a crucial role in the regulation of branching morphogenesis in lung development(13, 21, 191, 192, 194, 195). Studies have found that YAP controls the expression of Sox2 which is known to drive the development and differentiation of the proximal (upper) airways(13, 21, 191, 192). Additionally YAP has been shown to induce the expression of Shh, which as previously described plays a role in branching morphogenesis(194, 195).

During alveologenesis and subsequently in homeostasis YAP/TAZ have been shown to increase the expression of genes responsible for the differentiation of ATII cells to ATI cells, in this context the activity of YAP/TAZ is highly regulated and beneficial(21, 192, 194). In contrast to this, during disease dysregulated nuclear activation of YAP/TAZ has been observed. For example in IPF, increased ECM stiffness drives excessive nuclear translocation of YAP/TAZ and binding to TEAD transcription factors, which leads to the expression of pro-fibrotic genes including Twist1(13, 192, 194, 196).

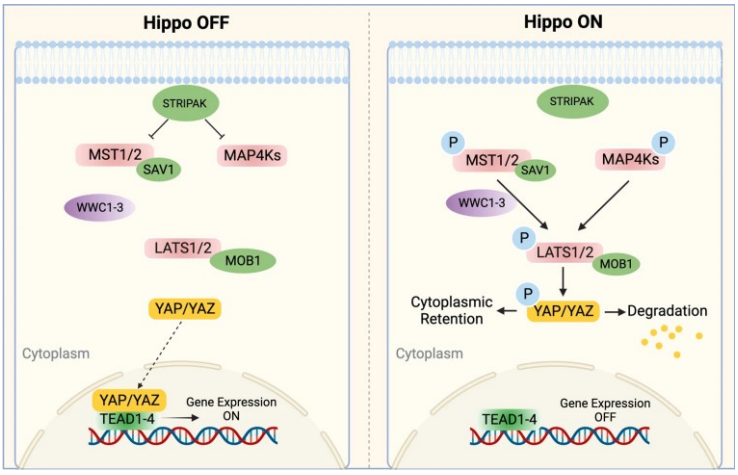

Figure 1.14. Hippo Signalling.

Schematic diagram summarising how the hippo signalling pathway is activated. Left hand side shows inactivate pathway and right-hand side shows activated pathway. The pathway is regulated by the STIRPAK complex which dephosphorylates MST1/2 and MAP4Ks. Inhibition of STIRPAK leads to the phosphorylation of MST1/2 and MAP4K leading to a cascade of phosphorylation events resulting in YAP/TAZ translocating into the nucleus and triggering gene expression via TEAD transcription factors**.** Adapted from Fu M, Hu Y, Lan T, Guan KL, Luo T, Luo M. The Hippo signalling pathway and its implications in human health and diseases. Signal Transduct Target Ther. 2022 Sep 19;7(1):376. (197).

1.3.5 Notch signalling

NOTCH is a juxtracrine signalling pathway (Figure. 1.15), ligand expressing cells interact directly with receptor expressing cells(13, 198, 199). Upon direct binding, the NOTCH intracellular domain (NCID) is cleaved from the NOTCH receptor by γ secretase and is able to translocate into the nucleus to activate target genes(13, 198, 199). There are 5 NOTCH ligands; Jagged 1, Jagged 2 and the Delta-like canonical Notch Ligands (Dll1,3,4) and 4 conserved Notch receptors (Notch1-4)(13, 198). During lung development NOTCH signalling regulates patterning along the proximo-distal axis, cell fate, epithelial differentiation and alveolarisation(13, 198). Studies have shown a key role for NOTCH signalling in alveolarisation(198). Notch2^{cNull} mutant mice, that lack Notch 2 found enlarged airspaces reminiscent of an emphysema like phenotype (198, 200). Highlighting that NOTCH signalling is required for alveolar development(198, 200) NOTCH signalling also regulates cell fate in resident stem cells, maintaining the balance between secretory and ciliated cell differentiation after injury. (5, 11, 13, 201).

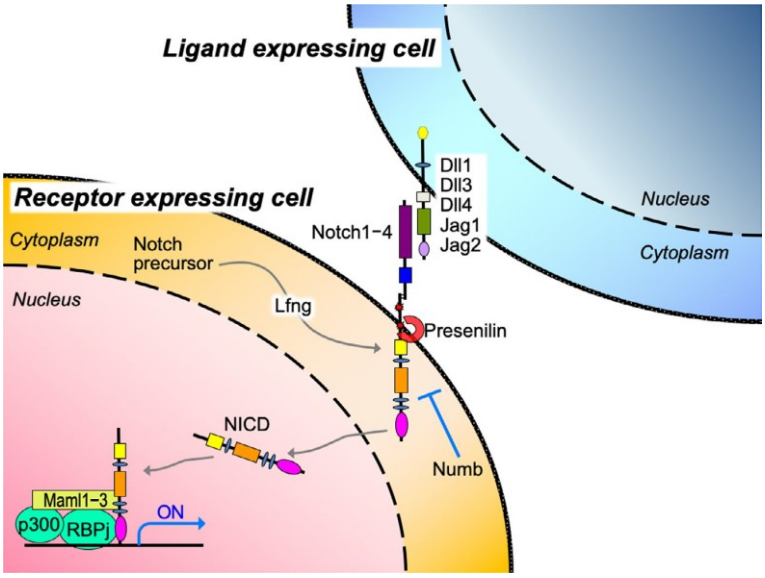

***Figure 1.15. Notch signalling pathway*.**

Schematic outlining Notch signalling pathway. The pathway is activated by interactions between ligand expressing cells (blue) and receptor expressing cells (orange). Binding of ligands to receptors leads to the cleavage of NICD, enabling NICD to translocate into the nucleus to activate target genes. Adapted from Kiyokawa H, Morimoto M. Notch signaling in the mammalian respiratory system, specifically the trachea and lungs, in development, homeostasis, regeneration, and disease. Dev Growth Differ. 2020 Jan;62(1):67-79. (198).

1.3.6 Vascular endothelial growth factor signalling pathway

There are several isoforms of VEGF which are activated upon interaction with tyrosine kinase receptors; VEGFR-1/Flt-1, VEGFR-2/Flk-1 (KDR), and VEGFR-3 (Flt-4)(8, 202, 203). VEGF signalling mediates pulmonary vascular development (angiogenesis and vasculogenesis) (Figure. 1.16)(8, 202, 203). VEGF signalling is first activated during the embryonic stage of lung development(202, 203). In addition, VEGF and VEGFR-2 are expressed during branching morphogenesis, and are involved in the regulation of crosstalk between endothelial, epithelial and mesenchymal cellular compartments, leading to simultaneous and coordinated vascular and epithelial branching morphogenesis(8, 202, 203). Coordination of development of the epithelial and endothelial cellular compartments is critical for successful development of the respiratory tree(202, 203); coordinated development between these compartments is driven by a gradient of VEGF expression in the distal tips of the branching airways(202, 203). A decrease in VEGF mRNA expression and VEGF protein has been found in clinical studies of lung tissue taken post-mortem from infants with bronchopulmonary dysplasia (BPD), further highlighting the importance of VEGF signalling at early stages of lung development(202-

204).Studies have also reported high expression of VEGF in alveoli, leading to more investigations into the role of VEGF during alveolarisation(202, 203, 205); interestingly, studies have shown that alveolarisation decreases in rats administered with VEGFR inhibitors(202, 203, 205, 206). Further to this, studies have demonstrated that treatment with VEGF leads to an increase in alveolarisation following pneumonectomy in mice (207) and after injury induced from exposure to hypoxic environments in rats(208).Interestingly, a study demonstrated that a reduction in VEGF led to a reduction in RA secretion, suggesting that VEGF induces RA secretion(209). The interaction between VEGF and RA plays an important role in regulating both alveolar and vascular development(209). The role of RA in development and the potential role of RA in repair and regeneration is explored in further detail in section 1.3.8.

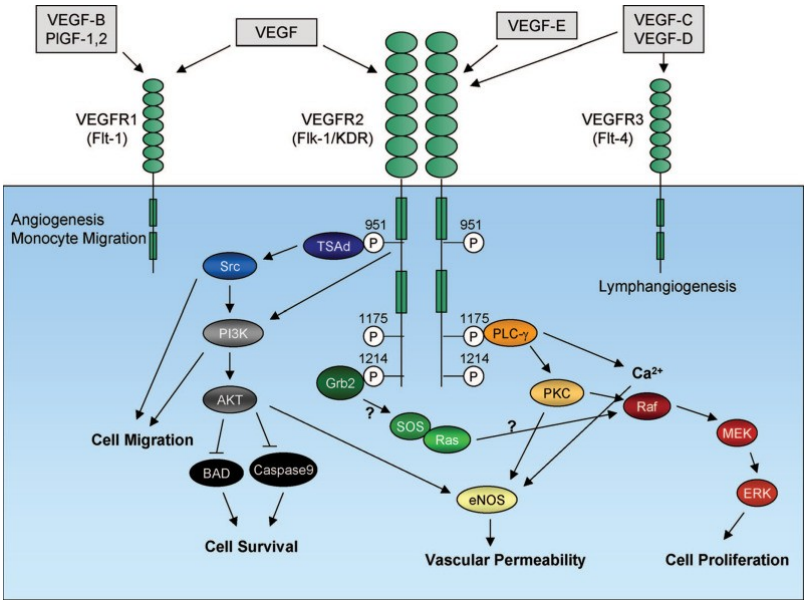

Figure 1.16. VEGF signalling.

VEGF ligands bind to tyrosine kinase VEGF receptors. This triggers dimerization, autophosphorylation and activation of several downstream signalling pathways including PLCγ, PI3K, AKT, Ras, Src and MPK. VEGF signalling can regulate cell migration, survival, proliferation and vascular permeability. Adapted from Nilsson M, Heymach JV. Vascular Endothelial Growth Factor (VEGF) Pathway. J Thorac Oncol. 2006 Nov;1(8):768-70.(210).

1.3.7 WNT signalling pathways

There are three distinct intracellular WNT signalling cascades: canonical WNT/β-catenin dependent (Figure. 1.17), and two non-canonical pathways, the planar cell polarity (PCP) and WNT/Ca^{2+} pathways(211-215). All three cascades are initiated when WNT ligands bind to 1 of 10 Frizzled (FZD_1-FZD_{10}) transmembrane receptors(213, 215). 19 mammalian WNT proteins

have been identified, that regulate a wide range of cellular processes (211, 213, 216, 217). Although the canonical WNT/β- catenin pathway is the most well characterised, WNT ligands can activate any of the three pathways depending on the cellular context, receptor availability and interactions with co-receptors(211-214). While WNT ligands exhibit this pleiotropic potential, some exhibit a bias for signalling via one pathway in particular, for example, WNT5A predominantly signals through the non-canonical PCP pathway.(218) Therefore, it is important to understand precisely which pathway(s) are active during lung development and repair (211-214). During early lung development WNT signalling has been found to regulate epithelial-mesenchymal interactions that promote branching morphogenesis, spatial patterning and cellular differentiation, with specific WNT ligands linked to the differentiation of distinct cell populations(11, 13, 211, 213, 214). For example, WNT2/2B is expressed in the mesenchyme, WNT7B in the epithelium and WNT11 has been observed in both the mesenchyme and epithelium during development(13, 211, 212). Non-canonical WNT signalling contributes cytoskeletal remodelling and the maintenance of planar cell orientation, these processes are essential for coordinated tissue morphogenesis during lung development (219-222). During lung development, WNT5A-PCP signalling has been shown to play a particularly important role in proximal-distal patterning of the airways, being expressed in both mesenchymal and epithelial cell compartments(220, 223). At the same time, WNT5A has been found to play a role in regulating proliferation and differentiation during branching morphogenesis (220, 223).

Dysregulation of both canonical and non-canonical WNT signalling pathways has associated with defective lung development and with respiratory diseases including, pulmonary fibrosis, lung cancer and pulmonary arterial hypertension (PAH)(211-214).

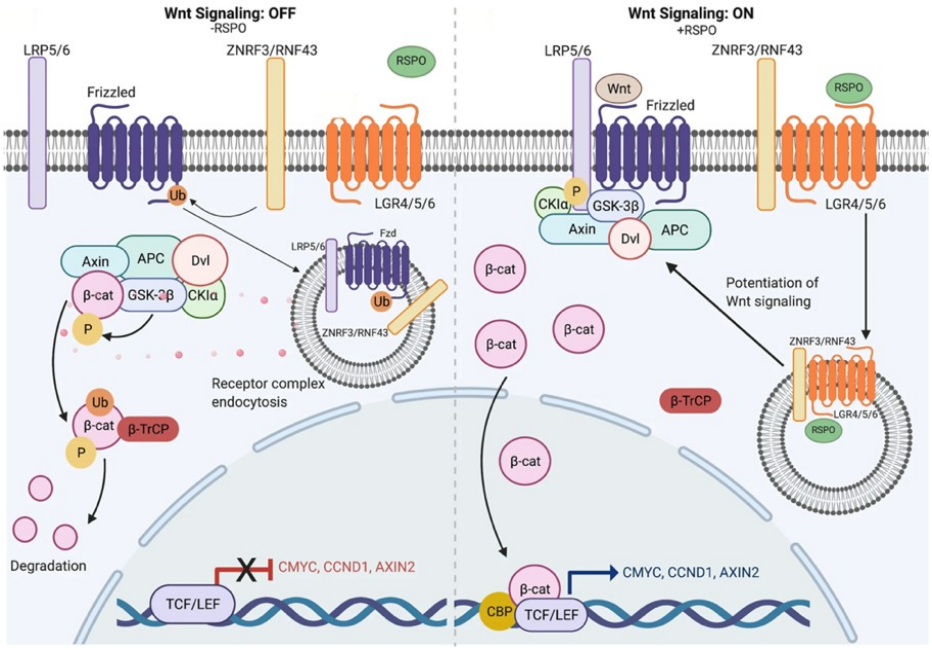

Figure 1.17. Canonical WNT signalling pathway.

Inactive WNT signalling is presented on the left-hand side, while activate WNT signalling is presented on the right side. Adapted from Aros CJ, Pantoja CJ, Gomperts BN. Wnt signaling in lung development, regeneration, and disease progression. Commun Biol. 2021 Sep 3;4(1):601. (224).

1.3.8 Retinoic acid

Retinoic acid (RA) is derived from vitamin A (retinol) and has been found to play an important role in lung development particularly during the embryonic phase, branching morphogenesis and alveolar development and differentiation(8, 13, 225, 226). RA has been shown to mediate these processes spatially and temporally(227, 228). Furthermore, experimental investigations have demonstrated the importance of RA in lung development. Notably functional defects were observed in the respiratory epithelium of vitamin A deficient mice (229) and embryonic explants from retinaldehyde dehydrogenase-2 (*Raldh2*) knockout mice failed to develop while addition of exogenous RA induced development(230). In addition to this, it has been demonstrated that the lung function of infants born to vitamin A deficient mothers is impaired(231-233).

RA is produced from retinol following two enzymatic reactions. Retinol is oxidised into retinal by alcohol dehydrogenases (ADH) and retinol dehydrogenases(225, 227). Then retinal is oxidised into retinoic acid by retinaldehyde dehydrogenases (RALDHs). Once produced, RA

binds to retinoic acid receptors (RARs)(225, 227). There are three RAR subtypes – RARα, RARβ and RARγ. Then RARs bind to retinoid x receptors (RXRs) forming heterodimers(225, 227). RAR-RXR heterodimers bind to retinoic acid response elements (RAREs) which leads to the regulation of gene transcription (Figure. 1.18)(225, 227).

RA signalling and retinoids have been found to play a role in lung repair and regeneration, in particular, RA has been found to play an important role in alveolar regeneration(226). Some experimental investigations have been conducted to investigate the role of RA in regeneration. Using a rat model of emphysema, it was demonstrated that daily administration of all trans RA injections led to the restoration of the alveolar structure(234). This was measured by a decrease in emphysematous lesions and an improvement in elastic recoil(234).

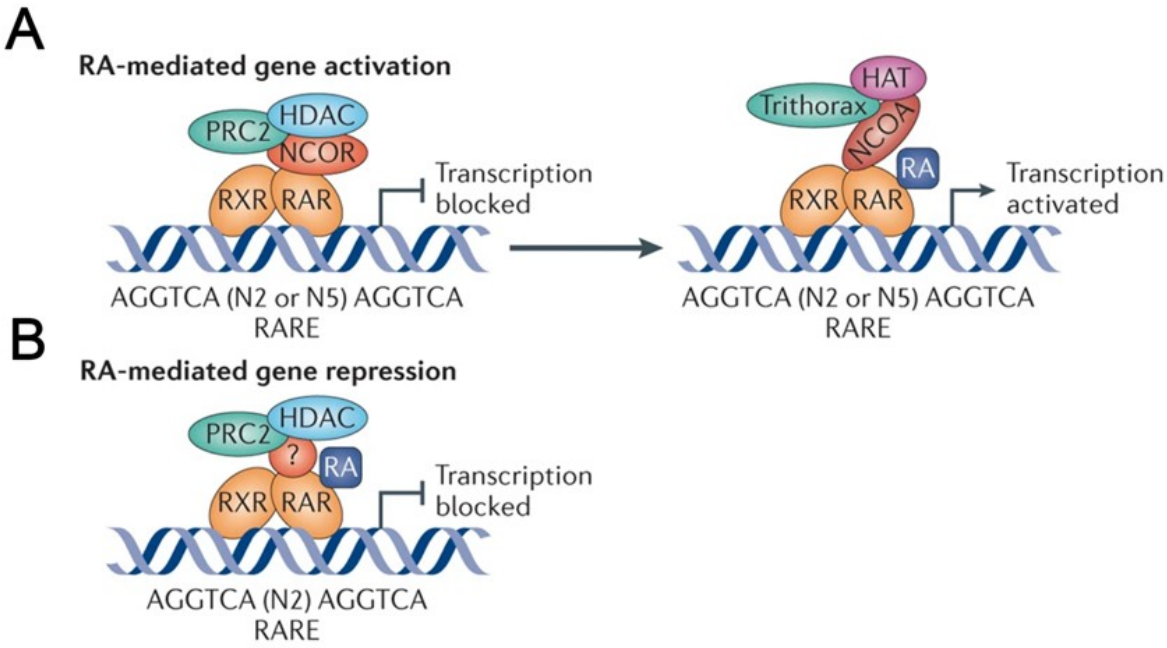

Figure 1.18. Retinoic acid signalling.
(A) Schematic summarising RA pathway activation in the absence of repressors. (B) Schematic summarising RA pathway inactivation Adapted from Cunningham TJ, Duester G. Mechanisms of retinoic acid signalling and its roles in organ and limb development. Nat Rev Mol Cell Biol. 2015 Feb;16(2):110-23. (235).

1.4 Models to study lung repair and regeneration

Despite growing evidence of key roles for developmental signalling pathways in lung repair and regeneration, our knowledge of the exact mechanisms through which these pathways

drive repair is still limited(37). One of the major challenges is the lack of advanced translational models that replicate the complexity of the human lung environment(236, 237). Experimental models are essential for studying the lungs, their deep anatomical position in the body and importantly their requirement for life make direct *in situ* investigation challenging(238). To overcome this problem and enable respiratory investigations to be conducted, a variety *in vitro*, *ex vivo* and *in vivo* models have been designed overtime to facilitate lung research (Figure. 1.19).

1.4.1 *In vitro* models

In vitro models have provided invaluable information that has shaped our understanding of lung cell biology. There are several different *in vitro* models which have been used and continue to be used to investigate various mechanisms in the lungs. (Figure. 1.20).

1.4.1.1 2D Cell culture

Two-dimensional (2D) Cell culture remains one of the most commonly employed techniques for basic laboratory research and can be used to investigate a variety of different cellular processes including, cell metabolism, proliferation, differentiation and cellular responses to different stimuli, in order to elucidate cell function(237, 239, 240). Furthermore, tumour-derived, immortalised or primary cells can be utilised depending on the investigation being conducted and the objective, making the use of cell culture broadly applicable(239). The choice of cell type has an impact on the relevance of data collected. Primary cell culture can be used to increase physiological relevance; however cell culture overall has the disadvantage of not accurately resembling the air-liquid interface which is characteristic of the airway microenvironment, cell cultures yield data which can be built upon using more complex models(239, 240). For this reason, cell culture is often employed for initial drug screening studies and pre-clinical research(239). Cell culture models have the advantage of being highly reproducible, cost-effective and high throughput (237, 239, 240).

1.4.1.2 Co-cultures

Co-culture models can be divided into direct and indirect contact co-culturing models (240).

Direct contact co-culture

Direct co-cultures are established by seeding two or more cells in the same well or culturing plate, enabling physical cell-cell interactions(241, 242). The close contact of cells mimics *in vivo* cell-cell communication and supports both juxtracrine and paracrine signalling, which can be assessed by measuring the secretion of growth factors, cytokines or ECM proteins(241, 242). Prior knowledge of interactions between cell types is ideal for this model system, however direct co-cultures also allow for discovery of previously unknown interactions to some extent(242).

Indirect contact co-culture

In Indirect contact co-cultures, cells are cultured in close proximity but are separated by a physical barrier (241, 242). Examples include transwell migration assays (or Boyden chamber assay), where cells are seeded on opposite sides of a porous membrane, these assays are used to study cell migration and can also be employed to investigate paracrine signalling and chemotaxis (243, 244). Another example is two-well culture systems, for example the Ibidi™ 2 well inserts, where cells are initially separated by a removable barrier, which is lifted once cells are confluent, to study cell migration and cell-cell interactions (245, 246). Another widely used approach is conditioned medium, where one cell type is cultured in medium that has been collected from another cultured cell type (conditioned medium), this allows the analysis of the effect of growth factors/secreted factors, in the conditioned medium(241).

1.4.1.3 3D cell culture

The development of three-dimensional (3D) cell culture systems including organoids and scaffolds has improved our understanding of lung development, as well as lung disease and regeneration(236, 237, 247, 248). Compared to 2D culturing methods, these models more

accurately mimic the complex architecture and cellular microenvironment of the lung, by supporting multi-directional cell growth and facilitating the study of cell-cell interactions(236, 237, 247, 248).

Air-liquid interface (ALI) culture

Air-liquid interface (ALI) culture models were developed to more closely resemble the lung microenvironment, and therefore, improve physiological relevance compared to simpler culture models. (237, 239, 240). The development of this culturing method in the late 1980s was a major milestone in the field, enabling researchers to more accurately mimic the *in vivo* airways(237, 249). In ALI cultures, epithelial cells are seeded onto a microporous membrane, that separates the apical side, exposed to air, from the basolateral side, which is submerged in culture medium(237, 239, 247). Furthermore, ALI cultures support epithelial cell differentiation into different cells including basal, ciliated and goblet cells, closely resembling the pseudostratified epithelium of the human airways(237, 247). Importantly, ALI cultures can be adapted to model different compartments of the respiratory tract including the nasal cavity, larynx, bronchi and alveoli, making these cultures versatile (239). To date ALI cultures have been used to investigate and inform our knowledge about lung diseases as well as important processes including, mucociliary clearance, epithelial barrier function, host-pathogen interactions and epithelial regeneration(237, 239).

Organoids

Lung organoids are self-assembling, stem cell derived 3D models which can be harnessed to recapitulate key features of the complex multicellular lung environment(237, 250-252). They can be generated from embryonic stem cells, human pluripotent stem cells (hPSCs) and induced pluripotent stem cells (iPSCs)(237, 250-252). Furthermore, they can be used to form region specific spheres such as “bronchospheres” or “alveolospheres”, which model the bronchial and alveolar regions of the lung respectively(236, 250, 251).

Organoids have been used to study lung development and have advanced our understanding of epithelial progenitor cell populations(236, 239, 252). Notably, organoid models have been used to characterise ATII cell differentiation and ATI cell de-differentiation(71, 79, 252). In addition to this, organoids support investigations into cellular crosstalk, for example, epithelial-mesenchymal interactions which play an important role in tissue repair(151, 239, 251, 252). Despite these advantages, organoids have some limitations, they do not accurately recapitulate the ECM or vascular networks within the lung, and their use is relatively costly and labour intensive, requiring long periods for culturing to observe cellular differentiation(236, 239, 252).

Scaffolds

Scaffold based 3D culture models are produced by culturing cells on synthetic or natural biomaterials and are generated to study the ECM and cell-ECM interactions, which play an important role in lung development, homeostasis, repair and regeneration(237, 248, 253, 254). In the context of lung disease and repair scaffolds are an important model that can be utilised to study ECM remodelling and cellular response to structural cues(237, 248, 254, 255). Natural scaffolds are typically derived from decellularised isolated human or animal lung cells, while synthetic scaffolds employ bioengineering approaches to mimic the lung environment and architecture(237, 248, 256-259). Scaffolds have been used to inform the development of microfluidic devices such as lung-on-a-chip(248).

1.4.1.4 Lung-on-a-chip

Organ-on-a-chip devices, such as lung-on-a-chip are microfluidic devices that are engineered to replicate key structural and functional features of an organ(236, 239, 247, 248, 260, 261). Lung-on-a-chip devices mimic aspects of the lung microenvironment and enable investigations of complex kinetic processes such as breathing motions and fluid flow, which are difficult to reproduce in other models (236, 239, 248, 260). Further to this, the models can also be harnessed to study cell-

cell interactions and to model the alveolar capillary membrane (ACM) (239, 247, 248, 261). However, these models remain relatively simplistic, as they typically only allow the study of two and in some cases three cell types, additionally, each lung-on-a-chip device, can only mimic one region of the lung, e.g. the alveolar region(260, 262). The key benefit of these models is the ability to control stretch, flow and mechanical cues of the lung microenvironment(239, 260, 262).

In vitro models are a good basis for preliminary studies, they are generally quick to set up, high throughput and yield a lot of data, although models such as lung-on-a-chip and organoid systems are not high throughput. Furthermore, there are a large range of established *in vitro* models, as outlined, therefore many of the methods are standardised. However, there are some limitations in the translation of *in vitro* models due to their simplicity when compared to the *in vivo* lungs, therefore findings from *in vitro* investigations should be corroborated using relevant *in vivo* or *ex vivo* models.

1.4.2 *In vivo* models (animal models)

In vivo models, including rodents (mice and rats) and larger mammals such as primates, have been instrumental in advancing our understanding of lung development, homeostasis, disease pathology and responses to injury/insults(236, 263). Rodents, in particular have been harnessed to enhance our understanding of repair and regeneration, specifically due to the ability to genetically manipulate these species by developing knockouts which allow researchers to investigate and understand molecular pathways and identify key mechanisms involved in repair(263-265).

However, while these *in vivo* models offer valuable physiological context and whole-organism complexity, there are some important limitations to consider. Some species-specific differences exist in the structure and composition of the airways(10, 14, 34), as presented in Figure 1.4, these differences have a direct impact on the translational relevance of findings in the context of human repair and regeneration. Furthermore, animal models are costly and have ethical constraints(236, 239, 263, 266). In line with the implementation of the 3Rs (replacement, reduction and refinement) principles of animal work(263, 266, 267), there is an

increasing emphasis on developing and adopting non-animal methodologies (NAMs), also referred to as new approach methodologies (NATs) (236, 239, 263, 268). These alternative strategies aim to reduce the reliance on animal studies while still generating meaningful insights into lung biology and repair(239, 263, 268).

1.4.3 *Ex vivo* models

In vitro models have enhanced our understanding of cellular and molecular mechanisms associated with lung cell damage and repair; however, these models do not reflect the complexity of the human lung. Whilst *in vivo* models provide the advantage of a full organism for investigations, issues arise with these models based on species specificity and ethics. *Ex vivo* models have been developed to bridge the gap between *in vitro* and *in vivo* models (Figure. 1.19).

1.4.3.1 Precision cut lung slices (PCLS)

Precision cut lung slices (PCLS) are versatile *ex vivo* model that can be employed to study lung development, disease, immune response, repair and regeneration (239, 263, 269-273). First described in 1993, PCLS have since become a well-established and reproducible platform due to the availability of standardised protocols for their generation(236, 274). Furthermore, PCLS can be prepared using tissue derived from a range of species including rodents and humans (biopsy samples)(239, 269, 275). In addition to this, PCLS can be generated using both healthy/control and diseased lung tissue samples to investigate cellular and mechanistic changes(239, 275). Importantly, PCLS retain the native lung architecture, native-cell-cell interactions can be observed as well as cell-ECM interactions(263, 269-273, 275, 276). Unlike other model systems such as organoids, PCLS can also be used to study the vasculature(269, 275). These advantages make PCLS particularly valuable for studying lung biology, while also supporting translational research(239, 269, 275). However, although PCLS can be used to study some tissue resident immune cells including macrophages, there is no circulation therefore immune cell recruitment cannot be studied(277, 278). This is important to note since the immune response also plays a critical role in repair. Furthermore, PCLS models cannot currently be used for long term studies due to a decline in viability, the maximum

culturing duration for PCLS is 5-7 days(277, 278). Some studies are focusing on optimising methods to maximise the use of PCLS by cryopreservation(278-280).

1.4.3.2 The Acid Injury and Repair (AIR) model

The Acid Injury and Repair (AIR) model is an *ex vivo* model of lung injury, that was established in the Dean lab(271, 276). The AIR model provides a "bridge between the current *in vitro* and *in vivo* models for studying lung injury and repair"(271, 273, 276); it is produced by injuring an isolated region of a precision-cut lung slice (PCLS) with hydrochloric acid (HCl)(271, 273, 276). This model has been designed to mimic the heterogenous pattern of lung injury frequently present in lung diseases by having an area of injured tissue adjacent to uninjured tissue(271, 276). The use of HCl makes this a clinically relevant model, since the major component of gastric acid is HCl; gastric acid aspiration is a major cause of acute lung injury (ALI) as well as exacerbations in patients with chronic lung diseases (271, 276). Furthermore, the AIR model can be used to label and track specific cell populations to precisely visualise and quantify alveolar repair. As previously mentioned there are several markers of progenitor cells which have been identified at different anatomical regions in the lungs (Figure. 1.7) (271, 276). Changes to the ECM can also be visualised in PCLS, this has been shown in preliminary studies conducted in the Dean lab group (unpublished data).

In chapter 3 of this thesis the mouse AIR model is employed to study alveolar repair and in chapter 5 I demonstrate that the AIR model can be translated into a human model. Highlighting the versatility and reproducibility of the model.

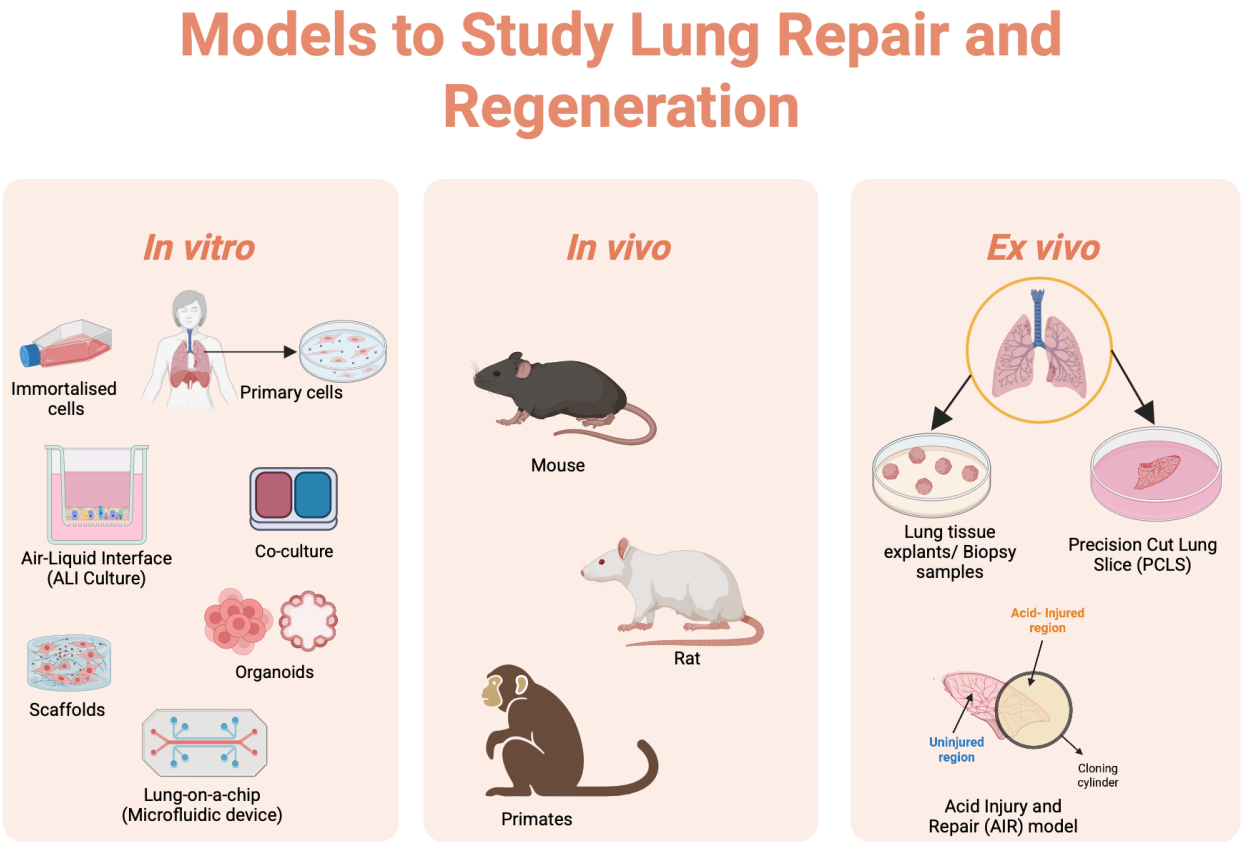

Figure 1.19. Models to study lung repair and regeneration.
Visual summary of *in vitro*, *in vivo* and *ex vivo* models that can be used to study the lungs. Adapted from Soto Veliz D, Lin KL, Sahlgren C. Organ-on-a-chip technologies for biomedical research and drug development: A focus on the vasculature. Smart Med. 2023 Jan 1;2(1):e20220030.(281) and Miller AJ, Spence JR. *In vitro* models to study human lung development, disease and homeostasis. Physiology (Bethesda). 2017 May;32(3):246-60. (237) and da Silva ACG, Valadares MC. The application of new approach methodologies in respiratory disease research: their role in improving translational medicine from bench to bedside. Altern Lab Anim. 2023 Jun;51(3):161-74.(239). Figure generated using Biorender.

1.5 Hypothesis and Aims

The overarching hypothesis of my thesis is that signalling pathways essential for lung development also play critical roles in alveolar repair and/or regeneration. Therefore, targeting these developmental pathways may offer a promising therapeutic strategy to promote the regeneration of damaged lung tissue.

To test this hypothesis, the following specific aims have been defined:

1) To use *in vitro* assays including wound healing assays to screen the effects of major developmental signalling pathways on repair and select one candidate pathway for detailed investigation into its role.

2) To investigate how the chosen pathway (SHH) regulates lung repair at a cellular and molecular level using *in vitro* wound healing and co-culture migration assays as well as an *ex-vivo* model of lung injury.

3) To translate the findings about the role of SHH from cell culture and mouse studies into a translationally relevant human lung model.

4) To use bioinformatic approaches to interrogate publicly available single-cell RNA sequencing (scRNA-seq) datasets and identify potential changes in SHH pathway activity in disease.

Chapter 2

Materials and Methods

Materials and Methods

2.1 Microscopy

Microscopy was conducted at the Facility for Imaging by Light Microscopy (FILM) at Imperial College London using a Zeiss Axio Observer, inverted widefield microscope with LED illumination (Zeiss Colibri 7) and motorised stage (Carl Zeiss MicroImaging GmbH, Göttingen, Germany) and Zeiss Apotome 3 attachment, to obtain confocal like images using optical sectioning of widefield images. Images were captured using Zen acquisition software and a Hamamatsu ORCA-Flash 4.0 camera (Hamamatsu Photonics K.K., Japan).

2.2 Animals and Ethics

All procedures carried out with mice were conducted under the personal licence PIL number: I80785100 and the project license entitled “Identifying genetic and cellular mechanisms of alveolar development and repair” (PPL number 30/3372), in accordance with the Animal (Scientific Procedures) Act 1986. Procedures conducted as part of this project were approved by the Imperial College London Animal Welfare and Ethical Review Body (AWERB).

2.3 Human tissue samples

Normal adult human lung tissue samples were collected from the Respiratory Biomedical Unit (BRU) Biobank at the Royal Brompton hospital from patients undergoing surgical lung resection for suspected lung cancer. Emphysematous tissue was obtained from patients undergoing lung volume reduction surgery for radiological emphysema. Normal Lung tissue samples and emphysematous tissue samples were classified by a histopathologist. The Biobank ethics number for this research is 20/SC/0142. All samples were obtained following informed consent from patients. Patient demographics were recorded.

2.4 Precision cut lung slices (PCLS)

2.4.1 Harvesting lungs from mice

Adult female mice (C57BL/6), aged 9-12 weeks, purchased from Charles River were euthanised humanely by anaesthetic overdose through intraperitoneal administration of pentobarbitone followed by severing of the femoral artery. The trachea was exposed by carefully excising the anterior chest wall and then cannulated using 21G rigid metal cannula from a small incision made below the cricoid cartilage. The canula was held in place with a loose suture then lungs were inflated in situ with approximately 1 mL 37°C 2 % low gelling point agarose (Sigma-Aldrich-Aldrich; A9414) prepared with 1X Hanks balanced salt solution (HBSS) (Life Technology; 14025-050) supplemented with 1 % HEPES buffer (Gibco; 15630056). Ice was indirectly applied (ice wrapped in tissue) to the chest cavity for 1 min to solidify the agarose. Then the lungs were excised from the chest cavity and placed in ice cold 1X HBSS + 1 % HEPES until generation of PCLS.

2.4.2 Generation of mouse PCLS (mPCLS)

A scalpel was used to isolate individual lung lobes which were then cut transversely using an automated vibrating microtome –VF-510-0Z Tissue Slicer (Precisionary Instruments LLC, USA) into slices of 300 µm thickness. Cold 1X HBSS supplemented with 1 % HEPES was used as the slicing buffer. mPCLS were transferred to 24 well culture plates containing Serum Free Dulbecco's Modified Eagle Medium (SF-DMEM) (Gibco, ThermoFisher Scientific) supplemented with 1 % (v/v) penicillin-streptomycin (Life Technologies; 15140122) and incubated overnight at 37°C with 5 % CO2. Prior to carrying out experiments mPCLS were washed three times with pre-warmed SF-DMEM.

2.4.3 Generation of human PCLS (hPCLS)

Adult human lung tissue was collected from RBHT within 24 hours post-surgery and stored at 4°C in SF-RPMI (Gibco, ThermoFisher Scientific; 61870010) supplemented with 1 % (v/v) penicillin-streptomycin (Gibco, ThermoFisher Scientific; 15140122), and 0.5 % (v/v)

gentamycin (Gibco, ThermoFisher Scientific; 15710064) and 0.1 % amphotericin B (Gibco, ThermoFisher Scientific; 15290-018) until time of PCLS production. To prevent leakage of agarose from the inflated tissue, an artificial pleura was first formed around the outside of the lung tissue by coating it with 3 % sodium alginate (Sigma-Aldrich; W201502), prepared in ddH20, for a few seconds, followed by submersion in 3 % calcium chloride (Sigma-Aldrich; C3306), prepared with ddH20, to solidify the hydrogel. Then the tissue was transferred to a falcon tube containing ice cold buffer (1X HBSS supplemented with 1 % (v/v) penicillin-streptomycin) for 5-10 minutes. The lung tissue was then point inflated with 3 % low melting point agarose (Sigma-Aldrich; A9414) using a 3 mL syringe and 21G BD Microlance™ 3 needle; the tissue was injected at several different points until the entire piece of tissue was evenly inflated. In between point inflation steps, the tissue was placed back into the ice-cold buffer to ensure that agarose solidified. Following inflation, an 8 mm biopsy punch (Selles Medical; BP-80F) was used to generate 8 mm cores of lung tissue to ensure that hPCLS generated were of equal size. Tissue cores were mounted onto a Compresstome® VF-510-0Z Tissue Slicer (Precisionary instruments), and 500 µm slices were cut. hPCLS were transferred to 24 well culture plates containing SF-RPMI supplemented with 1 % (v/v) penicillin-streptomycin and incubated overnight at 37°C with 5 % CO2. Prior to carrying out further experiments hPCLS were washed three times with prewarmed SF-RPMI to remove excess agarose.

2.5 AIR model

The acid injury and repair (AIR) model was generated using the method described by Kim *et al* (271, 276). An isolated region of PCLS was injured so that experiments could be set up to investigate differences or similarities in the repair response of adjacent injured and uninjured regions of PCLS.

PCLS were centred in the well and medium was removed following HBSS wash steps described previously, at the end of PCLS generation (in section 2.4.3 and 2.4.4). The isolated region of injury was established using a Pyrex® cloning cylinder (Sigma-Aldrich; CLS31668), which was coated at one end with sterile silicone grease, this end was applied to a region of the PCLS using gentle pressure to seal the cloning cylinder onto the tissue. Where the AIR model was

generated using human precision cut lung slices (hPCLS), an alcohol resistant marker was used to mark the side of the PCLS within the cloning cylinder, since hPCLS are circular.

Following this, 500 µL medium (SF-DMEM for mPCLS, SF-RPMI for hPCLS) was added to the area outside the isolated region and the region inside the cloning cylinder was examined to ensure that the medium did not leak through. To administer injury, HCl was diluted using SF-medium and Pluronic gel (Sigma-Aldrich; P2443). 30 % (w/v) Pluronic gel, prepared with SF-DMEM was left to dissolve slowly on ice at 4°C, the day prior to injuring PCLS. Pluronic gel was used as a vehicle to make the acid solution more viscous, further preventing the possibility of leakage from inside the cloning cylinder. The use of pluronic gel has been applied successfully previously in drug delivery studies, particularly for the administration of topical pharmaceutical agents (279). The working concentration (0.1 M) of HCl contained 15 % w/v pluronic gel. 100 µL of 0.1 M HCl for 1 min to the isolated region inside the cloning cylinder. The colour of the medium outside the cylinder was used to monitor if HCl leaked out i.e. a change from pink to yellow would indicate a change in pH due to increased acidity and therefore a leak of HCl. After 1 min of HCl treatment, the isolated region was washed five times with 200 µL SF-DMEM, to remove any trace of acid, whilst ensuring the seal between the two regions was undisturbed. The cloning cylinder was then removed and PCLS were transferred to a 24-well plate containing SF-medium only or SF-medium plus treatment and incubated at 37°C with 5 % CO2 for 48 hrs post injury.

2.5.1 Treatment of AIR PCLS with developmental signalling pathway modulators

Modulators of signalling pathways and exposure concentrations were chosen based on data in the literature; either agonists or antagonists, or both, of key significant pathways were selected and prepared as follows:

Table 2.1. Summary of chosen modulators of signalling pathways

Modulator	Diluent	Stock concentration	Working concentration	Manufacturer and CAT #
Recombinant SHH-N protein	PBS containing 0.1 % BSA	100 µg/mL	0.1, 0.25,0.5 µg/mL	R&D systems; 464-SH-025
Cyclopamine	95 % Ethanol	4 mg/mL	2.5 µg/mL, 5 µg/mL, 10 µg/mL	Tocris; C988400
WNT 5A	PBS containing 0.1 % BSA	100 µg/mL	0.1 µg/mL	R&D systems; 645-WN-010
WNT 9A	PBS containing 0.1 % BSA	250 µg/mL	0.04 µg/mL	R&D systems; 8148-WN-025
Retinoic acid	95 % Ethanol	10 mM	10 µM	Sigma- Aldrich; R2625-50MG

2.6 PCLS viability

2.6.1 MTT assay

3-(4, 5-dimethylthiazol-2-yl)-2, 5-diphenyl tetrazolium bromide (MTT), colourimetric assays measure metabolic activity and are used to as an indirect measure of viability. MTT is a yellow solution that is reduced to formazan (purple) by mitochondrial dehydrogenases (metabolic enzymes) (282, 283). There is a linear correlation between the amount of formazan produced and the intensity of colour; darker purple indicates higher metabolic activity (282, 283); conversely, when the purple colour is lower than the unexposed control, this indicates reduced metabolic activity and cell death.

To determine viability, PCLS of equal size were placed into wells of a 48-well plate (1 PCLS per well), in triplicate for each experimental condition. To ensure injury/treatment was kept consistent between PCLS for each condition, whole slices were injured/treated. 48 hrs post injury/treatment, medium was removed from each well and 250 µL 10 % MTT solution (Sigma-

Aldrich; M2128) was added. Then the 48-well plate was incubated for 1 hr at 37°C. 10 % MTT (5 mg/mL Stock) was prepared by diluting MTT in SF-DMEM. After 1 hr the MTT was removed, and 250 µL dimethyl sulfoxide (DMSO) was added to solubilise the cells and formazan crystals that formed. The plate was incubated for 10 mins. Then 200 µL of the formazan solution produced was transferred to a 96 well plate and absorbance was measured at 570 nm and corrected at 690 nm using a SpectraMax iD3 Multi-Mode Microplate Reader (Molecular Devices, USA).

2.6.2 Live/Dead® Viability Kit

Cell viability was also assessed in situ, using fluorescent dyes. The LIVE/DEAD® Viability/Cytotoxicity Kit (ThermoFisher Scientific; L3224) was used to assess viability in AIR model injured PCLS. PCLS treated with 70 % methanol were used as a positive control for dead cells and uninjured/untreated PCLS were used as a positive control for live cells/tissue. Calcein acetoxymethyl ester (calcein AM) and ethidium homodimer-1 (EthD-1) were brought to room temperature (RT) prior to use. Calcein AM permeates through the cell membrane and enters into live cells(284-286). Intracellular esterases present in live cells cleave acetoxymethyl (AM) from calcein AM (non-fluorescent compound), forming calcein (fluorescent compound) which binds to calcium ions to emit green fluorescence (excitation ~494 nm/ emission~517 nm)(284-286). Calcein is retained in the nucleus and cytoplasm of live cells. Calcein AM cannot be cleaved in dead cells and thus diffuses out(284-286). EthD-1 is membrane-impermeable in normal live cells, but is able to enter damaged or dead cells(287, 288). EthD-1 has a high affinity for nucleic acids and binds to the nucleus of dead cells, staining dead cells red (excitation~517 nm/ emission~617 nm)(287, 288).

PCLS were incubated with 2 µM Calcien AM and 2 µM EthD-1 in 250 µL warmed HBSS for 30 min at 37°C. PCLS were washed twice briefly with phosphate buffered saline (PBS) (ThermoFisher Scientific; 28908). Then PCLS were mounted onto glass slides using ProLong® Gold Antifade Mountant (ThermoFisher Scientific; P36930) and were left to set for 30 min at RT and then imaged immediately. To obtain an image of the entire PCLS, tiled images were taken using a 10x air objective on an inverted Zeiss Axio Observer widefield microscope. Image

tiling ensures that a large field of view can be imaged at a high resolution(289). PCLS images were taken at the central Z plane (the middle of the slice) of each PCLS, which was ~50 μm into each slice, in order to avoid staining artefacts and to ensure that imaging of slices was consistent across all experiments. Zen acquisition software was used to acquire images from the microscope.

2.7 Cell culture

Cells were cultured in a humidified incubator at 37°C with 5 % CO2. Cells were passaged routinely once they reached 80 % confluency.

2.7.1 Human Alveolar Adenocarcinoma Epithelial cell (A459)

Human alveolar adenocarcinoma epithelial cells (A549) (290, 291) are an adherent alveolar type II-like epithelial cell line (ATCC; CCL-185). A549 cells were maintained in DMEM supplemented with 10 % (v/v) foetal bovine serum (FBS) (Gibco; 11533387) and 1 % (v/v) penicillin-streptomycin at 37°C with 5 % CO2. To passage A549 cells, medium was removed from culturing flasks and cells were washed with sterile PBS, then cells were incubated with 5 mL TrypLE Express Enzyme (1X) (Gibco, 12604013) for 5 min to detach cells from a T75 culture flask. 10 mL (double the volume of TrypLE used) of complete DMEM was used to neutralise TrypLE in T75 flask and the cell suspension was transferred to a falcon tube and centrifuged at 1500 rpm for 3 min. Then the supernatant was discarded and the cell pellet was resuspended in 5 mL complete DMEM. Cells were counted using a haemocytometer and then diluted to obtain cell densities required for downstream experiments.

2.7.2 Human umbilical vein endothelial cells (HUVEC)

Primary human umbilical vein endothelial cells (HUVECs) (292) (Promocell; C-12200) are adherent primary cells. HUVECs were maintained in Endothelial Cell Growth Medium (EGM) (Promocell; C-22010) which includes the supplements: 2 % Foetal Calf Serum, 0.4 % Endothelial Cell Growth Supplement, 0.1 ng/mL Epidermal Growth Factor (recombinant

human, 1 ng/mL Basic Fibroblast Growth Factor (recombinant human), 90 µg /mL Heparin and 1 µg /mL Hydrocortisone. The Promocell Detach Kit (Promocell; C-41200) was used to passage HUVECs. Medium was removed from culture flasks and cells were washed with sterile HEPES buffered Balanced Salt Solution (HEPES BSS) (Promocell; C-41200), then cells were detached from the flask using 2 mL of the Trypsin/EDTA ratio of 0.04 %/0.03 % (Promocell; C-41200) for 5 min. An equal volume of trypsin neutralisation solution (0.05 % Trypsin Inhibitor in 0.1 % BSA) (Promocell; C-41200) was added to cells and the cell suspension solution was transferred to a falcon tube. Cells were centrifuged at 220g for 3 min. The supernatant was discarded and the cell pellet was resuspended in 1 mL EGM. Then cells were counted using a haemocytometer and diluted appropriately to achieve required seeding densities for downstream experiments. Cells were purchased and supplied by Promocell at passage 3 and were used for experiments up until passage 8.

2.7.3 Human pulmonary microvascular endothelial cells (HPMVEC)

Human pulmonary microvascular endothelial cells (HPMVECs) (293) (Promocell; C-12281) are adherent primary cells. HPMVECs were maintained in endothelial growth media-microvascular vessels (Ready to use) (EGM-MV) (Promocell; C-22020) which includes the supplements; 5 % foetal calf serum (FCS), 0.4 % endothelial cell growth supplement, 0.1 ng/mL epidermal growth factor (recombinant human, 1 ng/mL basic fibroblast growth factor (recombinant human), 90 µg / mL heparin and 1 µg / mL hydrocortisone. HPMVECs were passaged using the Promocell DetachKit, as described for HUVECs above. HMPVECs were purchased and supplied by Promocell at passage 3 and were used for experiments up until passage 8.

2.7.4 Isolating fibroblasts from human tissue samples

Human lung tissue biopsy samples were obtained from consenting patients by the RBHT Biobank following diagnostic lung resection (see section 2.4 Human tissue samples). To maximise use of lung tissue samples, human lung fibroblasts were isolated from the same tissue as human alveolar epithelial cells type II (ATII cells). Therefore the protocol used was

chosen to be compatible for isolation of both fibroblasts and ATII cells (294). ATII cells were isolated and used by other lab members. Tissue samples were bathed in sterile PBS to remove excess blood. Then samples were washed with PBS by point injection using a 19G needle attached to a syringe, until the fluid was clear. This washing stage removes the blood cells and at the same time most of the alveolar macrophages are removed. Next the tissue was cut into small pieces roughly 5 cm3 in size or less and left to incubate in a large petri dish with 40 mL 0.25 % Trypsin from bovine pancreas (Sigma-Aldrich; T8003) made up with HBSS, for 45 min. After incubation, tissue pieces were transferred to a clean petri dish and 10-15 mL trypsin was injected into each piece using a 19G needle and syringe. Excess trypsin that leaked into the petri dish was discarded and tissue pieces were incubated in petri dish at 37°C for 15 min. This step was then repeated again, followed by a third incubation with trypsin for 45 min. Excess trypsin was discarded then, 5-10 mL New-born Calf Serum (NCS) (Sigma-Aldrich; N4637-100 mL) was added to each piece of tissue to deactivate trypsin. Tissue pieces were cut into smaller 1-2 mm3 pieces, then 10 mL 250 µg/mL DNAse I (Sigma-Aldrich; 10104159001) made up with HBSS was added and the tissue suspension was mixed to aid degradation of DNA. The tissue suspension was aspirated into a 50 mL falcon tube and topped up to 40 mL using 250 µg/mL DNase I solution. Then the falcon tube was inverted to gently mix for a few minutes. The tissue suspension was filtered through a sterile gauge mesh filter (400 – 500 µm). Then tissue suspension was filtered again using several 40 µm Falcon™ Cell Strainers (Fisher Scientific; 10737821) to remove all debris. The suspension was centrifuged at 1300 rpm for 10 min and the pellet was resuspended in 35 mL 1:5 solution of 250 µg/mL DNase I and Hybridoma serum free medium (Gibco, 12045084). Hybridoma medium was used here specifically because ATII cells were isolated at the same time. This cell suspension was divided into 3 T75 flasks and placed in an incubator at 37°C with 5 % CO_2 overnight to allow fibroblasts to adhere fibroblasts. The next day medium was removed from T75 flasks and replaced with DMEM supplemented with 10 % (v/v) FBS and 1 % (v/v) penicillin-streptomycin. Fibroblast growth and density was monitored overtime using an EVOS XL core light microscope (Invitrogen, USA).

2.7.5 Primary Human pulmonary lung fibroblasts

Primary human pulmonary lung fibroblasts (Primary HLF) isolated from tissue samples obtained from the RBHT Biobank were maintained in DMEM supplemented with 10 % (v/v) foetal bovine serum (FBS) and 1 % (v/v) penicillin-streptomycin in an incubator at 37°C with 5 % CO2. To passage cells, they were washed using sterile PBS and detached from tissue culture flasks using TrypLE as described for A549 cells. The cell suspension was centrifuged at 1000 rpm for 5 min then the cell pellet was resuspended in 5 mL complete DMEM and cells were counted using a haemocytometer.

2.8 RNA extraction

The RNeasy Mini kit (Qiagen; 74104) was used to extract RNA from cells, lung tissue and PCLS.

2.8.1 Lysing/Homogenising cells for RNA extraction

Cells were seeded at 1x106 per well in 6 well plates the day before RNA extraction. Cells were lysed directly from culture plates by addition of 350 µL Lysis Buffer RLT Plus/ β-mercaptoethanol mix per well. An appropriate volume of lysis buffer was prepared based on the number of wells to extract RNA from by adding 10 µL β-mercaptoethanol (β-ME) to every 1 mL of Buffer RLT Plus. The homogenised lysate was transferred to a QIAshredder spin column placed in a 2 mL collection tube, and centrifuged for 2 min at full speed to further homogenise cell lysate. The spin column was discarded and the flow through (homogenised lysate) was saved.

2.8.2 Homogenisation of lung tissue and PCLS for RNA extraction

Lung tissue samples or PCLS were homogenised using the FastPrep-24™ Classic bead beating grinder and lysis system (MP Biomedicals, USA). Lysing matrix D 1.4mm ceramic spheres (MP Biomedicals, 116540434) were added to MP FastPrep- 24™ lysing matrix tubes (MP Biomedicals, 115076200) with 600 µL Lysis Buffer RLT Plus/ β-mercaptoethanol mix and 10 -

20 mg of lung tissue sample or 3 PCLS. Then tubes were put onto the rotor of the FastPrep-24™ Classic bead beating grinder and lysis system (homogeniser). The homogeniser was run twice for 40 seconds, with a 1 min interval. The resulting tissue lysate was centrifuged for 3 min at 4°C at 15,000 rpm. Then the supernatant (approx. 500 µL homogenised lysate) was transferred to a microcentrifuge tube. To ensure complete breakdown of tissue, the lysate was transferred to a QIAshredder tube and centrifuged.

2.8.3 RNA extraction following homogenisation

One volume of 70 % ethanol was added to the homogenised lysate (350 µL for cells, 500 µL for tissue lysate) and mixed by gently pipetting. 700 µL of the sample was then transferred to a RNeasy spin column placed in a 2 mL collection tube and centrifuged for 15 seconds at ≥10,000 rpm. The flow through was discarded, this step was repeated as required until all of homogenised lysate had been applied to the RNAeasy spin column. Then 350 µL Buffer RWI was added to the RNeasy spin column and centrifuged for 15 seconds at ≥10,000 rpm to wash the spin column membrane. The flow through was discarded. On-column DNase digestion was performed using RNase- Free DNase Set (QIAGEN; 79254). 80 µL DNase I Incubation mix was prepared in a microcentrifuge tube by adding 10 µL DNase I stock solution to 70 µL Buffer RDD and gently inverting the tube to mix. The DNase I Incubation mix (80 µl) was added directly to the RNeasy spin column membrane, and left to incubate for 15 mins on the benchtop (20-30□C). After 15 min 350 µL Buffer RWI was added to the RNeasy spin column and centrifuged for 15 seconds at ≥10,000 rpm, then the flow through was discarded. 500 µL Buffer RPE was added to further wash the RNeasy spin column and centrifuged for 15 seconds at ≥10,000 rpm. The flow through was discarded and 500 µL Buffer RPE was added to the RNeasy spin column again, this time the RNeasy spin column was centrifuged for 2 minutes at ≥10,000 rpm. The flow through was discarded. To dry the spin column membrane, the RNeasy spin column was placed in new 2 mL collection tube and centrifuge at full speed for 1 min.

To elute the RNA the RNeasy spin column was placed in a new 1.5 mL collection tube. Then 30-50 µL RNase free water was added to the spin column membrane and centrifuged for 1 min at ≥10,000 rpm. To increase the yield of RNA, the eluate was re-applied to the spin column

membrane and centrifuged again. RNA was stored at -80^{o}C until ready to carry out reverse transcription (cDNA synthesis).

2.8.4 Determining the quality of extracted RNA

The quality of extracted RNA was measured routinely using a Nanodrop 2000/2000c Spectrophotometer (ThermoFisher Scientific, USA). However for experiments where RNA was extracted from human lung tissue, the Nanodrop and TapeStation System 2200 (Agilent Technologies, USA) were both used to measure the quality of extracted RNA.

The concentration of RNA was recorded from the nanodrop. The quality of RNA was assessed using the nanodrop by recording the ratio of 260/280 and 260/230 wavelengths.

The nanodrop was calibrated using 1 µL RNase free water and measurements were taken by applying 1 µL sample to nanodrop pedestal. Nanodrop uses ultraviolet- visible light (UV-Vis) spectrophotometry, when the sample is applied to the pedestal it is exposed to a light source ranging from the wavelength of UV to visible light (~ 190 – 900 nm)(295, 296). The nanodrop then measures the amount of light that is absorbed or reflected by the sample at different wavelengths and determines the wavelength at which the sample absorbs the most light(295, 296). The light absorbed by the sample correlates directly with the concentration of the sample(296). 260 nm is the maximal wavelength at which nucleic acids (DNA and RNA) absorb light(295, 297, 298). Whilst 280 nm is the maximal wavelength at which many purified proteins absorb light and 230 nm is the maximal wavelength at which contaminants such as organic solvents from the extraction process absorb light (295, 297, 298). Therefore a lower value for the 260/280 ratio indicates contamination with proteins and a lower value for the 260/230 ratio indicates contamination with organic solvents. The 260 nm/280 nm value for RNA should be ~ 2.0 and the 260 nm/230 nm value for all nucleic acids should be between 2.0-2.2 if the quality is high (297, 298).

TapeStation was used to get a more accurate reading of RNA quality. TapeStation provides a more sensitive and comprehensive assessment of RNA quality, it uses capillary electrophoresis to measure concentration, purity and integrity of nucleic acids(299, 300). This bioanalyser can more accurately distinguish between RNA and DNA and additional contaminants(299, 300).

Before setting up, TapeStation reagents were left to equilibrate at room temp for 30 min and were vortexed briefly before using. RNA samples were thawed slowly and kept on ice to ensure they did not degrade. Samples were prepared by mixing 1 µL RNA with 5 µL RNA sample buffer, then were spun down in a microcentrifuge and vortexed using an IKA vortexer and adaptor at 2000 rpm for 1 min. Samples were spun down again, then were denatured by heating at 72°C for 3 min and placing on ice for 2 mins. Samples were spun down again, then loaded into the TapeStation 2200 with the RNA ScreenTape (reads RNA ≥ 25 ng/µL).

The ScreenTape records the concentration of RNA samples and the integrity of the RNA, by recording an RNA integrity number (RIN) which is ranked on a scale from 1 to 10. A RIN of 7-10 is considered high quality (300). RIN numbers are calculated by the TapeStation algorithm using data from electropherograms (graph of distribution of RNA fragments) generated for each RNA sample(299, 300). In particular 18S and 28S fragments are studied. Intact RNA should have a larger 28S peak, with a ratio of roughly 2:1. The presence of smaller fragments or smearing, indicative of RNA degradation is also taken into account, resulting in a lower RIN value(299, 300).

2.9 cDNA synthesis

Extracted RNA was normalised to ensure all samples were at the same concentration (between 1-2 µg per 10 µl), then RNA was converted into cDNA using High-Capacity cDNA reverse transcription (RT) kit (Applied Biosystems; 4368814). The components of the kit were allowed to thaw on ice, then a master mix was prepared as outlined in table 2.2.

Table 2.2. High-Capacity cDNA Reverse Transcription (RT) Kit master mix components

Components	Volumes (µL)	
	With RNase Inhibitor	Without RNase Inhibitor
10x RT Buffer	2	2
25x dNTP Mix (100mM)	0.8	0.8
10x RT Random Primers	2	2
Multiscribe Reverse Transcriptase	1	1
RNase Inhibitor	1	--
Nuclease Free H_20	3.2	4.2
Total	10	10

10 µL of RT master mix was added to 10 µL (1-2 µg) RNA for each sample to make up a total 20ul reaction mix. Then reactions were run in a thermal cycler using conditions outlined in the table below (Table. 2.3). cDNA samples were stored at -20oC until ready to carry out qPCR.

Table 2.3. Thermal cycler conditions for cDNA synthesis

Settings	Step 1	Step 2	Step 3	Step 4
Temp	25	37	85	4
Time (minutes)	10	120	5	∞

2.10 Quantitative real team polymerase chain reaction (qPCR)

Quantitative real time polymerase (qPCR) was performed using TaqMan® Fast Advanced Master Mix (ThermoFisher Scientific; 4444556) and TaqMan® Gene Expression Assays (FAM) (qPCR primers/qPCR probes, listed in table 2.4).

Table 2.4. Summary of TaqMan Gene expression assays used

TaqMan® Gene Expression Assay Code	Target
Hs00187842_m1	*B2M*
Hs03929097_g1	*GAPDH*
Hs00939627_m1	*GUSB*
Hs00180254_m1	*ALDH1A1*
Hs00977140_m1	*RAR*β
Hs01559230_m1	*RAR*γ
Hs00998537_m1	*WNT5A*
Hs01573829_m1	*WNT9A*
Hs00179843_m1	*SHH*
Hs00181117_m1	*PTCH1*
Hs01090242_m1	*SMO*
Hs00171790_m1	*GLI1*
Hs01119974_m1	*GLI2*
Hs01011015_m1	*HHIP*

qPCR reactions were set up in MicroAmp™ Fast Optical 96-Well Reaction Plate (Applied Biosystems; 4346907) and then run on the StepOnePlus™ Real-Time PCR System (ThermoFisher Scientifc, USA). qPCR reaction mixes were made up to a total volume of 10 µL as outlined in table 2.5.

Table 2.5. qPCR reaction components

Component	Volume (µL) per well
TaqMan Fast Advanced Master Mix (2x)	5.0
TaqMan Gene Expression Assay (20x)	0.5
cDNA template	2µL of 50ng/µL cDNA (Total: 100 ng)
Nuclease-free water	2.5
TOTAL	**10**

A minimum of three biological replicates were included in each qPCR experiment (n=3). Within each experiment, three technical replicates were included for each cDNA per gene being investigated. To investigate gene expression levels the cycle threshold (CT) values for

each target gene was normalised to the average CT value of housekeeping genes. B2M, GAPDH and GUSB were housekeeping genes used. Fold change was investigated by normalising diseased/injured samples to control samples. Housekeeping genes were chosen based on prior lab knowledge and published literature describing the most stable genes within the lungs(301-303).

2.11 Immunostaining

2.11.1 Fixing cells and tissue

PCLS or cells were fixed with 4 % Paraformaldehyde (PFA) for 15 mins, then washed three times with PBS. Cells or PCLS are fixed so that they can be preserved for downstream investigation such as immunostaining.

2.11.2 Immunofluorescence of PCLS

PCLS were permeabilised with 0.5 % Triton™ X-100 (ThermoFisher Scientific; 28313) on a plate rocker at room temperature (RT) for 30 min then washed 3x5 min in PBS. Then, PCLS were incubated in blocking buffer PBS-BT (PBS with 1 % BSA and 0.2 % Triton™ X-100) for 1hr to prevent non-specific binding of antibodies. Primary antibodies diluted in PBS-BT (Table 6) were added to the culture wells and PCLS were incubated overnight at 4°C. PCLS were incubated overnight on a plate rocker. The following day PCLS were washed with PBS 3x 5 min, before incubation with secondary antibodies diluted in PBS-BT (Table. 2.6) for 2hr. PCLS were washed briefly with PBS three times and counterstained with DAPI (ThermoFisher Scientific; D1306) diluted 1:500 in PBS-BT for 15 mins at RT. Finally, PCLS were washed with PBS, and mounted onto glass slides with ProLong® Gold antifade mountant (ThermoFisher Scientific; P36930).

2.11.3 Immunofluorescence of cells

A similar protocol was used to the protocol followed for immunofluorescence of PCLS. Cells were permeabilised with 0.5 % Triton™ X-100 at room temperature (RT) for 30 min then washed 3x5 min in PBS. Cells were only permeabilised when markers for intracellular proteins were used. Then cells were incubated in blocking buffer PBS-BT (PBS with 1 % BSA and 0.2 % Triton™ X-100) for 1hr. Primary antibodies diluted in PBS-BT (Table. 2.6) were added to the culture wells and cells were incubated overnight at 4°C.The following day cells were washed with PBS 3x 5 min, before incubation with secondary antibodies diluted in PBS-BT (Table 6) for 2hr. Cells were washed briefly with PBS three times and counterstained with DAPI diluted 1:500 in PBS-BT for 15 mins at RT. Finally, cells were washed with PBS, and mounted onto glass slides with ProLong® Gold antifade mountant. Where cells were in 8 well chamber slides, the chamber walls were removed leaving the glass slide before mounting with ProLong® Gold antifade mountant.

Table 2.6. Antibodies and dilution factors used for immunofluorescence

Antibody	Host/Derivative Species	Dilution Factor	Manufacturer	CAT #
Primary antibodies				
ADRP	Rabbit	1:200	Abcam	ab52356
α-SMA	Mouse	1:500	eBioscience	14-9760-82
ERG	Rabbit	1:200	Abcam	ab92513
HTII-280	Mouse	1:150	Terrace Biotech	TB-27AHT2-280
Ki67	Rat	1:500	eBioscience	14-5698-82
Pancytokeratin	Mouse	1:200	Merck	C5992
ProSP-C	Rabbit	1:500	Millipore	AB3786
Vimentin	Rabbit	1:200	Biorbyt	orb304659
Vimentin BioTracker TiY live cell dye	N/A	1:2000	Merck	SCT059
Secondary antibodies				
Alexa Fluor 488 anti-Rabbit IgG (H+L) Cross-Adsorbed	Goat	1:500	Invitrogen	A-11008
Alexa Fluor 555 anti-Rabbit IgG (H+L) Cross-Adsorbed	Donkey	1:500	Invitrogen	A-31572
Alexa Fluor 568 anti-Mouse IgG (H+L) Cross-Adsorbed	Goat	1:500	Invitrogen	A-11004
Alexa Fluor 568 anti-Rat IgG (H+L) Cross-Adsorbed	Goat	1:500	Invitrogen	A-11077
Alexa Fluor 647 anti Hamster IgG (H+L) Cross-Adsorbed	Goat	1:500	Invitrogen	A-21451
Alexa Fluor 647 anti-Mouse IgG (H+L) Cross-Adsorbed	Donkey	1:500	Invitrogen	A-31571
Alexa Fluor 647 anti-Rabbit IgG (H+L) Cross-Adsorbed	Goat	1:500	Invitrogen	A-21245

2.12 Image quantification

2.12.1 Automated image quantification: PCLS

Mounted PCLS were imaged at Imperial College Facility for Imaging by Light Microscopy (FILM) using a Zeiss Axio Observer inverted widefield microscope with Apotome. Three technical replicates were included per experimental group within each experiment (biological replicate) and a minimum of three experiments was carried out per investigation, n=3. Images were taken at three separate fields of view per PCLS (technical replicate) for each region of interest (Figure. 2.1).

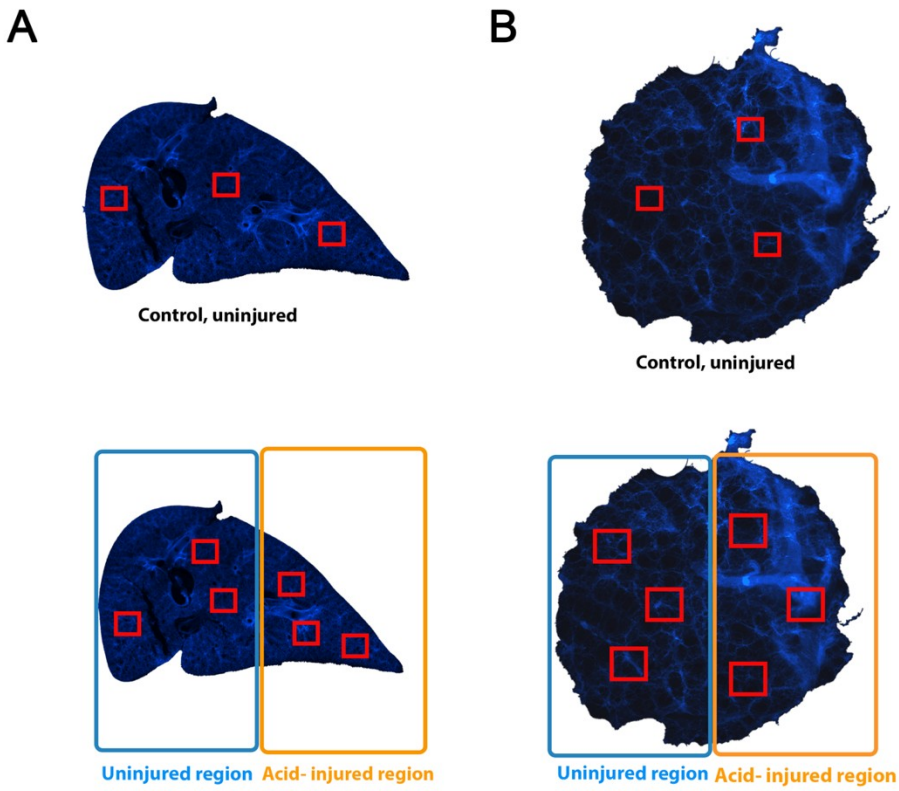

Figure 2.1. **Imaging** ***Precision Cut Lung Slices (PCLS).***
(A) Schematic diagrams showing three regions of control, uninjured PCLS images and 3 regions of the uninjured and acid-injured regions of AIR model mPCLS imaged. (B) Schematic diagrams showing three regions of control, uninjured PCLS images and 3 regions of the uninjured and acid-injured regions of AIR model hPCLS imaged.

The percentage of positive cells for markers of interest was calculated relative to the total number of cells (determined by DAPI positive nuclei). An automated ImageJ counting macro developed by Stephen Rothery (Facility for Imaging by Light Microscopy, Imperial College

London) was used to quantify the number of DAPI positive nuclei and separately, the number of cells positive for each marker of interest e.g. Ki67, proSP-C (271). Once automatic counting was complete for each image, they were exported to a folder with an overlay that marked each 'counted' cell with a cross (Figure. 2.2). Overlays were then manually viewed to check that cells had been accurately labelled and adjustments to the thresholds were made if necessary.

A mean percentage of positive cells from three technical replicates was calculated per experimental group for each experiment (biological replicate). In total a minimum of 9 technical replicates from n=3 biological replicates were used for quantification.

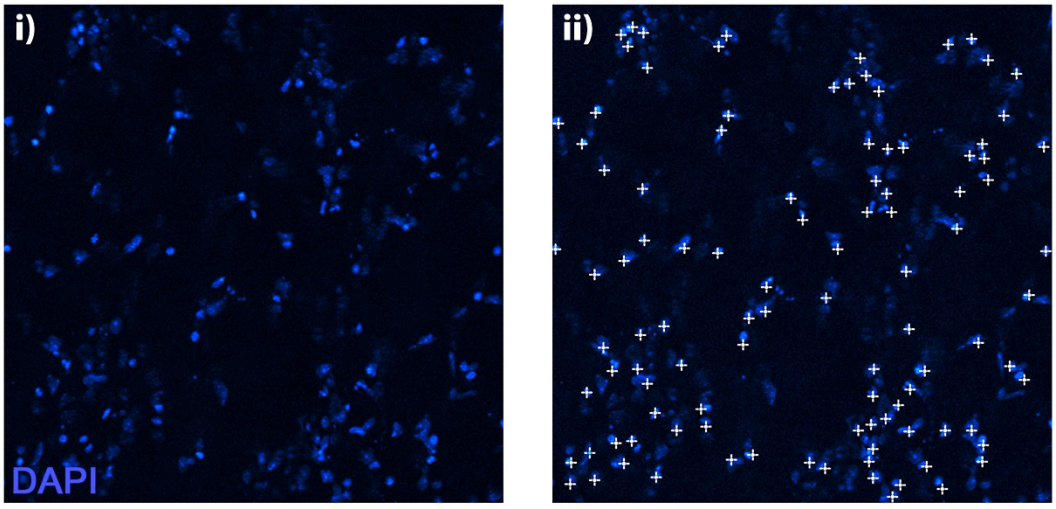

Figure 2.2. Automatic counting macro-overlay.
Shows (i) DAPI channel without overlay and (ii) DAPI channel with overlay that marked each counted cell with a cross.

2.12.2 Automated image quantification: Cells

A similar protocol was followed for quantification of cells. Mounted cells were imaged at Imperial College Facility for Imaging by Light Microscopy (FILM) using a Zeiss Axio Observer inverted widefield microscope with Apotome. Three technical replicates were included per experimental group within each experiment (biological replicate) and a minimum of three experiments was carried out per investigation, n=3. Images were taken from three separate fields of view for mounted cells. Then the automated macro was used to quantify the percentage of positive cells for markers as was done for PCLS.

2.12.3 Quantification of Vimentin staining area

To quantify the amount of vimentin staining in PCLS, a separate macro was developed by FILM facility at Imperial College. Here the macro calculates the total tissue area per field of view and the area with positive vimentin staining per field of view to quantify the amount of vimentin staining as a percentage of tissue area. A mean percentage of vimentin positive cells from three technical replicates was calculated per experimental group for each experiment (biological replicate). A minimum of n=3 biological replicates were used to determine statistical significance.

2.13 Scratch assay/ wound healing assay

8 well chamber slides were coated with 50 µg/mL collagen (Gibco; A1048301) for A549 and primary HLF cells or 2 µg/mL fibronectin (Sigma- Aldrich; F1141-2MG) for HUVECs and HPMVECs for a minimum of 2 hours at room temperature. Cells were seeded 5 x 104 per well (2x104 was sufficient for primary HLF) 24 hr before scratch injury to ensure a confluent monolayer of cells. A P1000 pipette tip was used to make a single scratch along the middle of each well. The media containing cell debris was removed from the well and cells were washed twice with SF media before adding the experimental media. Complete medium (prepared as previously outlined in section 2.7) was used as a positive control for wound closure, where A549 cells or HLF cells were used, this was prepared using DMEM + 10 % FBS, where HUVECs were used this was prepared using complete endothelial growth media (basal media + 2 % foetal calf serum, 0.4 % endothelial cell growth supplement, 0.1 ng/mL epidermal growth factor (recombinant human, 1 ng/mL basic fibroblast growth factor (recombinant human), 90 µg / mL heparin and 1 µg / mL hydrocortisone) and where HPMVECs were used this was prepared using endothelial growth media for microvascular vessels (5 % foetal calf serum (FCS), 0.4 % endothelial cell growth supplement, 0.1 ng/mL epidermal growth factor (recombinant human, 1 ng/mL Basic Fibroblast Growth Factor (recombinant human), 90 µg / mL heparin and 1 µg /mL hydrocortisone). Low serum media was used as a negative control for wound closure, where A549 cells or HLF cells were used this was prepared using DMEM +

0.5 % FBS, where HUVECs were used this was prepared using basal media + 1 % FCS and where HPMVECs were used this was prepared using basal media + 2 % FCS. The relevant low serum/control media was used as a basal media into which relevant signalling pathway modulators were diluted (concentrations of modulators used for experiments are summarised in table 2.1 in section 2.5.1).

Images of each well were taken at t=0, immediately after the scratch was applied, and also following incubation for 20 hrs for A549s and HUVECs or 24 hrs for HPMVECs and HLF. The end point for scratch assays was dependant on how quickly cells migrated and this was determined after pilot experiments and using information from previous lab studies conducted by other members of the lab. The % of wound closure was calculated by measuring the difference between the area of the scratch at T=0 and T=20/24. The scratch area in images taken at t=0 and images taken at t=20/24 was drawn around using a region of interest (ROI) macro on Fiji (ImageJ 2) and subsequently measured. Once the area of the scratch was measured at T=0 and T-20/24 the following calculation was used.

$$\%\ of\ wound\ closure = \frac{(wound\ area\ at\ 0h - wound\ area\ at\ 20/24h)}{wound\ area\ at\ 0h}$$

2.14 Co-culture migration assays

Ibidi™ 2 well inserts (Thistle Scientific, 80209-150) were placed into individual wells of a pre-coated 24 well plate (coated with collagen for A549 cells and primary human lung fibroblasts as described for wound healing assays in section 2.14). Cells were seeded at a density of $2x10^5$ per well, with A549 cells seeded in one well of the 2 well insert and primary HLF in the other (Figure. 2.3). The 2-well insert has been designed to allow reproducible culture of up to two different cell types cells for migration assays (244, 245). The insert is made up of two wells with a volume capacity of 70 µl separated by a cell free gap, ~ 500 µm (Figure. 2.3). After 24 hr, once a confluent monolayer formed on both sides of the insert, the insert was removed, leaving a cell free gap between the A549 and HLF cells of ~ 500 µm (Figure. 2.3). Cells were cultured in DMEM + 10 % FBS or DMEM + 0.5 % FBS + treatment (either SHH or Cyclopamine).

Images of cells were taken at T=0 and T=20 hr as described in section 2.13. The percentage change in cell free gap area was calculated using Fiji (using macro, followed by calculation as described in section 2.13) and the cell morphology and migration characteristics were also recorded.

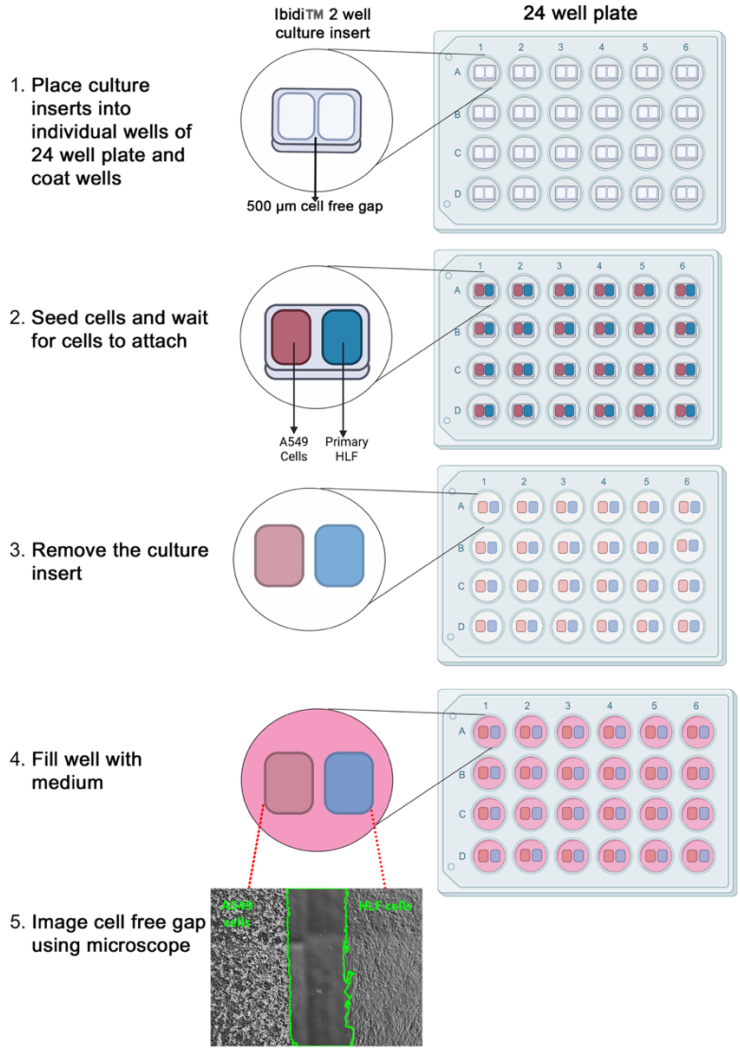

***Figure 2.3. Setting up co-culture*.**

Diagram of 2 well inserts showing A549 cells cultured on one side and primary HLF cultured on the other side before the insert is removed and following removal of the insert for the cells to interact.

2.15 Data analysis

2.15.1 Software

Data was analysed using Microsoft Excel and GraphPad Prism (version 9). All graphs were produced using GraphPad Prism. Heatmaps were generated using pheatmap package (version 1.0.13) in R (version 4.51). Schematic diagrams included were produced using Biorender,

unless otherwise stated. Microscopy images, graphs and diagrams were imported to Adobe Photoshop and final figures were assembled/produced using Adobe Photoshop.

2.15.2 Statistical tests

Graphs show the mean percentage of experimental (biological) replicates. Individual data points shown on graphs represent a single biological replicate (n=1). Biological replicates were calculated using the mean of three technical replicates for each experimental group. The variation between each biological replicate is shown on graphs as ± the standard error of the mean (SEM). Biological replicates are denoted 'n = x', in corresponding figure legends. Datasets comparing results from a minimum of three biological replicates were analysed using a Kruskal-Wallis test and Dunn's multiple comparisons post-test. Whilst where datasets were used to compare two groups a Mann-Whitney U test was employed. Differences were considered statistically significant for p values <0.05.

2.15.3 Bioinformatics

Gene expression heatmaps were generated using the pheatmap package in R to visualize differential expression patterns for target genes across cell types (A549, HUVECS, HPMVECs and HLF) identified through qPCR experiments.

To complement experimental findings, bioinformatic analysis was also conducted using publicly accessible transcriptomic and genomic data. The COPD Cell Atlas, an open-access tool developed by the Kaminski lab was utilised. This database provides single cell RNA sequencing (scRNA-seq) data from lung tissue samples of both healthy individuals and COPD patients(304, 305). I specifically used this platform to assess the expression profile of key genes across different lung cell populations. I compared the gene expression patterns in between healthy and COPD samples and generated cell type specific expression plots for genes of interest using the platform's visualization tools.

Chapter 3

Identifying the potential role of modulators from key lung developmental pathways in lung repair

3.1 Introduction

The adult lung is a largely quiescent organ, with lung tissue homeostasis maintained through minimal cellular turnover under normal physiological conditions(2, 5, 37, 306). It was previously believed that the lungs had a limited capacity for repair post injury(2). However, despite the low rate of cell turnover, the lungs possess a remarkable intrinsic ability to repair and regenerate damaged tissue following injury (2, 306).

Lung repair and regeneration is a complex process, involving interactions between multiple cell types and the integration of diverse signalling pathways(4, 11, 13, 112). Emerging evidence suggests that many of the signalling pathways essential for lung development are reactivated in response to injury, orchestrating key cellular processes such as cell migration, differentiation and proliferation (11, 13, 19, 37, 112). While, lung development occurs in five distinct stages; embryonic, pseudoglandular, canalicular, saccular, alveolar, this thesis focuses primarily on alveolarisation and the activation of pathways during alveolar repair (7, 9, 10, 11).

Alveolarisation is the final stage of lung development during which the alveoli, the functional units of gas exchange are formed (8, 12, 27). In humans, alveolarisation begins *in utero* and occurs in two phases; bulk (from 36 pcw to ~ 3 years) and continued alveolarisation. Studies have demonstrated that this process extends into early adulthood, with the number of alveoli continuing to increase up until ~21 years (8, 14, 16, 21).

Mouse models have been instrumental in advancing our understanding of the role of signalling pathways at different stages of lung development (Figure. 3.1) (8, 10, 11, 14). Numerous signalling pathways; including FGF, Hh, Hippo, Notch, RA, TGF-β, VEGF and Wnt have been identified as key regulators of alveolarisation (Figure. 3.1)(8-14).

Despite growing evidence that these developmental pathways also contribute to lung repair and regeneration (11, 13, 37), the precise molecular and cellular mechanisms through which

these pathways drive repair remain poorly understood. Gaining deeper insights into the function of these pathways post injury is essential for the development of effective regenerative therapeutics for respiratory diseases.

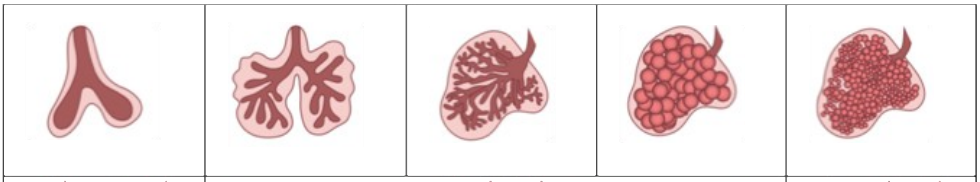

	Embryonic Period	Foetal Period			Postnatal Period
Stages & Timeline of Development:	Embryonic	Pseudoglandular	Canalicular	Saccular	Alveolar
	4-7 pcw E9-E12	5-17 pcw E12-E15	16-26 pcw E15-E17	26-36 pcw E17- P5	36pcw- Adult Birth- P20
Pathways Activated	FGF Hedgehog Notch Retinoic Acid TGF-β Wnt	FGF Hedgehog Hippo Notch Retinoic Acid TGF-β VEGF Wnt	FGF Hedgehog Notch TGF-β VEGF Wnt	FGF Notch TGF-β VEGF Wnt	FGF Hedgehog Hippo Notch Retinoic Acid TGF-β VEGF Wnt

Figure 3.1. Schematic diagram outlining stages of lung development.

Lung morphology at each stage of development is presented and key signalling pathways activated at each stage are listed. The timeline for development is also presented in post conception weeks (pcw) for humans and embryonic days (E) and postnatal days (P) for mice. Adapted from Allen-Hyttinen J, Yung H, Nikolić MZ. Lung development. In: Nikolić M, Hogan BLM, editors. Lung Stem Cells in Development, Health and Disease (ERS Monograph). Sheffield: European Respiratory Society; 2021. p. 1–16, (2) (14).

Moreover, deciphering the impact of these pathways on different cellular populations within the alveolar niche is critical to determine precisely how each pathway affects alveolar repair. The alveoli are composed of several specialised alveolar cells, including alveolar epithelial cells (ATI and ATII), endothelial cells, fibroblasts (e.g. pericytes, lipofibroblasts and myofibroblasts) and immune cells, most notably alveolar macrophages(36, 39, 112, 117). Additionally, these cells are organised into distinct tissue compartments; the alveolar epithelium, vascular endothelium and the interstitial stroma (39, 112).Repair and regeneration following injury is a complex process that requires multicellular cross talk across these compartments(2, 3, 36, 37, 112).

Facultative stem cell populations have been identified at different anatomical locations in the lungs (2, 28, 36, 111, 112). Within the alveoli, ATII cells are central to repair and serve as facultative stem cells, which are capable of self-renewal and differentiation into ATI cells, to regenerate the alveolar epithelium(2, 28, 36, 38, 111, 112). During homeostasis, the stem cell activity of ATII cells is low, however, in response to injury, these facultative stem cells are

activated (38). This regenerative process is further supported by paracrine signalling between the alveolar epithelium and PDGFR-α^+ fibroblasts, which have been demonstrated to secrete Wnt ligands, notably WNT5A, promoting ATII cell differentiation and self-renewal(27, 79, 201, 224). Furthermore, VEGF is another driver of epithelial cell proliferation and differentiation(27, 111, 201).

To effectively study cellular responses in lung repair further, it is essential to utilise relevant experimental models that enable the assessment of the repair capacity and the effects of specific pathway modulators. Over time, a wide range of models have been developed to investigate the cellular and molecular mechanisms that underpin lung development, homeostasis and importantly, repair(236, 237, 239, 263, 268, 273, 307). These include simpler *in vitro* approaches such as monocultures, co-cultures, and scratch wound assays, which employ immortalised cell lines or primary cell cultures(237). While, these models lack the complexity of the *in vivo* lung environment, they are particularly well suited to screening studies and for generating preliminary data to inform more complex experimental investigations, due to their speed, scalability and their relative cost-effectiveness(237, 239).

To overcome limitations of traditional 2D cultures, more complex 3D models have been developed to better recapitulate the structural and cellular complexity of lung tissue (239, 308). These 3D models include lung-on-a-chip microfluidic devices, organoids, ECM/hydrogel-based systems, and precision-cut lung slices (PCLS), each enabling the study of repair within a more complex environment(236, 239, 263, 268, 307). PCLS, in particular, retain the complex native architecture, cellular diversity and spatial organisation of the lung, making them a valuable *ex vivo* model for studying lung repair and regeneration(269-273, 276).

The Dean lab established the Acid Injury and Repair (AIR) model, a novel *ex vivo* model, using PCLS, in which a spatially restricted injury is induced by HCl(271, 276). This approach creates an injury pattern where damaged and healthy lung tissue are adjacent, mimicking the heterogeneity observed in many respiratory diseases(37, 309). The AIR model serves as an invaluable and physiologically relevant model for investigating cellular and molecular mechanisms that underlie lung repair and regeneration.

3.1.1 Hypothesis and Aims

Signalling pathways that are critical for lung development have also been suggested to play a crucial role in lung repair, suggesting a conserved role across developmental and regenerative processes. Based on this, it was hypothesised that modulation of selected developmental signalling pathways will influence key cellular and molecular processes involved in lung repair and regeneration, including proliferation, differentiation and migration. These pathways therefore represent promising targets for further mechanistic investigation and therapeutic targeting post lung injury.

In order to investigate this hypothesis, the following aims were defined:

1. To conduct a thorough literature review to identify signalling pathways that are critical for lung development and have also been shown to play a potential role in lung repair.

2. To conduct wound healing (scratch) assays to investigate and determine the role of selected signalling pathways particularly in cell migration during repair. Based on the findings from these assays, one pathway will be selected for further in-depth investigation.

3. To apply the AIR model to investigate the cellular and molecular mechanisms through which the selected signalling pathway influences lung repair. Specifically, I aim to assess the impact of pathway modulation on cell proliferation and differentiation.

3.2 Results

3.2.1 Identifying key lung development and repair signalling pathways

The Signalling pathways chosen for experimental investigation in this thesis were selected following several stages (Figure. 3.2). First a list of known seminal pathways in developmental biology were made, which included FGF, TGF-β, Wnt/, Hedgehog, Hippo, Notch (310, 311) . Previous work conducted by members of the Dean lab on Wnt and RA signalling pathways was also incorporated to further refine the list to the following: FGF, TGF-β, Wnt, Hedgehog, Hippo, Notch and RA.

Next, literature searches were performed using primary sources such as research papers and secondary sources such as review articles and textbooks to obtain a comprehensive picture of known data about the role of each of these pathways in lung development as well as any existing information on their role in repair and regeneration. To reduce selection bias, PubMed search was used to identify published literature. Boolean search operators (AND, OR, NOT, parentheses, quotation marks) were used to define search parameters. Synonyms were also used where necessary to make the search more comprehensive. An example of search terms used on PubMed include:

- Signalling pathways AND lungs
- Pulmonary development AND signalling pathways
- Wnt AND lung development
- Shh AND lung repair OR regeneration

I conducted the literature search using search terms and Boolean search operators in order to maximise the identification of relevant studies. A Preferred Reporting Items for Systematic reviews and Meta-Analyses (PRISMA) flow diagram was not included in this project because the literature search did not follow the methodology of a traditional systematic review, where inclusion and exclusion criteria are predefined and studies are screened in multiple stages of inclusion and exclusion(312). The search strategy used was exploratory and was used to

identify relevant studies. However, some research papers were excluded where the content was not relevant to my research question or where insufficient information was provided.

As part of the literature search, I obtained information on the life stages when each of these signalling pathways was active (Figure. 3.1). Because this thesis focused on identifying signalling pathways involved in alveolar repair, I was particularly interested in identifying which pathways played a role in generation of alveoli (alveologenesis).

Based on the literature searches, 3 signalling pathways were selected for further experimental investigation: Hedgehog (Hh), Retinoic Acid (RA), Wnt.

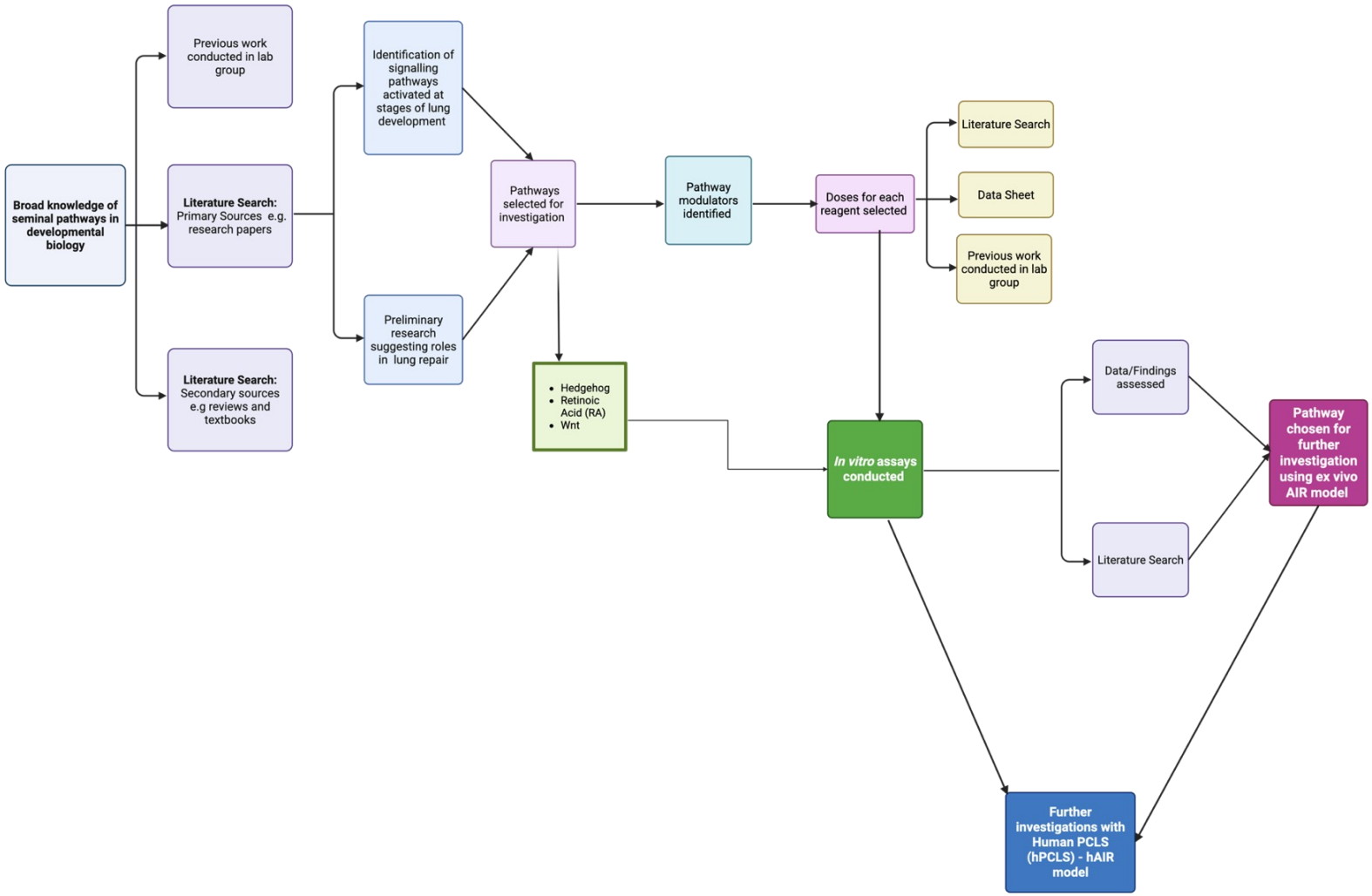

Figure 3.2. Flowchart summarising pathway selection.
Outlines the key steps undertaken to identify and select signalling pathways investigated in this thesis.

3.2.2 Selecting pathway modulators

Table 3.1. Summary of Pathways selected for further experimental investigation, following literature search

Signalling Pathway	Stimulatory agent/factor	Inhibitory agent/factor	References
Sonic Hedgehog (SHH)	SHH-N recombinant protein	Cyclopamine	(11, 13, 171, 172, 174, 180-182, 184, 190, 313-318)
Retinoic Acid (RA)	Retinoic Acid (RA)	4-diethylaminobenzaldehyde (DEAB)	(227, 228, 230, 234, 319-326)
WNT	WNT5A recombinant protein	Box5	(4, 11, 102, 190, 211-213, 220, 223, 224, 327-334)

3.2.3 Investigating endogenous levels of pathway target genes

To begin to investigate the role that each of the chosen pathways play in lung repair at the cellular level, I began by using *in vitro* scratch assays as a simple model of lung repair to screen our chosen signalling pathways for their potential role in lung repair.

Prior to conducting scratch assays, the endogenous levels of key genes within each of the signalling pathways being investigated was assessed in A549 and HUVEC cells using qPCR. Determining the endogenous or baseline expression of genes is imperative because this provides a reference point to determine whether the patterns observed in experiments are due to the selected pathway modulators or the natural expression of target genes. For example, if the endogenous expression level of a target gene is already highly expressed in a cell type, addition of an agonist or recombinant protein may not have a significant impact on wound closure in a scratch assay. Equally, if the endogenous gene expression levels are low, then an antagonist may not have any effect. By understanding the endogenous expression of target genes, the working concentration of agonists and antagonists can also be adjusted to ensure experimental investigations are informative. Since scratch assays were conducted to

screen the effect of signalling pathways, only one concentration of each pathway modulator was used.

3.2.3.1 Selecting appropriate reference genes for normalisation of gene expression

Three reference genes, beta-2 microglobulin (*B2M*), glyceraldehyde 3-phosphate dehydrogenase (*GAPDH*) and glucuronidase beta (*GUSB*), were selected based on prior validation conducted within the lab group and published literature identifying them among the most stably expressed genes in lung tissue and related cell types (301-303). Multiple reference genes were examined to improve the reliability and accuracy of gene expression normalisation(335, 336).

To confirm their suitability, the expression stability of *B2M*, *GAPDH* and *GUSB* was assessed in both A549 cells and HUVECs, by examining the mean cycle threshold (Ct) values across biological replicates (Figure. 3.3). Three biological replicates were included for each reference gene and within each experiment there were three technical replicates. For each biological replicate, RNA was extracted from cells at different passages to accurately demonstrate biological variability. In qPCR, the Ct value represents the number of amplification cycles required for the gene of interest to be detected (337, 338). Importantly, Ct values are inversely proportional to gene expression levels, therefore, the lower Ct values indicate higher levels of gene expression (337).

Ideal reference genes should have consistent and moderate expression across all experimental conditions. Therefore, selected reference genes were expected to have low Ct variability between biological replicates (335, 336, 338), with Ct values that were neither too low (to avoid detection saturation) nor too high (to avoid unreliable quantification). The mean Ct value for *GUSB* was 31.1 in A549 cells (Figure. 3.3A) and 29.7 in HUVECS (Figure. 3.3B), both values are too high for reliable normalisation. Furthermore *GUSB* showed more sample variability across replicates (Figure. 3.3). In contrast, *B2M* and *GAPDH* displayed stable expression across replicates with mean Ct values of 26.2 and 21.9, respectively in A549 cells (Figure. 3.3A), and 23.9 and 20.8 in HUVECs (Figure. 3.3B). Therefore both *B2M* and *GAPDH*

were used as reference genes for normalisation of target gene expression in both cell types. According to minimum information for publication of quantitative real-time PCR experiments: MIQE guidelines, using one reference for normalisation is not robust(336). So two were used to improve the accuracy and reproducibility of the gene expression data.

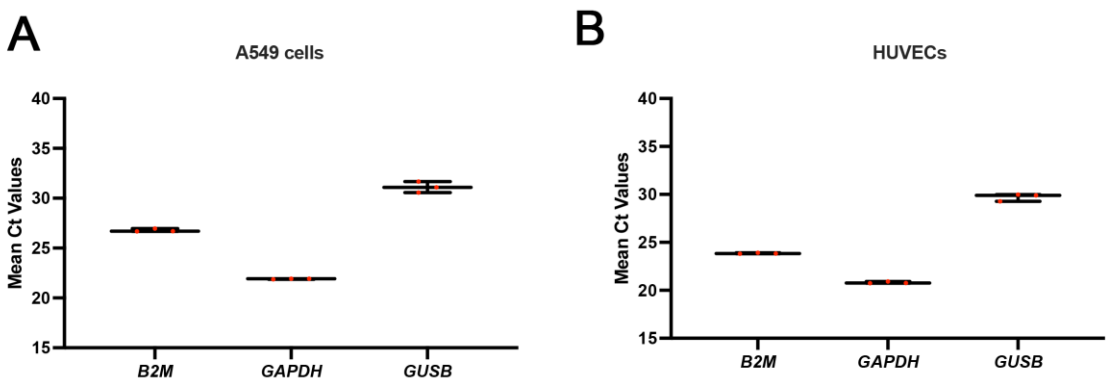

Figure 3.3. Mean Ct values of candidate reference genes in A549 cells and HUVECs.
The stability of B2M, GAPDH and GUSB expression was assessed in (A) A549 cells and (B) HUVECs using qPCR. Boxplots show the mean Ct values across biological replicates for each gene. Points overlaid on boxplots represent biological replicates (n=3).

Table 3.2. Mean Ct values for candidate reference genes

	A549	HUVEC
B2M	26.8	23.9
GAPDH	21.9	20.8
GUSB	31.1	29.7

3.2.3.2 Determining the relative expression of target genes in A549 and HUVECs

Target gene expression levels were normalised to the references *B2M* and *GAPDH*, as outlined in the previous section to calculate the ΔCt value. Then the relative expression was determined using the 2^ (- ΔCt) method(336, 337). Fold change (2^ (- ΔΔCt)) was not calculated, as this investigation did not include a treatment group or experimental condition for comparison(336, 337, 339). The aim of this investigation was to assess and compare baseline expression levels of target genes in A549 cells and HUVECs.

The expression levels of 11 target genes associated with selected signalling pathways were analysed in A549 cells. Specifically, *WNT5A* and *WNT9A* were examined as representatives of the WNT signalling pathway; *RARβ*, *RARγ* and *ALDH1A1* for retinoic acid signalling; and *SHH*, *PTCH1*, *SMO*, *GLI1, GLI2* and *HHIP* for SHH signalling (Figure. 3.4).

Among the genes investigated, *ALDH1A1* exhibited the highest relative expression in A549 cells (Figure. 3.4A). This gene encodes retinaldehyde dehydrogenase 1, which is one of the enzymes that catalyses retinoic acid synthesis(340). The mean relative expression of aldh1a1 was 3.9, which was markedly higher than all other genes investigated, to the extent that it obscured relative differences in expression levels when plotted on the same graph (Figure. 3.4A). To address this, an additional bar chart excluding *ALDH1A1* was generated, allowing for clearer visualisation of the expression of the remaining genes (Figure. 3.4B). From this adjusted representation, it was evident that *GLI1, GLI2* and *SMO*, with mean relative expression levels ranging from~0.03 to 0.16, were moderately expressed in A549 cells. Whilst *RARβ* and *RARγ* exhibited low but measurable expression levels of 0.0086 and 0.0046 respectively, while *HHIP* and P*TCH1* were very low at 0.002 and 0.0016 respectively. *WNT5A*, *WNT9A* and *SHH* were all expressed at <0.001. To improve the interpretation of data, data were transformed into a $\log_{10}$ scale (Figure. 3.4C). Using $\log_{10}$ reduces the skewness caused by wide differences in expression levels, therefore this made subtle variations between low expressing genes easier to discern and compare(341, 342). A heatmap was also generated to summarise the expression profile of genes (Figure. 3.4D), the heatmap highlights the pronounced difference between the very high relative expression of *ALDH1A1* and the low expression of the remaining genes, while also enabling clearer distinction between low expressing genes.

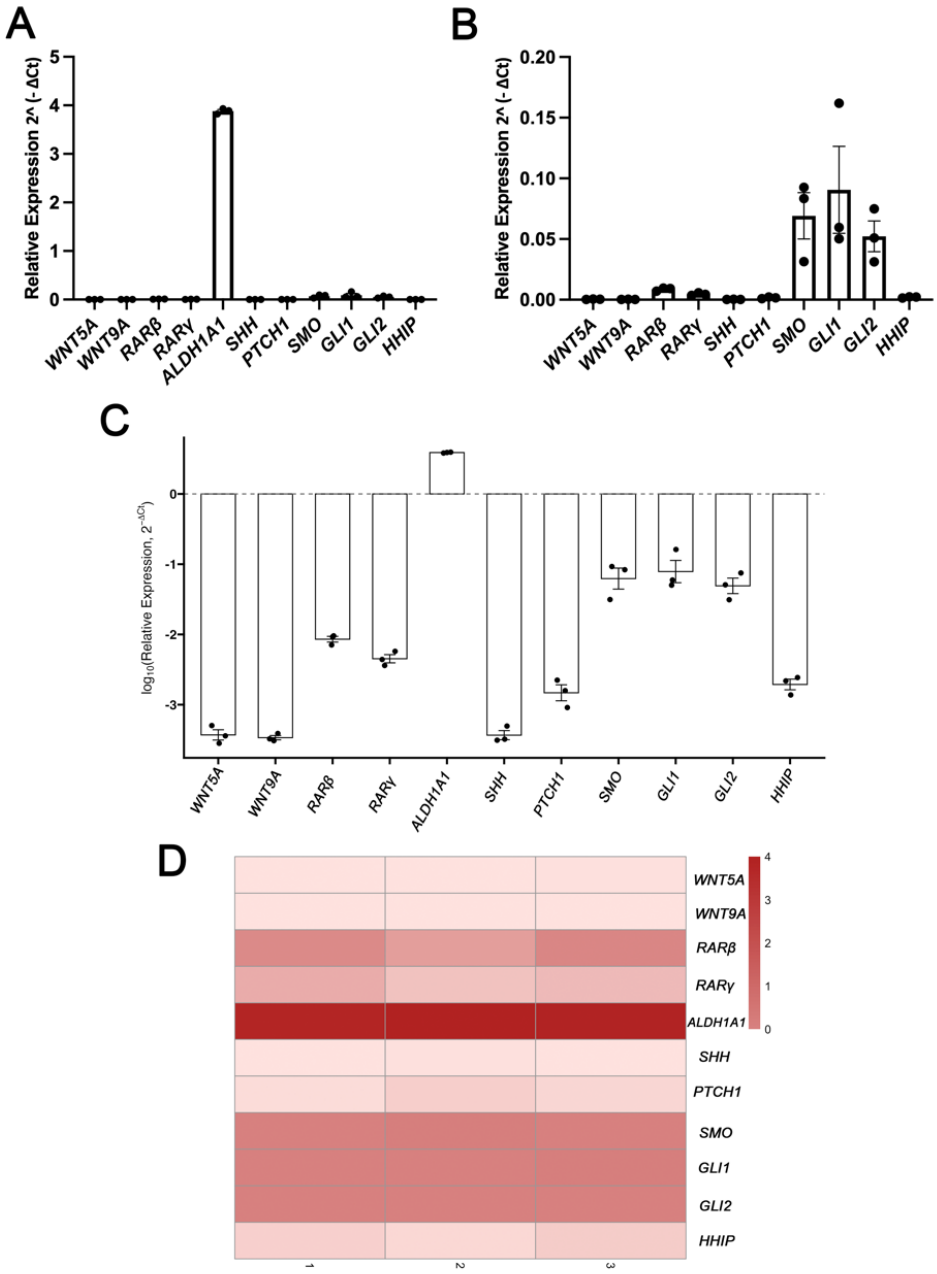

Figure 3.4. Relative gene expression of target genes in A549 cells.
(A) Bar chart showing the relative expression of target genes in A549 cells calculated using 2^ (- ΔCt) method. (B) Bar chart showing relative expression of target genes excluding ALDH1A1 to enhance visualisation genes with lower expression. (C) Bar chart displaying relative expression values converted to a $\log_{10}$ scale to facilitate data interpretation. (D) Heatmap summarising the relative expression of target genes calculated using 2^ (- ΔCt) method. Colour intensity ranges from light pink (low expression) to red (high expression), as shown in the scale bar. The heatmap was generated using pheatmap package in R.

Next, target gene expression was analysed in HUVECS (Figure. 3.5A). *HHIP* showed the highest relative expression at 0.2, exceeding the relative expression of all other genes (Figure. 3.5), additionally the expression of *HHIP* was higher in HUVECs than in A549 cells (Figure. 3.4-3.5).

ALDH1A1 expression was lower than in A549 cells but remained relatively high at 0.04 compared to other genes (Figure. 3.4-3.5), while *RARβ* showed moderate expression at 0.015 (Figure. 3.5). The remaining genes of interest were expressed at very low levels (<0.002) (Figure. 3.5).

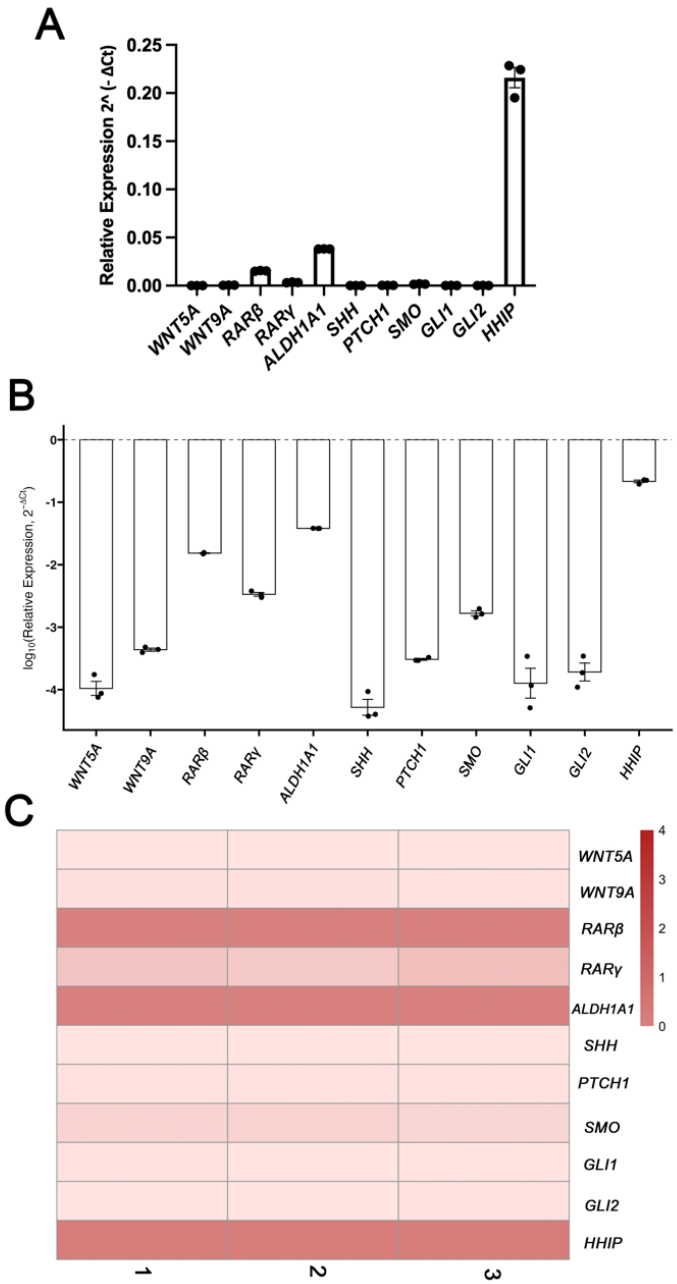

Figure 3.5. Relative gene expression of target genes in HUVECs.

(A) Bar chart showing the relative expression of target genes in HUVECS calculated using 2^ (- ΔCt) method. (B) Bar chart displaying relative expression values converted to a log10 scale to facilitate data interpretation. (C) Heatmap summarising the relative expression of target genes calculated using 2^ (- ΔCt) method. Colour intensity ranges from light pink (low expression) to red (high expression), as shown in the scale bar. The heatmap was generated using pheatmap package in R. Kolde R (2025). pheatmap: Pretty Heatmaps. R package version 1.0.13.

Although qPCR analyses for A549 and HUVECs were performed at different times, a heatmap was generated to summarise differences in the relative gene expression of targets in both cell types (Figure. 3.6).

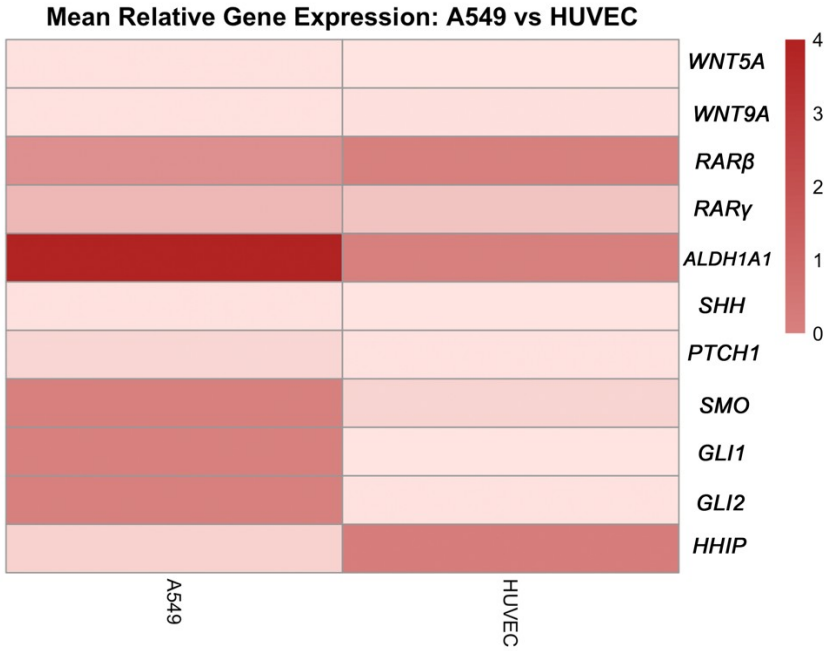

Figure 3.6. Comparison of relative gene expression of target genes in A549 cells and HUVECs.
Heatmap summarising mean relative expression values of *WNT5A, WNT9A, RARβ AND RARγ, ALDH1A1, SHH, PTCH1, SMO, GLI1, GLI2* and *HHIP* in A549 cells and HUVECs obtained after conducting qPCR and analyses using 2^ (- ΔCt) method. Colour intensity ranges from light pink (low expression) to red (high expression), as shown in the scale bar. The heatmap was generated using pheatmap package in R. Kolde R (2025). pheatmap: Pretty Heatmaps. R package version 1.0.13

3.2.4 Screening selected lung developmental pathways using wound healing assay

Lung repair and regeneration is a process that requires multicellular interactions(2, 4, 5, 343). It is important to note that although stem cells play a key role in repair and/or regeneration, these processes do not just involve stem cells. There are other biological mechanisms that are critical roles, such as cell migration (343, 344). Cell migration is critical for development to facilitate the formation of organs and is also crucial for repair and regeneration, particularly for facilitating wound closure (343, 344).

Scratch assays are a widely used, reproducible *in vitro* model generated by applying a scratch to a monolayer of cells and then calculating the subsequent number/percent of cells to migrate to close the wound gap (345, 346). Since the scratch induces cellular injury, this model is similar to aspects of *in vivo* tissue damage, making this a good and relevant model for studying wound repair. In addition to this, the assay enables high throughput analysis, making scratch assays particularly suitable for primary investigation (345, 346).

Although there are numerous cell types in the lungs I focused on the potential reparative role of the chosen factors on two cell types that are critical for alveolar function, type II alveolar epithelial cells and endothelial cells (Human Alveolar Adenocarcinoma Epithelial cells – A549) cells and endothelial cells (Human Umbilical Vein Endothelial cells – HUVECs) to determine whether modulating the selected pathways would have an impact on wound healing. The A549 cell line was chosen for experimental investigations rather than primary ATII cells because primary cells are hard to isolate, culture and maintain over time when compared to cell lines which are obtained commercially(78, 347). Moreover, A549 cells have been used extensively in research studies due to their ease of use, low cost and the flexibility to conduct long term studies since the cells are immortalised(347). It is also widely understood that primary ATII cells differentiate and transform over time leading to a loss of their phenotype. Specifically, researchers have observed primary ATII cells differentiate to an ATI phenotype(263, 347). Whereas, A549 cells do not differentiate, they maintain their ATII phenotype (263, 347). Despite this, it is also important to acknowledge that there are some limitations to using A549 cells. A549 cells are a cancer cell line, originally isolated from alveolar basal cell adenocarcinoma (290, 291), therefore A549 cells lack contact inhibition. This can lead to excessive cell proliferation even at very high cell densities in contrast to normal epithelial cells which cease to divide when packed too closely together (263, 347, 348).

Similarly, HUVEC cells were used to model endothelial cells in this chapter due to their ease of use in comparison to Human Pulmonary Microvascular Endothelial Cells (HPMVECs). HUVECs exhibit greater stability in culture and are able to undergo a higher number of passages, making them more suitable for preliminary experiments. Furthermore, I aimed to

assess the impact of the chosen pathway modulators on HUVEC wound closure with the intention of subsequently conducting investigations using HPMVECs.

Scratch assays were set up by seeding A549 cells at a concentration of 5 x 10^4 per well into collagen coated 8 well slide chambers (as described in chapter 2 section 2.14) and applying a scratch to the middle of each well and then treating with selected signalling pathway modulators.

3.2.4.1 WNT *treatment increases wound closure in A549 cells*

Previous scratch assay experiments in the Dean lab found that WNT5A had a pro-repair effect on A549 cells (330). Therefore, initial scratch assay experiments were set up with 1 μg/mL WNT5A in DMEM + 0.5 % FBS, along with a control group with medium only (DMEM + 0.5 % FBS), to ensure that this data was reproducible and that the scratch assay method was working. A549 cells treated with DMEM + 10 % FBS was also included as a positive control for increased wound closure (Figure. 3.7A (i-ii), Figure. 3.7B). After 20 hr, A549 cells in DMEM + 10 % FBS had a mean percentage of wound closure of 65.6 % (Figure. 3.7A (i-ii), Figure. 3.7B), whereas cells in DMEM + 0.5 % FBS alone had a mean percentage wound closure of 22.5 % (Figure. 3.7A (iii-iv), Figure. 3.7B). Consistent with previous findings, treatment with 1 μg/mL Wnt5a led to a higher wound closure compared to the DMEM+0.5 % FBS control, with a mean percentage of wound closure of 32.3 % after 20 hr (Figure. 3.7A (v-vi), Figure. 3.7B). This corresponds to a 1.4-fold difference (≈ 44 % increase), which was statistically significant ($p = 0.0286$), supporting a pro-repair role for WNT5A in A549 cells.

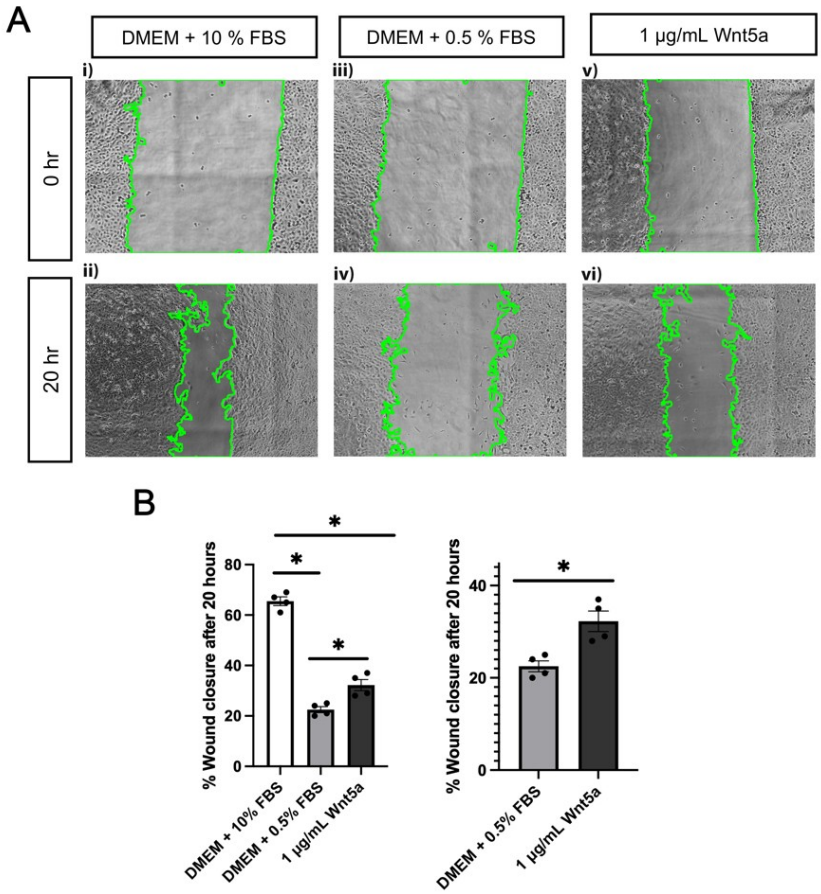

Figure 3.7. Effect of 1µg/mL Wnt5a treatment on A549 wound closure.

(A) Representative light microscope images showing A549 wound closure following 20 hr culture with (i-ii)DMEM + 10 % FBS, (iii-iv)DMEM + 0.5 % and (v-vi) 1µg/mL WNT5A (experimental group). Widefield images taken at 10× using Zeiss Axio Observer (B) Graphs showing quantification of % wound closure in A549 after 20 hr of culture. Data are presented as mean ± SEM (n = 4; Mann – Whitney U-test. *p < 0.05).

3.2.4.2 Treatment of A549 cells with retinoic acid does not promote wound closure

The effect of retinoic acid (RA) on A549 cell wound closure was investigated next. As with the WNT5A experiments, the aim of conducting this assay was to validate previously published findings from the Dean lab, which reported that RA had no significant effect on A549 cell wound closure(323). A549 cells were treated with 10 µM RA in DMEM + 0.5 % FBS. Since RA required reconstitution in 0.01 % ethanol (EtOH), an additional control condition (DMEM + 0.001 % EtOH) was included to assess whether EtOH alone had an influence on wound closure. A549 cells in DMEM+ 10 % FBS had a mean percentage of wound closure of 53.5 % (Figure. 3.8A (i-ii), Figure. 3.8B) after 20 hr, whilst A549 cells in DMEM + 0.5 % FBS had a mean percentage of wound closure of 27.8 % (Figure. 3.8A (iii-iv), Figure. 3.8B) and cells in 0.01 % EtOH had a mean percentage of wound closure of 24.8 % (Figure. 3.8A (v-vi), Figure. 3.8B).

A549 cells treated with 10 μM RA had a wound closure of 27.3 % (Figure. 3.8A (vii-viii), Figure. 3.8B). When compared to the DMEM + 0.5 % FBS, there was no significant difference in wound closure of cells treated with DMEM + 0.01 % EtOH (p= 0.4571) after 20 hr and in agreement with previous studies no significant change in wound closure was observed after 20 hr of RA treatment compared with A549 cells treated with DMEM + 0.5 % FBS (p= 0.6782).

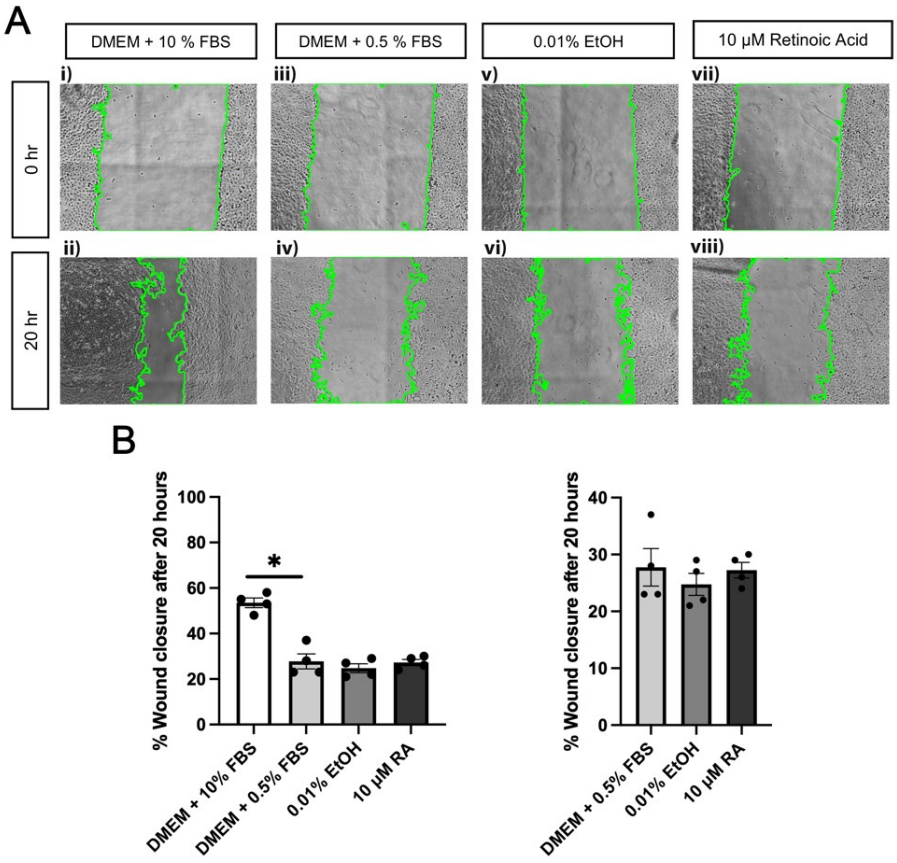

Figure 3.8. Effect of 10 μM Retinoic Acid (RA) treatment on A549 wound closure.

(A) Representative light microscope images showing A549 wound closure following 20 hr culture with (i-ii) DMEM + 10 % FBS, (iii-iv) DMEM + 0.5 % FBS, (v-vi) 0.01 % EtOH (vehicle control) and (vii-viii) 10 μM RA (experimental group). Widefield images taken at 10× using Zeiss Axio Observer (B) Graphs showing quantification of % wound closure in A549 cells after culturing for 20 hr. Data are presented as mean ± SEM (n = 4; Mann – Whitney U-test. *p < 0.05).

3.2.4.3 Wnt9a treatment does not promote wound closure in A549 cells

Having established reproducible scratch assays and confirmed previous findings regarding the effects of WNT5A and RA on wound repair, additional factors (potentiators or inhibitors) from our pathways of interest were tested. Beyond WNT5A, the mammalian Wnt family comprises 18 other ligands, many of which are expressed in the lungs (211, 213). Among these, Wnt9a

has been shown to play a role in lung development(349). Studies using embryonic chick lungs detected Wnt9a expression at the distal tips of the bronchi, suggesting a role in branching morphogenesis (349). Moreover, a genome-wide association study (GWAS) revealed that *WNT9A* is associated with adult lung function (333) and further to this another GWAS linked *WNT9A* biomarkers to acute respiratory distress syndrome (ARDS) (350). However, the role of *WNT9A* in lung repair remains unclear. To investigate this, I assessed whether WNT9A treatment affects wound closure in A549 cells. After 20 hr, cells cultured in DMEM + 10 % FBS had a mean percentage of wound closure of 69 % (Figure. 3.9A(i-ii), Figure. 3.9A) cells, while cells in DMEM + 0.5 % FBS alone had a mean wound closure of 23.3 % (Figure. 3.9A(iii-iv), Figure. 3.9B). Cells treated with 0.04 μg/mL WNT9A had a mean wound closure of 24.3 % (Figure. 3.9A(v-vi), Figure. 3.9B), which was a 1-fold change (≈ 4 % increase) and was not significantly different from the DMEM + 0.5 % FBS control (p = 0.6857). These results suggest that Wnt9a does not significantly influence A549 wound closure.

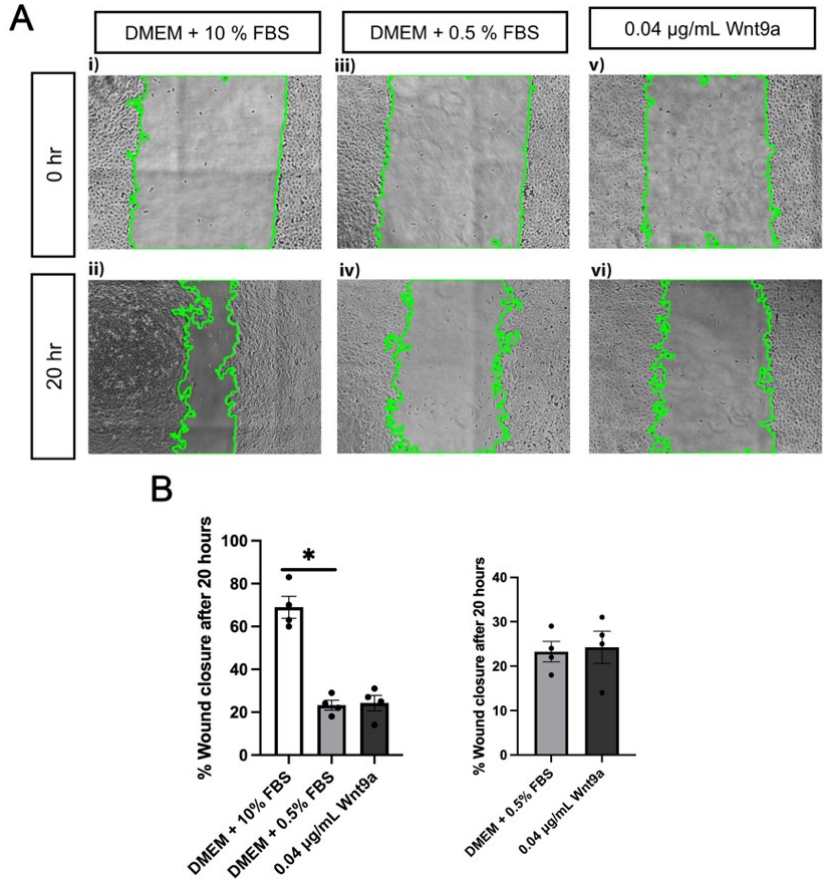

Figure 3.9. Effect of 0.04 μg/mL Wnt9a treatment on A549 wound closure.

*(*A) Representative light microscope images showing A549 wound closure following 20 hr culture with (i-ii) DMEM + 10 % FBS, (iii-iv) DMEM + 0.5 % FBS and (v-vi) 0.04 μg/mL Wnt9a (experimental group). Widefield images taken at 10× using Zeiss Axio Observer (B) Graphs showing quantification of % wound closure in A549 cells after culturing for 20 hr. Data are presented as mean ± SEM (n = 4; Mann – Whitney U-test. *p < 0.05).

3.2.4.4 SHH-N treatment leads to a reduction in wound closure of A549 cells

The impact of SHH on A549 cell wound closure was investigated next. SHH signalling plays an important role in lung development and is also involved in maintaining adult lung homeostasis, where it regulates mesenchymal cell proliferation and differentiation (13, 180, 181). In this investigation, A549 cells cultured in DMEM + 10 % FBS had a mean percentage of wound closure of 63 % (Figure. 3.10A(i-ii), Figure. 3.10B), while cells in DMEM + 0.5 % FBS had a mean percentage of wound closure of 31 % (Figure. 3.10A(iii-iv), Figure. 3.10B). Treatment with 0.25 µg/mL SHH resulted in a mean percentage wound closure of 25 % (Figure. 3.10A v-vi, Figure. 3.10B). This represented a 6 % difference or a 0.8- fold change (≈ 20 % decrease) in percentage closure compared to cells in the DMEM + 0.5 % control group, furthermore the difference was statistically significant (p= 0.0286). These findings suggest that SHH may negatively impact wound closure in A549 cells.

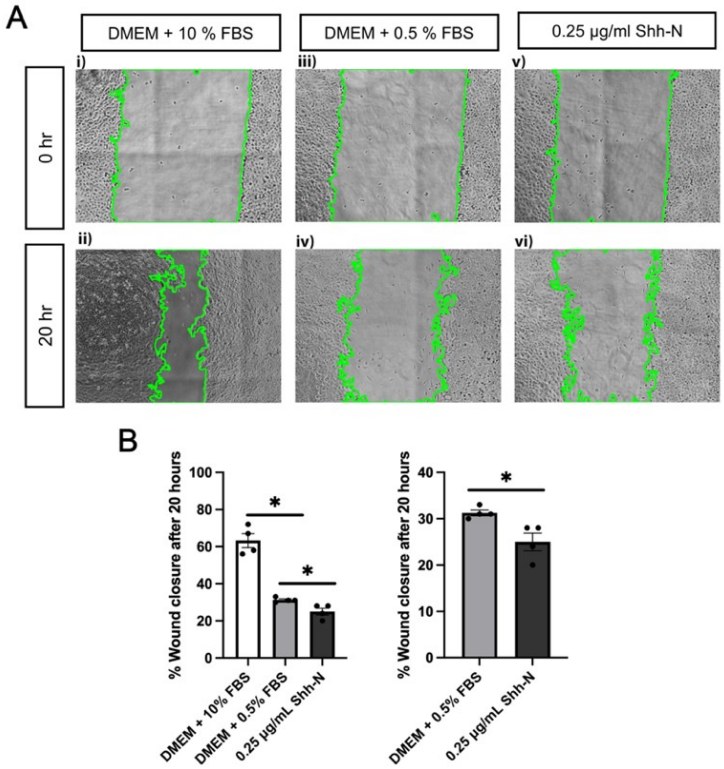

Figure 3.10. Effect of 0.25 µg/mL SHH treatment on A549 wound closure.
(A) Representative light microscope images demonstrating A549 wound closure following 20 hr culture with (i-ii) DMEM + 10 % FBS, (iii-iv) DMEM + 0.5 % FBS and (v-vi) 0.25µg/mL SHH (experimental group). Widefield images taken at 10× using Zeiss Axio Observer (B) Graphs showing quantification of % wound closure in A549 cells after culturing for 20 hr. Data are presented as mean ± SEM (n = 4; Mann – Whitney U-test. *p < 0.05).

3.2.4.5 *Cyclopamine treatment does not have a significant impact on A549 wound closure*

Having found a small but significant inhibitory effect of SHH on wound closure in A549 cells, the effect of cyclopamine, a well characterised inhibitor of Hh signalling(351), was investigated next. Cyclopamine inhibits the smoothened (Smo) receptor, therefore blocking Hh pathway activation. As cyclopamine was dissolved in EtOH prior to dilution in culture medium, an ethanol control (0.001 % EtOH in DMEM + 0.5 % FBS) was included to assess potential solvent effects. A549 cells cultured in DMEM + 10 % FBS had a mean wound closure of 61.3 % (Figure. 3.11A(i-ii), Figure. 3.11B), while cells in DMEM + 0.5 % FBS had a mean wound closure of 26.3 % (Figure. 3.11A(iii-iv), Figure. 3.11B). Cells in 0.001 % EtOH had a mean wound closure of 22 % (Figure. 3.11A(v-vi), Figure. 3.11B). No significant difference in wound closure was observed between the EtOH control and the DMEM + 0.5 % FBS control group (p=0.1143), indicating that the solvent did not adversely affect wound closure. Treatment with 0.5 μg/mL cyclopamine led to a mean percentage wound closure of 31 % (Figure. 3.11A(vii-viii), Figure. 3.11B) after 20 hr, compared to 26.3 % in the DMEM + 0.5 % FBS control. This was a 1.2-fold change (≈ 18 % increase); however, this difference was not statistically significant (p=0.3429).

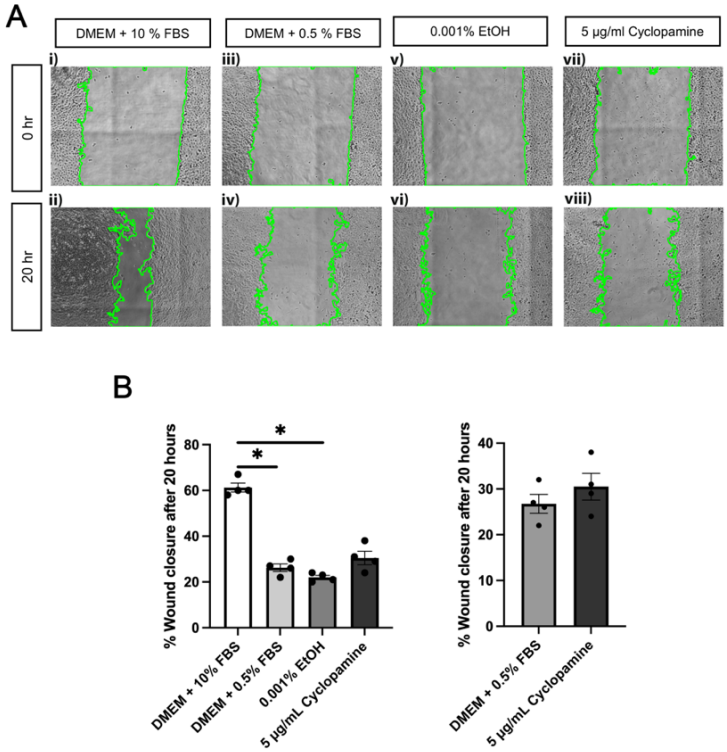

Figure 3.11. Effect of 5 μg/mL Cyclopamine treatment on A549 wound closure.

(A) Representative light microscope images showing A549 wound closure following 20 hr culture with (i-ii) DMEM + 10 % FBS, (iii-iv) DMEM + 0.5 % FBS, (v-vi) 0.001 % EtOH (vehicle control) and (vii-viii) 5 μg/mL cyclopamine (experimental group). Widefield images taken at 10× using Zeiss Axio Observer (B) Graphs showing quantification of % wound closure in A549 cells after culturing for 20 hr. Data are presented as mean ± SEM (n = 4; Mann – Whitney U-test. *p < 0.05).

3.2.4.6 Treatment of HUVECs with retinoic acid promotes wound closure

After investigating the effect of pathway modulators on the A549 epithelial cell line, the effects of pathway modulators on endothelial cell wound healing was investigated, using HUVECs. As previously highlighted, HUVECs were chosen for preliminary endothelial scratch assays before moving on to lung specific primary endothelial cells because they are easier to maintain and grow. For HUVEC scratch assays, cells were seeded at 5 x 10^4 cells per well into 8 well slide chambers which were pre-coated with 2 μg/mL fibronectin and HUVEC cells were cultured until confluent. Once confluent, a scratch wound was made through the middle of each well as described in methods (chapter 2 section 2.14) and cells were treated with selected signalling pathway modulators.

Previous experiments in the Dean lab demonstrated that while RA did not affect wound repair in A549 cells (as shown in section 3.2.4.2) it did promote wound closure in HUVECs. These studies also identified 10 μM RA as an optimal concentration for treatment, with lower concentrations producing a reduced effect and higher concentrations having a cytotoxic effect. Further to this, RA was found to stimulate tube formation in HPMVECs (323). Therefore, scratch assays were conducted with HUVECs treated with RA first to validate the method with HUVECs, with plans to move onto further investigations with HPMVECs.

HUVECs were treated with 10 μM RA prepared in basal medium + 1 % FCS. Since RA was diluted in 0.01 % EtOH, wound healing assays were also set up with 0.01 % EtOH, to determine whether the EtOH had a cytotoxic affect. HUVECs were also treated with complete Endothelial Growth Medium (Basal medium + 2 % Foetal Calf Serum (FCS), 0.4 % Endothelial Cell Growth Supplement, 0.1 ng/mL Epidermal Growth Factor (recombinant human, 1 ng/mL Basic Fibroblast Growth Factor (recombinant human), 90 μg / mL Heparin and 1 μg / mL Hydrocortisone), which was included as a positive control for a high level of wound closure or control medium only (Basal medium + 1 % FCS).

After 20 hr, cells cultured in complete endothelial growth medium had a mean percentage of wound closure of 74 % (Figure. 3.12A(i-ii), Figure. 3.12B), while cells cultured in Basal medium

+ 1 % FCS had a wound closure of 19.7 % (Figure. 3.12A(iii-iv), Figure. 3.12B) and cells cultured in 0.01 % EtOH had a wound closure of 14.7 % (Figure. 3.12A(v-vi), Figure. 3.12B). The difference between the mean percentage of wound closure in the HUVECs treated with 0.01 % EtOH (14.7 %) (Figure. 3.12A(v-vi), Figure. 3.12B) and the mean percentage of wound closure in HUVECs treated with basal medium + 1 % FCS (19.7 %) (Figure. 3.12A(iii-iv), Figure. 3.12B) was not significant (p = 0.5391), indicating that EtOH did not have an impact on wound closure. HUVECs treated with 10 µM RA showed a mean percentage wound closure of 66.7 % (Figure. 3.12A(vii-viii), Figure. 3.12B), compared to a mean of 19.7 % in HUVECs cultured in basal medium + 1 % FCS, which was a 3.4-fold change (≈ 239 % increase) (Figure. 3.12A(iii-iv), Figure. 3.12B) (p= 0.0219).

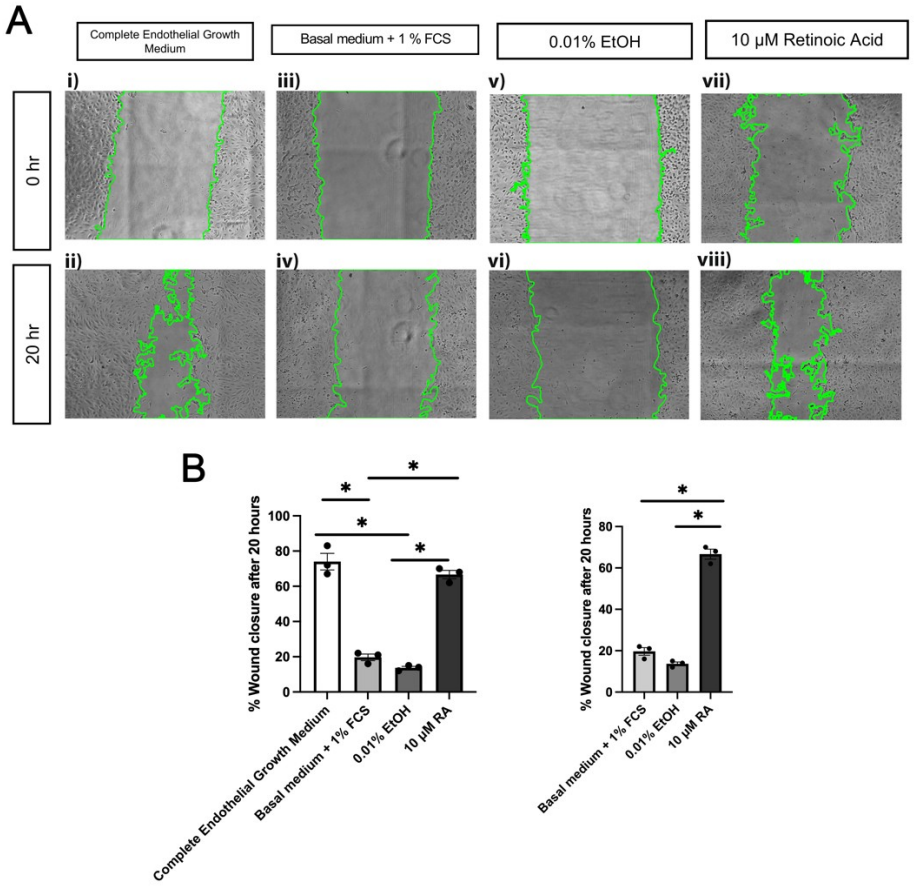

Figure 3.12. Effect of 10 µM Retinoic Acid (RA) treatment on HUVEC wound closure.

(A) Representative light microscope images showing HUVEC wound closure following 20 hr culture with (i-ii) complete endothelial growth medium, (iii-iv) basal medium + 1 % FCS, (v-vi) 0.01 % EtOH (vehicle control) and (vii-viii) 10 µM RA (experimental group). Widefield images taken at 10× using Zeiss Axio Observer (B) Graphs showing quantification of % wound in A549 cells after culturing for 20 hr. Data are presented as mean ± SEM (n = 3; Mann – Whitney U-test. *p < 0.05).

3.2.4.7 Wnt5a treatment does not promote wound closure in HUVECs

Whilst information about the effect of WNT5A in the epithelial cell population is growing (330, 331), information about the role of WNT5A on endothelial cells is limited. To address this knowledge gap, scratch assays were performed on HUVECs treated with 1 µg/mL WNT5A or basal medium + 1 % FCS for 20 hours. HUVECs were also treated with complete endothelial growth medium as a positive control for increased wound closure. HUVECs cultured in complete endothelial growth medium had a mean percentage of wound closure of 75 % (Figure. 3.13A(i-ii), Figure. 3.13B). HUVECS treated with Basal medium had a mean percentage of wound closure of 19.6 % (Figure. 3.13A(iii-iv), Figure. 3.13B). Treatment with 1 µg/mL WNT5A resulted in a mean wound closure of 19 %, (Figure. 3.13A(v-vi), Figure. 3.13B) which was almost identical to the percentage of wound closure in HUVEC cultured with basal medium + 1 % FCS alone (Figure. 3.13A (iii-iv), Figure. 3.13B) (p=0.8000).

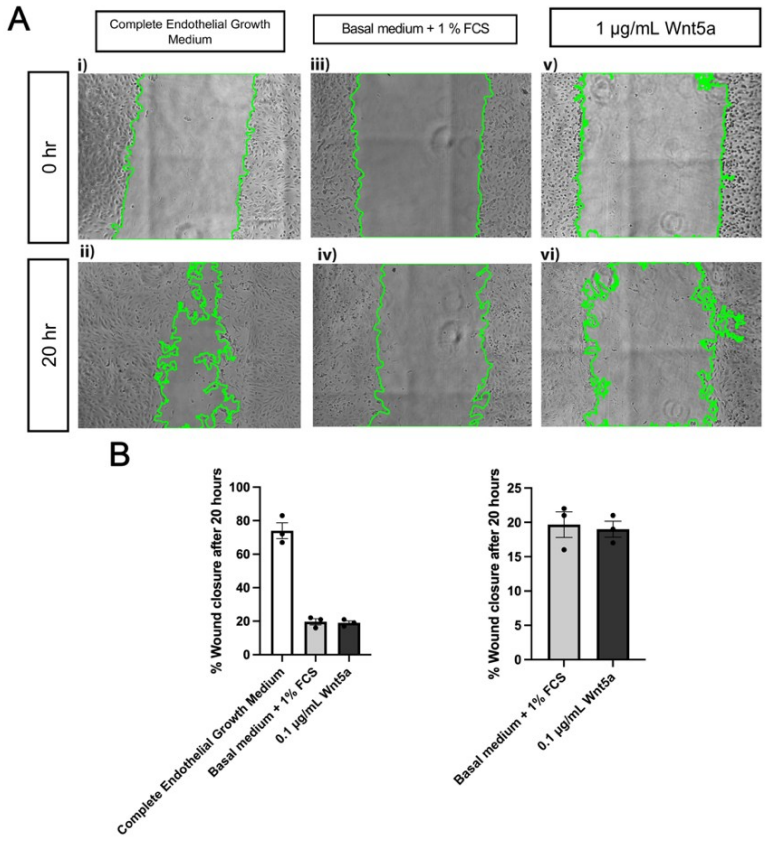

Figure 3.13. Effect of 1µg/mL Wnt5a treatment on HUVEC wound closure.

(A) Representative light microscope images showing HUVEC wound closure following 20 hr culture with (i-ii) complete endothelial growth medium, (iii-iv) basal medium + 1 % FCS and (v-vi) 1µg/mL WNT5A (experimental group). Widefield images taken at 10× using Zeiss Axio Observer (B) Graphs showing quantification of % wound closure in HUVECs after culturing for 20 hr. Data are presented as mean ± SEM (n = 3; Mann – Whitney U-test. *p < 0.05).

3.2.4.8 Wnt9a treatment does not have a significant impact on HUVEC wound closure

Then the effect of WNT9A on endothelial cell repair was investigated (Figure 3.14). HUVECs were treated with 0.04 µg/mL WNT9A in basal medium + 1 % FCS or basal medium + 1 % FCS alone for 20 hours. Complete endothelial growth medium was included as a positive control for maximal wound closure. HUVECs cultured in complete endothelial medium had a mean percentage of wound closure of 73 % (Figure. 3.14A(i-ii), Figure. 3.14B), while cells cultured in basal medium + 1 % FCS had a mean percentage wound closure of 19 % (Figure. 3.14A(iii-iv), Figure. 3.14B). Treatment with 0.04 µg/mL WNT9A resulted in a mean wound closure of 17 % (Figure. 3.14A(v-vi), Figure. 3.14B), there was no significant difference in percentage wound closure between HUVECs treated with WNT9A and HUVECs cultured with basal medium + 1 % FCS alone (Figure. 3.14A (iii-iv), Figure. 3.14B) (p=0.4000).

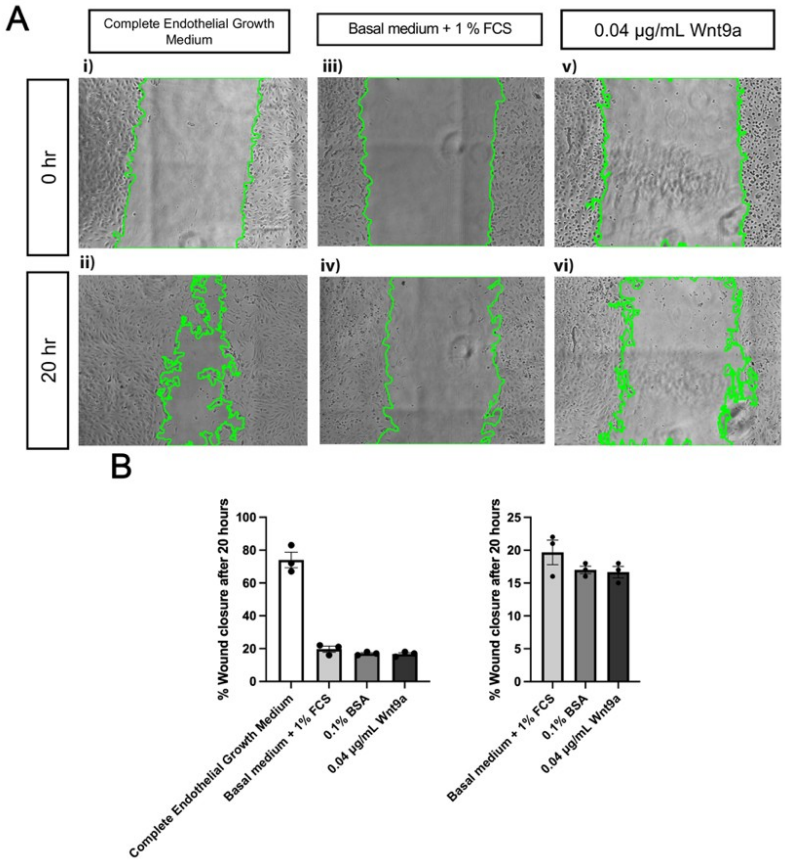

Figure 3.14. Effect of 0.04µg/mL Wnt9a treatment on HUVEC wound closure.

(A) Representative light microscope images showing HUVEC wound closure following 20 hr culture with (i-ii) complete endothelial growth medium (iii-iv) basal medium + 1 % FCS and (v-vi) 0.04 µg/mL WNT9A (experimental group). Widefield images taken at 10× using Zeiss Axio Observer (B) Graphs showing quantification of % wound closure in HUVECs after culturing for 20 hr. Data are presented as mean ± SEM (n = 3; Mann – Whitney U-test. *p < 0.05).

3.2.4.9 *Treatment of HUVECs with SHH-N does not have an impact on wound closure*

The effect of SHH treatment on HUVEC wound closure was investigated next. Since a small reduction in wound closure was observed following SHH treatment of A549 cells, it was important to determine whether SHH treatment also has an effect on the endothelial cell population. HUVECs were treated with 0.25 µg/mL in basal medium + 1 % FCS, basal medium + 1 % FCS alone, or complete endothelial growth medium (positive control for increased wound closure). After 20 hr, HUVECs cultured in complete endothelial growth medium had a mean wound closure of 60 % (Figure. 3.15A(i-ii), Figure. 3.15B), cells in basal medium + 1 % FCS had a mean wound closure of 19.5 % (Figure. 3.15A(iii-iv), Figure. 3.15B) and HUVECs treated with 0.25 µg/mL SHH showed a mean of 21.6 % (Figure. 3.15A(v-vi), Figure. 3.15B), which a 1.1-fold change (≈ 11 % increase) and was not a significant difference when compared to HUVECs cultured with basal medium + 1 % FCS (Figure. 3.15A(iii-iv), Figure. 3.15B) ($p>0.9999$).

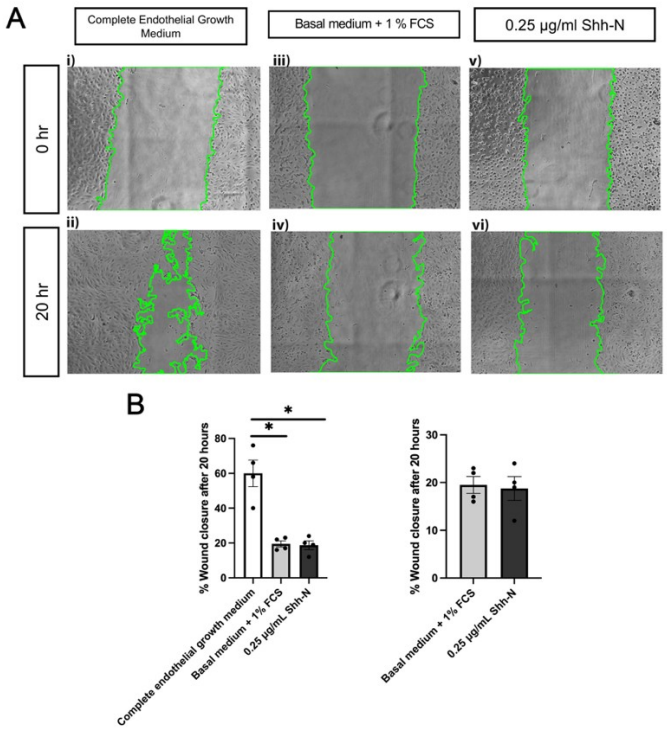

Figure 3.15. Effect of 0.25µg/mL SHH treatment on HUVEC wound closure.

(A) Representative light microscope images showing HUVEC wound closure following 20 hr culture of HUVECs with (i-ii) complete endothelial growth medium, (iii-iv) basal medium + 1 % FCS and (v-vi) 0.25 µg/mL SHH (experimental group). Widefield images taken at 10× using Zeiss Axio Observer (B) Graphs showing quantification of % wound closure in HUVECs after culturing for 20 hr. Data are presented as mean ± SEM (n = 4; Mann – Whitney U-test. *$p < 0.05$).

3.2.4.10 Treatment of HUVECs with Cyclopamine does not have an impact on wound closure

The effect of the SHH inhibitor, cyclopamine on HUVEC wound closure was also investigated. HUVECs were treated with 5 µg/mL cyclopamine in basal medium + 1 % FCS, basal medium + 1 % FCS alone or complete endothelial growth medium. As previously mentioned in section 3.2.4.5 cyclopamine was dissolved in EtOH prior to dilution in basal medium + 1 % FCS, resulting in a final EtOH concentration of 0.001 %. Therefore, HUVECs were treated with an equal concentration of EtOH in basal medium + 1 % FCS to ensure that EtOH did not have a cytotoxic effect on HUVECs. HUVECs cultured in complete endothelial medium had a mean percentage of wound closure of 70 % (Figure. 3.16A(i-ii), Figure. 3.16B), while cells in basal medium had a mean percentage of wound closure of 21.5 % (Figure. 3.16A(iii-iv), Figure. 3.16B). No significant difference was observed between the HUVECs treated with EtOH, which had a mean percentage of wound closure of 17 % (Figure. 3.16A(v-vi), Figure. 3.16B) and HUVECs treated with basal medium + 1 % FCS (Figure. 3.16A(iii-iv), Figure. 3.16B) (p =0.1429). Treatment with 5 µg/mL cyclopamine led to a mean wound percentage wound closure of 19.5 % (Figure. 3.16A vii-viii, Figure. 3.16B), which was not significantly different from HUVECs in basal medium + 1 % FCS (Figure. 3.16A(iii-iv), Figure. 3.16B) (P =0.3429).

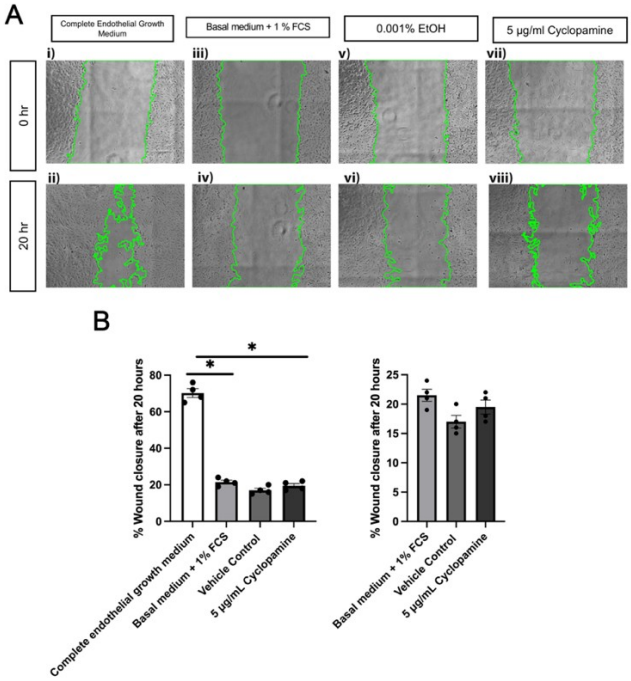

Figure 3.16. Effect of 5 µg/mL Cyclopamine treatment on HUVEC wound closure.

(A) Representative light microscope images showing HUVEC wound closure following 20 hr culture with (i-ii) complete endothelial growth (iii-iv) basal medium + 1 % FCS, (v-vi) 0.001 % EtOH (vehicle control) and (vii-viii) 5 µg/mL Cyclopamine(experimental group). Widefield images taken at 10× using Zeiss Axio Observer (B) Graphs showing quantification of % wound closure in HUVECs after culturing for 20 hr. Data are presented as mean ± SEM (n = 4; Mann – Whitney U-test. *p < 0.05.

3.2.5 Summary of main findings from wound healing assays

Investigation of Wnt, RA and SHH pathway modulators in wound repair revealed that WNT5A promoted repair in epithelial cells but had no effect on endothelial cells, while WNT9A showed no effect on either cell type. RA enhanced repair in endothelial cells but not in epithelial cells.

Modulation of SHH signalling inhibited repair in epithelial cells, and a slight, though not statistically significant increase in repair was also observed in epithelial cells following Shh inhibition with cyclopamine. Based on the findings from these wound healing assays (Table 3) and supporting evidence from published literature, the SHH signalling pathway was selected for further investigation in the context of alveolar repair following injury. To explore this, a more complex 3D model of lung injury; the Acid injury and Repair (AIR) model was employed to investigate the potential role of SHH.

Table 3.3. Table summarising the effects of Wnt, RA and SHH pathway modulators on repair of A549 cells and HUVECs

Factor	A549	HUVECs
WNT5A	↑	X
WNT9A	X	X
Retinoic Acid (RA)	X	↑
SHH-N	↓	X
Cyclopamine	X	X

3.2.6 Investigating the impacts of SHH pathway modulation in a 3D model of lung injury and repair

3.2.6.1 Generation of the Acid Injury and Repair (AIR) model

The Acid Injury and Repair (AIR) model is an *ex vivo* model that enables investigation of the cellular mechanisms of repair following injury(271, 276). To generate the AIR model, lung tissue is harvested from mice (Figure. 3.17(i)) and precision cut lung slices (PCLS) are prepared (Figure. 3.17(ii). A spatially restricted region of PCLS is generated by placing a cloning cylinder at one end of PCLS (Figure. 3.17(iii)). 500 µl of 0.1M HCl SF-DMEM is added to the region outside of the cloning cylinder and 100 µl HCl is applied to the restricted region for 1 min to produce injury. This results in a region of injured tissue adjacent to healthy, undamaged tissue (271, 276) (Figure. 3.17- 3.18A). After 1 min, the acid-injured region (Figure. 3.17(iii)) is washed 5 times with SF-DMEM to ensure that residual acid is removed and the cloning cylinder is removed. Acid-injured PCLS are then transferred to a 24-well plate and cultured in SF-DMEM at 37°C for 48h.

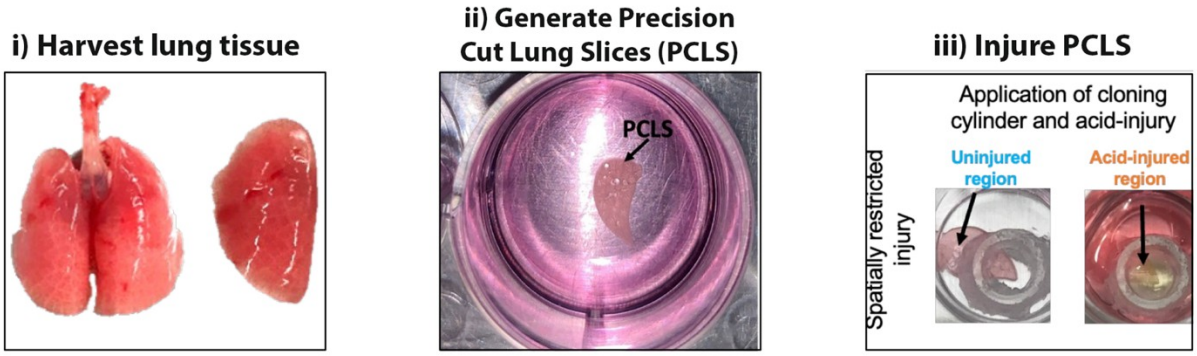

Figure 3.17. Generation of the AIR model using mouse precision cut lung slices (mPCLS).

Shows (i) Harvested lung tissue from mouse that is inflated using agarose. (ii) 300 µm PCLS generated after lobes are cut using a vibratome and (iii) Demonstrates how the AIR model is established using PCLS. A cloning cylinder and silicone grease is used to create a restricted area of injury. HCl is applied inside cloning cylinder to produce injury. Adapted from Kim SY, Mongey R, Wang P, Rothery S, Gaboriau DCA, Hind M, et al. The acid injury and repair (AIR) model: A novel ex-vivo tool to understand lung repair. Biomaterials. 2021; 267:120480.(271).

3.2.6.2 Live/Dead staining confirms restricted region of injury in AIR-PCLS

To confirm that PCLS treated with acid contained a distinct region of injury, as previously shown in Kim *et al*.(271), live/dead staining was conducted by incubating PCLS with calcein-

AM to identify live cells (yellow) and ethidium homodimer-1 (EthD-1) to identify dead cells (magenta). Widefield fluorescent images were taken at 10× magnification to capture the entire slice (Figure. 3.18B). Calcein-AM, is retained in the nucleus and cytoplasm of live cells, however, it is not retained by dead cells due to their compromised membrane integrity. Whereas EthD-1 is cell impermeant and cannot penetrate through the cell membrane of live cells, it therefore only stains dead cells. Control, uninjured PCLS contained mostly calcein positive, live cells (yellow) (Figure. 3.18B(i)) whilst methanol treated PCLS, used as a control for dead cells since methanol is toxic, contained EthD-1 positive, dead cells (magenta) (Figure. 3.18B(ii)). The majority of cells in the acid-injured region of AIR-PCLS showed EthD-1 positive staining in comparison to the uninjured region which contained a higher proportion of live calcein positive cells (Figure. 3.18B(iii)). This confirms that there was a restricted region of injury distinct from the uninjured region.

3.2.6.3 Modification of HCl concentration can be used alter the severity of injury

To determine the optimal concentration of HCl to use for further investigation and to confirm the suitability of 0.1 M HCl for acid injury, a dose response experiment was conducted (Figure 3.18C). Whole slice PCLS were injured for 1 min with either 0.01, 0.1 or 0.75 M HCl (Figure. 3.18C). MTT assays were then conducted as described in methods section 2.6.1, to assess the level of injury caused by increasing HCl concentrations. PCLS treated with 70 % methanol, which kills the cells thus arresting metabolic activity, were used as a control for no metabolic activity. Control, uninjured PCLS were included as positive controls, from which high metabolic activity would be expected. Control, uninjured PCLS were therefore used as a baseline reference for other treatments to be compared to. Changes in percentage viability of PCLS, were assessed relative to control, uninjured PCLS. As expected, there was a significant decrease in metabolic activity of PCLS treated with methanol (5 % viability) when compared to control, uninjured PCLS (p= 0.026) (Figure. 3.18C). Treatment with 0.75 M HCl resulted in a 94 % reduction in viability compared to control (0.06-fold-change), uninjured PCLS (p = 0.019) whilst treatment with 0.1 M resulted in a 55 % reduction in viability compared to control (0.45-fold change), uninjured PCLS (p= 0.05) (Figure. 3.18C). Confirming that 0.1 M induced significant injury but did not result in death of all cells, this HCl concentration was chosen for

all subsequent AIR model experiments. Whilst treatment with 0.01 M HCl resulted in a 20 % reduction in viability compared to the control (0.80-fold change).

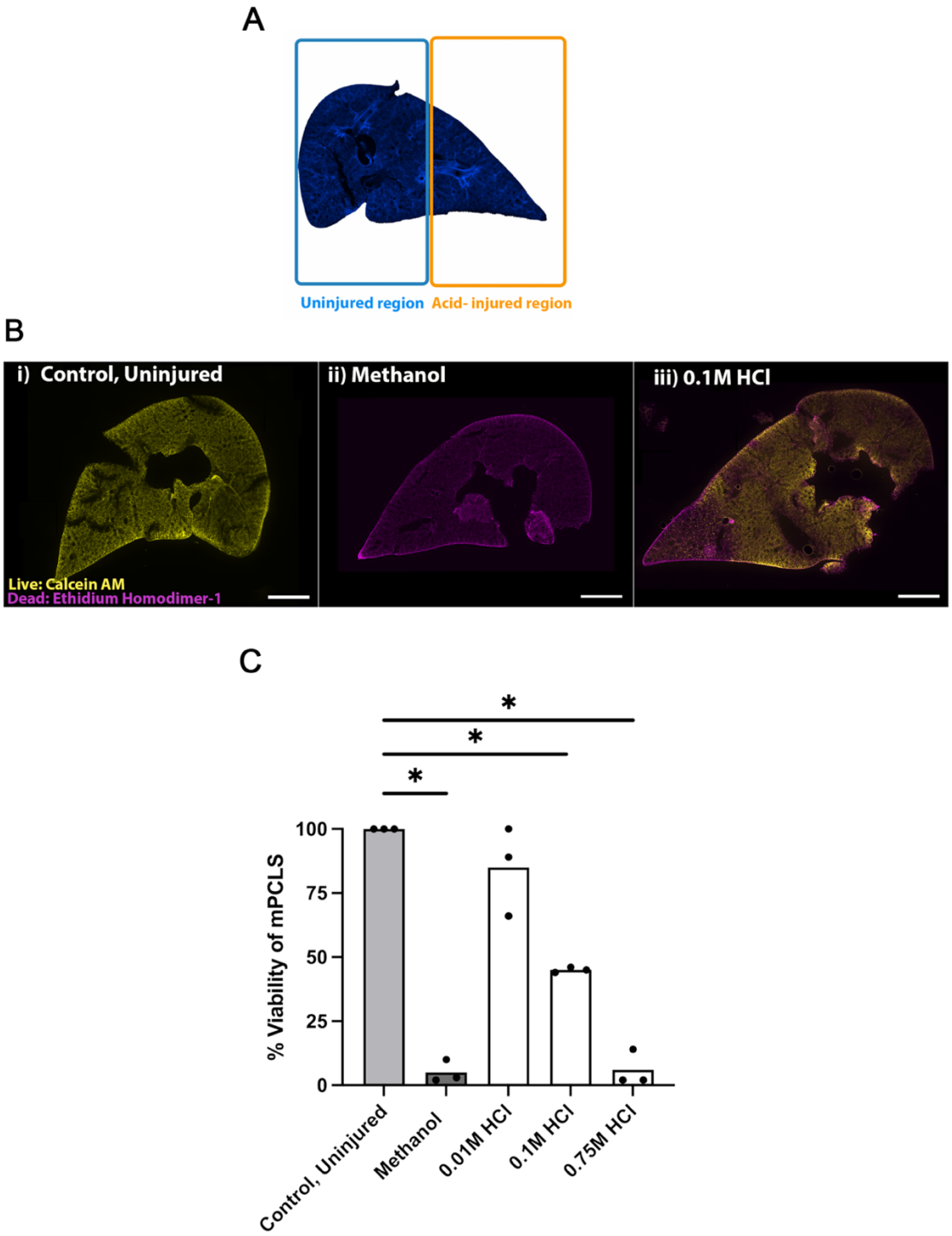

Figure 3.18. Viability assays to assess the use of 0.1M HCl for injury.

(A) Schematic illustrating the uninjured region (blue box) and the acid-injured region (orange box) of AIR- PCLS (B) Whole slice PCLS images taken at 10× using widefield microscopy showing live (Calcein AM, yellow) and dead (Ethidium Homodimer-1, magenta) cells in (i)control, uninjured, (ii) methanol and (iii) 0.1M acid-injured slices (n=3). Scale bars:Widefield whole slice = 1000 µm (B) MTT assay demonstrating reduction in PCLS viability with addition of increasing concentrations of HCl and methanol treatment (negative control) in comparison to control uninjured hPCLS (n = 3; Kruskal-Wallis test, Dunn's multiple comparisons test. *$p < 0.05$).

3.2.6.4 Use of the AIR model to investigate alveolar repair

Using the AIR model, specific cell populations, including alveolar epithelial cells, endothelial cells and fibroblasts can be labelled and tracked to precisely visualise and quantify alveolar repair. Two previously established markers, Ki67 for proliferating cells and proSP-C for progenitor cells were chosen to quantify repair (271, 276).

PCLS were generated and a spatially restricted injury was applied, as previously outlined in Kim *et al.* (271, 276). 48hr after injury, slices were fixed and immunostained with anti-prosurfactant protein-C(anti-proSP-C) (Figure. 3.19). Subsequently, slices were imaged and changes in proSP-C^+ cells were visualised. In these preliminary investigations, conducted to establish the model as previously described (271), markers of repair were not quantified (for quantification see section3.2.7. below). However, consistent with published data(271), an increase in proSP-C^+ cells was qualitatively observed in the acid-injured region of AIR-PCLS (Figure. 3.19(vii-viii)) compared to the uninjured region of AIR-PCLS (Figure. 3.19(v-vi)) and control, uninjured PCLS (Figure. 3.19(ii-iv)), indicating an active repair response

Cell proliferation was also assessed by immunostaining control, uninjured and AIR-PCLS with anti-Ki67 (Figure. 3.20). A higher number of $Ki67^+$ cells was observed in the uninjured region of AIR-PCLS (Figure. 3.20A(v-vi)) compared to both controls, uninjured PCLS (Figure. 2.20(iii-iv)), and the acid-injured region of AIR-PCLS (Figure. 3.20(vii-viii)), consistent with previous findings (271).

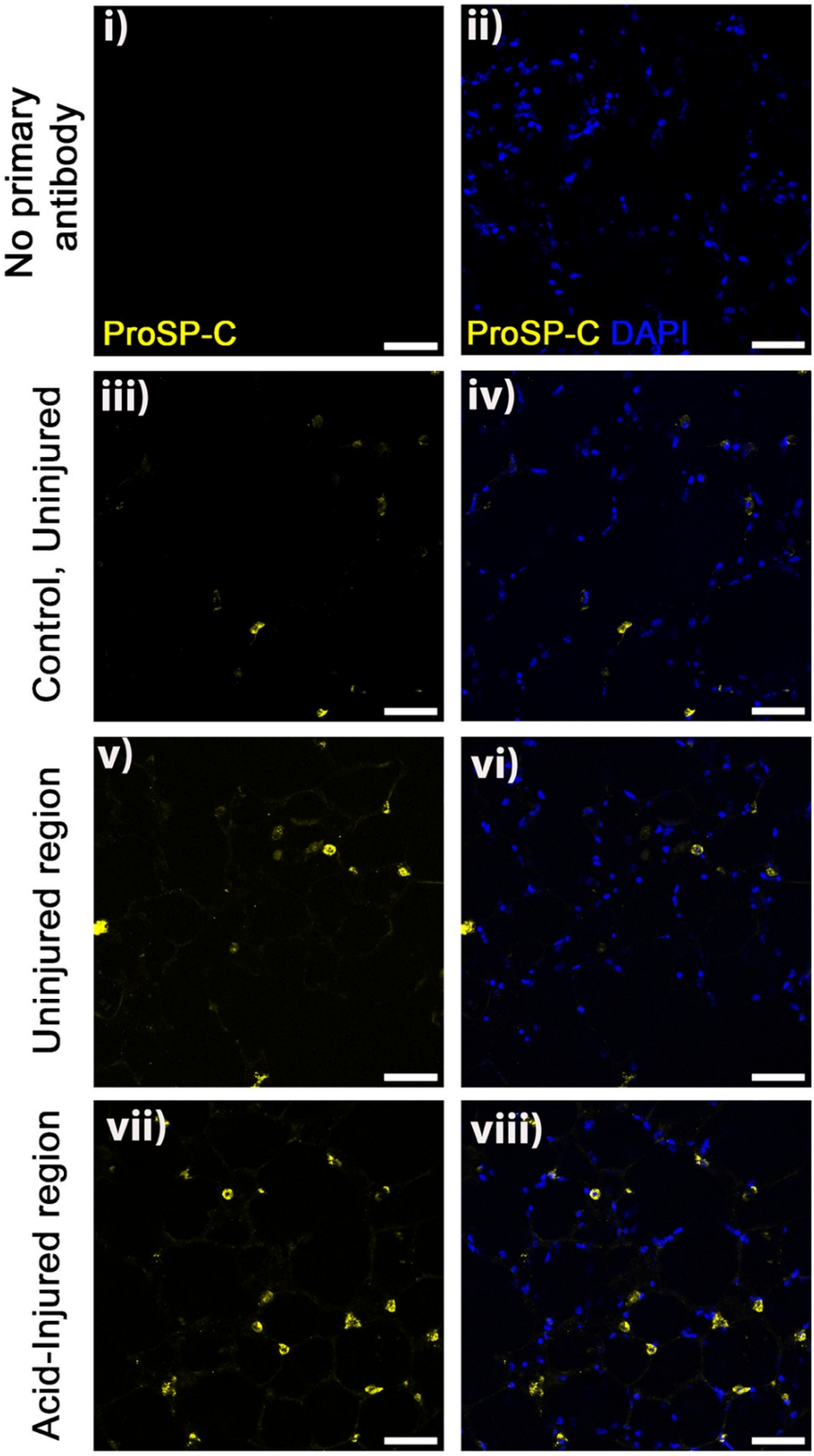

Figure 3.19. ProSP-C increases in the acid-injured region of AIR-PCLS post injury.

(i-ii) Shows no primary antibody staining for proSP-C in control, uninjured PCLS. Immunofluorescence staining for ProSP-C (yellow) and DAPI (blue) in (iii-iv) control, uninjured PCLS and (v-vi) uninjured region and (vii-viii)acid-injured regions of PCLS with spatial acid injury (AIR model), Widefield images taken at 40× magnification, scale bar= 50 µm.

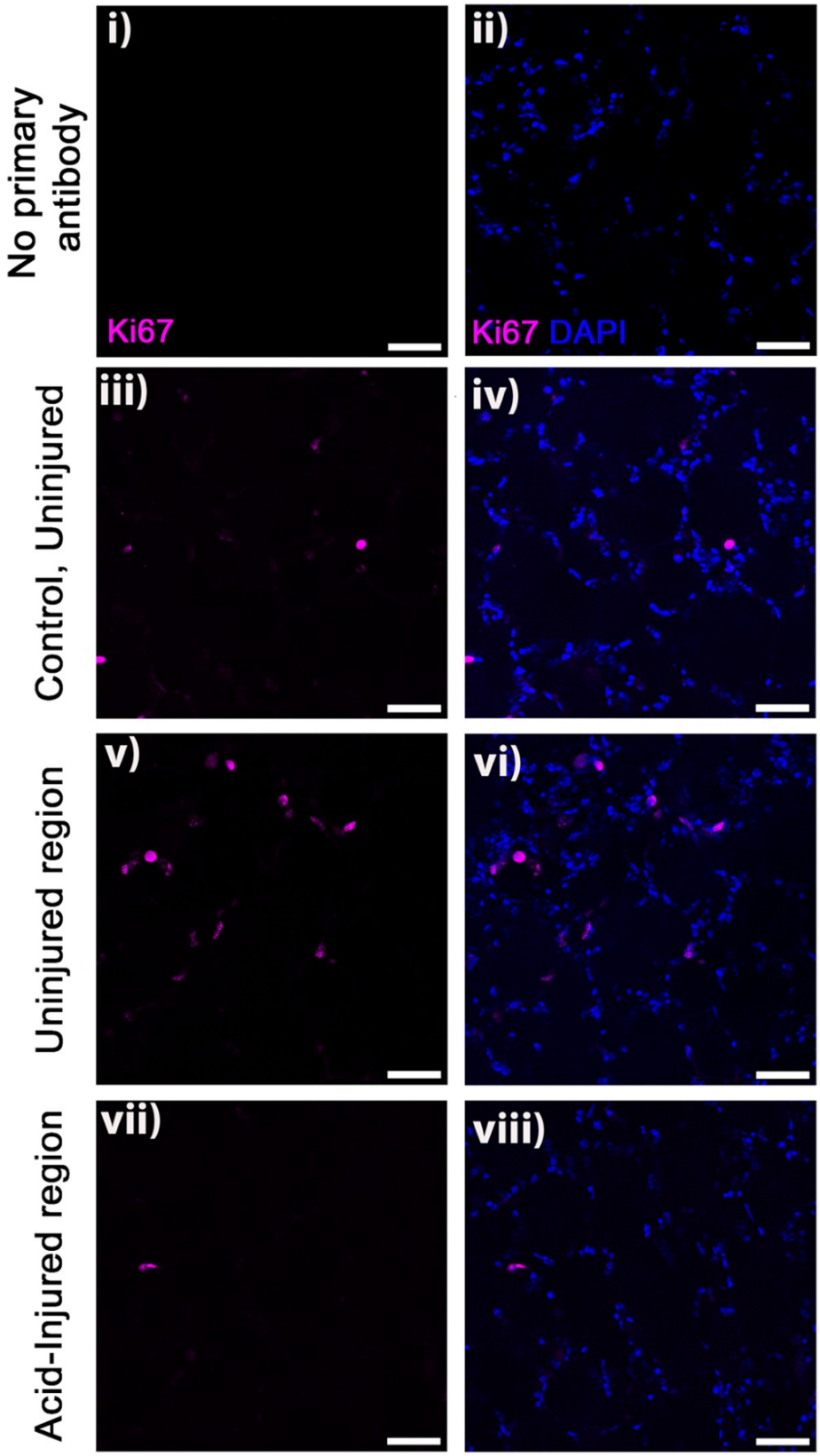

Figure 3.20. Ki67 increases in the uninjured region of AIR-PCLS post injury.

(i-ii) Shows no primary antibody staining for Ki67 in control, uninjured PCLS. Immunofluorescence staining for Ki67 (pink) and DAPI (blue) in (iii-iv) control, uninjured PCLS and (v-vi) uninjured region and (vii-viii)acid-injured regions of PCLS with spatial acid injury (AIR model), Widefield images taken at 40× magnification, scale bar= 50 µm.

Having successfully generated the AIR model in PCLS and observed an increase in the percentage of proSP-C^{+} progenitor cells in the injured region of PCLS and a corresponding increase in ki67^{+} proliferating cells in the uninjured region, AIR-PCLS were treated with either SHH or cyclopamine, to investigate the effects of SHH signalling on alveolar repair.

3.2.6.5 Determining appropriate concentrations of Shh for investigation

As previously stated, pathways were selected and modulators to potentiate and block each pathway were identified. Next, the appropriate concentration range was chosen for each factor. Concentrations to be used in experiments were chosen by using both information from published research and the ED_{50} values provided in the company datasheets that factors were purchased from. Since wound healing assays were conducted to obtain preliminary information, only one concentration was chosen within a range. Taking into account findings from wound healing assays and existing published literature I chose to focus investigations for this section on the impact of SHH on repair. The activity range of SHH was studied further to determine a high, mid and low concentration to use (352). The working concentrations used for SHH were 0.1, 0.25,0.5 µg/mL, whilst the working concentrations used for the SHH inhibitor cyclopamine were 2.5 µg/mL, 5 µg/mL, 10 µg/mL.

3.2.6.6 Investigating viability of PCLS treated with SHH

As previously highlighted, after studying the literature and data sheets, the following 3 concentrations of SHH were chosen to conduct investigations: 0.1, 0.25 or 0.5 µg/mL. To investigate the potential role of the SHH pathway in lung repair, the pathway was stimulated with 0.1, 0.25 or 0.5 µg/mL SHH- N recombinant protein. Whole slice PCLS were treated with each concentration of SHH for 48 hrs. Following this, MTT assays were conducted to determine whether factors had a detrimental effect on PCLS in the absence of acid injury before setting up the AIR model with treatments. The assay was repeated three times (three biological replicates), with 3 technical replicates for each condition within an individual biological replicate (Figure. 3.21). When compared to control, uninjured PCLS, treatment with 0.1 µg/mL SHH resulted in a viability of 88 % ($p=0.4061$), there was no statistically significant difference. Similarly, there was no statistically significant difference in PCLS treated with 0.25

µg/mL SHH with a viability of 95 % (p > 0.9999) or 0.5 µg/mL SHH with a viability of 97 % (p > 0.9999) (Figure. 3.21). These findings indicate that SHH treatment does not compromise tissue viability and therefore supports the use of the AIR model to investigate the potential role of SHH in lung repair without introducing further injury to the lung tissue.

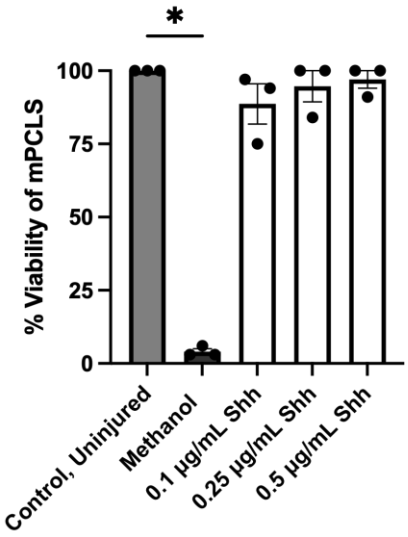

Figure 3.21. SHH treatment does not have a significant impact on PCLS viability.
MTT assay demonstrating that SHH-N treatment does not lead to a significant reduction in PCLS viability compared to control-uninjured PCLS and methanol treated PCLS (n=3; Kruskal-Wallis test, Dunn's multiple comparisons test. *p < 0.05).

3.2.6.7 Sonic Hedgehog (SHH) treatment led to a trend towards an increase in progenitor cells in the acid-injured region of AIR-PCLS

Next, the effect of SHH treatment on alveolar markers of repair following injury was investigated using the AIR model. 48hr after injury and following 48 hr treatment with selected concentrations of SHH, slices were fixed and immunostained with anti-prosurfactant protein-C(anti-proSP-C). Subsequently, slices were imaged and for each PCLS, proSP-C$^+$ cells were quantified at three distinct fields of view within both the uninjured and acid-injured regions of AIR-PCLS, as well as in control, uninjured PCLS, as detailed in methods (chapter 2 section 2.13.1). Untreated slices were included as controls to assess changes in the progenitor cell population following injury. As data for untreated slices has been previously published (271) and the findings were similarly observed in section 3.2.6.4, showing an increase in the proSP-C$^+$ progenitor cell population in the acid-injured region of AIR slices compared to both the uninjured region and control, uninjured PCLS, these findings serve as a baseline for comparison with SHH treated PCLS.

Quantification of samples without SHH treatment showed that the mean percentage of proSP-C^+ cells in the acid-injured region of AIR-PCLS was 12 % (Figure. 3.22) compared to 8.6 % in uninjured region of AIR-PCLS (Figure. 3.22, p >0.9999) and 7 % in control, uninjured PCLS (Figure. 3.22, p >0.9999), indicating an active repair response, as previously published (3, 274). However findings were not statistically significant.

SHH treatment across all concentrations tested (0.1, 0.25 or 0.5 µg/mL), did not result in significant changes in the proSP-C^+ cell population (Figure. 3.22). In the uninjured region of AIR-PCLS, treatment with 0.1 µg/mL SHH led to a a 1.1- fold change (≈ 8.1 % increase) in proSP-C^+ cells in comparison to the uninjured region of untreated AIR-PCLS (Figure. 3.22A(i), Figure. 3.22B, p >0.9999), while 0.25µg/mL SHH led to a 0.81-fold change (≈ 19 % decrease) compared to the uninjured region of untreated AIR-PCLS (Figure. 3.22A(iii), Figure. 3.22B, P >0.9999), and 0.5 µg/mL SHH resulted in a 1.4-fold change (≈ 40 % increase, Figure. 3.22A(v), Figure. 3.22B).

Whereas when the acid-injured region of untreated AIR-PCLS (mean percentage of proSP-C^+ cells of 12 %) was compared to the acid-injured region of AIR-PCLS treated with 0.1 µg/mL SHH there was a 1-fold change (≈ 2.5 % increase, mean=12.3 %, Figure. 3.22A(ii), Figure. 3.22B, p >0.9999), a 0.8-fold change (≈ 16.7 % decrease) with 0.25 µg/mL SHH treatment (mean= 10 %, Figure. 3.22A(iv), Figure. 3.22B, p >0.9999) and a 0.94- fold change (≈ 5.8 % decrease) with 0.5 µg/mL SHH treatment (mean=11.3 %, Figure. 3.22A(vi), Figure. 3.22B, p >0.9999).

Overall, when comparing data from the uninjured regions and acid-injured regions of AIR-PCLS treated with different concentration of SHH, differences observed were not statistically significant.

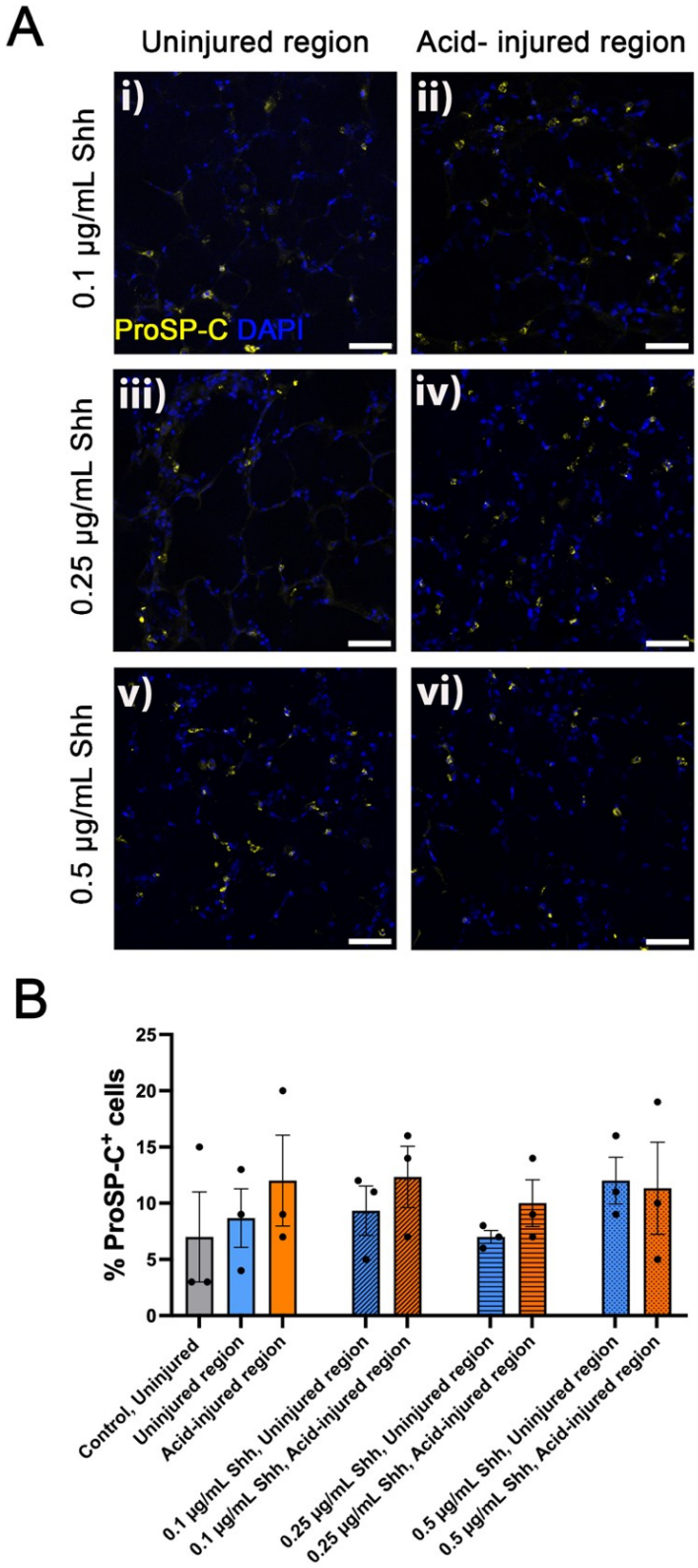

Figure 3.22. Investigating the impact of SHH treatment on changes in ProSP-C post injury using the AIR model.

(A) Immunofluorescence staining for ProSP-C (yellow) and DAPI (blue) in the uninjured and acid-injured regions of AIR-PCLS treated with (i-ii) 0.1 µg/ml, (iii-iv) 0.25 µg/ml, (v-vi) 0.5 µg/ml Shh, Widefield images taken at 40× magnification, scale bar= 50 µm. (B) Graph showing quantification of ProSP-C$^+$ cells in untreated controls and the uninjured and acid-injured regions of Shh treated AIR-PCLS (n = 3; Kruskal-Wallis test, Dunn's multiple comparisons test. *$p < 0.05$).

3.2.6.8 Sonic Hedgehog (Shh) treatment did not have an effect on proliferation in AIR-PCLS

Changes in cell proliferation were also assessed by immunostaining Shh treated AIR-PCLS with anti-Ki67. Here, untreated samples were included as controls to assess changes in proliferating cells following injury. Concordant with previously published data (271), I found a 3.5-fold change (≈ 253 % increase) in $Ki67^+$ cells in the uninjured region of AIR-PCLS (mean= 6 %, Figure. 3.23) compared to the acid-injured region of AIR-PCLS (mean = 1.7 %, Figure. 3.23, p= 0.5982), and a 1.5-fold change (≈ 50 % increase) in $Ki67^+$ cells in the uninjured region of AIR-PCLS compared to control, uninjured PCLS (mean=4 %, Figure. 3.23, p=0.8718). However, this was not statistically significant.

Similar to proSP-C data, SHH treatment across all concentrations tested (0.1, 0.25 or 0.5 µg/mL), did not lead to a significant difference in the $KI67^+$ cell population (Figure. 3.23). In the uninjured region of AIR-PCLS, the general trend was an increase in $Ki67^+$ cells in the uninjured region when compared to the acid-injured region irrespective of the concentration of SHH treatment.

In the uninjured region of AIR-PCLS, treatment with 0.1 µg/mL SHH led to a 0.88- fold change (≈ 11.7 % decrease) in $Ki67^+$ cells compared to the uninjured region of untreated AIR-PCLS (mean = 5.3 %, Figure. 3.23A(i), Figure. 3.23B, p >0.9999). Treatment with 0.25µg/mL resulted in a mean of 6 % $Ki67^+$ cells, which was identical to the uninjured region of untreated AIR-PCLS (Figure. 3.23A(iii), Figure. 3.23B, P >0.9999). 0.5 µg/mL SHH resulted in a 0.83- fold change (≈ 16.7 % decrease in $Ki67^+$ cells (mean= 5 %, Figure. 3.23A(v), Figure. 3.23B).

Whereas when the acid-injured region of untreated AIR-PCLS (mean percentage of $Ki67^+$ cells of 1.7 %) was compared to the acid-injured region of AIR-PCLS treated with 0.1 µg/mL SHH a 1.18-fold change (≈ 17.6 % increase) was observed (mean=2 %, Figure. 3.23A(ii), Figure. 3.23B, p >0.9999). Treatment with 0.25 µg/mL SHH led to a 0.76-fold change (≈ 23.5 % decrease) in $Ki67^+$ cells (mean= 1.3 %, Figure. 3.23A(iv), Figure. 3.22B, p >0.9999) and 0.5 µg/mL SHH treatment also led to a 0.76-fold change (≈ 23.5 % decrease) in Ki67+ cells (mean=1.3 %, Figure. 3.23A(vi), Figure. 3.23B, p >0.9999).

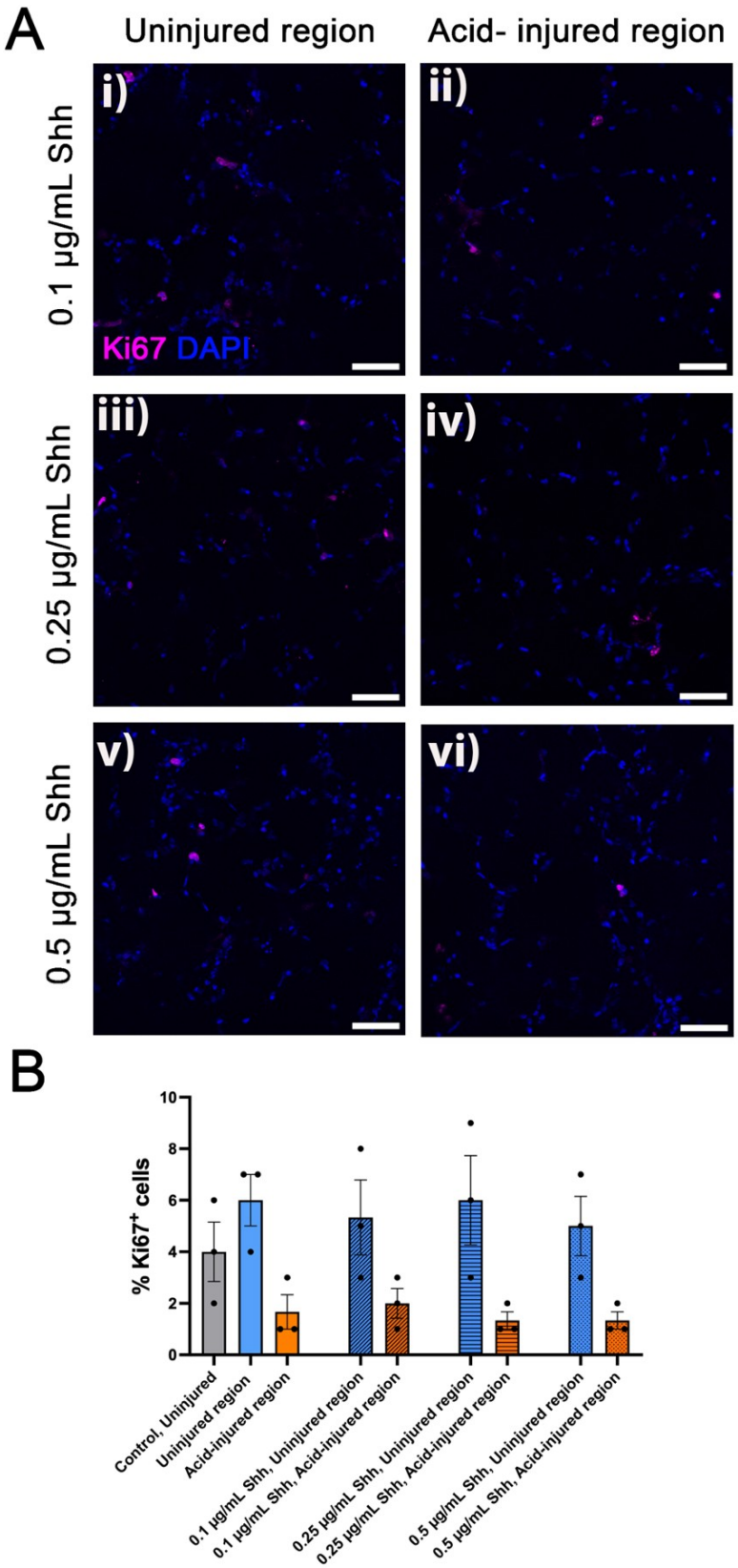

Figure 3.23. Investigating the impact of SHH treatment on changes in Ki67 post injury using the AIR model.
(A) Immunofluorescence staining for Ki67 (pink) and DAPI (blue) in the uninjured and acid-injured regions of AIR-PCLS treated with (i-ii) 0.1 µg/ml, (iii-iv) 0.25 µg/ml, (v-vi) 0.5 µg/ml SHH, Widefield images taken at 40× magnification, scale bar= 50 µm. (B) Graph showing quantification of $Ki67^+$ cells in untreated controls and the uninjured and acid-injured regions of SHH treated AIR-PCLS(n = 3; Kruskal-Wallis test, Dunn's multiple comparisons test. *$p < 0.05$).

3.2.6.9 Selection of cyclopamine concentrations and viability assessment

To determine the impact of blocking the SHH pathway, PCLS were treated with the smoothened inhibitor cyclopamine, at concentrations of 2.5, 5 and 10 µg/mL for 1 min, following a similar protocol to section 3.2.6.3. An MTT assay was conducted to determine whether cyclopamine had an impact on the viability/metabolic activity of whole slice PCLS. Each PCLS slice was treated for 1 min with the respective concentration of cyclopamine. Cyclopamine was resuspended in ethanol (as summarised in table. 2.1 in section 2.5.2 of the materials and methods), therefore, to determine whether EtOH had a cytotoxic effect, an equivalent volume of EtOH was applied to a separate group of PCLS. The assay was repeated three times (three biological replicates), with 3 technical replicates per condition (Figure. 3.24).

When compared to control, uninjured PCLS treatment with 2.5 µg/mL cyclopamine resulted in a viability of 95 % ($p > 0.9999$), with no statistically significant difference. Similarly, PCLS treated with 5 µg/mL cyclopamine had a viability of 94 %, which was also not statistically significantly different compared to control, uninjured PCLS ($p > 0.9999$). Treatment with 10 µg/mL cyclopamine yielded a viability of 82 %, which was also not statistically significantly different ($p = 0.2903$). Additionally, EtOH treated PCLS, with a viability of 81 %, did not have a significant impact on the viability of PCLS in comparison to control, uninjured PCLS ($p=0.2215$) (Figure. 3.24). A significant difference was only observed between control, uninjured PCLS and methanol treated PCLS which had a viability of 3 % ($p=0.0058$) (Figure. 20). As previously stated methanol was used as a positive control for no metabolic activity i.e. cell death.

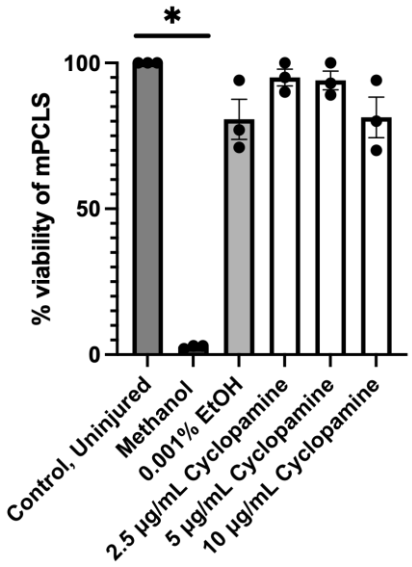

Figure 3.24. Cyclopamine treatment does not have a significant impact on PCLS viability.
MTT assay demonstrating that Cyclopamine treatment does not lead to a significant reduction in PCLS viability compared to control-uninjured PCLS and methanol treated PCLS (n=3; Kruskal-Wallis test, Dunn's multiple comparisons test. *p < 0.05).

3.2.6.10 Cyclopamine treatment causes a decrease in proSP-C⁺ cells in the acid-injured region of AIR-PCLS

Following cell viability studies, the impact of cyclopamine treatment on the alveolar markers of repair was investigated. First, changes in progenitor cells (proSP-C) were investigated in AIR -PCLS, as previously performed for SHH treated AIR-PCLS (section 3.2.7.3-3.2.7.4). Quantification of samples without cyclopamine treatment showed that the mean percentage of proSP-C$^+$ cells in the acid-injured region of AIR-PCLS was 18 % (Figure. 3.25) compared to 11 % in uninjured region of AIR-PCLS (Figure. 3.25, p = 0.2137) and 9 % in control, uninjured PCLS (Figure. 3.25, p =0.0724), indicating an active repair response, as previously published (3, 274). However findings were not statistically significant.

Since cyclopamine was resuspended in EtOH (as summarised in table. 2.1 in section 2.5.2 of the materials and methods), AIR-PCLS were also treated with an equivalent concentration of EtOH (0.001 %) to assess whether EtOH affected the repair capability of PCLS in the absence of cyclopamine. Changes in the proportion of proSP-C$^+$ cells were quantified to determine any potential impact of EtOH on tissue repair (Figure. 3.25A, Figure. 3.25C). In the uninjured region of AIR-PCLS treated with 0.001 % EtOH, the mean percentage of proSP-C$^+$ cells was 10 %, which was not significantly different from the uninjured region of untreated AIR-PCLS where the

mean percentage of proSP-C$^+$ cells was 11 % (Figure. 3.25A, Figure. 3.25C, p>0.9999). Similarly, in the acid-injured region of AIR-PCLS treated with 0.001 % EtOH, the mean percentage of proSP-C$^+$ cells was 14 %, compared to 18 % in the acid-injured region of untreated AIR-PCLS, no statistically significant difference was observed (Figure. 3.25A, Figure. 3.25C, p>0.9999). To further ensure that the EtOH (vehicle) did not significantly affect changes in the proSP-C$^+$ cell population, control, uninjured PCLS were treated with the selected concentrations of cyclopamine and changes in the proSP-C$^+$ cells were assessed along with AIR-PCLS (Figure. 3.25B-3.25C).

When control, uninjured PCLS treated with 2.5 µg/mL cyclopamine were compared to untreated PCLS, there was a 0.78-fold change (≈ 22 % decrease) observed; however, this difference was not statistically significant (mean = 7%, Figure. 3.25B(i-iii), Figure. 3.25C, p>0.9999). In contrast, treatment with 5 µg/mL cyclopamine led to a 1.2- fold change (≈ 22 % increase) (mean = 11 %, Figure. 3.25B(iv-vi), Figure. 3.25C), while treatment with 10 µg/mL cyclopamine led to a 0.89-fold change (≈ 11 % decrease) in the uninjured region (mean = 8 %, Figure. 3.25B(vii-ix), Figure. 3.25C) (p>0.9999); neither change were statistically significant.

In the uninjured region of AIR-PCLS treated with 2.5 µg/mL cyclopamine, the mean proSP-C$^+$ cell percentage was 10 %, a 0.91-fold change (≈ 9.1 % decrease) compared to the uninjured region of untreated AIR-PCLS (Figure. 3.25B(i-iii), Figure. 3.25C, p>0.9999). Treatment with 5 µg/mL cyclopamine, led to a mean of 11 %, identical to the treatment group (Figure. 3.25B(iv-vi), Figure. 3.25C, p>0.9999). In uninjured region of AIR-PCLS treated with 10 µg/mL cyclopamine, the mean was 13 %, a 1.2- fold change (≈ 18 % increase) compared to the untreated group (Figure. 3.25B(vii-ix), Figure. 3.25C, p>0.9999).

In the acid-injured region of AIR-PCLS treated 2.5 µg/mL cyclopamine, the mean proSP-C$^+$ cell percentage was 8 %, a 0.44- fold change (≈56 % decrease) compared to the acid-injured region of untreated AIR-PCLS (Figure. 3.25B(i-iii), Figure. 3.25C, p=0.0566). Similarly, treatment with 5 µg/mL cyclopamine, led to a mean of 8 % (Figure. 3.25B(iv-vi), Figure. 3.25C, p=0.0566). In contrast, treatment with 10 µg/mL cyclopamine led to a mean of 11 %, a 0.61-fold change (≈ 39 % decrease) compared to untreated AIR-PCLS, this difference was not statistically significant. (Figure. 3.25B(vii-ix), Figure. 3.25C, p=0.8777).

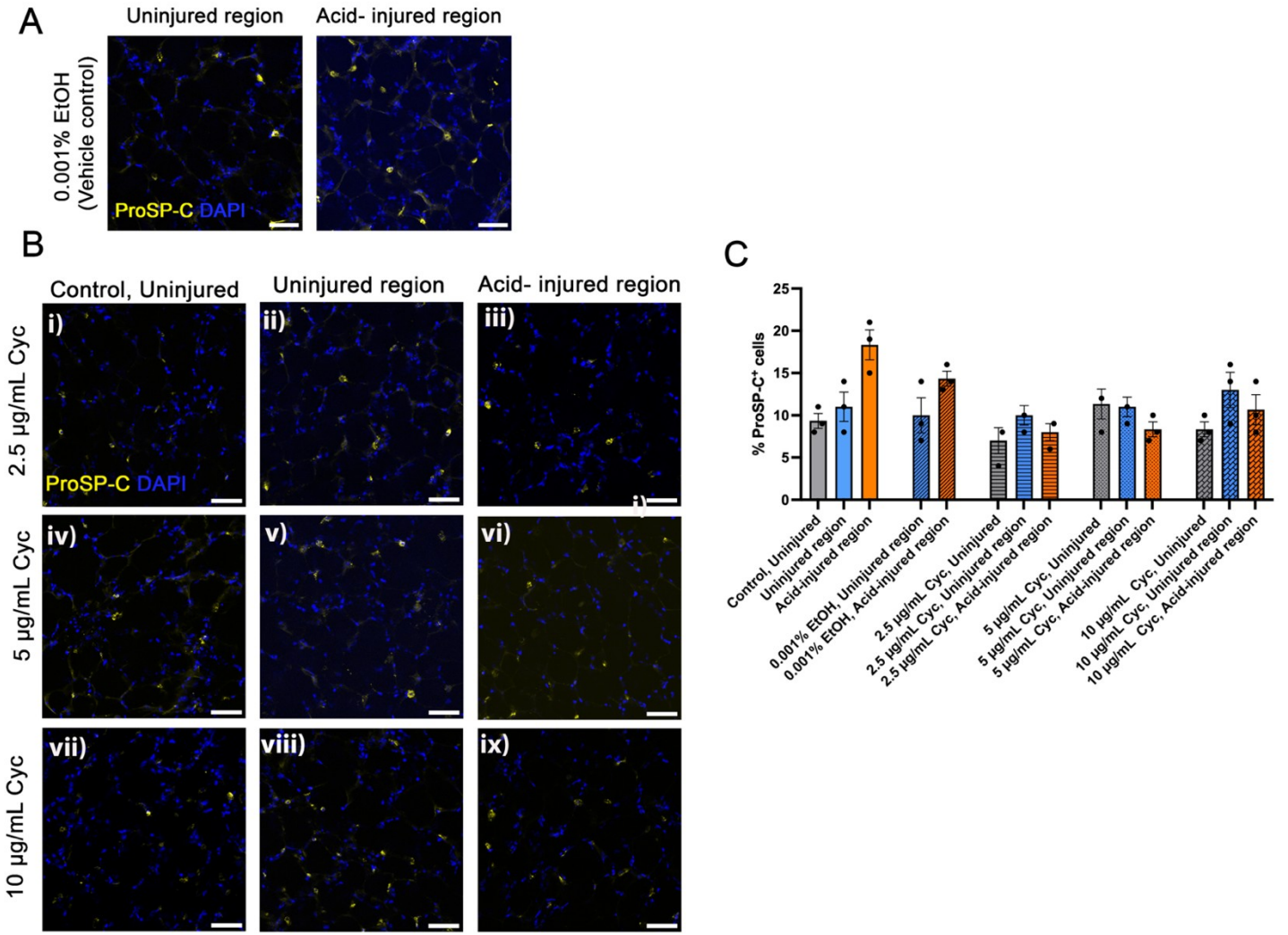

Figure 3.25. Investigating the impact of Cyclopamine treatment on changes in ProSP-C post injury using the AIR model.

(A)Immunofluorescence staining for ProSP-C (yellow) and DAPI (blue) in AIR-PCLS treated with 0.001 % EtOH(vehicle) (B) Immunofluorescence staining for ProSP-C (yellow) and DAPI (blue) in control, uninjured PCLS and the uninjured region and acid-injured region with (i-iii) 2.5 µg/mL, (iv-vi) 5 µg/mL, (vii-ix) 10 µg/mL cyclopamine, Widefield images taken at 40× magnification, scale bar= 50 µm. (C) Graph showing quantification of ProSP-C$^+$ cells in untreated controls, the uninjured and acid-injured regions of EtOH treated AIR-PCLS and in control, uninjured PCLS treated with cyclopamine and the uninjured and acid-injured regions of cyclopamine treated AIR-PCLS(n = 3; Kruskal-Wallis test, Dunn's multiple comparisons test. *p < 0.05).

3.2.6.11 Treatment with Cyclopamine an inhibitor of Sonic Hedgehog (Shh) does not have an impact on the Ki67⁺ cell population

Next, changes in proliferating cells were investigated in AIR-PCLS treated with cyclopamine. Untreated samples were included as controls to assess proliferation in the absence of cyclopamine. In control, uninjured PCLS, the mean percentage of $Ki67^+$ cells was 6 % (Figure. 3.26). In the uninjured region of AIR-PCLS, a 1.3-fold change (≈ 33 % increase) was observed, with a mean of 8 %, compared to control, uninjured PCLS (Figure. 3.26, $p>0.9999$) and the acid-injured region of AIR-PCLS, which had a mean of 4 % (Figure. 3.26, $p>0.9999$), which was a 0.67-fold change (≈ 33 % decrease). Although these findings were not statistically significant, the trend was consistent with previously published data (271).

Changes in the proportion of $Ki67^+$ cells were also quantified in AIR-PCLS treated with 0.001 % EtOH to determine any potential impact of EtOH on tissue repair in the absence of cyclopamine since cyclopamine was reconstituted in this concentration of EtOH (Figure. 3.26A, Figure. 3.26C). In the uninjured region of AIR-PCLS treated with 0.001 % EtOH, the mean percentage of $Ki67^+$ cells was 5 %, which was not significantly different from the uninjured region of untreated AIR-PCLS where the mean percentage of $Ki67^+$ cells was 8 % (Figure. 3.26A, Figure. 3.26C, $p=0.9346$). Similarly, in the acid-injured region of AIR-PCLS treated with 0.001 % EtOH the mean was 4 % which was identical to untreated AIR-PCLS (Figure. 3.26A, Figure. 3.26C, $p>0.9999$).

When control, uninjured PCLS treated with 2.5 µg/mL cyclopamine were compared to untreated PCLS, a 1 % decrease was observed; however, this difference was not statistically significant (mean= 5 %, Figure. 3.26B(i-iii), Figure. 3.26C, $p>0.9999$). In contrast, treatment with 5 µg/mL cyclopamine led to a 1 % increase (mean = 7 %, Figure. 3.26B(iv-vi), Figure. 3.26C, $p>0.9999$), while treatment with 10 µg/mL cyclopamine led to a mean of 6 % which was identical to untreated PCLS (3.26B(vii-ix), Figure. 3.26C, $p>0.9999$).

In the uninjured region of AIR-PCLS treated with 2.5 µg/mL cyclopamine, the mean percentage of $Ki67^+$ cells was 5.3, a 0.66-fold change (≈ 34 % decrease) compared to the uninjured region of untreated AIR-PCLS (Figure. 3.26B(i-iii), Figure. 26C, $p=0.4623$). Treatment with 5 µg/mL

cyclopamine resulted in a mean of 4.6 %, a 0.58-fold change (≈ 43 % decrease) (Figure. 3.26B(iv-vi), Figure. 3.26C, p=0.3760). Similarly, treatment with 10 µg/mL cyclopamine led to a mean of 5.3 % (Figure. 3.26B(vii-ix), Figure. 3.26C, p=0.4623).

In the acid-injured region of AIR-PCLS, none of the changes observed were statistically significant. Treatment with 2.5 µg/mL cyclopamine resulted in a mean $Ki67^+$ cell percentage of 4.3 %, a 1.1-fold change (≈ 7.5 % increase) compared to the acid-injured region of untreated AIR-PCLS (Figure. 3.26B(i-iii), Figure. 26C, p>0.9999). Treatment with 5 µg/mL cyclopamine resulted in a mean of 5.3 %, a 1.4-fold change (≈ 32.5 % increase) (Figure. 3.26B(iv-vi), Figure. 3.26C, p>0.9999), and treatment with 10 µg/mL cyclopamine led to a mean of 5.7 %, a 1.43-fold change (≈ 42.5 % increase) (Figure. 3.26B(vii-ix), Figure. 3.26C, p=0.6869).

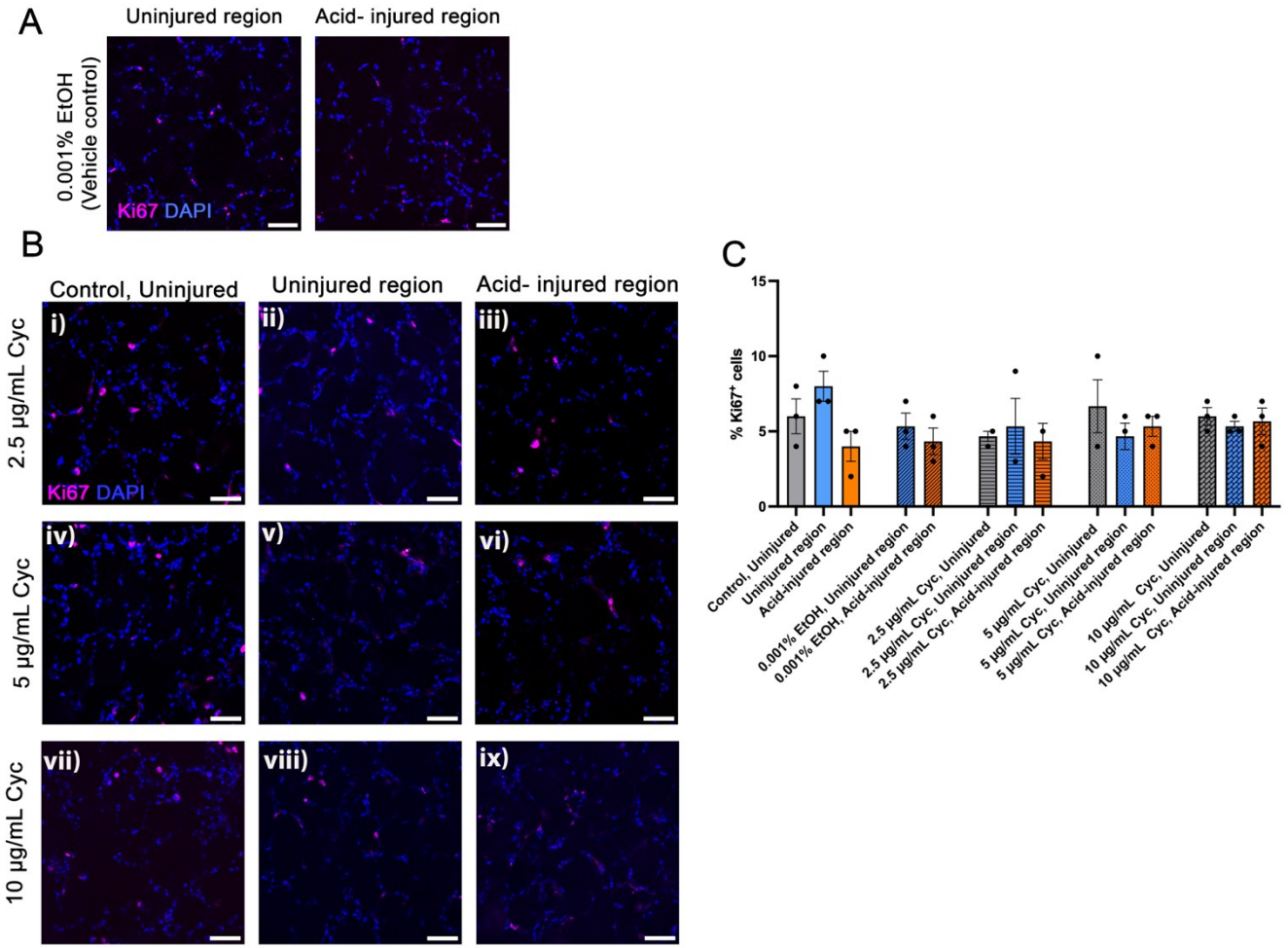

Figure 3.26. Investigating the impact of Cyclopamine treatment on changes in Ki67 post injury using the AIR model.

(A)Immunofluorescence staining for Ki67 (pink) and DAPI (blue) in AIR-PCLS treated with 0.001 % EtOH(vehicle) (B) Immunofluorescence staining for Ki67 (pink) and DAPI (blue) in control, uninjured PCLS and the uninjured region and acid-injured region with (i-iii) 2.5 µg/mL, (iv-vi) 5 µg/mL, (vii-ix) 10 µg/mL cyclopamine, Widefield images taken at 40× magnification, scale bar= 50 µm. (C) Graph showing quantification of $Ki67^{+}$cells in untreated controls, the uninjured and acid-injured regions of EtOH treated AIR-PCLS and in control, uninjured PCLS treated with cyclopamine and the uninjured and acid-injured regions of cyclopamine treated AIR-PCLS(n = 3; Kruskal-Wallis, test, Dunn's multiple comparisons test. *$p < 0.05$).

3.2.6.12 *Sample size analysis highlights need for additional replicates to reach statistical significance*

After analysing the results from the AIR model investigations, where AIR-PCLS were treated with either SHH or cyclopamine, and observing a lack of statistically significant findings, I conducted sample size calculations to determine whether the lack of statistical power was due to an insufficient sample size. These calculations were performed using the GraphPad Prism Cloud power analysis and sample size calculator. In experiments where AIR-PCLS were treated with SHH, there were 9 experimental groups (Figure. 3.22-3.23), each with 3 biological replicates (as summarised in section 3.2.7.3). There were 14 experimental groups, each with 3 biological replicates where AIR-PCLS were treated with cyclopamine (Figure. 3.25-3.24). Statistical analysis was performed using the Kruskal-Wallis test with Dunn's post-test, a non-parametric alternative to the one-way ANOVA. Sample size calculations were based on these test parameters (Figure. 3.27). The results indicated that a sample size of 3 biological replicates was inadequate. Specifically, to obtain statistically significant results (80 % power), at least 6 biological replicates would be required for AIR-PCLS treated with SHH and at least 5 biological replicates would be required for those treated with cyclopamine (Figure. 3.27).

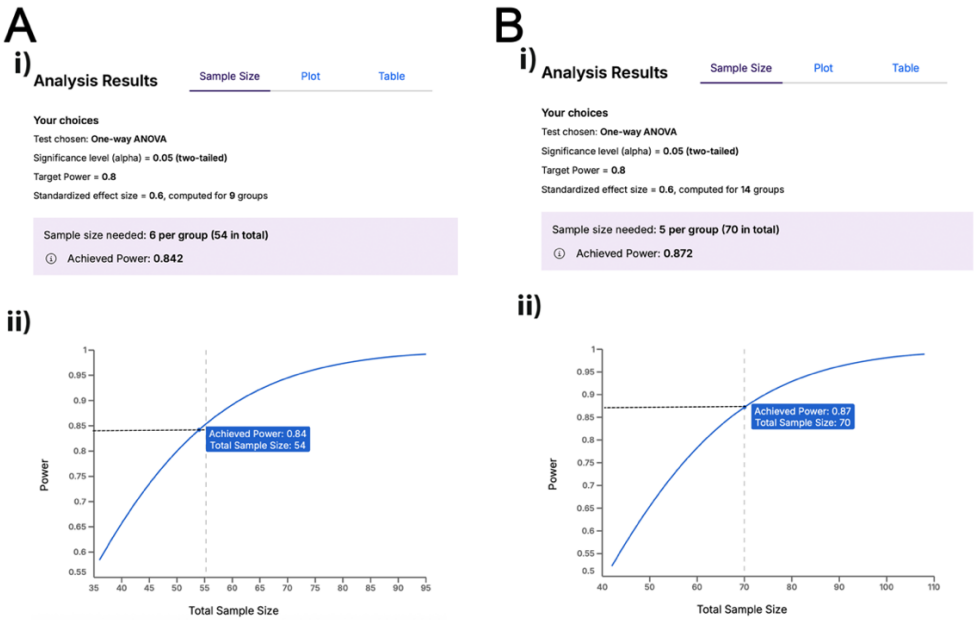

Figure 3.27. Sample size calculations following AIR model investigations with* SHH *and cyclopamine treatment.
Sample size calculations conducted to determine whether lack of statistically significant results in AIR-PCLS experiments was due to insufficient biological replicates. (A) Results for AIR-PCLS treated with SHH (i) Shows output summary indicating the required sample size per experimental group to achieve adequate power (ii) Graph showing the relationship between statistical power (y axis) and total sample size (x axis). (B) Results for AIR-PCLS treated with Cyclopamine (i) Output summary of required sample size per experimental group to achieve adequate power (ii) Graph showing the relationship between statistical power (y axis) and total sample size (x axis).

3.2.6.13 SHH treatment led to an increase in vimentin labelling in AIR-PCLS

Mouse models have contributed significantly to our understanding of SHH signalling in the lung. Notably, these studies have demonstrated that SHH signalling plays a key role in regulating the mesenchymal cell population during lung development and homeostasis(13, 181, 184, 353). Following the investigation of SHH pathway modulation on ATII cells and proliferating cells post injury, additional alveolar cell populations were assessed. Since previous studies have shown Shh can stimulate mesenchymal cell differentiation and proliferation(13, 181, 184, 187), further analysis focused on the fibroblast population during repair. To investigate this, control, uninjured and AIR-PCLS were labelled with BioTracker™ TiY Vimentin Live Cell Dye after 48hr culture. Vimentin, a type III intermediate filament protein is constitutively expressed in fibroblasts and therefore serves as a marker for the fibroblast population(354). A no antibody control was included to rule out non-specific staining or autofluorescence (Figure. 3.28A). Although this live-cell vimentin dye was only used for preliminary studies due to challenges imaging live tissue, some informative observations were made. In the uninjured regions of AIR-PCLS, vimentin labelling appeared relatively uniform across all concentrations of SHH treatment (Figure. 3.28B). In contrast, a visible increase in vimentin labelling was observed in the injured regions of AIR-PCLS following SHH treatment (Figure. 3.28C). This increase appeared to be dose-dependent, with stronger fluorescence observed as the concentration of SHH increased, while lower concentrations of SHH produced weaker labelling. Although untreated AIR-PCLS controls (i.e. not treated with SHH) were not included in these preliminary experiments, this was addressed in the subsequent phase of this study.

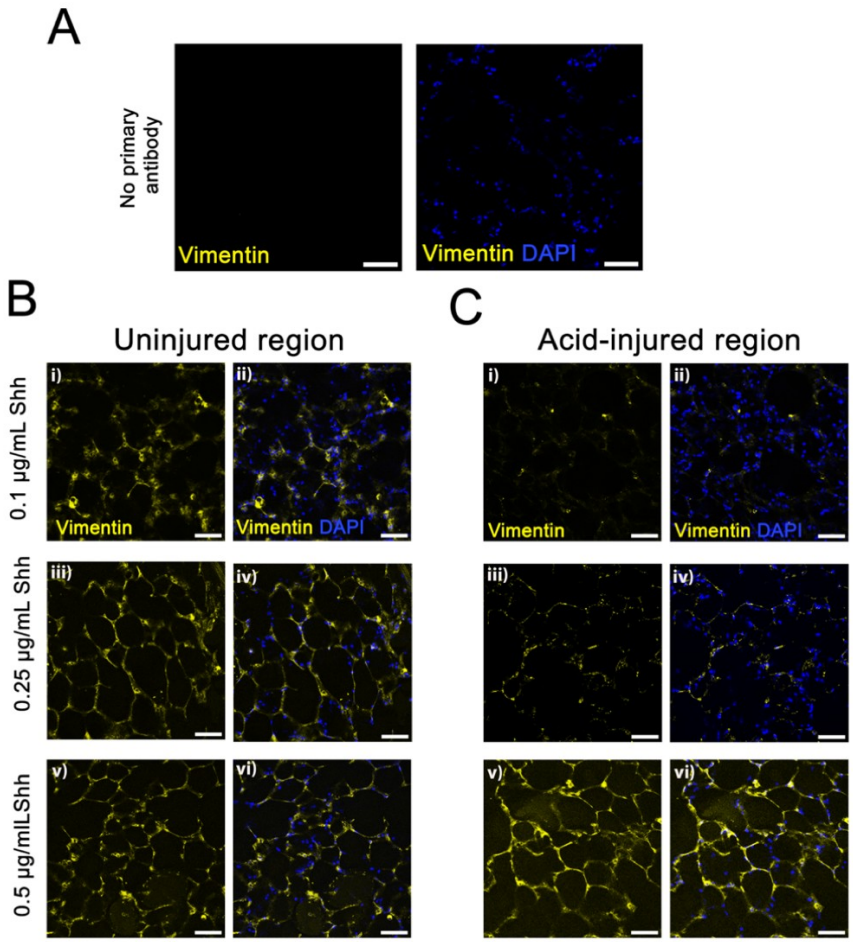

Figure 3.28. Expression of BioTracker™ TiY Vimentin Live Cell Dye in AIR-PCLS treated with increasing concentrations of SHH-N recombinant protein.

(A) Shows no primary antibody staining for Vimentin BioTracker in control, uninjured PCLS. (B) Immunofluoresecence staining for Vimentin (yellow) and DAPI (blue) in the uninjured region of AIR PCLS treated with (i-ii) 0.1 µg/mL, (iii-iv) 0.25 µg/mL, (v-vi) 0.5 µg/mL SHH. (C) Immunofluoresecence staining for Vimentin (yellow) and DAPI (blue) in the acid-injured region of AIR PCLS treated with (i-ii) 0.1 µg/mL, (iii-iv) 0.25 µg/mL, (v-vi) 0.5 µg/mL Shh.Widefield images taken with Apotome at 40× magnification, scale bars = 50 µm.

3.2.6.14 Further Vimentin staining confirms a dose-dependent increase in fibroblast expression in the acid-injured region of Shh treated AIR- PCLS

As the BioTracker™ TiY Vimentin is a live cell dye, both staining and imaging had to be conducted within a limited time window. Additionally, preliminary experiments revealed that the dye was not compatible for co-labelling. To enable more detailed investigation of fibroblasts in AIR-PCLS, immunostaining was performed using Rabbit anti-Vimentin antibody (Biorbyt, orb304659) and visualised using Alexa Fluor 555 anti-Rabbit IgG (H+L) secondary antibody (Invitrogen, A-11008). To quantify vimentin positive staining, an image analysis

macro developed by the FILM facility at Imperial College London was employed. As described in section 2.13.2, this macro calculates the total tissue area and the area of vimentin positive staining per field of view, so that the vimentin expression as a percentage of total tissue area can be determined. The experiment was repeated five times (n=5), with three technical replicates per experimental group in each biological replicate.

A no primary antibody control was included to rule out non-specific staining (Figure. 3.29A. In untreated PCLS, the percentage of vimentin staining was similar between control uninjured PCLS, which had a percentage of 49 % (Figure. 3.29B(i), Figure. 3.30A-B) and the uninjured region of AIR-PCLS, which had a percentage of 50 % (Figure. 3.29B(ii), Figure. 3.30A-B, p>0.9999). However, a significant reduction in vimentin staining was observed in the acid-injured region of untreated AIR-PCLS, which had a percentage of 21 %, a 0.43- fold change (≈ 57 % decrease) compared to control, uninjured PCLS (Figure. 3.29B(i, iii), Figure. 3.30A-B, p=0.0436) and a 0.42- fold change (≈ 58 % decrease) compared to the uninjured region of AIR-PCLS (Figure. 3.29(ii-iii)-3.30, p=0.0226).

In the uninjured region of AIR-PCLS treated with increasing concentrations of SHH, the percentage of vimentin positive area remained relatively consistent and showed no statistically significant differences. Specifically, AIR-PCLS treated with 0.1 μg/mL SHH had a mean of 51 %, a 1 .02-fold change (≈ 2 % increase) compared to the uninjured region of untreated AIR-PCLS (Figure. 3.29C(i), Figure.3.30A-B, p>0.9999). Treatment with 0.25 μg/mL SHH led to a mean of 48 % in the uninjured region of AIR-PCLS, a 0.96-fold change (≈ 4 % decrease) (Figure. 3.29(iii), Figure. 3.30A-B), while treatment with 0.5 μg/mL led to a mean of 51 %, again showing no significant difference from the untreated group (Figure. 3.29C(v), Figure. 3.30A-B), p>0.9999).

In contrast, quantification of the acid-injured region revealed a dose-dependent increase in vimentin staining following SHH treatment. At 0.1 μg/mL SHH the mean percentage of vimentin positive area remained 21 %, identical to that of the acid-injured region of untreated AIR-PCLS (Figure. 3.29C(ii), Figure. 3.30A, C, p>0.9999). Treatment with 0.25 μg/mL SHH led to a vimentin positive area of 33 %, a 1.57-fold change (≈ 57 % increase) (Figure. 3.29C(iv),

Figure. 3.30A, C, p=0.0614), while 0.5 μg/mL SHH led to a mean of 41 % (Figure. 3.29C(vi), Figure. 3.30A, C, p=0.5469), a 1.95-fold change (≈ 95 % increase). Although comparison between the untreated acid-injured region and individual treatment of SHH did not reach statistical significance, there was a significant overall increase in vimentin positive area between the 0.1 μg/mL and 0.5 μg/mL SHH treatment groups (Figure. 3.29-3.30, P= 0.0244, n=5).

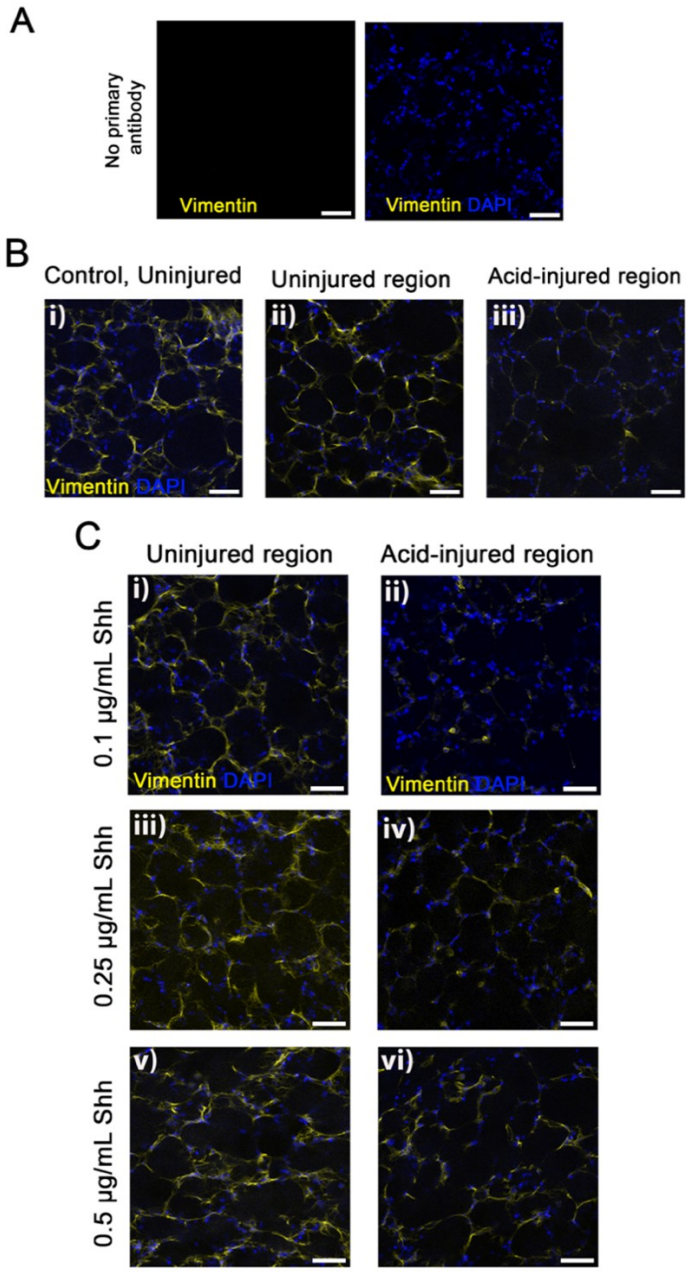

Figure 3.29. Expression of Vimentin in AIR-PCLS treated with increasing concentrations of SHH-N recombinant protein.
(A) Shows no primary antibody staining for Vimentin (antibody) in control, uninjured PCLS. (B) Immunofluoresecence staining for Vimentin (yellow) and DAPI (blue) in (I) untreated, control, uninjured PCLS (ii) the uninjured region of untreated AIR-PCLS and (iii) the acid-injured region of AIR-PCLS. (C) Immunofluoresecence staining for Vimentin (yellow) and DAPI (blue) in the uninjured region and acid-injured region of AIR PCLS treated with (i-ii) 0.1 μg/mL, (iii-iv) 0.25 μg/mL, (v-vi) 0.5 μg/mL SHH.Widefield images taken with Apotome at 40× magnification, scale bars = 50 μm.

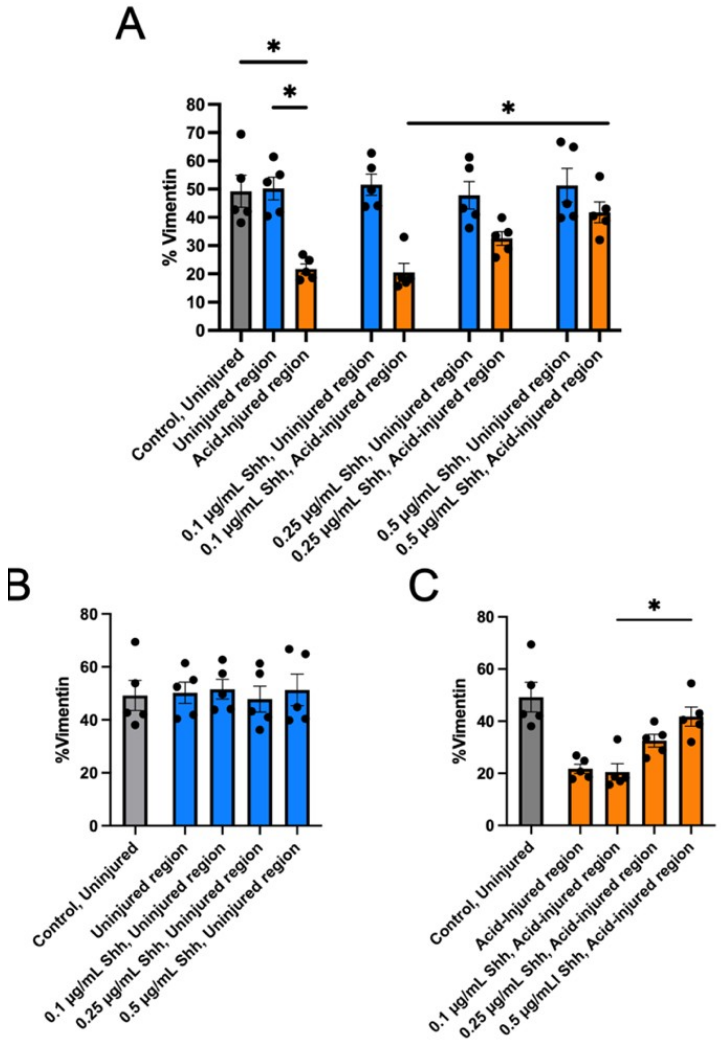

Figure 3.30. Quantification of percentage vimentin staining of Shh treated AIR-PCLS.
(A) Graph outlining the percentage of vimentin positive tissue in untreated PCLS (control, uninjured and AIR model) and Shh treated AIR-PCLS (B) Graph outlining the percentage of vimentin positive tissue in control uninjured PCLS, untreated uninjured region of AIR-PCLS and the uninjured region of SHH treated AIR-PCLS. (C) Graph outlining the percentage of vimentin positive tissue in control uninjured PCLS, untreated acid- injured region of AIR-PCLS and the acid- injured region of Shh treated AIR-PCLS.

3.2.6.15 Determining the impact of SHH treatment on fibroblast subpopulations

The results from vimentin staining indicate a relationship between SHH signalling and the restoration of the fibroblast population following injury. This is in agreement with previously published literature which suggests that Shh plays a role in fibroblast expansion post injury (13, 181). However, it is important to note that vimentin is a non-specific marker for fibroblasts. The lung is comprised of multiple fibroblast subtypes, each contributing to homeostasis, repair and regeneration. Notably, both myofibroblasts and lipofibroblasts have been shown to play active roles in alveologenesis and subsequent lung homeostasis (95, 355-

357). Additionally, fibroblasts have also been found to be activated post injury (108, 353-355). Having identified that SHH treatment led to an increase in vimentin staining within the acid-injured region of AIR-PCLS, the next objective was to determine whether Shh modulates the entire fibroblast population or selectively influences specific subtypes.

To explore this, AIR-PCLS were treated with recombinant SHH, cultured for 48 hr and subsequently fixed and immunostained with markers specific to distinct fibroblast subpopulations. Lipofibroblasts were identified using an anti-adipose differentiation related protein (ADRP) antibody, which localises to lipid droplets of lipofibroblasts and is a well-established marker of this subtype(104). Myofibroblasts were identified using an anti- alpha-smooth muscle actin (α-SMA) antibody. Myofibroblasts express alpha smooth muscle actin (α- SMA) therefore this is a commonly used marker for myofibroblasts(95, 96).

Given the strong association between SHH signalling and myofibroblast differentiation and activation reported in previously published studies(13, 314, 358), initial investigations focused on co-staining with vimentin and α-SMA to assess the presence and spatial distribution of myofibroblasts following injury and SHH treatment (Figure. 3.31). A no primary antibody control was included and confirmed that there was no non-specific staining or autofluorescence (Figure. 3.31A). I observed stellate, web-like α-SMA$^+$ cells, consistent with the characteristic morphology of myofibroblasts(184, 359), confirming their presence within PCLS. Additionally, while some α-SMA$^+$ cells co-localised with vimentin, others did not, indicating cell type specificity. This variation in marker expression confirms the presence of distinct fibroblast subpopulations within the tissue. As highlighted the key fibroblast subpopulations in the alveoli are myofibroblasts and lipofibroblasts.

Although this dataset was not quantified due to sample availability (one biological replicate conducted), I observed a general trend in α-SMA$^+$ cell proportion that was similar to vimentin staining results (Figure. 3.31B-C). α-SMA staining was reduced in the acid-injured region of untreated AIR-PCLS compared to both the uninjured region of untreated AIR-PCLS and untreated control, uninjured PCLS (Figure. 3.31B). In AIR-PCLS treated with SHH, α-SMA staining in the uninjured region appeared relatively consistent across all concentrations of Shh

(Figure. 3.31C(i, iii, v). In contrast, in the acid-injured region there appeared to be a dose-dependent increase in α-SMA staining (Figure. 3.31C(ii, iv, vi), which was previously observed with vimentin staining (Figure. 3.28-3.30).

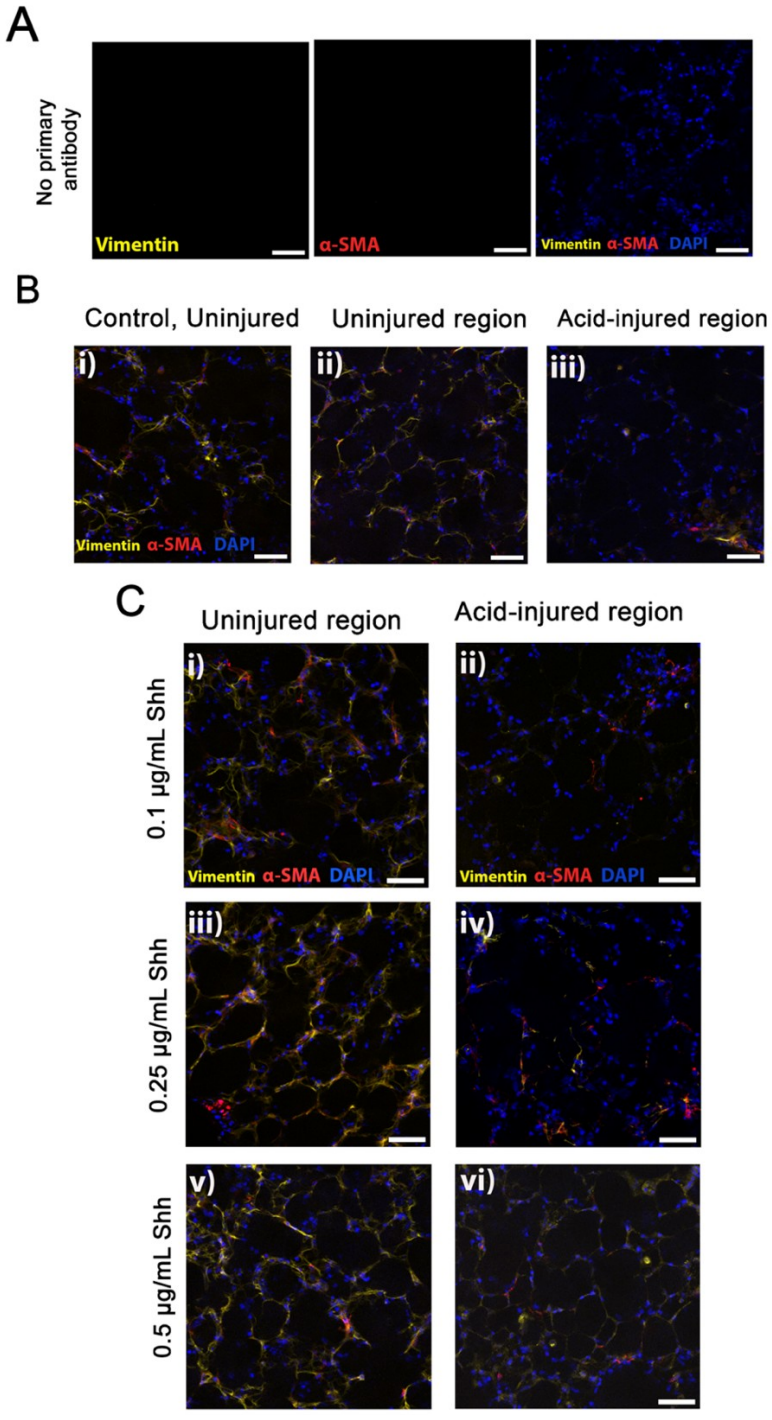

Figure 3.31. Co-staining Vimentin and α-SMA in AIR-PCLS treated with increasing concentrations of SHH-N recombinant protein.

(A) Shows no primary antibody staining for Vimentin and α-SMA in control, uninjured PCLS. (B) Immunofluoresecence staining for Vimentin (yellow), α-SMA (red) and DAPI (blue) in (I) untreated, control, uninjured PCLS (ii) the uninjured region of untreated AIR-PCLS and (iii) the acid-injured region of AIR-PCLS. (C) Immunofluoresecence staining for Vimentin (yellow), α-SMA (red) and DAPI (blue) in the uninjured region and acid-injured region of AIR PCLS treated with (i-ii) 0.1 µg/mL, (iii-iv) 0.25 µg/mL, (v-vi) 0.5 µg/mL SHH.Widefield images taken with Apotome at 40× magnification, scale bars = 50 µm.

Following the investigation of myofibroblast, I examined the presence and distribution of lipofibroblasts in both control, uninjured PCLS and AIR-PCLS, including untreated samples and those treated with 0.1, 0.25 or 0.5 μg/mL SHH. Preliminary attempts to co-stain ADRP and vimentin were unsuccessful, and due to time constraints, optimisation of this protocol was not feasible. For this reason, I prioritised staining with ADRP alone, to assess changes in lipofibroblast expression and localisation in response to injury and SHH treatment. Investigating lipofibroblasts using the AIR model was particularly important, since there is a limited understanding of the relationship between SHH signalling and lipofibroblasts during alveolar repair. Although only two biological replicates of ADRP staining alone were conducted, the data was quantified to obtain preliminary insights into the potential role of lipofibroblasts in Shh mediated repair. These initial findings may help to guide future studies exploring the interplay between SHH signalling and lipofibroblast function during lung repair and regeneration.

Due to the small sample size, statistical analysis could not be performed, however observable trends were still examined (Figure. 3.32-33). In untreated AIR-PCLS, the acid-injured region exhibited a higher proportion of $ADRP^+$ cells, with a mean of 8.5 %, compared to the uninjured region, which had a mean of 5.5 %, this was a 0.65-fold change (≈ 35.3 % decrease) and the untreated control, uninjured PCLS, which had a mean of 6 % (Figure. 3.32B, Figure. 3.33), a 0.71-fold change (≈ 29 % decrease). When the uninjured regions of AIR-PCLS treated with SHH were analysed, a concentration dependent increase in $ADRP^+$ cells was observed. Specifically, treatment with 0.1 μg/mL SHH led to a mean of 6.5 % $ADRP^+$ cells, a 1.18-fold change (≈ 18.2 % increase) compared to the uninjured region of untreated AIR-PCLS (Figure. 3.32C(i), Figure. 3.33). Treatment with 0.25 μg/mL SHH, increased the mean to 7.5 %, a 1.36-fold change (≈ 36.4 % increase) (Figure. 3.32C(iii), Figure. 3.33)., while treatment with 0.5 μg/mL SHH led to a mean of 8 %, a 1.45-fold change (≈ 45.5 % increase) (Figure. 3.32C(v), Figure. 3.33). A similar pattern was observed in the acid-injured regions of AIR-PCLS treated with SHH. The mean percentage of $ADRP^+$ cells increased to 9.5 % with 0.1 μg/mL SHH, which is a 1.12-fold change (≈ 11.8 % increase) compared to untreated AIR-PCLS (Figure. 3.32C(ii), Figure. 3.33). Treatment with 0.25 μg/mL SHH further increased this mean to 10.5 %, a 1.24-fold change (≈

23.5 % increase) (Figure. 3.32C(iv), Figure. 3.33)., and treatment with 0.5 µg/mL SHH led to a mean of 11.5 %, a 1.35-fold change (≈ 35.3 % increase) (Figure. 3.32C(vi), Figure. 3.33).

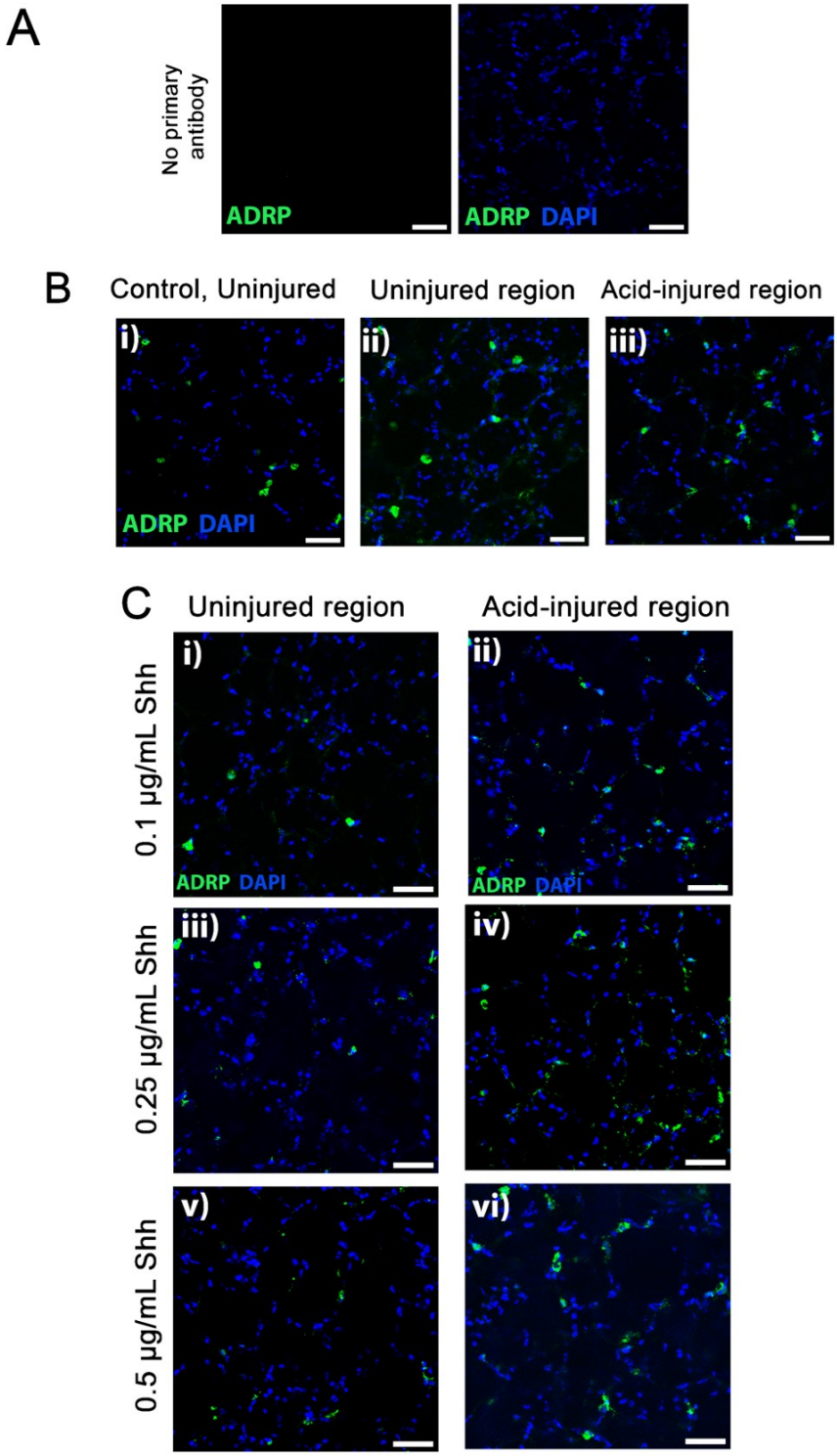

Figure 3.32**. **Expression of ADRP in AIR-PCLS treated with increasing concentrations of SHH-N recombinant protein. (A) Shows no primary antibody staining for ADRP in control, uninjured PCLS. (B) Immunofluoresecence staining for ADRP (green) and DAPI (blue) in (I) untreated, control, uninjured PCLS (ii) the uninjured region of untreated AIR-PCLS and (iii) the acid-injured region of AIR-PCLS. (C) Immunofluoresecence staining for ADRP (green) and DAPI (blue) in the uninjured region and acid-injured region of AIR PCLS treated with (i-ii) 0.1 µg/mL, (iii-iv) 0.25 µg/mL, (v-vi) 0.5 µg/mL Shh.Widefield images taken with Apotome at 40× magnification, scale bars = 50 µm.

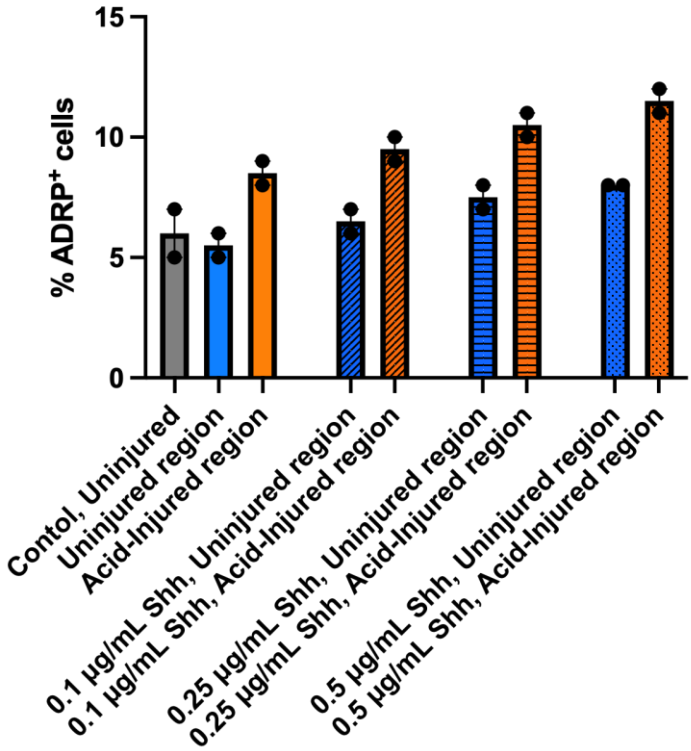

Figure 3.33. Quantification of changes in ADRP cell population following SHH treatment.
Graph showing quantification of ADRP+ cells in untreated controls and the uninjured and acid-injured regions of Shh treated AIR-PCLS (n=2 biological replicates, statistics were not conducted).

Finally, after investigating the presence of lipofibroblasts, a similar experiment was set up where AIR-PCLS were treated with Shh and co-stained with anti-ADRP and anti-α-SMA (Figure. 3.33). The aim of this investigation was to determine whether the two distinct fibroblast subpopulations could be morphologically distinguished within the AIR model, and to assess the presence of co-localisation. Additionally I sought to examine whether SHH treatment influenced the expression of these markers, in order to determine the impact on fibroblast subtype dynamics post injury.

Due to time constraints and limited sample availability, this dataset was not quantified. Nonetheless, qualitative analysis yielded informative preliminary findings. As with previous immunostaining, a no primary antibody control was included to confirm the absence of non-specific binding (Figure. 3.33A). ADRP staining revealed circular shaped structures reminiscent of lipid droplets, characteristic of lipofibroblasts. In contrast, α-SMA staining revealed stellate, web-like cells, typical of myofibroblast morphology. Notably, co-localisation of ADRP and α-SMA was not observed, further supporting the presence of distinct fibroblast subpopulations.

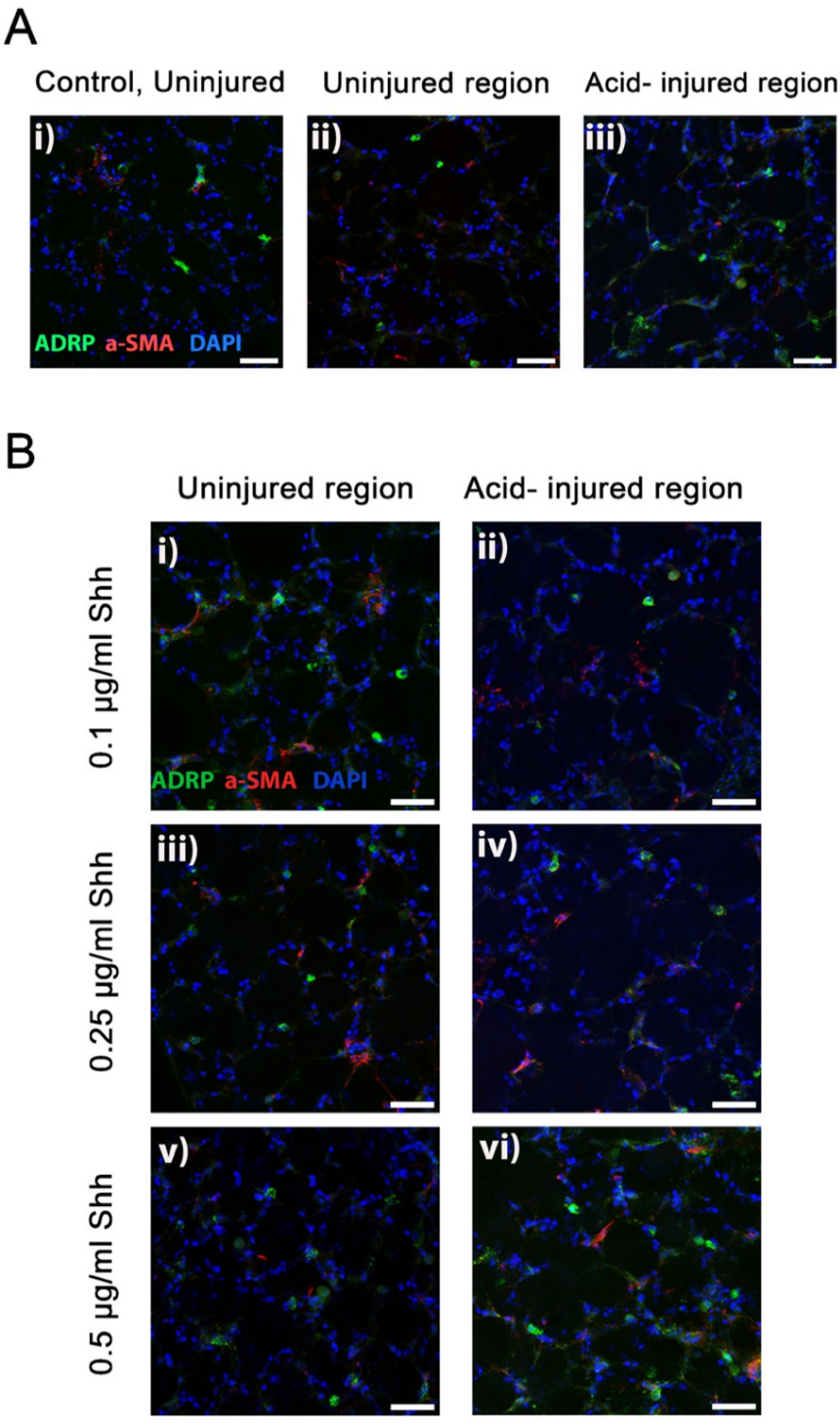

Figure 3.34. Co-staining ADRP and α-SMA in AIR-PCLS treated with increasing concentrations of SHH-N recombinant protein.

(A) Shows no primary antibody staining for ADRP and α-SMA in control, uninjured PCLS. (B) Immunofluoresecence staining for ADRP (green), α-SMA (red) and DAPI (blue) in (I) untreated, control, uninjured PCLS (ii) the uninjured region of untreated AIR-PCLS and (iii) the acid-injured region of AIR-PCLS. (C) Immunofluoresecence staining for ADRP (green), α-SMA (red) and DAPI (blue) in the uninjured region and acid-injured region of AIR PCLS treated with (i-ii) 0.1 µg/mL, (iii-iv) 0.25 µg/mL, (v-vi) 0.5 µg/mL SHH.Widefield images taken with Apotome at 40× magnification, scale bars = 50 µm.

3.3 Discussion

The aim of this chapter was to investigate and develop a deeper understanding of key signalling pathways involved in lung development, and to evaluate their potential roles in promoting lung repair following injury, using a combination of *in vitro* and *ex vivo* models of lung injury. The experimental investigations presented in this chapter were designed as an initial screening approach to assess multiple pathways, with the objective of identifying the most promising for further investigation. Understanding how signalling pathways influence lung repair could ultimately inform the development of targeted therapeutics aimed at enhancing repair and regeneration.

The first set of experiments focused on *in vitro* models, specifically examining the impact of modulating three developmentally important pathways: WNT, RA and SHH signalling. These pathways were selected based on an extensive literature review highlighting their roles in lung development, homeostasis and their potential roles in lung repair and regeneration (Figure. 3.2, Table 3.1). I identified a range of commercially available pathway modulators that act as either agonists or antagonists (Table 3.1). Working concentrations for each modulator were determined based on a combination of published data, EC50 values provided by suppliers and prior lab knowledge. While the selected concentrations were sufficient for preliminary screening, it is important to acknowledge that future work would benefit from more robust dose-response experiments to refine the concentrations used and enhance our understanding of the role of these pathways in the context of repair.

To evaluate the impact of pathway modulation, scratch assays were conducted in structural lung cells; A549 cells (epithelial) and HUVECs (endothelial). Some of the assays set up were to build on and validate previous work that has been conducted by the lab group which has focused primarily on the effect of Wnt5a and RA treatment. It was important to conduct these investigations to develop an understanding of the technique.

Prior to performing the scratch assays, I assessed the baseline relative expression of key components and downstream targets of the WNT, RA and SHH signalling pathways in both

A549 cells and HUVECs using qPCR (Figure. 3.4-3.6). This was carried out to evaluate the capacity of each of the cell types to respond to exogenous treatment, based on the endogenous expression of ligands, relevant receptors and transcriptional targets. The qPCR analysis (Figure. 3.4-3.6) revealed distinct expression profiles between the two cell types, suggesting differing responsiveness to specific pathways. This information is critical for interpreting data from scratch assays, as the relative expression of pathway components may influence the observed effects following treatment. Therefore, the findings from treatment with each pathway modulator will be evaluated and interpreted in relation to the relative expression of key signalling components. This will help to contextualise the observed effects on cell migration and wound closure, providing a more comprehensive understanding of how modulating each pathway correlates with gene expression profiles in A549 and HUVECs.

3.3.1 Investigation of Wnt mediated repair in epithelial and endothelial cells

The WNT signalling pathway is well-established as a key regulator of lung development and has more recently been shown to play an important role in repair and regeneration, therefore, WNT signalling has emerged as a promising target for the development of novel regenerative therapies(11, 13, 214). Among the WNT ligands, there has been an increased focus on Wnt5a since it has been shown to promote epithelial migration, which is an important process in both repair and regeneration (330, 331). Supporting this, studies using the AIR model have demonstrated that treatment with 1 μg/mL WNT5A significantly increases the proportion of facultative alveolar epithelial progenitor cells, specially marked by an increase in proSP-C$^+$ and transmembrane 4 L Six Family Member 1$^+$ (TM4SF1$^+$) cells in the acid-injured regions of AIR-PCLS. This pro-repair effect was attenuated by the WNT5A inhibitor Box5, further confirming the importance of Wnt5a in epithelial repair. Consistent with these findings I observed that treatment of A549 cells with 1 μg/mL WNT5A significantly increased wound closure after 20 hr of culture (Figure. 3.7), supporting the pro-repair role for WNT5A in epithelial cells. This experiment not only validated existing data but also provided the opportunity to establish and optimise the scratch assay method for further investigation into the selected signalling pathways.

In contrast, no significant change in wound closure was observed in HUVECs following treatment with 1 μg/mL WNT5A after 20 hr of culture (Figure. 3.13), indicating a lack of responsiveness in endothelial cells under similar conditions. Interestingly, qPCR analysis revealed low endogenous expression of *WNT5A* in both A549 and HUVEC cells, suggesting that the differential effect of exogenous Wnt5a is not solely due to basal expression levels, but may also reflect cell type specific responsiveness. This differential response may be due to variations in the expression of Wnt5a receptors including *ROR1, ROR2, RYK, PTK7* and the FZD family of receptors (329, 360, 361), as well as differences in downstream signalling components that are necessary for transducing pro-repair signals in both cell types. This highlights the necessity of accounting for cell type specific differences in WNT signalling responsiveness when investigating its role in repair.

Although some published studies have reported that WNT5A can promote endothelial cell migration and differentiation(362, 363), the lack of response observed in HUVECs in this study may also reflect differences in sensitivity to WNT5A dosage. It is possible that higher or lower concentration of WNT5A, or exposure over a longer period of time might yield a response in HUVECs. Furthermore, scratch assays are limited in their ability to capture complex multicellular interactions, particularly paracrine signalling that may be critical for endothelial repair *in vivo*. It has been shown that endothelial differentiation is abrogated in wntless (Wls) deficient mouse lungs, wls is an epithelial transmembrane protein that drives wnt ligand secretion(223, 363).

To further investigate the role of other WNT ligands in lung repair, I examined the effect of Wnt9a, which remains less-well characterised. Treatment with 0.04 μg/mL WNT9A had no significant effect on wound closure in either A549 cells (Figure. 3.9) or HUVECs (Figure. 3.14). Similar to WNT5A, endogenous WNT9A expression was low in both cell types, and the lack of response again raises the question of whether appropriate receptors or co-receptors for Wnt9a are expressed in these cells.

To deepen our understanding of WNT mediated repair, it would be important to characterise the expression profiles of relevant WNT receptors and downstream signalling factors in both

cell types. This could clarify our understanding of the observed responses on a molecular level. Additionally, it may be interesting to investigate the impact of treating A549 cells or HUVECs with WNT5A and WN9A simultaneously to determine the potential for synergistic interactions.

3.3.2 Investigating RA mediated repair in epithelial and endothelial cells

Following the investigation of WNT signalling, subsequent experiments were conducted to explore the role of retinoic acid signalling in lung repair. Similar to the WNT scratch assays, these experiments were established during the earlier phase of the project to develop technical proficiency with the scratch assay methodology and to validate previously generated data from the lab group as well as published literature.

In vivo mouse and rat models have been used to investigate the role of RA signalling during alveolar formation and regeneration in models of induced alveolar loss or destruction(234, 319-321, 324). Importantly, *in vivo* mouse and rat models have shown that RA administration can induce regeneration(234, 319, 322, 325).

Consistent with previous findings from our lab group (323), treatment with 10 μM RA did not significantly increase wound closure in A549 cells (Figure. 3.8), whereas a significant increase in wound closure was observed in HUVECs (Figure. 3.12). Similar to WNT studies, this differential response may be as a result of distinct endogenous RA signalling capacities between the two cell types. Gene expression analysis revealed high levels of *ALDH1A1*, the gene that encodes one of the key enzymes responsible for RA biosynthesis(340), in A549 cells. This suggests high endogenous production of RA and therefore high endogenous expression of RA which may have a direct impact on the sensitivity of A549 cells to exogenous RA. Furthermore, A549 cells expressed moderate levels of RAR-β and low RAR-γ, indicating a limited receptor capacity to respond to RA signalling (Figure. 3.4-3.6). In contrast, HUVECs expressed high levels of *RAR-β.* Although the level of *ALDH1A1* expression was high in HUVECs, it was relatively lower than in A549 cells, suggesting that HUVECs were more likely to respond to exogenous RA (Figure. 3.4-3.6). These findings further highlight the importance

of both endogenous ligand availability and receptor expression in modulating cellular responsiveness to signalling molecules.

3.3.3 Investigating Shh mediated repair in epithelial and endothelial cells

Next, I investigated the role of SHH signalling in epithelial and endothelial repair using scratch assays. Previously published studies have demonstrated that an increase in SHH promotes cell proliferation in both the epithelial and fibroblast cell populations, contributing to tissue maintenance and potentially repair post lung injury (201, 353). Interestingly, in contrast to these findings, I observed that treatment of A549 cells with 0.25 μg/mL SHH resulted in a significant reduction in wound closure after 20 hours (Figure. 3.10), whilst in HUVECs no significant difference in wound closure was observed.

It is important to note that whilst this reduction in wound closure was observed in A549 cells treated with 0.25 μg/mL SHH, the mean percentage of wound closure in the control group (DMEM + 0.5 % FBS alone) in the SHH dataset was 31 %, which is higher than the control values observed in the WNT and RA datasets (22-27.8 %, Figure. 3.7-3.9). This elevated percentage of wound closure in the DMEM + 0.5 % FBS alone group may reflect biological variability. It is important to consider that the rate of cell growth and in turn the rate of wound healing and cell migration can vary between biological replicates and is dependent on the passage number of cells(364). The mean percentage of wound closure in A549 cells treated with SHH was 25 %; this value is more consistent with the control ranges from other experiments. This may indicate that the observed reduction in wound closure in the SHH dataset may be relative to a potentially anomalous control.

To gain a better understanding of these findings, I assessed the expression of key SHH signalling pathway components (Figure. 3.4-3.6). In A549 cells, low expression of *SHH, PTCH1* (receptor), and *HHIP* (negative regulator) was observed, while *SMO* (signal transducer), *GLI1* and *GLI2* (downstream transcriptional factors) were expressed at moderate levels (Figure. 3.4-3.6). This suggests that although upstream activation is limited, the downstream transcriptional factors are sufficiently expressed. Based on this, it would be expected that

exogenous SHH treatment would activate the pathway and promote cell proliferation and migration. While A549 cells are useful for technical reproducibility and ease of use, primary alveolar epithelial cells are a more physiologically relevant model and could be used to validate our findings. However, primary epithelial cells pose a challenge to use because of time taken to isolate and because they do not remain phenotypically stable for long(308, 364). The reduction in wound closure may also suggest that SHH directed epithelial repair is dependent on cross-talk with other cells and pathways.

In contrast, HUVECs exhibited low expression of *SHH, PTCH1, GLI1 AND GLI2*, but had moderate *SMO* expression and high expression of *HHIP* (Figure. 3.4-3.6). The elevated expression of Hhip is likely to contribute to the reduced responsiveness of HUVECs to exogenous Shh. Furthermore, low levels of *GLI1* and *GLI2* suggest that there is minimal transcriptional activity downstream which is also indicative of the lack of responsiveness.

Next, A549 cells and HUVECs were treated with the SHH inhibitor cyclopamine to determine whether the reverse trend would be observed. Treatment with 5 μg/mL cyclopamine led to a moderate increase in wound closure in A549 cells (Figure. 3.11), although findings were not significant, this was an opposing trend to what was observed in A549 cells treated with SHH. This validates the previous finding. No significant difference in wound closure was observed in HUVECs treated with 5 μg/mL cyclopamine (Figure. 3.16).

Apart from in RA treated HUVECs, no significant changes were observed in HUVEC wound closure in the remaining treatment groups. This may reflect the importance of cell-cell interaction and paracrine signalling in lung repair and regeneration. Studies have demonstrated that interactions between endothelial cells and epithelial cells drive repair and regeneration in the alveoli(3, 365).

A limitation of the study is that the endothelial cell line used for investigations was not derived from the lungs. Since endothelial cell lines are much harder to culture than epithelial cell lines such as A549 cells. These experimental investigations provided a foundation for our understanding of the role of pathway modulators on endothelial cells. Having practised the

technique using HUVECs, scratch assays will be conducted to investigate the impact of treating Human Pulmonary Microvascular endothelial cells (HPMVECs) with SHH and Cyclopamine on wound closure. This will broaden our understanding of the impact of SHH and Cyclopamine on pulmonary endothelial cells specifically.

Following analysis of scratch assays I decided to streamline our investigations and focus on one pathway. I decided to focus on the SHH pathway because of the interesting findings observed when A549 cells were treated with Shh or cyclopamine and because little is known about the role of SHH in alveolar repair, while our lab group has previously studied the impact of WNT and RA.

Given that tissue repair is a complex, coordinated process involving multiple signalling pathways, future studies should also explore how the SHH pathway interacts with other key regulators which are known to modulate lung development and which have been suggested to play a role in repair and regeneration. Several studies have suggested cross-talk between SHH and WNT, FGF, TGF-β particularly during branching morphogenesis and in cell maintenance(8, 9, 21, 201). These interactions may also be important in repair and regeneration of the lung, further highlighting that successful repair is governed by an integrated network of signalling pathways(4, 11, 13, 112).

3.3.4 Using the AIR model to investigate changes in alveolar markers of repair following SHH treatment

The second set of experiments focused on using an *ex vivo* model of lung injury, the AIR model (Figure. 3.17, Figure. 3.18A) to investigate the role of SHH signalling on repair post injury. The AIR model provides a reproducible tool for investigating lung repair and examining changes in markers of repair (271, 276). In this chapter, the methodology required to successfully produce PCLS and subsequently set up the AIR model using PCLS was harnessed as demonstrated in Figure. 3.17. In agreement with data published when the model was first established (276), I demonstrated, using live/dead staining, that an area of restricted injury was successfully generated in AIR-PCLS (Figure. 3.18B). Furthermore, I show that although 0.1

M HCl successfully injures PCLS (Figure. 3.18B-C), there are still some live cells present in the acid-injured region of AIR-PCLS. This demonstrates the heterogeneity that is usually observed in lung disease, where damaged lung tissue is often adjacent to healthy lung tissue, as well as showing that there is still a capability of the tissue to repair.

As previously demonstrated by Kim *et al* (276) the AIR model can be used to investigate changes in cellular populations by immunostaining AIR-PCLS with different markers, specifically the AIR model has been used to demonstrate changes in alveolar progenitor cells and proliferating cells post injury to investigate alveolar repair.

In response to injury, regeneration can occur by proliferation and/or through cellular de-differentiation or trans-differentiation(2, 36, 37, 366). In the lungs, resident stem cells exist and are distributed across distinct anatomical locations(2, 36). In the alveolar epithelium, proSP-C^{+} cells, which mark ATII cells, function as resident progenitor cells. These ATII cells contribute to the regeneration of damaged lung tissue by self-renewing and differentiating into both ATII and ATI cells(2, 28, 36, 38). Therefore, to assess this regenerative response, I immunostained AIR-PCLS for proSP-C^{+} cells. I observed an increase in proSP-C^{+} cells in the acid-injured region of AIR-PCLS compared to the uninjured region and control, uninjured PCLS (Figure. 3.19), which is in agreement with previously published results (276). Proliferation also plays a very important role in repair and regeneration. I also observed similar results when I immunostained AIR-PCLS for Ki67. The findings showed a higher number of Ki67^{+} cells in the uninjured region of AIR-PCLS when compared to the acid-injured region and control, uninjured PCLS (Figure. 3.20), again, in agreement with published results (276). This highlights the reproducibility and the validity of this model for this project.

Since findings from scratch assays indicated a decreased percentage of wound closure in epithelial cells treated with SHH (Figure. 3.10), I decided to focus on broadening my understanding of the role of Shh in lung repair post injury. After successfully harnessing the AIR model, it was employed to determine changes in the population of the selected markers of alveolar repair (ProSP-C and Ki67) when AIR-PCLS were treated with SHH or cyclopamine. The AIR model has previously been used to investigate the effect of WNT signalling,

particularly using WNT5A treatment and the WNT inhibitor WntC59 (271), further validating the application of the AIR model for investigating repair and regeneration.

Although scratch assays were conducted with one concentration of SHH, for investigations using the AIR model I investigated the effect of SHH treatment on proSP-C$^+$ and Ki67$^+$ cells in AIR-PCLS at three different concentrations (0.1, 0.25 and 0.5 μg/mL). I demonstrated, using the MTT cell viability assay, that Shh did not have a significant impact on PCLS viability, then changes in markers of alveolar repair were assessed (Figure. 3.21). My findings showed that SHH treatment did not have a significant impact on the number of proSP-C$^+$ cells in the acid-injured or uninjured region of AIR-PCLS, irrespective of the concentration of SHH (Figure. 3.22). However, similar to untreated AIR-PCLS, when AIR-PCLS were treated with 0.1 μg/mL or 0.25 μg/mL SHH, there was a higher number of proSP-C$^+$ cells in the acid-injured region when compared to the uninjured region (Figure. 3.22). In contrast, treatment with 0.5 μg/mL SHH led to a higher number of proSP-C$^+$ cells in the uninured region compared to the acid-injured region. Furthermore, although at 0.1 μg/mL and 0.25 μg/mL there were still more proSP-C$^+$ cells in the acid-injured region, there was a trend toward a general decrease in the level of proSP-C$^+$ cells in the acid-injured region of PCLS treated with SHH (Figure. 3.22). However, none of the observed changes were statistically significant. These results suggest that Shh does not stimulate repair of alveolar epithelial cells, corroborating scratch assay data where I observed that SHH led to a decrease in A549 wound closure (Figure. 3.10).

To further investigate the role of SHH, I treated AIR-PCLS with three different concentrations (2.5, 5 and 10 μg/mL) of cyclopamine, the SHH pathway inhibitor and assessed whether this led to changes in the proSP-C$^+$ cell population (Figure. 3.25). Prior to this, MTT assay of cell viability revealed that although cyclopamine appeared to have a small impact on PCLS viability, this was not statistically significant (Figure. 3.24). Interestingly, I observed minimal changes in the uninjured region of AIR-PCLS but there was a trend towards a reduction in proSP-C$^+$ cells in the acid-injured region at all concentrations (Figure. 3.25). However, these findings were not statistically significant.

Building on this, changes in cell proliferation were assessed by measuring changes in the population of $Ki67^+$ cells in AIR-PCLS treated with either SHH or cyclopamine. Similar to untreated AIR-PCLS, results show an increase in the proportion of $Ki67^+$ cells in the uninjured region when compared with the acid-injured region of AIR-PCLS, at all concentrations of SHH treatment (Figure. 3.23). Further to this SHH treatment led to minimal changes in the number of $Ki67^+$ cells in the uninjured and acid-injured region of AIR-PCLS when compared to untreated AIR-PCLS. This suggests that treatment with SHH has no impact on the number of proliferating cells post injury. Interestingly, when AIR-PCLS were treated with cyclopamine, there was a trend toward a reduction in $Ki67^+$ cells with 2.5 and 5 μg/mL cyclopamine, however at 10 μg/mL no change was observed compared to the untreated AIR-PCLS. Conversely in the acid-injured region, following cyclopamine there was a dose-dependent trend toward an increase in $Ki67^+$ cells. This suggests that SHH signalling inhibits cell proliferation post injury. However, these findings were not statistically significant.

Whilst the results presented provide a good basis for further investigation into the role of the SHH pathway, definitive conclusions cannot be made about the role of Shh on alveolar repair since findings from AIR model investigations were not statistically significant. To improve our understanding and to contextualise our findings, sample size calculations were performed to assess whether the lack of statistically significant was due to the number of biological replicates included (n=3). The number of biological replicates, or the sample size included in a study directly affects the observed effect size and consequently the statistical power (367). The power analysis revealed that to reach statistical significance, where AIR-PCLS were treated with Shh, 6 biological replicates would be required and where AIR-PCLS were treated with cyclopamine, 5 would be required (Figure. 3.27). Thus, increasing the number of biological replicates for future investigations would improve the statistical power and could potentially yield more conclusive results.

3.3.5 Determining the impact of SHH treatment on fibroblasts post injury

Whilst our findings suggest that SHH signalling does not have a direct impact on alveolar epithelial repair, previous studies have indicated a relationship between SHH and the

mesenchymal cell population, particularly fibroblasts(13, 181, 184, 353). Additionally studies have identified cross-talk between the SHH signalling pathway and the FGF pathway at different stages of lung development and during homeostasis(8, 9, 181, 220). Therefore, it was important to determine the impact of SHH treatment on the fibroblast cell population post injury. I treated AIR-PCLS with SHH then determined changes in the level of fibroblast cells using markers for fibroblasts (Figure. 3.28-3.34). Our first investigations were conducted using vimentin, which is a widely used fibroblast marker(354). In the uninjured region of AIR-PCLS, treatment with increasing concentrations of SHH did not appear to have an impact on the level of fibroblast staining (Figure. 3.28-3.29). Vimentin staining appeared relatively stable across all concentrations of SHH and quantification of vimentin positive tissue confirmed this (Figure. 3.30). Conversely, I demonstrated that in the acid-injured region of AIR-PCLS, there was a dose-dependent increase in the percent of vimentin positive tissue (Figure. 3.29-3.30). This aligns with published studies, which have shown that an increase in SHH signalling is associated with fibroblast expansion(13, 181, 314). Intriguingly many of these studies also suggest that SHH signalling may play a role in the pathogenesis of lung fibrosis(13, 181, 314), raising the possibility that SHH signalling could be modulated to prevent or limit the progression of lung fibrosis. It is important to note that fibroblasts play a key role in the early stages of wound healing by producing ECM and driving ECM deposition; however, excessive ECM deposition leads to fibrosis(368). This further highlights the importance of investigating SHH signalling in the context of lung repair and regeneration and also the importance of understanding which specific fibroblast subtypes Shh has an influence on.

The current studies investigating the relationship between Shh and fibroblasts, have indicated that Shh has a relationship with myofibroblasts in particular(13, 314, 358). SHH pathway downstream transcription factors, Gli1 and Gli2 were found to be expressed in α-SMA^{+} cells in lung tissue harvested from a mouse bleomycin-induced fibrosis model(369). As previously stated, α- SMA is a commonly used marker for myofibroblasts(95, 96). Further to this, another study demonstrated that inhibition of human lung fibroblasts (HLF) isolated from control and IPF patients treated with cyclopamine exhibited decreased the expression of α-SMA (358). After observing promising results with vimentin, I co-stained vimentin and α-SMA (Figure.

3.31). It was important to conduct further investigation because whilst vimentin is widely used, it is a non-specific marker for fibroblasts. I observed a similar pattern of α-SMA staining (Figure. 3.31) compared to vimentin staining (Figure. 3.28-3.29), there appeared to be an increase in staining with increases in Shh concentration in the acid-injured region of AIR-PCLS (Figure. 3.31). However, overall there appeared to be relatively less α-SMA$^+$ cells than vimentin-stained cells, highlighting the distinction between the markers and the specificity of α-SMA. Furthermore, these findings are in agreement with published research which highlight a relationship between myofibroblasts and Shh. Further replicate experiments will need to be conducted and the data will need to be quantified before distinct conclusions can be made.

Despite growing research into the relationship between SHH signalling and fibroblast behaviour/phenotype, the specific relationship between SHH and lipofibroblasts is less well understood. However, the role that lipofibroblasts play in lung development and homeostasis, and particularly in surfactant synthesis and alveolar epithelial differentiation, is well characterised (94, 95, 103). In order to address the significant gap in our understanding of the relationship between SHH and this fibroblast population, I immunostained SHH treated AIR-PCLS for ADRP, a marker of lipofibroblasts (Figure. 3.32). Interestingly, I observed that SHH treatment led to a dose-dependent increase in ADRP$^+$ cells in both the uninjured and acid-injured regions of AIR-PCLS in comparison to untreated AIR-PCLS (Figure. 3.32-3.33). I also successfully demonstrated the presence of the two distinct fibroblast populations in SHH treated AIR-PCLS by co-staining α-SMA and ADRP (Figure. 3.34). These findings provide more evidence that Shh plays a role in maintaining fibroblast homeostasis and promoting fibroblast expansion. Although our findings from scratch assay analysis (Figure. 3.10) and changes in proSP-C and Ki67 cells in AIR-PCLS (Figure. 3.22-3.23, Figure. 3.25-3.26) suggest that Shh does not have a direct impact on the alveolar epithelial cell population, the observed changes in the fibroblast population raise the possibility that Shh may indirectly contribute to alveolar repair, through modulation of the fibroblast population. Particularly lipofibroblasts which are known to secrete factors that drive alveolar differentiation (94, 95, 101, 103). Equally, SHH may also stimulate the release of other mediators that in turn stimulate lipofibroblast multiplication enhancing lipofibroblast activity. However, further investigation with a larger

number of biological replicates is required, as well as investigations to determine the role of SHH on paracrine signalling.

3.4 Conclusion

Overall, the findings from these experiments enabled me to establish the techniques needed for the next investigations in my project and provided some interesting data which informed the design of the following experiments and investigations. Notably, the preliminary data indicates that Shh may have an effect on fibroblasts phenotype within the alveoli following injury.

Chapter 4

Investigating the impact of Sonic Hedgehog (Shh) signalling on alveolar repair using mono and co-culture *in vitro* assays

4.1 Introduction

Understanding and identifying mechanisms that promote tissue repair following lung injury is crucial to advance the development of novel therapeutics and improve patient outcomes
In the previous chapter, the role of key modulators of several signalling pathways required for lung development, specifically Wnt, RA and Shh, was investigated, using *in vitro* wound healing assays (section 3.2.4). Among these, the most notable effects were observed following SHH treatment. Using wound healing assays, I determined that treatment of A549 cells with Shh led to a significant reduction in wound closure (Figure. 3.10). Conversely, inhibition of the SHH pathway using cyclopamine led to an increased percentage of wound closure (Figure. 3.11), although this effect did not reach statistical significance. Nevertheless, the observation of an opposing trend with Shh activation and inhibition indicated that SHH signalling may play a modulatory role in alveolar epithelial repair. To build upon these *in vitro* findings, I employed the AIR model to investigate the response of several cell populations to SHH treatment following injury. Notably, I observed a dose-dependent increase in vimentin (a fibroblast marker) in the acid-injured region of AIR-PCLS treated with SHH, indicating a potential role for Shh in modulating the fibroblast response to injury during tissue repair (Figure. 3.28-3.30).

4.1.1 Sonic hedgehog (Shh) signalling in the alveoli

SHH signalling plays an essential role in lung development, particularly during branching morphogenesis and in the co-ordination of epithelial-mesenchymal interactions which drives mesenchymal cell proliferation and differentiation(180-183, 187). Disruption of SHH signalling during development leads to lung malformation, improper branching has been observed in Shh null mouse mutants (180-183). In the adult lung, SHH is relatively quiescent during homeostasis but is known to regulate the mesenchymal cell population(181, 185-187). Emerging studies also suggest that SHH signalling may play a role in alveolar repair post injury (13, 181). However, gaps remain in our understanding of the precise mechanisms through which SHH may modulate alveolar repair. Interestingly, researchers have found that Shh produced by epithelial cells is released and can act in a paracrine manner, signalling to the mesenchyme. Further to this, studies indicate that Shh released from the epithelium has the potential to modulate repair mechanisms in mesenchymal tissue by regulating expression of

fibroblast growth factors (FGFs) (181, 185, 370, 371). This highlights the importance of cell-cell crosstalk, specifically epithelial-mesenchymal cross-talk in coordinating effective repair post injury.

Our understanding of the specific effects of SHH signalling on different mesenchymal populations including fibroblasts such as lipofibroblasts and myofibroblasts remains poorly defined. Although previous studies have reported associations between SHH signalling and myofibroblast activation and expansion (13, 314, 358), the broader implications of SHH in modulating fibroblasts during alveolar repair are not fully understood.

4.1.2 The importance of cellular cross-talk in alveolar repair

As previously outlined in chapter 1 section 1.2.3, different stem cell and progenitor cell populations have been identified in different anatomical regions of the lung. To date, much of the research on alveolar repair and/or regeneration has focused on the role of alveolar epithelial regeneration. In particular the role of ATII cells, which act as facultative stem cells and are activated upon injury during which they proliferate and give rise to ATI cells to repopulate damaged alveolar epithelium (2, 28, 36, 38, 111, 112). Basal cells, club cells and BASCs in the airway epithelium have also been extensively characterised(33, 113, 116, 117, 137, 306). However, the epithelium alone cannot orchestrate successful alveolar repair. Other cellular populations including ECs, fibroblasts and immune cells play crucial roles in repair(3, 10, 95, 102). Furthermore, cross-talk between different cell and tissue components are essential for both lung development and repair(13, 201, 372, 373). During lung development, reciprocal interactions between the epithelium and mesenchyme regulates branching morphogenesis, cellular patterning and differentiation (13, 372, 373). These interactions are mediated by growth factors from conserved signalling pathways, including FGF, Shh, Wnt and BMP (13, 372, 373), whose roles in lung development I outlined the importance of in chapter 1, section 1.3. A key example is FGF10 and FGFR2 IIIb, FGF10 is secreted by mesenchymal cells and binds to FGFR2 IIIb on epithelial cells, this initiates a signalling cascade(13, 374), which promotes epithelial proliferation and branching during development (13, 374). As emphasised throughout this thesis, these developmental pathways are frequently reactivated to orchestrate alveolar repair which just like lung development is a complex multicellular

process(11-13, 19). An example of this during repair is the interaction between ATII cells and adjacent fibroblasts which secrete factors including WNT5A(150). Specifically, a study showed that WNT5A secreted by fibroblasts leads to the activation of ATII progenitor cells and this promotes repair following injury(150). In parallel, crosstalk between the epithelium and vasculature is also essential for alveolar repair, endothelial cells are responsible for secreting growth factors such as human growth factor (HGF) which drive epithelial repair(83).

Understanding the interactions between different cellular populations within the alveolar niche will enhance our understanding of alveolar repair. One key aspect of repair is cell migration, which enables cells to move to areas of damage to restore the tissue or lost cells(344). Therefore, it is also important to consider the migratory behaviours of cells in response to injury. Interestingly, there are differences in the migratory behaviours of different cell types. Epithelial cells typically migrate collectively while maintaining stable cell-cell junctions (375)(Figure. 4.1). In the context of wound healing, this co-ordinated movement is often described as sheet-like migration(375). This cohesive migration results in rapid initial movement but cells tend to be more spatially restricted due to the cohesive nature of the cell layer. In contrast, fibroblast migration is characterised by a lack of stable cell-cell junctions (Figure. 4.1) and proceeds in a non-uniform manner(375, 376).

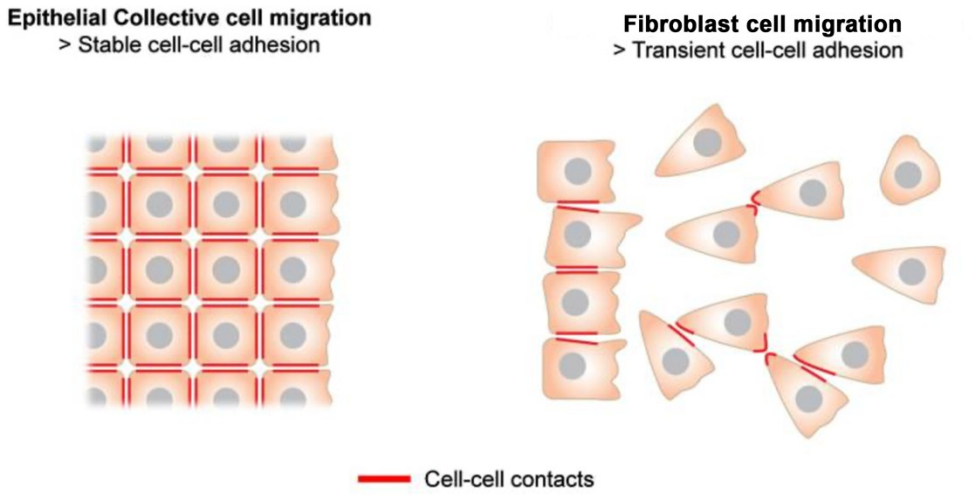

Figure 4.1 Differences in cellular migration between epithelial and fibroblast cells.
Shows differences in cell-cell adhesion mechanisms used by epithelial cells and fibroblasts during cell migration. Adapted from Theveneau E, Mayor R. Collective cell migration of epithelial and mesenchymal cells. Cell Mol Life Sci.2013;70(19):3481–3492.(1) (375).

4.1.3 Hypothesis and Aims

The hypothesis for this chapter was that Shh plays an important role in alveolar repair via cross talk between key cell types.

To test this hypothesis the following aims were developed:

1. To investigate whether SHH treatment promotes migration of key non- epithelial primary cell types, pulmonary microvascular endothelial cells and fibroblasts.

2. To investigate the potential role of SHH in driving alveolar repair through cellular crosstalk, by establishing a novel *in vitro* co-culture model.

4.2 Results

Although the lungs are comprised of many different cell types as outlined in the introduction (chapter 1, section 1.2.2). The three major structural cell types are epithelial, endothelial and fibroblast cells. Therefore, I chose to focus on investigating repair in these cell types. Beginning with mono-culture assays and then subsequently determining the response of these cell types to SHH treatment in co-cultures, to build a more complete picture about the role of Shh in alveolar repair.

Having established reproducible scratch assays investigating the role of SHH treatment on A549s and HUVECs in chapter 3 section, scratch assays were set up using HPMVECs, to gain a better understanding of the impact of SHH treatment on pulmonary endothelial cell migration specifically. Following this scratch assay were also conducted using primary human lung fibroblasts (HLF).

4.2.1 Investigating the endogenous gene expression of Key SHH signalling pathway genes in HPMVECs

As described in chapter 3, section 3.2.3, the endogenous expression levels of key SHH signalling pathway genes were initially assessed in A549 cells and HUVECs prior to conducting further experimental investigations. The same approach was followed with HPMVECs, the endogenous expression levels of Key SHH signalling pathway genes were assessed, to determine whether HPMVECs possess the necessary signalling components to respond to Shh stimulation. Specifically, it was important to determine whether cells express the relevant receptors and to also ensure that endogenous levels of *SHH* were not too high. High endogenous levels of expression could diminish observable effects of SHH treatment.

4.2.1.1 Selecting appropriate reference genes for normalisation of gene expression of Key SHH signalling pathway genes in HPMVECs

To ensure accurate normalisation of gene expression data, three commonly used reference genes; *B2M, GAPDH* and *GUSB,* were assessed for their suitability for gene expression normalisation, following the same approach previously described for A549 cells and HUVECS.

The mean Ct value for each reference gene was examined across three biological replicates, RNA was extracted from cells at varying passage numbers to demonstrate biological variability (Figure. 4.2).

The mean Ct value for *GUSB* was 30.6 in HPMVECs (Figure. 4.2), which exceeds the commonly accepted threshold for reliable quantification, the ideal reference gene has consistent and moderate expression (not too low and not too high) (335, 336, 338). Therefore, *GUSB* was not chosen for normalisation. In contrast, *B2M* and *GAPDH* exhibited lower Ct values in HPMVECS, with mean Ct values of 24.8 and 23.8 respectively (Figure. 4.2). *B2M* and *GAPDH* were selected as reference genes for normalisation of Shh target gene expression in HPMVECs.

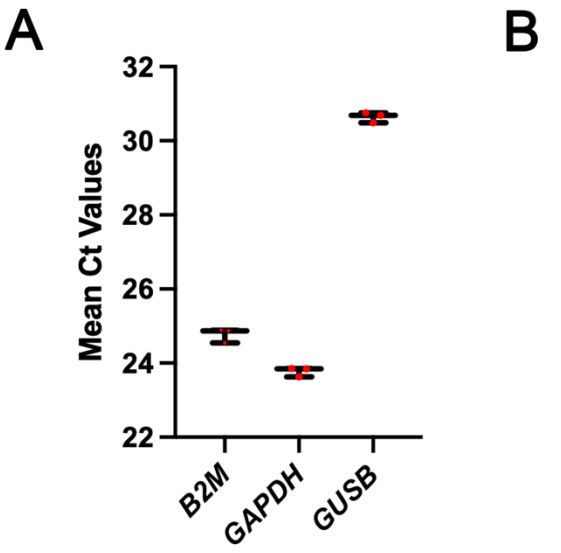

	Mean Ct
B2M	24.8
GAPDH	23.8
GUSB	30.6

Figure 4.2. Mean Ct values of candidate reference genes in HPMVECs.

The stability of *B2M, GAPDH* and *GUSB* expression was assessed in HPMVECs using qPCR. (A) Boxplot showing the mean Ct values across three biological replicates for each gene, points overlaid on boxplots represent biological replicates (n=3). (B) Table summarising mean Ct values for candidate reference genes.

4.2.1.2 Assessing the relative expression of Key SHH signalling pathway genes in HPMVECs

Shh target gene expression in HPMVECs was normalised to *B2M* and *GAPDH* to calculate ΔCt values and relative expression was determined using the 2^ (- ΔCt) method(336, 337). Fold change (2^ (- ΔΔCt)) was not calculated, as the aim of this investigation was to compare baseline expression in HPMVECs without a treatment group.

The relative expression levels of key components of the SHH signalling pathway were analysed in HPMVECS. This included, the ligand *SHH*, the receptor *PTCH1*, signal transducer *SMO*, transcription factors *GLI1* and *GLI2* and the negative regulator Hhip.

Overall, the relative gene expression level of all key SHH signalling pathway genes assessed was low in HPMVECs. Among the genes, *HHIP* had the highest relative expression at ~0.232 (Figure. 4.3A). Due to the comparatively high expression of *HHIP* against the remaining target gene, *HHIP* obscured the relative differences in expression levels of the remaining key SHH signalling pathway genes when plotted on the same graph. To resolve this, the mean relative expression of the remaining genes was plotted again in another graph excluding *HHIP* (Figure. 4.2B). This showed that the remaining genes had mean relative expression levels ranging from ~0.0013 – ~ 0.00084, with *PTCH1* being the next most highly expressed gene at ~0.0013. To further improve the ease of interpretation, the data was also transformed to a a $\log_{10}$ scale (Figure. 4.3C) and a heatmap was generated to visualise the overall expression profile of the genes (Figure. 4.3D). The heatmap highlights the high expression of *HHIP* in comparison to the other key SHH signalling pathway genes, while also highlighting the subtle differences in expression between the remaining genes.

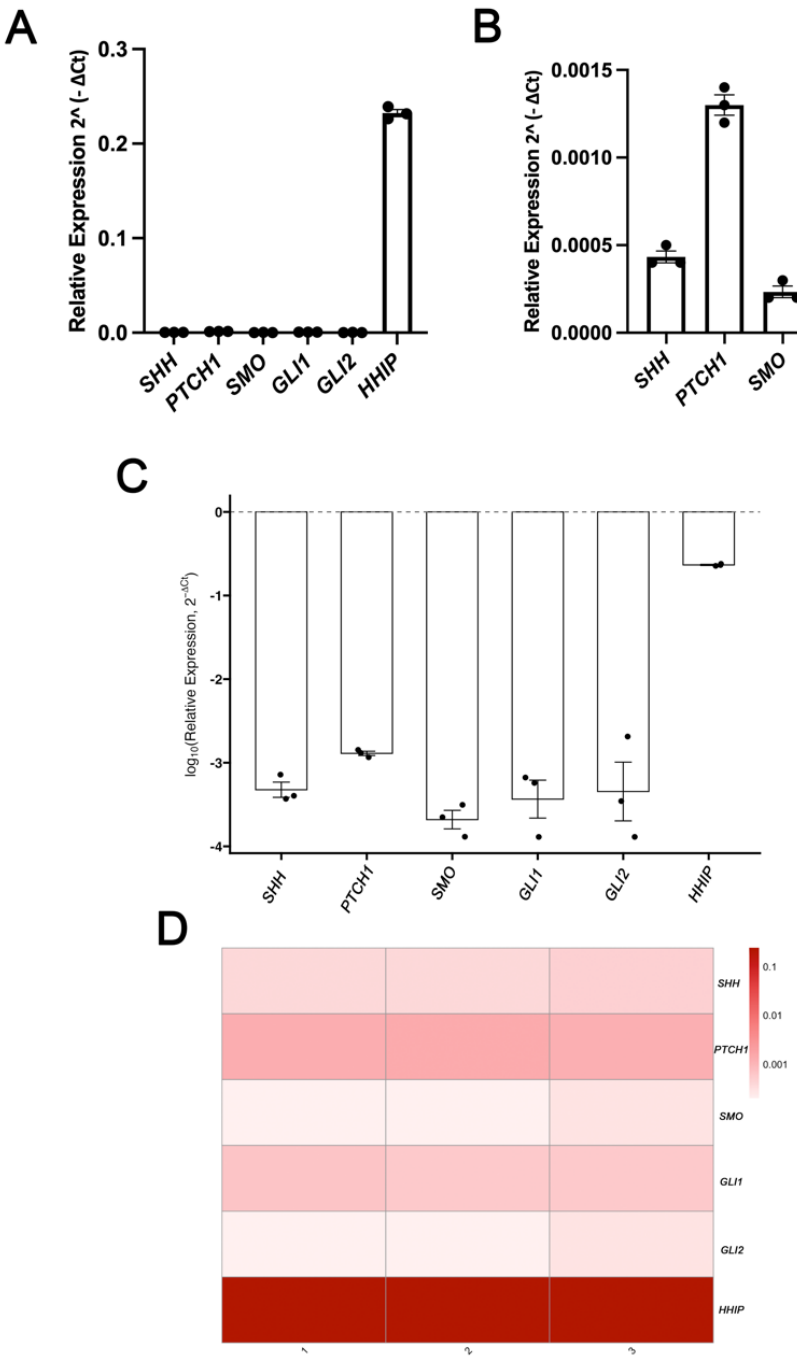

Figure 4.3. Relative gene expression of Key SHH signalling pathway genes in HPMVECs.

(A) Bar chart showing the relative expression of key SHH signalling pathway genes in HPMVECs calculated using 2^ (- ΔCt) method. (B) Bar chart showing relative expression of key SHH signalling pathway genes excluding Hhip to enhance visualisation genes with lower expression. (C) Bar chart displaying relative expression values converted to a log10 scale to facilitate data interpretation. (D) Heatmap summarising the relative expression of key SHH signalling pathway genes calculated using 2^ (- ΔCt) method. Colour intensity ranges from light pink (low expression) to red (high expression), as shown in the scale bar. The heatmap was generated using pheatmap package in R. Kolde R (2025). pheatmap: Pretty Heatmaps. R package version 1.0.13.

4.2.2 Determining the impact of SHH treatment on HPMVEC wound closure

4.2.2.1 Shh does not lead to an increase in HPMVEC wound closure

To set up HPMVEC scratch assays, 8 well chamber slides were coated with 2 µg/mL fibronectin then HPMVECs were seeded 5 x 10^4 per well and cultured in complete endothelial growth medium for microvascular vessels (5 % foetal calf serum (FCS), 0.4 % endothelial cell growth supplement, 0.1 ng/mL epidermal growth factor (recombinant human, 1 ng/mL basic fibroblast growth factor (recombinant human), 90 µg/mL heparin and 1 µg/mL hydrocortisone) for 24 hr until confluent. Then a scratch was made along the middle of each well as described in the methods chapter 2, section 2.13. Changes in the wound closure were assessed after 24 hr. I chose to culture scratch assays for 24 hr instead of the 20-hour duration used for HUVECS, because HPMVECs demonstrated a slower doubling time in culture relative to HUVECs.

Scratch assays experiments were set up with 0.25 µg/mL SHH in basal media + 2 % FCS, to determine whether SHH treatment had an impact on HPMVEC wound closure. This concentration of SHH was selected based on prior optimisation, representing a mid-range effective concentration within the working concentration of SHH recombinant protein. Additionally, this concentration was chosen to maintain consistency with previous experiments conducted using A549 cells and HUVECs. A control group with basal media + 2 % FCS only was also set up, HPMVECs were also treated with complete endothelial growth media as a positive control for increased wound closure (Figure. 4.4).

HMPVECs treated with complete endothelial growth medium, exhibited a mean of 45 % wound closure (Figure. 4.4A(i-ii), Figure. 4.4B) whereas HMPEVCs cultured in basal media + 2 % FCS only exhibited a mean of 14 % wound closure at 24 hr (Figure. 4.4A(iii-iv), Figure. 4.4B). Treatment with 0.25 µg/mL SHH resulted in a mean of wound closure of 18.3 %, which was a 1.31- fold change (≈ 31% increase), however this was not significantly different compared to 14 % in basal media + 2 % FCS ($p = 0.1500$) (Figure. 4.4A(v-vi), Figure. 4.4B). This lack of an effect on endothelial cells was in agreement with that previously found using HUVEC cells (see Chapter 3, section 3.2.4.9).

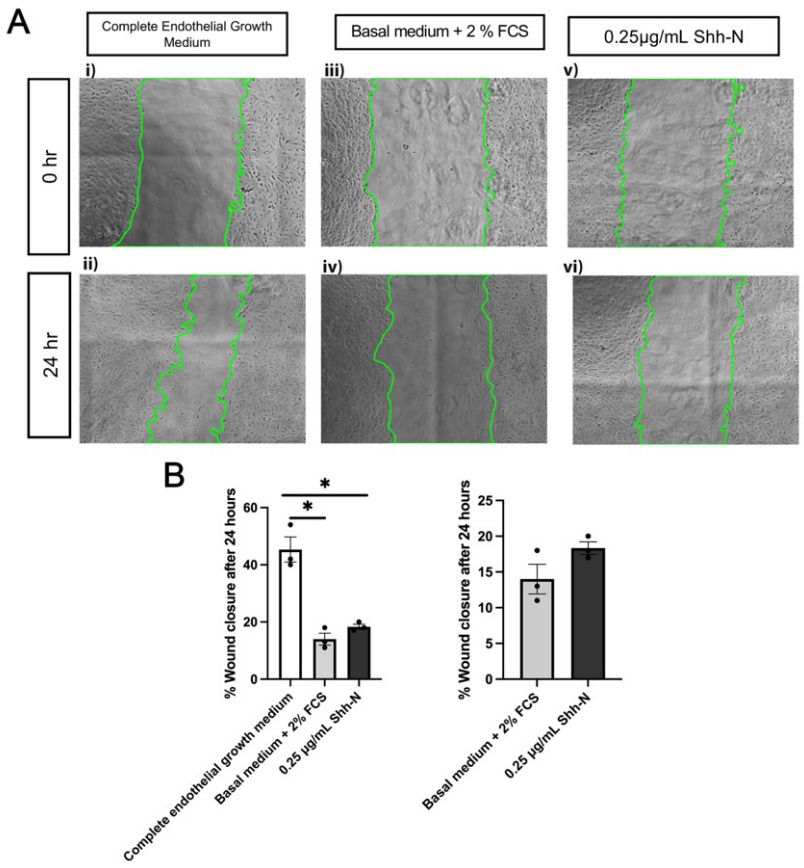

Figure 4.4. Effect of 0.25µg/mL SHHtreatment on HPMVEC wound closure.

(A) Representative light microscope images demonstrating HMPVEC wound closure following 24 hr culture with (i-ii) complete endothelial growth medium (iii-iv) basal media + 2 % FCS and (v-vi) 0.25 µg/mL SHH(experimental group). Widefield images taken at 10× using Zeiss Axio Observer (B) Graphs showing quantification of % wound closure in HMPVECs after culturing for 24 hr. Data are presented as mean ± SEM (n = 3; Mann – Whitney U-test. *p < 0.05.

4.2.2.2 Cyclopamine does not have an impact on HPMVEC wound closure

Following scratch assays investigating SHH treatment, the effects of inhibiting the SHH signalling pathway were investigated. Scratch assays were set up with 5 µg/mL cyclopamine in basal media + 2 % FCS, to determine whether the SHH pathway inhibitor had an impact on wound closure. As previously done a control was set up with basal media + 2 % FCS only and HPMVECs were also treated with complete endothelial growth media as a positive control for increased wound closure. As previously mentioned, (section 3.2.4.5) cyclopamine was reconstituted in EtOH before dilution in culture media. Therefore, HMPVECs were treated with an equal volume/ % EtOH in basal media + 2 % FCS to ensure that the EtOH did not have an impact on wound closure. HPMVECs cultured in complete endothelial media had a mean

wound closure of 45 % (Figure. 4.5A(i-ii), Figure. 4.5B), while cells in basal media + 2 % FCS had a mean wound closure of 14 % (Figure. 4.5A(iii-iv), Figure. 4.5B). HPMVECs cultured in 0.001 % EtOH had a mean wound closure of 12.3 % (Figure. 4.5A(v-vi), Figure. 4.5B). HPMVECs treated with 5 µg/mL cyclopamine had a mean percentage of wound closure was 15.7 % (Figure. 4.5A(vii-viii), Figure. 4.5B), which was a 1.12-fold change (≈ 12 % increase) compared to cells in Basal medium + 2 % FCS. There was no significant difference between the EtOH control and HPMVECs treated with Basal medium + 2 % FCS (p= 0.8000). Similarly, there was not a significant change in wound closure observed between HPMVECs treated with 5 µg/mL cyclopamine and HPMVECs cultured with Basal medium + 2 % FCS (p = 0.3500).

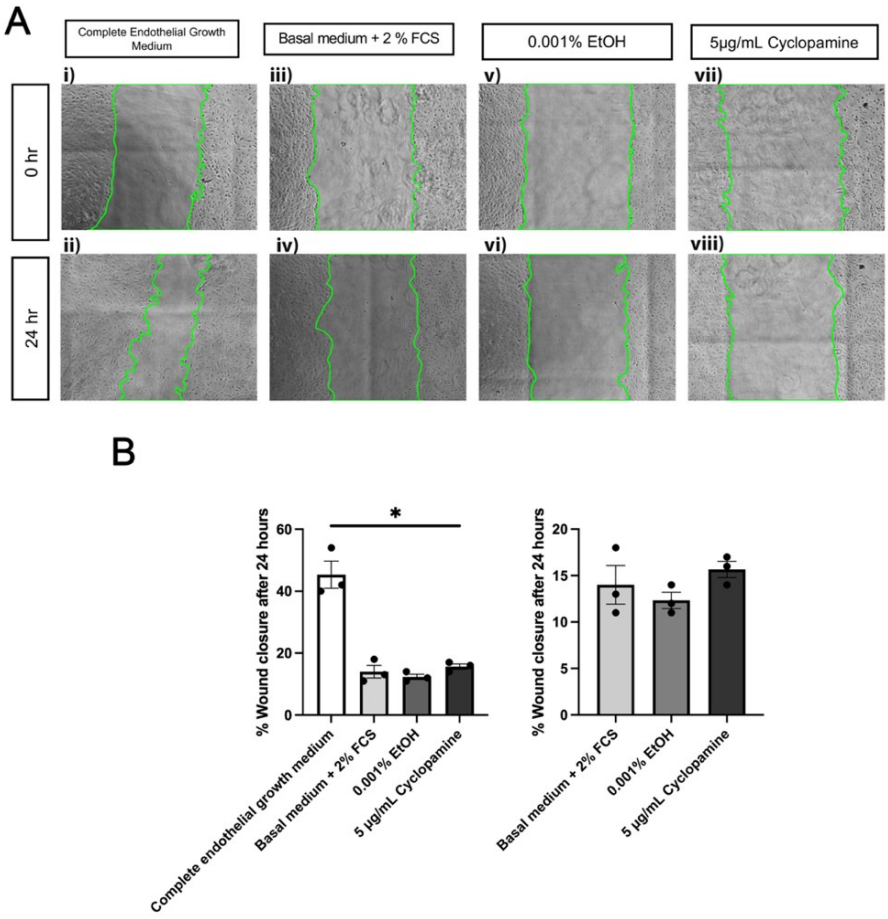

Figure 4.5. Effect of 5 µg/mL Cyclopamine treatment on HPMVEC wound closure.

(A) Representative light microscope images demonstrating HMPVEC wound closure following 24 hr culture with (i-ii) complete endothelial growth medium (iii-iv) basal media + 2 % FCS (v-vi) 0.001 % EtoH and (vii-viii) 5 µg/mL cyclopamine (experimental group). Widefield images taken at 10× using Zeiss Axio Observer (B) Graphs showing quantification of % wound closure in HMPVECs after culturing for 24 hr. Data are presented as mean ± SEM (n = 3; Mann – Whitney U-test. *p < 0.05.

4.2.3 Determining the impact of SHH treatment on primary lung fibroblasts

Primary human pulmonary/lung fibroblasts (HLF) were isolated from human lung tissue biopsy samples obtained from the Respiratory Biomedical Unit (BRU) Biobank at the Royal Brompton hospital (ethics reference number 20/SC/0142). Tissue samples were obtained from patients undergoing surgical resection for diagnosis of potential tumours, all samples used were confirmed to be histologically normal by a histopathologist prior to collection. HLF were isolated as described in methodology chapter 2 section 2.7.4.

4.2.3.1 Characterisation and verification of isolated fibroblast cell population

Following isolation, HLF cells were fixed and co-immunostained with antibodies to vimentin (Figure. 4.6(iii-iv)), a widely recognised marker for fibroblasts (354) and pan-cytokeratin (Figure. 4.6 v-vi), an epithelial cell marker (377), to confirm their cellular identity and purity. DAPI (Figure. 4.6(i-ii)) staining was used to visualise the cell nuclei. Immunostaining confirmed strong vimentin expression in the isolated cells, indicative of high fibroblast purity. Only occasional pan-cytokeratin positive cells were observed (Figure. 4.6).

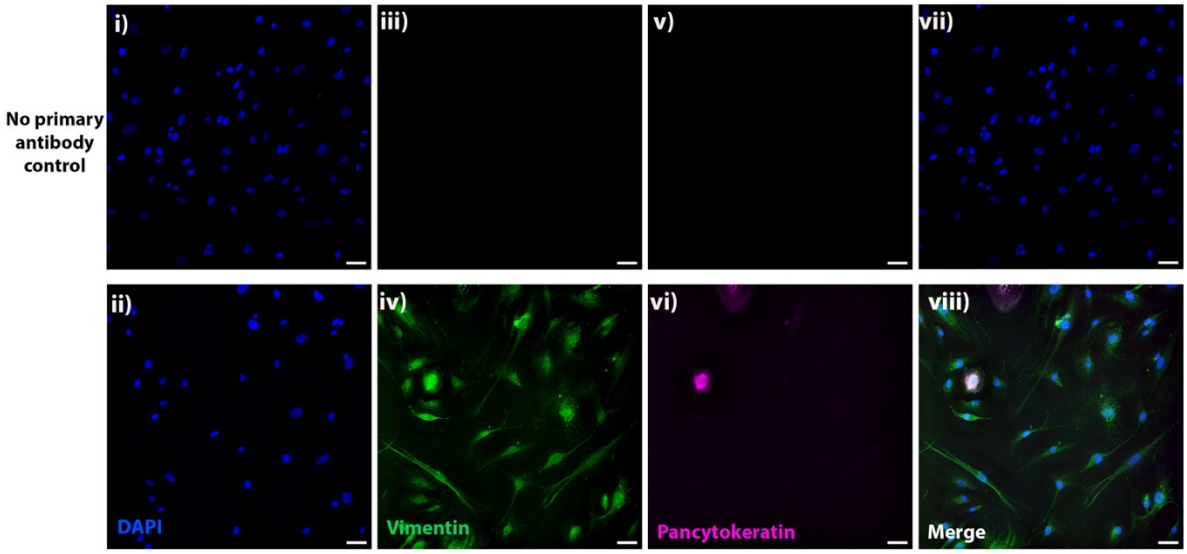

Figure 4.6. Confirmation of isolated HLF.

Immunofluorescence staining for (i-ii) DAPI (nuclear marker), (iii-iv) Vimentin (fibroblast marker), (v-vi) Pan-cytokeratin (epithelial cell marker) (vii-viii) Merged images. Panels i, iii, v and vii, represent the no primary antibody control. Widefield images taken at 20× magnification, scale bar= 50 µm.

4.2.4 Investigating the endogenous gene expression of Key SHH signalling pathway genes in HLF

After confirming the identity and purity of HLF isolated from lung tissue resections, the endogenous expression levels of Key SHH signalling pathway genes were assessed in HLF prior to undertaking further experimental investigations. Measuring endogenous expression of Key SHH signalling pathway genes was important to determine whether HLFs express the necessary receptors and downstream effectors required to respond to SHH stimulation. Further to this, it was important to assess the endogenous level of *SHH* specifically because elevated basal levels of Shh could diminish the effect of exogenous SHH treatment.

4.2.4.1 Selecting appropriate reference genes for normalisation of gene expression of Key SHH signalling pathway genes in HLF

To ensure accurate normalisation of Shh target gene expression in HLFs, three commonly used reference genes, *B2M, GAPDH* and *GUSB* were assessed, as previously done for A549, HUVECs and HPMVECs. Mean Ct values were examined across three biological replicates. To accurately take into account biological variability, RNA was extracted from cells at different passages

The mean Ct value for *GUSB* in HLFs was 30.3 (Figure. 4.7), exceeding the threshold for reliable quantification. Ideal reference genes show consistent, moderate expression across experimental conditions (335, 336, 338), therefore, *GUSB* was excluded. In contrast, *B2M* and *GAPDH* had lower Ct values of 24.6 and 22.3, respectively (Figure. 4.7), therefore they were selected for normalisation.

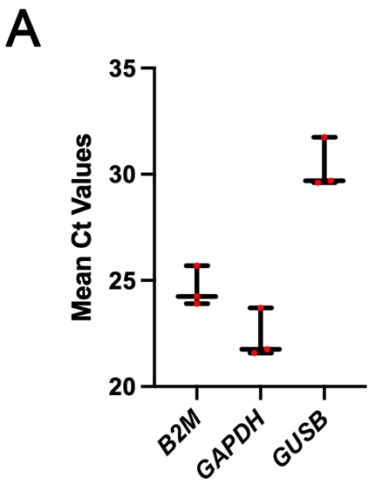

B

	Mean Ct
B2M	24.6
GAPDH	22.3
GUSB	30.3

Figure 4.7. Mean Ct values of candidate reference genes in HLFs.

The stability of *B2M, GAPDH* and *GUSB* expression was assessed in HLFs using qPCR. (A) Boxplot showing the mean Ct values across three biological replicates for each gene, points overlaid on boxplots represent biological replicates (n=3). (B) Table summarising mean Ct vakues for candidate reference genes.

4.2.4.2 Assessing the relative expression of Key SHH signalling pathway genes in HLFs

Relative expression levels of Key SHH signalling pathway genes in HLF were calculated using the 2^ (- ΔCt) method, with *B2M* and *GAPDH* used as reference genes. As with previous relative expression analysis, fold change (2^ (- ΔΔCt)) was not calculated, since the aim of this investigation was to assess the baseline gene expression of Key SHH signalling pathway genes in HLF in the absence of a treatment group.

The mean relative expression of Key SHH signalling pathway genes in HLFs was generally low (Figure. 4.8). Among the genes investigated, *GLI2* exhibited the highest mean relative expression at ~0.00556, followed by *PTCH1* at ~0.00136 and Smo at ~0.00106. The remaining genes, *GLI1, HHIP AND SHH*, had lower mean relative expression levels, with Shh exhibiting the lowest at ~0.00009. To improve the visualisation and interpretation of data, mean relative gene expression values were transformed using a $\log_{10}$ scale (Figure. 4.8B). A heatmap was also generated (Figure. 4.8C), summarising the overall expression profile of Key SHH signalling pathway genes in HLFs and highlighting the relatively higher expression of *GLI2* compared to the remaining genes.

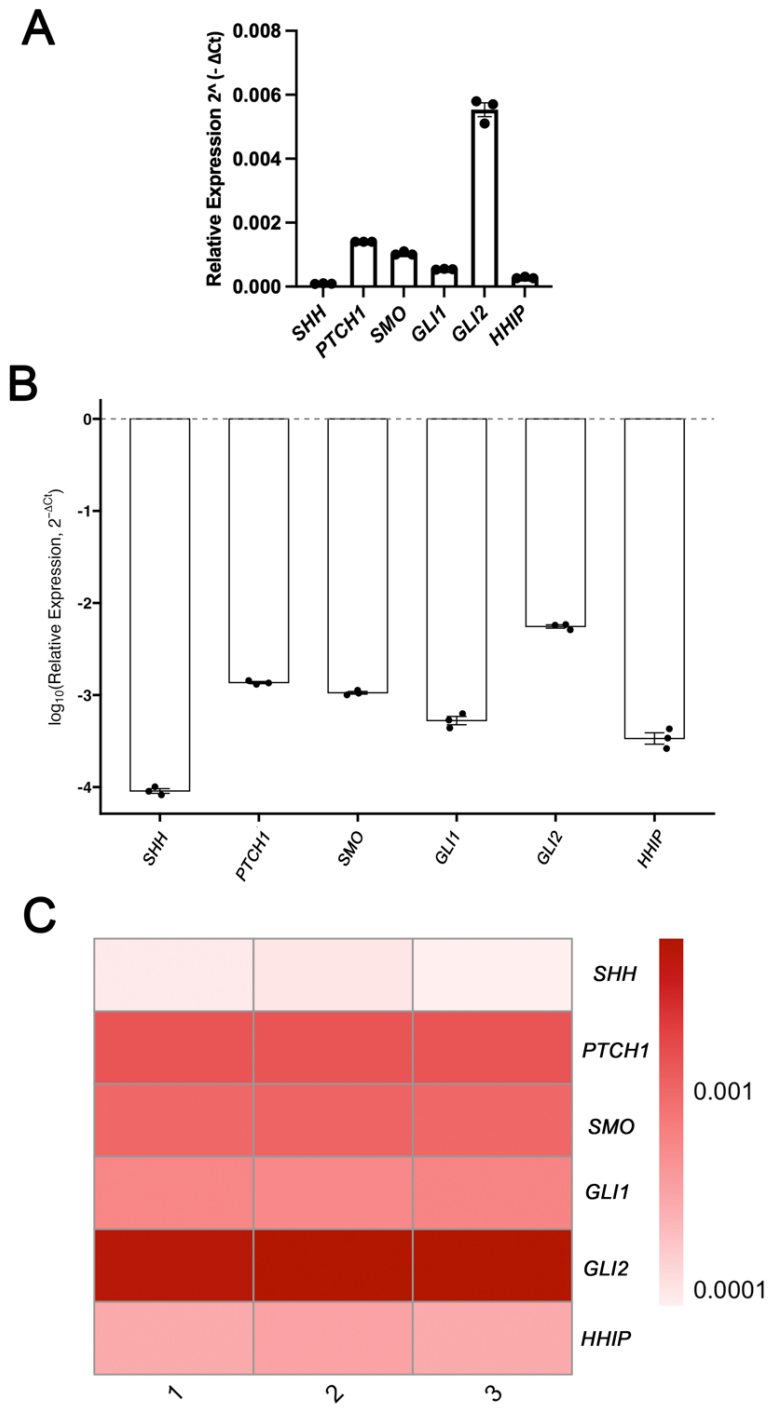

Figure 4.8. Relative gene expression of key SHH signalling pathway genes in HLFs.

(A) Bar chart showing the relative expression of key SHH signalling pathway genes in HLFs calculated using 2^ (- ΔCt) method. (B) Bar chart displaying relative expression values converted to a log10 scale to facilitate data interpretation. (C) Heatmap summarising the relative expression of key SHH signalling pathway genes calculated using 2^ (- ΔCt) method. Colour intensity ranges from light pink (low expression) to red (high expression), as shown in the scale bar. The heatmap was generated using pheatmap package in R. Kolde R (2025). pheatmap: Pretty Heatmaps. R package version 1.0.13.

4.2.4.3 *Differential expression of SHH pathway genes across epithelial, endothelial and fibroblast cells*

Despite being performed at different times, qPCR data from A549, HUVEC, HPMVEC and HLFs were combined into a heatmap to summarise relative gene expression of key SHH pathway genes difference across all four cell types (Figure. 4.9). The results demonstrate cell type specific differences in the expression of SHH pathway genes, spanning multiple orders of magnitude. Interestingly, Shh expression was low across all cell types. Contrastingly, *HHIP* expression was very high in both HUVECs and HPMVECs but low in A549 and HLF cells. The expression of *SMO, GLI1, GLI2* showed highest expression in A549 cells and was moderately expressed in other cell types. *PTCH1* expression was relatively consistent and moderate in all cell types.

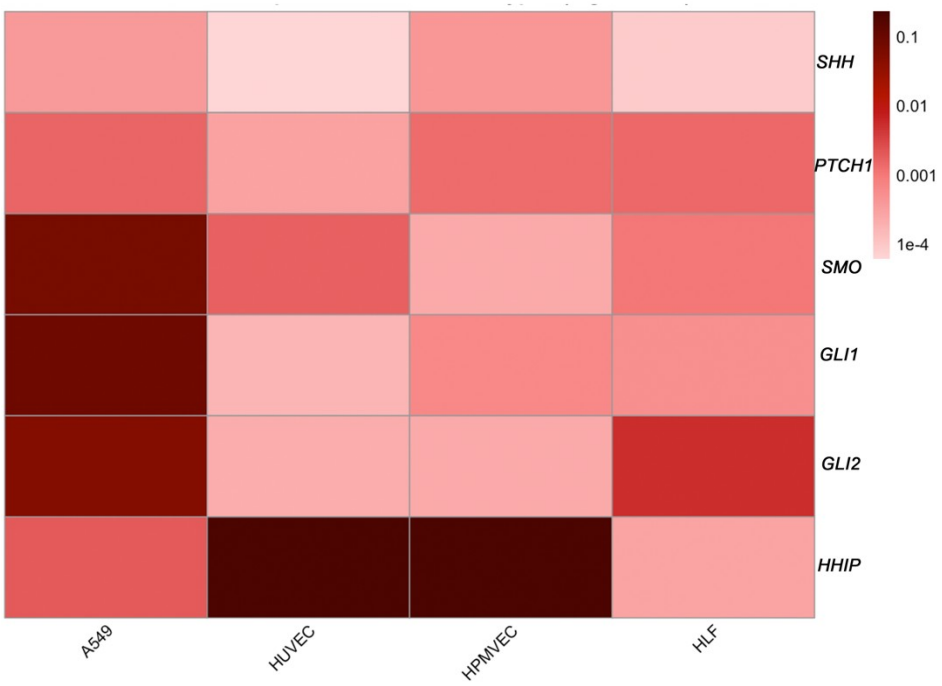

Figure 4.9. Relative gene expression of Shh target genes in structural pulmonary cells.
Heatmap summarising mean relative expression of *SHH, PTCH1, SMO, GLI1, GLI2, HHIP* in A549, HUVEC, HPMVEC and HLF cells obtained after conducting qPCR and analyses using 2^ (- ΔCt) method. Colour intensity ranges from light pink (low expression) to red (high expression), as shown in the scale bar. The heatmap was generated using pheatmap package in R. Kolde R (2025). pheatmap: Pretty Heatmaps. R package version 1.0.13.

4.2.4.4 SHH treatment led to an increase in HLF wound closure

Having isolated primary HLFs and investigated the relative expression levels of Key SHH signalling pathway genes in HLFs, scratch assays were set up to determine the impact of SHH treatment on HLF wound closure (Figure. 4.10). HLF cells were seeded at a concentration of $2x10^4$ per well into collagen coated 8 well slide chambers (as described in chapter 2 section 2.14). Once confluent, a scratch was made in the middle of each well and HLF were treated with 0.25 μg/mL SHH in DMEM + 0.5 % FBS or control media only (DMEM + 0.5 % FBS). This concentration of SHH was selected as a mid-range concentration and to ensure consistency was maintained between previous investigations conducted using A549 cells, HUVECs and HPMVECs. HLF cells treated with DMEM + 10 % FBS was also included as a positive control that induces wound closure (Figure. 4.10A(i-ii), Figure. 4.10B). 24 hr endpoint was used for scratch assays conducted with HLFs, based on prior optimisation conducted by previous lab members (data not shown here), which identified this as an optimal time duration for assessing HLF wound closure. After 24 hr, cells cultured in DMEM + 10 % FBS had a mean percentage of wound closure of 62 % (Figure. 4.10A(i-ii), Figure. 4.10B) cells, while cells in DMEM + 0.5 % FBS alone had a mean wound closure of 19.3 % (Figure. 4.10A(iii-iv), Figure. 4.10B). Cells treated with 0.25 μg/mL SHH had a mean wound closure of 26 % (Figure. 4.10A(v-vi), Figure. 4.10B), which was a 1.35-fold change (≈ 35 % increase) in comparison to the DMEM + 0.5 % FBS control, this increase was statistically significant ($p = 0.0500$).

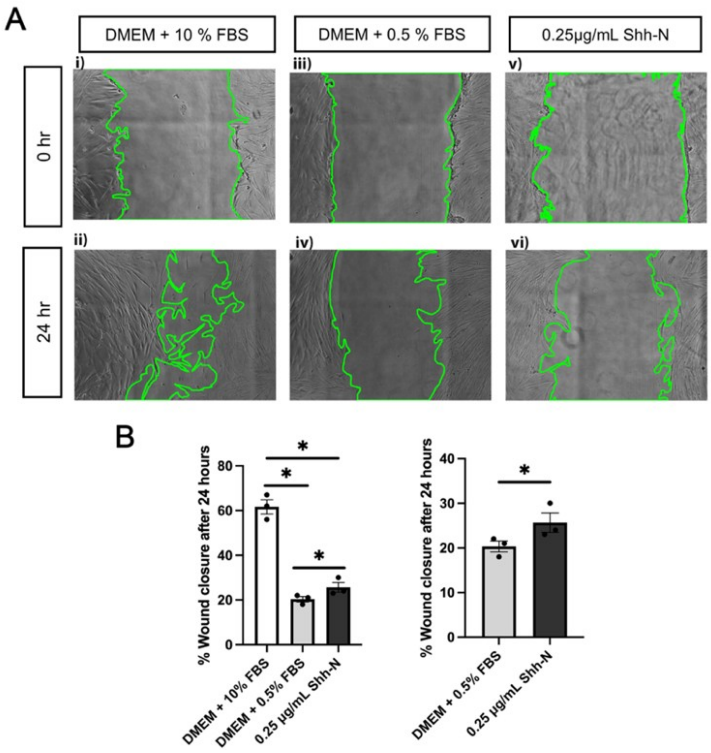

Figure 4.10. Effect of 0.25µg/mL SHH treatment on HLF wound closure.
(A) Representative light microscope images demonstrating HLF wound closure following 24 hr culture with (i-ii) DMEM + 10 % FBS (iii-iv) DMEM + 0.5 % FBS (v-vi) 0.25 µg/mL SHH(experimental group). Widefield images taken at 10× using Zeiss Axio Observer (B) Graphs showing quantification of % wound closure in HMPVECs after culturing for 24 hr. Data are presented as mean ± SEM (n = 3; Mann – Whitney U-test. *p < 0.05.

4.2.4.5 Cyclopamine treatment did not have a significant impact on HLF wound closure

Consistent with previous investigations conducted on other lung cell types (A549, HUVECs and HPMVECs), after investigating the impact of SHH treatment on HLF wound closure, the impact of the Shh inhibitor cyclopamine on HLF wound closure was investigated (Figure. 4.11). Scratch assays were set up with 5 µg/mL cyclopamine in DMEM + 0.5 % FBS, to determine whether the SHH pathway inhibitor had an impact on wound closure. As previously done a control was set up with DMEM + 0.5 % only and HLFs were also treated with DMEM + 10 % FBS as a positive control for increased wound closure. As previously described, (section 3.2.4.5) cyclopamine was reconstituted in EtOH prior to dilution in culture medium. To control for any potential effects of the solvent, HLFs were treated with the equivalent volume/ % EtOH in DMEM + 0.5 % FBS. HLFs cultured in DMEM + 10 % FBS had a mean wound closure of 62 % (Figure. 4.11A(i-ii), Figure. 4.11B), while cells in DMEM + 0.5 % FBS had a mean wound closure of 20.3 % (Figure. 4.11A(iii-iv), Figure. 4.11B). HLFs cultured in 0.001 % EtOH had a mean wound closure

of 18 % (Figure. 4.11A(v-vi), Figure. 4.11B) and HPMVECs treated with 5 μg/mL cyclopamine had a mean percentage of wound closure was 19 % (Figure. 4.11A(vii-viii), Figure. 4.11B). No significant difference was observed between HLF treated with DMEM + 0.5 % FBS (Figure. 4.11A(iii-iv), Figure. 4.11B) and HLF treated with 0.001 % EtOH Figure. 4.11A(v-vi), Figure. 4.11B) (p=0.1500). Additionally, no significant difference was observed between HLF treated with 5 μg/mL cyclopamine Figure. 4.11A(vii-viii), Figure. 4.11B) and HLF treated with DMEM + 0.5 % FBS Figure. 4.11A(iii-iv), Figure. 4.11B) (p=0.2500).

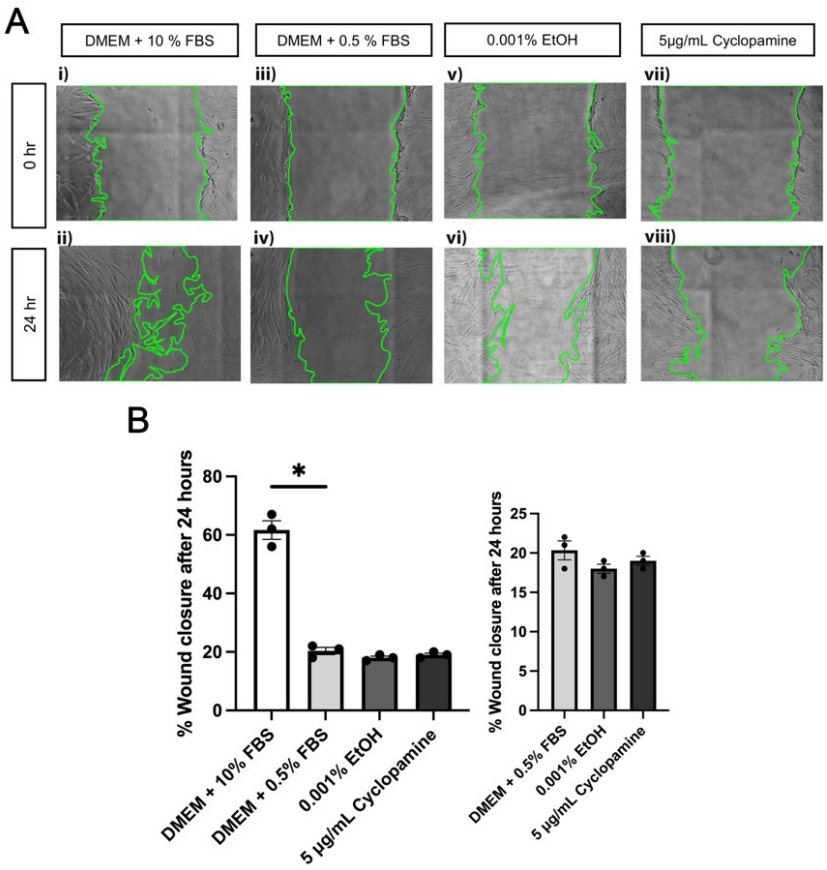

Figure 4.11. Effect of 5 μg/mL Cyclopamine treatment on HLF wound closure.
(A) Representative light microscope images demonstrating HLF wound closure following 24 hr culture with (i-ii) DMEM + 10 % FBS (iii-iv) DMEM + 0.5 % FBS (v-vi) 0.001 % EtoH and (vii-viii) 5 μg/mL cyclopamine (experimental group). Widefield images taken at 10× using Zeiss Axio Observer (B) Graphs showing quantification of % wound closure in HMPVECs after culturing for 24 hr. Data are presented as mean ± SEM (n = 3; Mann – Whitney U-test. *p < 0.05).

As previously outlined, lung repair and/or regeneration is a complex process that requires multicellular interaction (2, 28, 29, 51, 124). A systems level approach may therefore be essential to fully capture the intricacies of Shh-mediated repair. Furthermore, to gain a better

understanding of the mechanisms that underpin repair and regeneration in the alveoli post injury and specifically the role of the SHH signalling pathway, it is important to take into consideration the potential role of cellular cross-talk in facilitating repair. For this reason, following monolayer scratch assays, co-culture assays were established. Based on findings from scratch assays across different structural lung cell types (epithelial, endothelial and fibroblasts), as well as published literature, I focused on investigating the relationship between alveolar epithelial cells and fibroblasts. In addition to this, I investigated the effect of treating cells with SHH and cyclopamine while in co-culture.

4.2.5 Co-culture assays

4.2.5.1 Investigating cross-talk between the alveolar epithelial cell population and fibroblast cell population using a co-culture model

Scratch assay data demonstrated that SHH treatment reduced wound closure in alveolar epithelial cell (A549), but enhanced wound closure in fibroblasts (HLF). In contrast, endothelial cells showed no response to SHH treatment. These results informed the decision to establish co-culture assays using the two Shh responsive cell types, to explore the role of cell-cell interactions in Shh mediated alveolar repair.

To investigate migration in co-culture, I adapted a method previously described by Yuan *et al.,*(378), who utilised Ibidi™ 2-well inserts to study interactions between HPMVECs and pericytes. The complete methodology used for this thesis is detailed in chapter 2, section 2.14. Unlike monolayer scratch assays, where a wound is created by making a scratch, a cell free gap is generated by removing the culture insert once cells reach confluence (245, 246). The 2 well inserts were selected because they facilitate the simultaneous culture of two distinct cell populations and are reproducible because the cell free gap between cells is always 500 µm (245, 246)(Figure. 4.12). Since a physical scratch is not applied, this assay is more accurately described as a migration assay. Importantly, this model was adopted because it allowed the investigation of cell-cell communication.

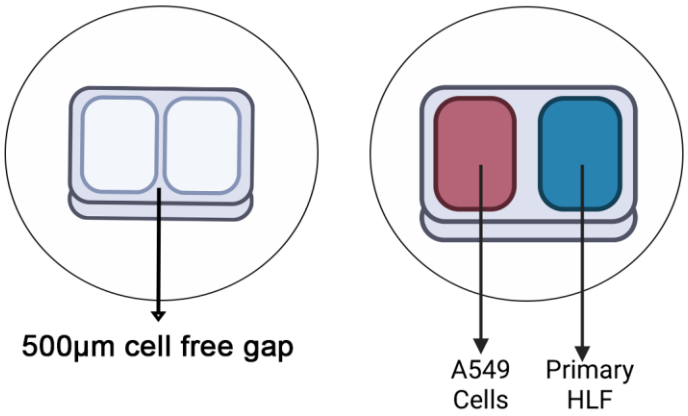

Figure 4.12. Ibidi™ 2-well inserts.
Schematic diagram of Ibidi™ 2- well insert cell, showing the cell free gap and demonstrating how two different cell types can be seeded on opposite sides of the insert.

4.2.5.2 Establishing optimal parameters for co-culture examining the role of Shh using Ibidi™ 2-well inserts

A step wise approach was used to establish co-cultures for examining the role of SHH signalling. First, A549 and HLF cells were selected based on their responsiveness to SHH treatment in monoculture wound healing assays. Then the Ibidi™ 2-well model was chosen to facilitate co-culture set-up and to enable the investigation of cell-cell cross-talk (Figure. 4.12). Following this, the parameters of the assay were optimised, this included the cell seeding density and the duration of the assay (end-point) for assessing cell migration using the 2 well inserts, as well as parameters to image the inserts.

To evaluate the suitability of the 2-well culture inserts for studying cell migration and to optimise imaging parameters, preliminary experiments were conducted using A549 cells alone, seeded on both sides of the insert at a density of $2x10^5$ per well, following the manufacturer's guidelines. After 24 hr of culture, cells reached confluence, indicating that the seeding density was optimal. Upon removal of the insert, revealing the cell-free gap, A549 cells were cultured in either DMEM+ 10 % FBS in which a high percentage of cell migration would be expected or in DMEM + 0.5 % FBS media, in which minimal cell migration was expected (Figure. 4.13). Images were taken at 0 and 20 hr using a 5× (Figure. 4.13A) and 10×

(Figure. 4.13B) air objective on an inverted Zeiss Axio Observer widefield microscope. From these experiments it was determined that a 20-hr incubation was a suitable time point for observing differences in cell migration. Based on image clarity and the field of view, the 10× objective was selected for all subsequent imaging using the 2-well inserts.

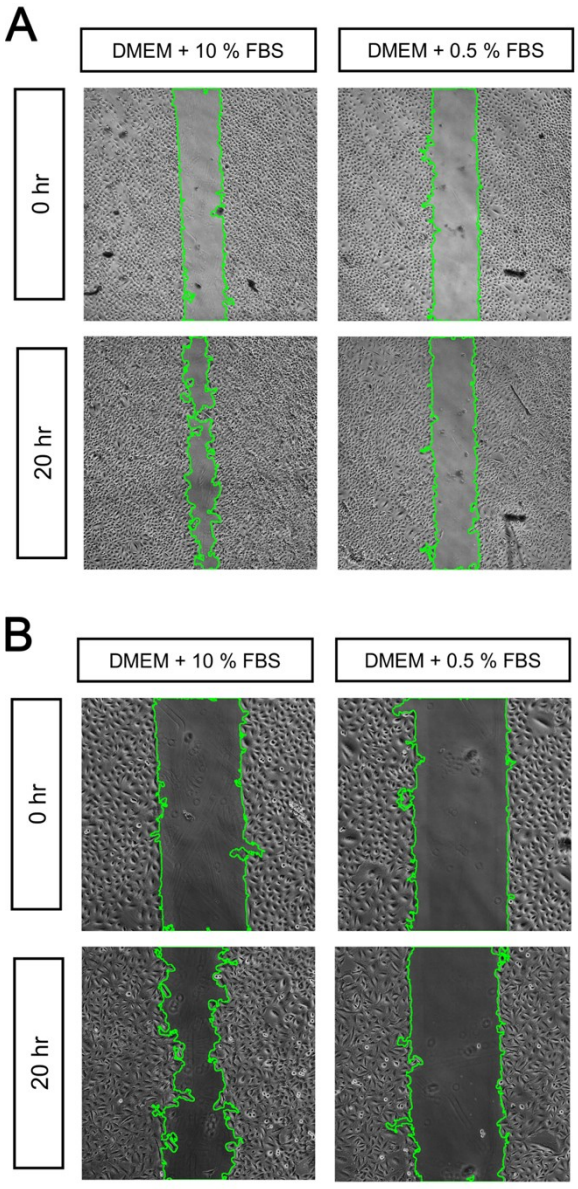

Figure 4.13. Optimisation of cell migration assay using Ibidi™ 2-well inserts.

(A) Representative light microscope images of A549 cells cultured in DMEM + 10 % FBS and DMEM + 0.5 % FBS in 2 well inserts with images taken at 5× using inverted Zeiss Axio Observer widefield microscope. (B) Represntative images of A549 cells cultured under the same consitions as (A), taken at 10×.

4.2.5.3 Investigating cell migration in A549 and HLF cell co-cultures

Co-culture assays were established by seeding A549 cells and HLF $2x10^5$ cells per well into opposite sides of the 2 well inserts (Figure. 4.14) 2 well inserts were placed in collagen coated 24-well plates for culturing, to allow for technical replicates (as shown in chapter 2 section 2.14). Each 24 well plate included three technical replicates per condition, and represented one biological replicate. The seeding density used for A549 cells was established by conducting preliminary experiments, as described in the previous section, and the same density was deemed suitable for HLFs based on data from a lab member working on another project (data not shown).

Similar to previously conducted wound healing assays, co-culture migration assays were performed using both DMEM + 10 % FBS (Figure. 4.14A(i-ii) and DMEM + 0.5 % FBS (Figure. 4.14A iii-iv) and culturing for 20 hr. There was a significant increase in migration between cells cultured in DMEM + 10 % FBS (Figure. 4.14A(i-ii), Figure. 4.14B), which had a mean percentage of migration of 59 % and cells cultured in DMEM + 0.5 % FBS (Figure. 4.14A-B), which had a mean percentage of migration of 8 % (p=0.0500). While quantitative analysis focused on measuring changes in the width of the cell free gap (Figure. 4.14B), qualitative analysis of images was also carried out to assess whether fibroblasts and epithelial cells appeared to be migrating towards one another equally. From assessment of co-cultured cells following 20 hr incubation with DMEM + 0.5 % FBS (Figure. 4.14A(iv)), it appears as though A549 cells have migrated more than HLF and some A549 cells can be seen in the middle of the cell free gap. However, after 20 hr the image of co-cultured cells incubated with DMEM + 10 % FBS appears to show a relatively equal distribution of both cell types across the cell free gap (Figure. 4.14 A(ii)).

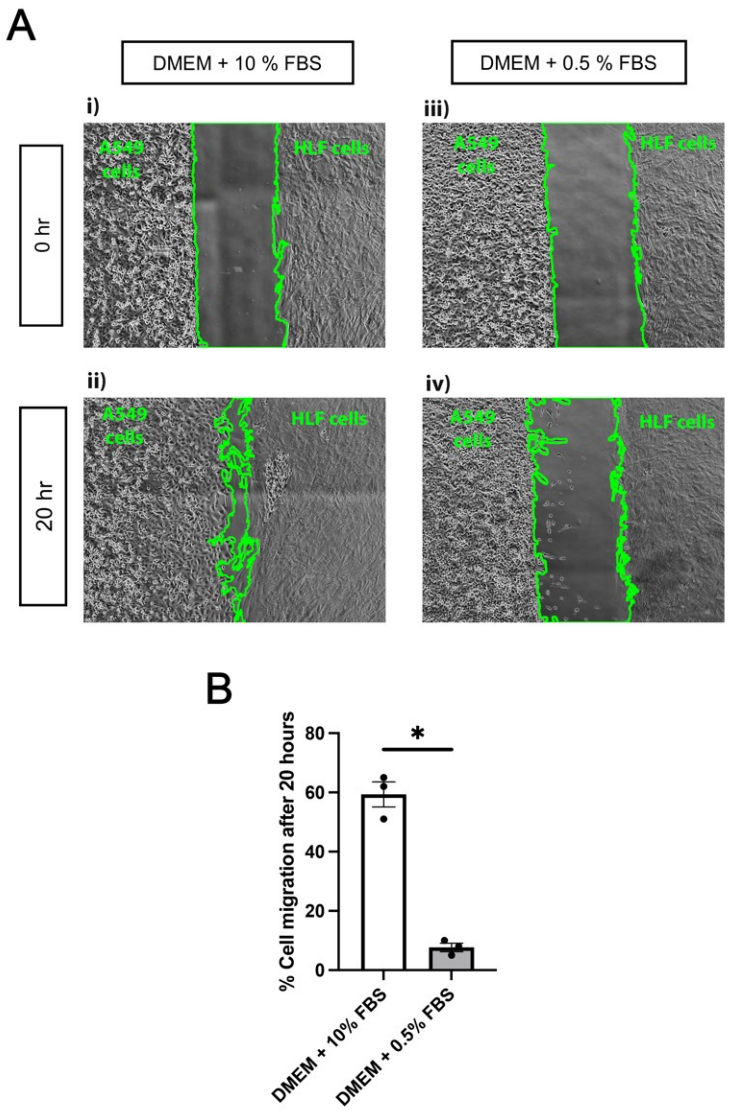

Figure 4.14. Cell migration of A549 and HLF cells in co-culture.

(A) Representative light microscope images showing A549 cells and HLF cell co-cultures following 20 hr culture with (i-ii) DMEM + 10 % FBS and (iii-iv) DMEM + 0.5 % FBS, images taken at 10× using inverted Zeiss Axio Observer widefield microscope. (B) Graphs showing quantification of % migration of co-cultured cells after 20 hr. Data are presented as mean ± SEM (n = 3; Mann – Whitney U-test. *p < 0.05).

4.2.5.4 *Investigating the role of Shh on cross cellular interactions between epithelial cells and fibroblast cells*

The effect of Shh on the migration of the co-cultured cells was investigated simultaneously within the same 24 well plate used for co-culture experiments where cells were cultured with DMEM + 0.5 % FBS alone and DMEM + 10 %, which was a positive control for induced migration for each biological replicate. Each 24 well plate included three technical replicates

per condition, and represented one biological replicate. Co-cultures were established as described in section 4.2.5.1, and once the insert was removed to reveal the cell free gap, cells were treated with 0.25 μg/mL SHH in DMEM + 0.5 % FBS. As outlined in the previous section, cell cultured in DMEM + 10 % FBS had a mean percentage migration of 59 %, while cells cultured in DMEM + 0.5 % FBS has a mean percentage migration of 8 %. Treatment with 0.25 μg/mL SHH (Figure. 4.15A(v-vi), Figure. 4.15B) significantly increased migration in co-cultured cells, with a mean percentage of migration of 25 %, in comparison to co-cultured cells in DMEM + 0.5 % FBS only (Figure. 4.15A(iii-iv), Figure. 4.15B) which had a mean percentage of migration of 8 % (p=0.0500), this was a fold change of 3.13 (≈ 213 % increase). Notably, after 20 hr SHH treatment, A549 and HLFs appeared to equidistant to each other, indicating that they migrated collectively towards each other (Figure. 4.15A(vi))

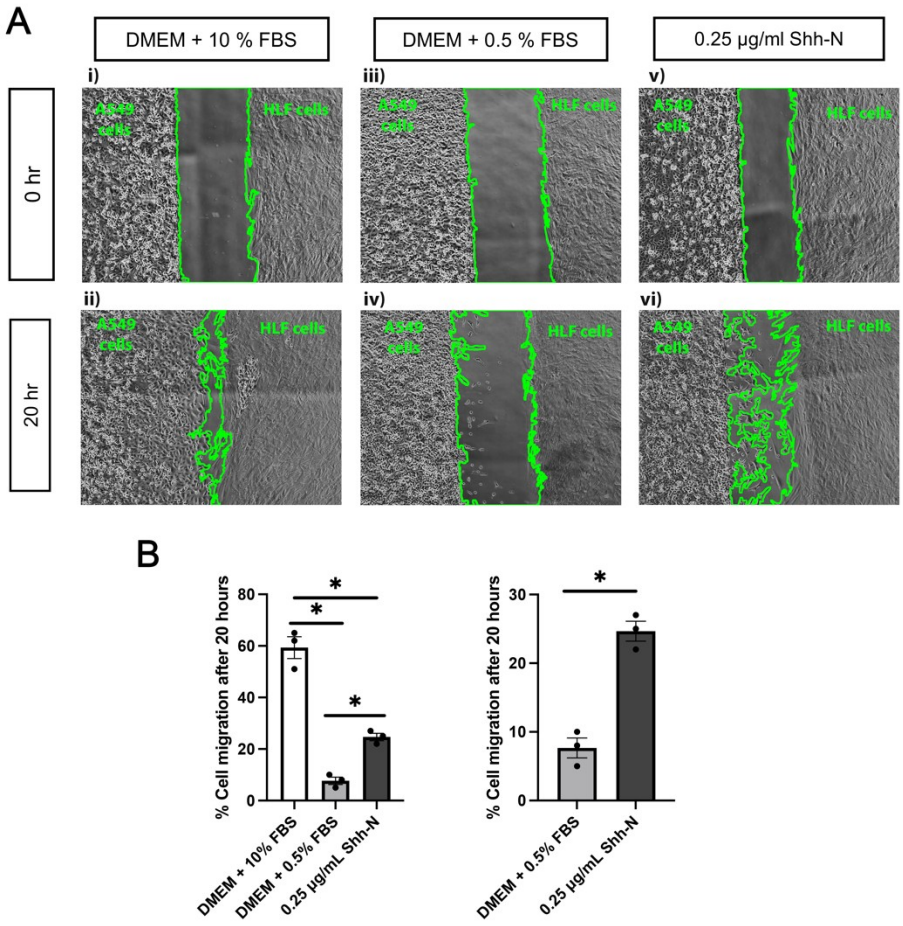

Figure 4.15. Cell migration of Shh treated A549 and HLF cells in co-culture.

(A) Representative light microscope images showing A549 cells and HLF cell co-cultures following 20 hr culture with (i-ii) DMEM + 10 % FBS, (iii-iv) DMEM + 0.5 % FBS and (v-vi) 0.25 μg/mL SHH (experimental group), images taken at 10× using inverted Zeiss Axio Observer widefield microscope. (B) Graphs showing quantification of % migration of co-cultured cells after 20 hr. Data are presented as mean ± SEM (n = 3; Mann – Whitney U-test. *p < 0.05).

4.2.5.5 *Detailed visual analysis of cell migration behaviour*

As summarised in chapter 2, sections 2.13-2.14, a macro was employed to quantify the changes in migration across the cell free area between 0 hr and 20 hr. The macro draws around the region of interest (ROI), i.e. the cell free gap, as illustrated in Figure. 4.13 To investigate cell migration behaviour in more detail, images were examined without the ROI outline (Figure. 4.16), to allow for clearer visualisation of the cells migrating within the gap. This revealed distinct differences in migration patterns between epithelial and fibroblast cells. After 20 hr, A549 cells appeared less tightly packed and cells appeared to be protruding towards the cell free gap and fibroblasts also appeared to spread towards the cell free gap, with some cells appearing to have moved more than others.

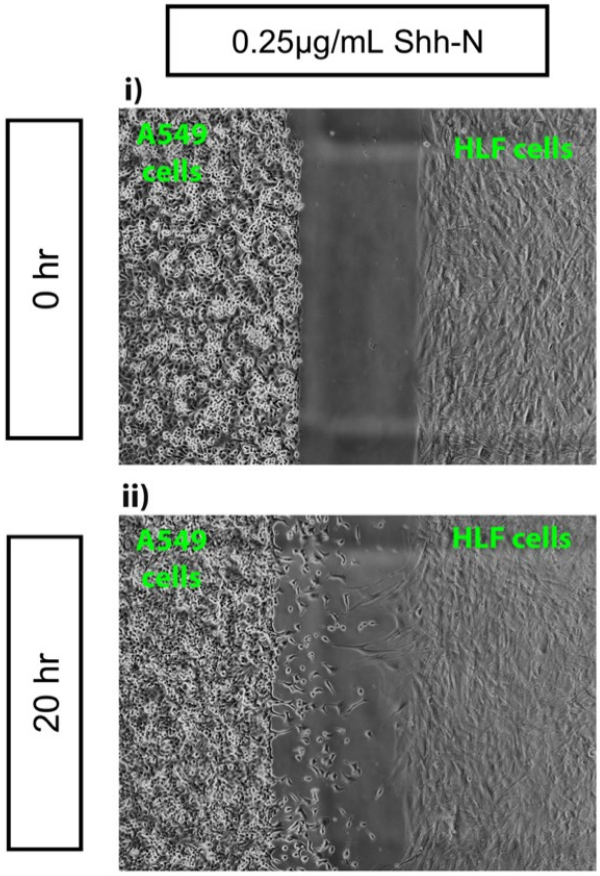

Figure 4.16. Detailed analysis of migratory behaviour of A549 and HLF in co-culture following Shh treatment.
Representative light microscope images showing A549 cells and HLF cell co-cultures treated with 0.25 µg/mL SHH at (i) 0 hr and (ii) 20 hr timepoints withough cell free gap outline, to allow detailed observation of cell migration. Images taken at 10× using inverted Zeiss Axio Observer widefield microscope.

4.2.5.6 *Investigating the role of cyclopamine on cross cellular interactions between epithelial cells and fibroblast cells*

The effect of the SHH signalling pathway inhibitor, cyclopamine was also investigated simultaneously for each biological replicate. The mean percentage of migration of cells treated with 5 μg/mL cyclopamine was 13 %. In comparison to cells co-cultured in DMEM + 0.5 % FBS only (Figure. 4.17A(iii-iv), Figure. 4.17B), which had a mean percentage of migration of 8 %, co-cultured cells treated with 5 μg/mL cyclopamine (Figure. 4.17A(v-vi), Figure. 4.17B) did not have a significant increase in migration following 20 hr (p=0.1000), with a fold-change of 1.63 (≈ 63 % increase). However, the distinct differences in migratory behaviour between epithelial and fibroblast cells can be observed.

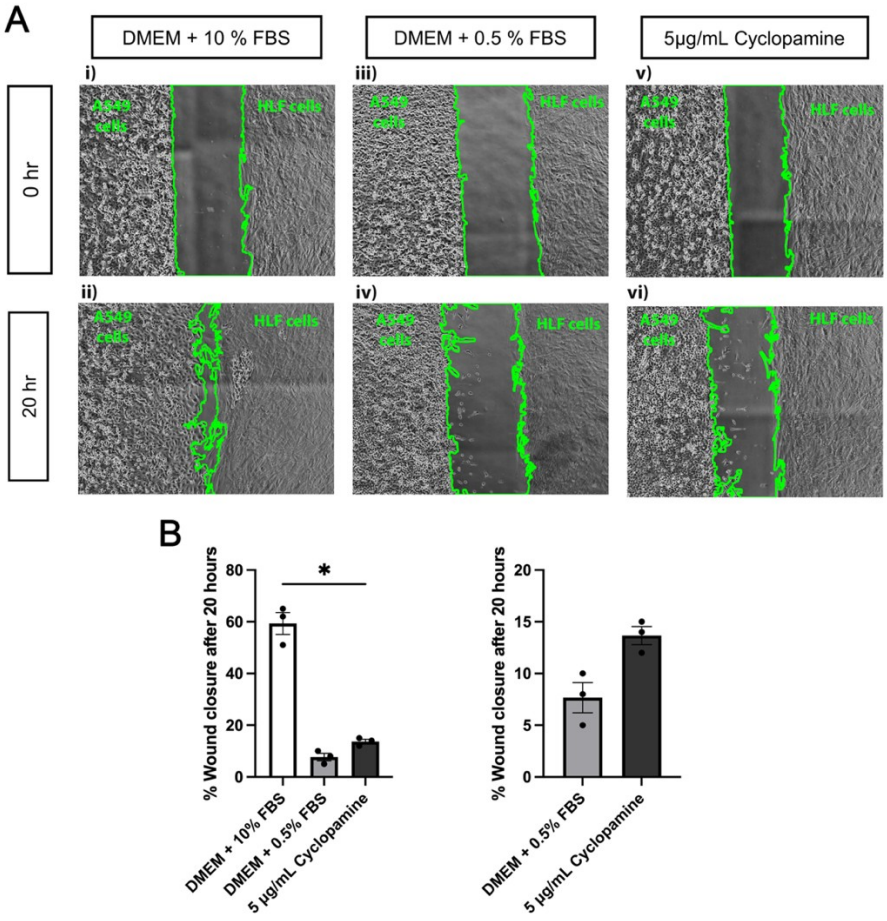

Figure 4.17. Cell migration of cyclopamine treated A549 and HLF cells in co-culture.
(A) Representative light microscope images showing A549 cells and HLF cell co-cultures following 20 hr culture with (i-ii) DMEM + 10 % FBS, (iii-iv) DMEM + 0.5 % FBS and (v-vi) 5 μg/mL cyclopamine (experimental group), images taken at 10× using inverted Zeiss Axio Observer widefield microscope.(B) Graphs showing quantification of % migration of co-cultured cells after 20 hr. Data are presented as mean ± SEM (n = 3; Mann – Whitney U-test. *p < 0.05)

4.3 Discussion

In this chapter, I sought to test the hypothesis that SHH signalling plays a role in alveolar repair by mediating cross-talk between key lung cell types. To address this hypothesis, I designed experimental investigations to determine the impact of Shh on cellular populations within the alveolar niche and to determine the significance of this in the context of repair. Initial experiments were focused on validating findings from chapter 3 by examining whether SHH treatment had an impact on endothelial cell migration using HPMVECs. Then the effects of SHH treatment on pulmonary fibroblast migration following cell isolation were assessed. Finally, I established an *in vitro* co-culture model to investigate the role of intercellular interactions on alveolar repair and/or regeneration.

4.3.1 Investigating the impact of SHH treatment on pulmonary endothelial cells

In the previous chapter, the effect of SHH treatment on endothelial cell wound closure was examined using HUVECs (section 3.2.4.9) and no significant effect on wound closure was observed. In this chapter, I repeated these experiments using HPMVECs (Figure. 4.4), which is a more physiologically relevant model for investigating the impact of Shh in alveolar repair. Both HUVECs and HPMVECs are primary endothelial cell types, and it is well established that endothelial cells display considerable structural and phenotypic heterogeneity across organs (379-382). Numerous studies have demonstrated that endothelial cell populations respond differently to the same stimuli, further emphasising the importance of using HPMVECs for follow up investigations (379-382).

Consistent with findings in HUVECs, SHH treatment did not have a significant effect on wound closure in HPMVECs (Figure. 4.4). Primary endothelial cell lines, such as HUVECs and HPMVECs, present challenges in culture due to their limited life span and reduced stability in comparison to immortalised cell lines (383, 384). Typically, these cells can only be passaged 9-10 times before losing viability or functional characteristics(383, 384). Additionally, because primary cells are derived from individual donors, studies have reported potential variability

between different cell batches, which may contribute to inconsistencies or discrepancies in experimental outcomes(383, 384). Despite these limitations, the data presented here demonstrate that SHH treatment does not have a significant effect on wound closure in either of the primary endothelial cell types tested.

Further to this, inconsistencies often observed when culturing primary cells were mitigated by conducting wound healing assays using cells at early passage (4-7) and cells from the same donor batch were used for HUVECs and HPMVECs respectively.

To further investigate the potential role of the SHH signalling pathway on endothelial repair, HPMVECs were treated with the Shh inhibitor, cyclopamine (Figure. 4.5) to determine whether inhibition of the pathway produced an opposite effect. Treatment with cyclopamine did not have an effect on wound closure, this finding was also consistent with previous observations from HUVEC wound healing assays. These findings suggest that Shh does not influence endothelial repair. However, some other studies have identified an important role for SHH signalling in modulating endothelial cells, specifically in angiogenesis, vascular differentiation and maturation, in the brain, and heart(385-390).Specifically, activation of SHH signalling has been demonstrated to induce endothelial progenitor cell differentiation, leading to vascular repair in cardiac tissue (385-389), as well as to maintain and regulate the integrity of the blood-brain barrier (390). Although evidence for a role in the lung vasculature remains limited.

Further investigations using a more physiologically relevant model of lung injury and repair, for example the AIR model (271, 276) are necessary to make more definitive conclusions about the role of Shh on the endothelial cell population. I have recently demonstrated that endothelial cells can be tracked in the AIR model by immunostaining AIR-PCLS with the endothelial cell marker ETS related gene (ERG) (277). This will facilitate investigations into the potential role of SHH in modulating the endothelial cell population post injury.

To further contextualise these findings and to evaluate the capacity of HPMVECs to respond to exogenous Shh I assessed the relative gene expression of SHH pathway genes in HPMVECs

(Figure. 4.3). I found that the expression of *SHH, PTCH1, SMO, GLI1* and *GLI2* were very low in HPMVECs with relative expression ranging from ~0.00023 for expression of both *SMO* and *GLI2* to ~0.00130. The expression of *HHIP* on the other hand was comparatively higher with a relative expression of ~0.23235. A relatively high expression of *HHIP* was also observed in HUVECs (Figure. 3.5), although *HHIP* expression levels were higher in HPMVECs than in HUVECs. The lack of responsiveness to exogenous SHH treatment, as evidenced by a lack of significant change in wound closure assays conducted using HUVECs or HPMVECs correlates with high expression of *HHIP.* Similar to findings with HUVECs the low expression of downstream transcription factors *GLI1/GLI2* also correlates with the lack of responsiveness to SHH treatment. Broadly this indicates that SHH signalling is minimal in endothelial cells and/or SHH signalling is regulated by factors from other pathways.

4.3.2 Investigating the impact of SHH treatment on HLF wound closure

As part of this project, I successfully isolated primary HLFs from histologically normal lung tissue. Immunostaining confirmed strong vimentin expression and minimal pan-cytokeratin^{+} cells, indicating high fibroblast purity (Figure. 4.6).

Next, I demonstrated that treatment with SHH enhances wound closure in HLFs (Figure. 4.10). This finding is both clinically relevant and novel, since the impact of SHH on primary HLF migration has not been previously reported in a scratch assay model.

The CCL-206 (MLg2908) cell line is a mouse lung fibroblast (MLg) cell line, which was originally isolated in 1974 from normal neonatal ddY mouse spontaneously transformed with C-type particles (391). These cells exhibit typical fibroblast morphology and have been widely used to investigate pulmonary fibrosis and cellular and molecular mechanisms underlying lung diseases(392-395). While a previous study performed scratch assays using the MLg cell line (391, 396) and treated cells with both SHH and cyclopamine (393), to our knowledge, our study is the first study to investigate and demonstrate the effect of SHH on wound closure in primary HLF. Our findings are consistent with those of Bermudez et al.,(393), who reported increased wound closure in the MLg cell line following SHH treatment. Interestingly, they also

observed a significant reduction in wound closure with cyclopamine treatment (393), whereas I found no significant difference in wound closure following cyclopamine treatment of HLF (Figure. 4.11). Notably, their experimental investigation involved 26-hour incubation, whereas as our assays were conducted for 24 hours, which may partly explain the differences observed(393). However, a 2-hr difference in incubation is unlikely to make a significant difference. The differing response to cyclopamine observed in our investigation may instead be as a result of using primary cells which exhibit greater heterogeneity than immortalised cells, however our model is more physiologically relevant than immortalised cells like MLg cells.

To contextualise the findings from the wound healing assays, I examined the expression of SHH pathway components in HLFs (Figure. 4.8). This analysis allowed me to correlate the functional response of HLFs to both SHH and cyclopamine treatment with the expression levels of key SHH pathway genes and also provided insight into the molecular mechanisms underlying the observed effects on fibroblast migration.

It was determined that the expression of all SHH pathway components were extremely low in HLFs, ranging from ~0.00009 for *SHH* expression to ~0.00140 for *PTCH1* expression. This suggests that the canonical SHH pathway is quiescent in HLFs and aligns with published studies which highlight that the origin of Shh in the lung is the epithelium (181, 187, 353). Interestingly, *SHH* expression was low across all cell types investigated as part of this thesis (A549, HUVEC, HPMVEC, HLF) (Figure. 4.9), highlighting a limitation of *in vitro* cell culture models. *In vivo* Shh is predominantly secreted by epithelial cells and signals to neighbouring mesenchymal populations. In monoculture, the absence of epithelial-mesenchymal interactions and the lack of a physiologically relevant lung microenvironment is likely to contribute to the minimal endogenous Shh expression, particularly in A549 cells(237, 347, 397). However, the enhanced wound closure following HLF treatment with exogenous Shh demonstrates that HLF retain the capacity to respond to SHH signalling and also highlights the greater physiological relevance of primary cells compared to immortalised cell lines(237). Future studies assessing the expression of pathway components in primary alveolar epithelial cells would provide valuable insight. Furthermore, to ascertain the role of Shh on the

fibroblast population in wound healing further experimental investigations can be conducted where HLF are treated with Shh and subsequently with the SHH inhibitor, cyclopamine. This approach is specifically important to determine whether the observed effects of SHH on wound closure are mediated through canonical SHH signalling.

4.3.3 Co-culture models are an effective model for investigating the relationship between epithelial cells and fibroblasts to drive cell migration

To increase the complexity of our alveolar repair model and further explore the role of Shh, the next aim of this chapter was to investigate and determine the importance of cellular crosstalk. Based on data from our wound healing assays, which showed that SHH treatment reduced A549 wound closure (Figure. 3.10) but increased HLF wound closure (Figure. 4.10), along with supporting evidence from previous studies highlighting the importance of epithelial-mesenchymal interactions in alveolar repair (9, 11, 13, 181). I successfully established co-culture experiments using the alveolar epithelial cell line, A549 and primary HLF to further explore the interactions between these two cell types during the repair process (Figure. 4.14-4.16).

These co-culture experiments provide important insight into the role of epithelial-fibroblast crosstalk in alveolar repair. In monoculture, SHH reduced wound closure in A549 cells, but enhanced wound closure n HLFs, whereas in co-culture, SHH promoted migration of both cell types (Figure. 4.15). This suggests that interactions between alveolar epithelial cells and fibroblasts can modulate SHH responsiveness, either through paracrine signalling or direct cell-cell interactions. The enhanced migration observed in co-culture highlights the physiological relevance of this model, this model recapitulates the *in vivo* alveolar microenvironment where epithelial-mesenchymal interactions are critical for repair. Importantly these findings highlight the role of Shh in alveolar repair and confirm that Shh repair is reliant on complex multicellular interactions(11, 13, 372, 373).

It is important to consider the potential mechanisms underlying the cross-talk between epithelial and HLF cells, which leads to the enhanced cell migration observed in co-culture.

For example, SHH treatment may induce the release of mediators from fibroblasts, which promote epithelial cell migration, a response that was not observed when epithelial cells in monoculture were treated with SHH. Additionally, many studies have shown that SHH interacts with other signalling pathways including TGF-β, FGF and Wnt (8, 13, 28, 398), these interactions may also have an impact on the production and regulation of mediators, therefore modulating the increase in migration observed in co-culture.

To further investigate the role of SHH on alveolar repair, I conducted similar experiments where A549 and HLF cells in co-culture were treated with the Shh inhibitor cyclopamine (Figure. 4.16). Interestingly, cyclopamine treatment had no significant impact on cellular migration of co-cultured cells. Relating this back to the gene expression data collected where endogenous *SHH* expression was low in both A549 and HLF cells (Figure. 4.9), the lack of change following cyclopamine treatment reaffirms that the enhanced migration is mediated by exogenous SHH treatment. However, similar to with monoculture HLF experiments, it would be informative to conduct further experiments where co-cultured cells are treated with SHH and subsequently cyclopamine.

While our findings are informative, our understanding of the interactions between epithelial and fibroblast cells following SHH treatment could be expanded by studying migration over multiple timepoints. The initial plan was to conduct time-lapse imaging experiments to observe the trends in early and late migration in co-cultures. This would provide deeper insight into temporal trends and would help us to understand if either of the cell types influence each other to migrate. This is specifically important because it is known that the migratory behaviour of these two cell types differs (375, 376).

Additionally, the breadth of experimental investigations possible using this co-culture model were not explored in this project due to time constraints. As demonstrated by Yuan *et al*., (378), who also utilised the Ibidi™ 2 well inserts culturing system, cellular interactions can be studied in greater detail by examining cellular polarisation. Yuan *et al*., (378) stained pericytes with pericentrin to assess pericyte polarisation towards endothelial cells, as well as with F-actin (also known as phalloidin) to examine cytoskeletal activity during cell migration. My

investigations can be optimised by staining co-cultured cells with F-actin and pericentrin as demonstrated by Yuan *et al*., (378) and further to this, we can stain for protein tyrosine kinases to assess fibroblast polarisation (399, 400). Investigating cell polarity would allow us to determine the direction of both epithelial and fibroblast cells and to determine whether the cells are actively moving towards each other. Staining for cell polarisation markers coupled with time lapse imaging as shown by Yuan *et al.,* (378) would deepen our understanding of the mechanisms which underlie epithelial-mesenchymal crosstalk during alveolar repair in the context of Shh modulation.

4.4 Conclusion

In this chapter, I confirmed that SHH does not have a significant effect on endothelial cell wound closure. In contrast, I identified a clear role for SHH in promoting fibroblast wound closure. I also previously showed that Shh had an impact on epithelial wound closure modelled using A549 cells. Building on these findings, I established a co-culture model to investigate how interactions between alveolar epithelial cells and human pulmonary fibroblasts influence the repair process, following SHH treatment. Remarkably, I demonstrated that co-culture resulted in a more potent effect of SHH on cell migration, with both A549 and HLF cells actively migrating. This is likely to reflect the more complex model system used and demonstrates that the co-culture model is a more physiologically relevant and translatable model to investigate *in vivo* repair responses. Collectively these findings further confirm the role of SHH in modulating alveolar repair.

Future work will focus on further optimisation of the co-culture model and extending its application to investigate cellular cross-talk between epithelial and endothelial cells, as well as to develop the epithelial cell and fibroblasts co-culture, which I show in this chapter.

Chapter 5

Investigating the effects of SHH pathway modulation in healthy and injured or diseased

5.1 Introduction

Current treatments available for respiratory diseases are not curative and primarily help patients to manage their symptoms and/or slow down disease progression (1, 5, 271). In recent years antifibrotic agents have been developed, including nintendanib and pirfenidone, which slow down disease progression in patients with IPF but cannot reverse fibrosis(401-404). Recent advances have also been made in the development of cystic fibrosis transmembrane conductance regulator (CFTR) channel modulators, including ivacaftor, lumacaftor and tezacaftor, which have led to improvements of patient lung function and overall quality of life (405-409). Despite these advances, in cases of severe lung damage, lung transplantation often remains the only viable therapeutic option(5). This highlights the urgent need to identify and develop novel treatments aimed at improving patient outcomes and potentially modifying the course of respiratory diseases. This lack of new treatments may in part, stem from our limited understanding of the role of signalling pathways in lung injury and repair, as well as from the absence of advanced translational models that can adequately replicate the complexity of the *in vivo* lungs.

5.1.1 Shh in Health and Disease

Emerging research suggests that SHH signalling is associated with various lung diseases including lung cancers, chronic obstructive pulmonary disease (COPD), pulmonary fibrosis and asthma(181, 410). However, our understanding of the precise role Shh plays in the pathogenesis of these diseases remains limited. In addition to this, it is crucial to determine whether SHH signalling is a driver of disease progression or whether it plays a protective role in response to injury or disease onset. Interestingly, recent genome-wide association studies (GWAS) have demonstrated that single nucleotide polymorphisms (SNPs) within Hedgehog Interacting Protein (*HHIP*) are associated with lung function(411-413). Furthermore, studies have identified single-nucleotide polymorphisms (SNPs) in *HHIP* as significant genetic risk factors for COPD and emphysema (68, 304, 412, 414). Emphysema, one of the pathologies within the COPD umbrella, it is characterised by damaged alveoli(414), further highlighting the importance of our research which has focused on investigating repair of structural cells within the alveolar niche.

HHIP encodes an endogenous secreted protein, HHIP that negatively regulates the SHH signalling pathway by binding directly to the Shh ligand and preventing its interaction with Ptch1 receptor, therefore inhibiting pathway activation(181, 415-417). Whilst other SHH signalling pathway inhibitors have been identified, HHIP is the only endogenous inhibitor(415-417). During lung development, HHIP modulates SHH signalling to prevent overactivation(181, 416, 417). Specifically during branching morphogenesis, Hhip mediated inhibition of the SHH pathway enables FGF10 expression, which is critical for secondary bud formation. This regulatory role of HHIP is maintained in the adult lung during homeostasis (418).

Additionally, findings from chapters 3 and 4 of this thesis support the growing evidence that SHH signalling plays a pivotal role in lung repair and regeneration. Taken together, this further highlights the importance of investigating and determining differences between SHH pathway activity between healthy and diseased lung tissue. Accurate human lung models are also crucial to investigate the role of signalling pathways, such as Shh in lung disease pathogenesis and to identify therapeutic targets.

5.1.2 Human models of lung injury and repair

The mammalian lungs are comprised of numerous cell types, each playing a distinct role within the lung niche(34-36). Traditional cell culture models lack many of the critical components of the lung, thus they fail to accurately replicate the *in vivo* environment(239, 308). This limitation has driven the development of 3D models that better capture the complexities and represent the environment of the lungs *in vivo*(239, 308).

Animal models have contributed significantly to the discovery and our understanding of processes within the lungs. However, the extent to which animal models accurately reflect human biology and the environment of the human lungs *in vivo* is limited, in addition the use of animal models poses ethical challenges(236, 239, 263). Human new approach methodologies (NAMs), also referred to as non-animal technologies (NATs) are being developed and adopted as alternatives to traditional animal models, offering more accurate

representations of the *in vivo* lung environment.(236, 239, 263). These include; cell culture, air-liquid interface (ALI) models, lung organoids, lung-on-a-chip microfluidic models and the use of precision cut lung slices (PCLS)(236, 239, 263, 268, 307). Furthermore, the Food and Drug Administration (FDA) have issued guidance encouraging the reduction of animal testing and announced a plan to phase out mandatory animal testing for novel therapeutics, highlighting the increasing shift away from animal models(419). In addition to this, the current Labour government's manifesto includes a commitment to phase out animal testing, again reflecting growing support for alternative research methods(420).

In parallel, there is a growing number of publicly available databases which have contributed to our understanding about human disease mechanisms. The Human Lung Cell Atlas (HLCA) (421, 422) provides a comprehensive single-cell reference atlas of the human lung, integrating data from single-cell transcriptomic studies to map cellular diversity and cell lineage as well to profile cell populations across healthy and diseased states (421, 422). Another useful database is LungMAP (39), which integrates transcriptomic, proteomic and imaging data to characterise lung development, cellular populations within the lungs and cellular changes across healthy and pathological states. Disease-specific databases that integrate single-cell RNA sequencing (scRNA-seq) data from both healthy and diseased lung samples further enable the identification and study of cell type–specific alterations associated with pathology. Examples include the Idiopathic Pulmonary Fibrosis (IPF) Cell Atlas (423), the COPD Cell Atlas (304) and COVID Cell Atlas (424).

Despite the wealth of information provided by these databases (39, 304, 421-424), experimental validation in physiologically relevant systems remains essential. PCLS are increasingly being employed for respiratory research and investigations due to their versatility and physiological relevance(239, 269-273). PCLS retain the complex 3D tissue architecture of the lungs. Additionally, PCLS closely replicate the *in vivo* lung physiology because native cell-cell and cell-ECM interactions are maintained (269-273, 276).

5.1.3 The AIR model

The AIR model was developed by the Dean lab group in mouse PCLS (271, 276). In this model, a spatially localised injury is generated by briefly applying HCl to a restricted region of the PCLS. The model allows for the investigation of repair and regeneration responses, with the ability to track and quantify relevant cell populations such as ATII cells by labelling with specific markers(271, 276). In chapter 3 the AIR model was successfully used to investigate the role of Shh in lung repair post injury.

Translation of the AIR model into human tissue will enable mechanistic studies of early lung repair and regeneration, providing a valuable pre-clinical platform for drug screening and ultimately therapeutic intervention. Specifically for this thesis, establishing the AIR model in human lung tissue (hAIR), provides a more complex model to investigate the role of Shh in lung repair and regeneration, and build upon the data collected in chapters 3 and 4.

5.1.4 Hypothesis and Aims

The primary hypothesis of this chapter is that a relationship exists between SHH signalling and the incidence or progression of lung diseases involving dysregulated repair, such as COPD.

I hypothesised that establishing the AIR model, in human PCLS would provide a translationally relevant, reproducible *ex vivo* model of lung injury and repair to facilitate mechanistic studies and address the current lack of suitable models required for effective drug discovery.

To test these hypotheses, the following aims were defined for this chapter:

1. To investigate and compare the expression of key SHH signalling pathway components in healthy versus emphysematous human lung tissue, in order to assess potential changes associated with disease.

2. To use the COPD Cell Atlas to examine and compare SHH pathway component expression across human lung cell types and identify alterations associated with disease pathology.

3. To establish the AIR model in human PCLS and to use this complex model to investigate the role of Shh in human lung repair and regeneration.

5.2 Results

Our investigations have focused on understanding the effects of Shh on different alveolar cell populations in order to build our understanding of this signalling pathway in repair and regeneration following injury. Wound healing assays revealed that Shh had an opposite effect on epithelial and fibroblast cells. SHH treatment led to a reduction in A549 wound closure compared to untreated controls (25 % wound closure vs 31 % in untreated cells), while SHH treatment significantly promoted repair in HLFs (26 % wound closure vs 19.3 % in untreated cells). Further analysis using a co-culture model demonstrated that SHH treatment increased cell migration from 8 % in untreated conditions to 25 %, with both A549 and HLF cells actively migrating. To build upon these findings in a more physiologically relevant model, I employed the AIR model. I observed a relationship between Shh and the fibroblast cell population, SHH treatment resulted in a dose-dependent increase in vimentin expression in the acid-injured region of AIR-PCLS. Consistent with this finding, a similar dose-dependent trend was observed when myofibroblasts (marked by α- SMA) and lipofibroblasts (marked with ADRP) were investigated.

Having identified a relationship between SHH signalling and fibroblasts as well as an effect of SHH signalling on epithelial-fibroblast interactions, I sought to determine whether these findings would be replicated in human lungs.

Adult-control and emphysematous human lung tissue samples were obtained from the Respiratory Biomedical Unit (BRU) Biobank at the Royal Brompton Hospital (methods section 2.3). Specifically, in this study tissue was obtained from 6 patients with histologically normal tissue and 6 age matched patients with emphysematous tissue. Full informed consent was provided by all participants and anonymised clinical data was used to record patient demographics (Table 5.1).

Table 5.1.Patient demographics and pulmonary function data for normal and emphysema samples included in study

Background Lung	Age at Tissue Collection	Sex	Diagnosis	FEV1 (Litres)	FVC (Litres)	Smoking history (cpd= cigarretes per day)
Emphysema	27	M	emphysema			
Emphysema	41	F	emphysema	0.83 (30.1%)	1.05 (33%)	Non smoker
Emphysema	53	F	emphysema	0.32 (13%)	1.53(52%)	Ex smoker, started aged 19yrs, stopped aged 51yrs, 10cpd
Emphysema	60	F	emphysema	1.25 (51%	2.68 (59%)	Current smoker, 5cpd
Emphysema	71	M	emphysema	0.53 (20%)	1.9	Ex smoker, 20 cpd
Emphysema	81	M	emphysema	2.24 (44%)	3.10 (76.4%)	Ex-smoker
'Normal'	28	F	Pneumothorax			
'Normal'	41	F	Metastatic Osteosarcoma	2.2	4.5	Non smoker
'Normal'	53	F	Non mucinous adenocarcinoma lepidic and acinar predominant pattern	1.9 (81%)	3.9 (132%)	Ex smoker, stopped for 14yrs, 20 cpd
'Normal'	60	F	Adenocarcinoma consistant with metastatic colorectal carcinoma			
'Normal'	71	M	Sarcoidosis	3.1	4	Ex-smoker, 70 cpd between ages 20-49
'Normal'	81	F	Adenocarcinoma, acinar predominant	2.25 (137%)	2.83 (139%)	Non smoker

*Where table is blank this data was not obtained from Biobank

5.2.1 qPCR comparison of SHH signalling in control and emphysema lungs

RNA was extracted from human tissue samples as described in methods section 2.9, subsequently cDNA was synthesised and qPCR was conducted to determine whether there were changes in the relative expression level of SHH pathway genes in normal vs. emphysematous lung tissue.

5.2.1.1 Selecting appropriate reference genes for normalisation of gene expression of key SHH pathway genes in control and emphysematous lung tissue

Accurate quantification of gene expression using qPCR requires normalisation to reference genes that have consistent and moderate levels of expression across all experimental conditions(335, 336, 338). For this investigation, it was important to select the appropriate reference gene to ensure reliable comparison of key SHH pathway gene expression between control and emphysematous lung tissue. Three reference genes, *B2M, GAPDH* and *GUSB* were selected to assess for stability in samples based on existing literature identifying stable housekeeping genes in lung tissue (301-303), as well as previous validation studies conducted

within the lab group. However, the expression stability of these reference genes in the context of pulmonary disease such as emphysema was not known.

To assess their suitability, expression stability of these candidate reference genes was compared across control and emphysematous lung tissue samples, by examining mean Ct values for consistency both within and between groups. Among the three candidate genes, *GAPDH* exhibited the most stable expression, with minimal variation in Ct values across all samples, normal and emphysematous. Further to this, *GAPDH* Ct values were moderately expressed (Ct mean between 21.2-22.6 across all samples) (Figure. 5.1). *B2M* Ct values were not as stable, with mean Ct values ranging from 20.7-23.3 across all samples (Figure. 5.1). *GUSB* Ct values were too high for reliable quantification, indicating low expression, and Ct values were not stable across samples (mean Ct between 27.8-31.1) (Figure. 5.1). Therefore, *GAPDH* was selected for normalisation of key SHH signalling pathway gene expression data.

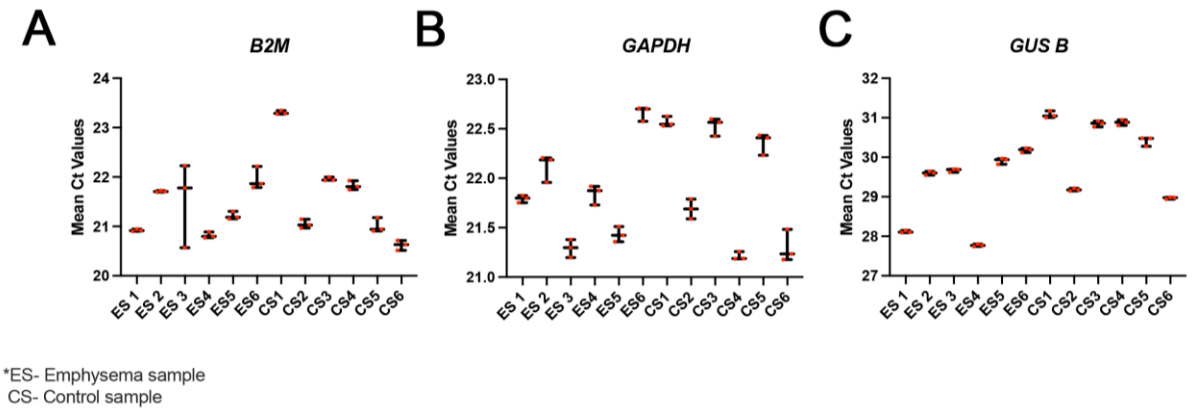

Figure 5.1. Mean Ct values of candidate reference genes in emphysema and control patient samples.
The stability of *B2M, GAPDH* and *GUSB* expression was assessed in emphysema samples (ES) and control samples (CS).

5.2.1.2 *Determining the relative expression of target genes in emphysema samples versus control samples*

After selecting *GAPDH* as the reference gene, target gene expression levels were normalised to *GAPDH* using the ΔΔCt method. For each target gene, the mean ΔCt values were calculated for both control and emphysema patient samples. Following this, the ΔΔCt values were calculated by comparing the mean ΔCt values of emphysema samples to control samples and

relative fold change was determined using 2^- ΔΔCt. Fold change is presented as gene expression in emphysema patient samples compared to control patient samples.

Technical replicates were included for each gene probe per qPCR plate and to ensure the reproducibility, each qPCR assay was repeated independently three times. Since the same biological starting material (emphysema or control patient samples) was used for each independent repeat, these cannot be referred to as biological repeats. However replicates served to confirm consistency of amplification.

Differential relative expression of key components of the SHH signalling pathway genes was observed in emphysematous lung tissue compared to controls (Figure. 5.2A). Shh expression was upregulated with a mean fold change of 1.41. Similarly, the pathway receptor *PTCH1* was upregulated and had a mean fold change of 1.38, as were transcription factors *GLI1* and *GLI2,* which had mean fold changes of 1.15 and 1.35 respectively. While *SMO* had a mean fold change of 1.11, indicating modest upregulation, remaining close to baseline level.

In contrast, *HHIP* was downregulated in emphysema patient samples compared to control samples, with a mean fold change of 0.84. There is an inverse relationship between Shh which is upregulated and *HHIP* which is downregulated (Figure. 5.2B).

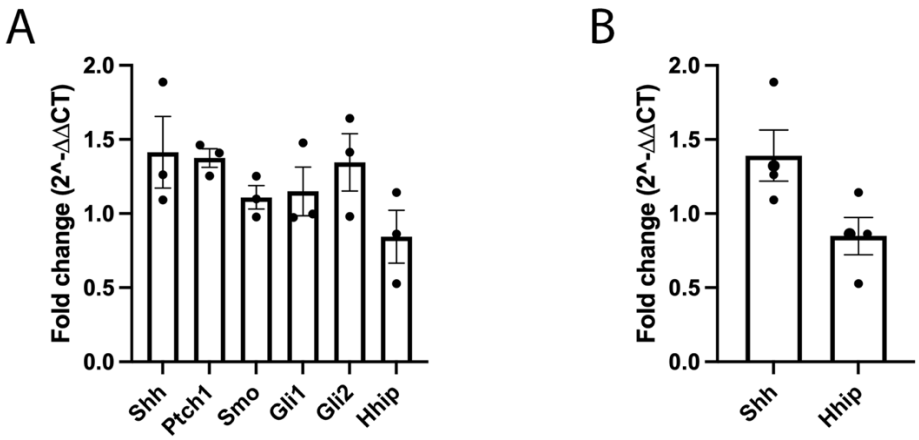

Figure 5.2. Expression of SHH pathway genes in emphysema patient samples compared to normal (control) patient samples.

Gene expression was normalised to *GAPDH* (housekeeping gene) and fold change is presented as gene expression in emphysema patient samples compared to normal patient samples. Values > 1.0 gene indicate upregulation in emphysema. Values < 1 indicate downregulation in emphysema. (A) Shows fold change for all SHH pathway genes in emphysema patient samples. (B) Shows fold change for *SHH* and *HHIP* specifically in emphysema patient samples.

5.2.1.3 Assessing differential gene expression in Emphysema samples using power analysis

Following analysis of qPCR data, GraphPad Prism was used to perform power analysis to assess how accurately our study could detect differences or changes in gene expression between emphysema and control samples. Based on study design, an unpaired t-test, two tailed (alpha=0.05), was chosen for analysis. The power analysis revealed that for a medium effect size (Cohen's d= 0.5)(425), 64 samples per group (128 in total) (Figure. 5.3A) would be needed to reach the commonly accepted power of 80 %. To achieve a large effect size (Cohen's d=0.8) (425), the number of samples required reduces to 26 per group (52 in total) (Figure. 5.3B). In this study there were only 6 samples per group, therefore the estimated statistical power to detect medium changes was low (~21 %), while the power to detect large effects was ~81 %. This indicates that the sample number is sufficient for detecting large effects but reveals that there is not enough power to detect smaller changes.

The power analysis was done for the whole dataset (Figure); however it is important to take into consideration differences for each gene. Ideally, power analysis should be conducted for each gene separately but a general approach was taken due to our small sample size.

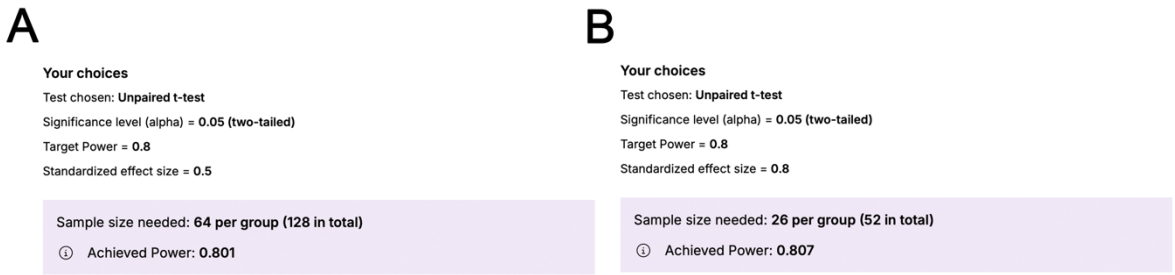

Figure 5.3.Power analysis of differential gene expression in emphysema patient samples.
Power analysis was performed to determine whether the study sample size could reliably be used to detect change in gene between emphysema and controls (A) Shows power calculation for a medium effect size (Cohen's d= 0.5) (4) (B) Shows power calculation for a large effect size (Cohen's d=0.8) (4).

5.2.2 Investigating expression levels of SHH signalling pathway genes in healthy and COPD lungs using the COPD Cell Atlas

To build on the data collected from our qPCR investigation using normal and emphysema patient samples, I decided to explore publicly accessible genomic and transcriptomic databases to determine whether our findings aligned with existing datasets. Specifically, I utilised the COPD Cell Atlas, which is an open access web tool developed by the Kaminski lab(304, 305). The COPD atlas provides single cell RNA sequencing (scRNA-seq) data from lung tissue samples of both healthy individuals and COPD patients(304, 305).

The COPD atlas was developed as part of a project aimed at characterising gene expression across different cell types in lung tissue from healthy individuals and COPD patients(304, 305). I chose to use this resource because it enables users to input genes of interest and generate cell type specific graphs and expression maps(304, 305). This web tool helped us to further examine the expression patterns of the key genes within the SHH pathway across distinct cell populations and to investigate differences between healthy and COPD tissue samples. I decided to investigate and assess the gene expression profile of *SHH*, *PTCH1*, *SMO*, *GLI1*, *GLI2* and *HHIP (Figure. 5.4-5.6)*, as had been done when I conducted qPCR investigations.

I divided the analysis by cell type using the web tool, selecting to focus on the epithelial, endothelial and stromal cell populations. Then I focused the analysis further by examining differential expression of the key SHH pathway genes in cellular subtypes within each cell population.

The output from the COPD Cell Atlas was in the form of dot plots where the intensity of the colour of each dot represents the average level of gene expression within a cell type and the size of each dot which indicates the percentage of cells within the population expressing the gene.

5.2.2.1 *Observations in epithelial cells*

The paper published alongside the development of the COPD cell atlas outlines that using scRNA-seq 9 distinct epithelial cells types were identifies based on the expression of cell specific markers(304). The cells identified were PNECs, goblet, ciliated, basal, ATII, ATI and aberrant basaloid cells. Two clusters of ATII cells were identified, $ATII_A$ expressed *SFTPC*, while $ATII_B$ cells expressed *SFTPC* as well as *SFTPA1, SFTPA2, and ETV5(304).*

Analysis of SHH pathway gene expression across the identified epithelial subtypes revealed distinct patterns in expression (Figure. 5.4). Interestingly, *HHIP* was highly expressed in $ATII_B$ cells from both COPD and control samples. $ATII_B$ cells showed both high average expression of *HHIP* (indicated by strong colour intensity) and a high proportion of expressing cells (reflected by large dot size) (Figure. 5.4). This expression pattern suggests potential role for *HHIP* in alveolar epithelial function and highlights *HHIP* as a gene of interest for COPD pathogenesis. *GLI1* was not found expressed in any of the epithelial cells but *GLI2* expression was high in PNECs of control samples. Both *GLI2* and *PTCH1* showed low expression of aberrant basaloid cells restricted to COPD patient samples, which could be associated to disease pathology. Finally, *SHH* and *SMO* exhibited minimal to no expression across all cell types, as reflected by negligible dots and faint colour intensity of dots on plot (Figure. 5.5).

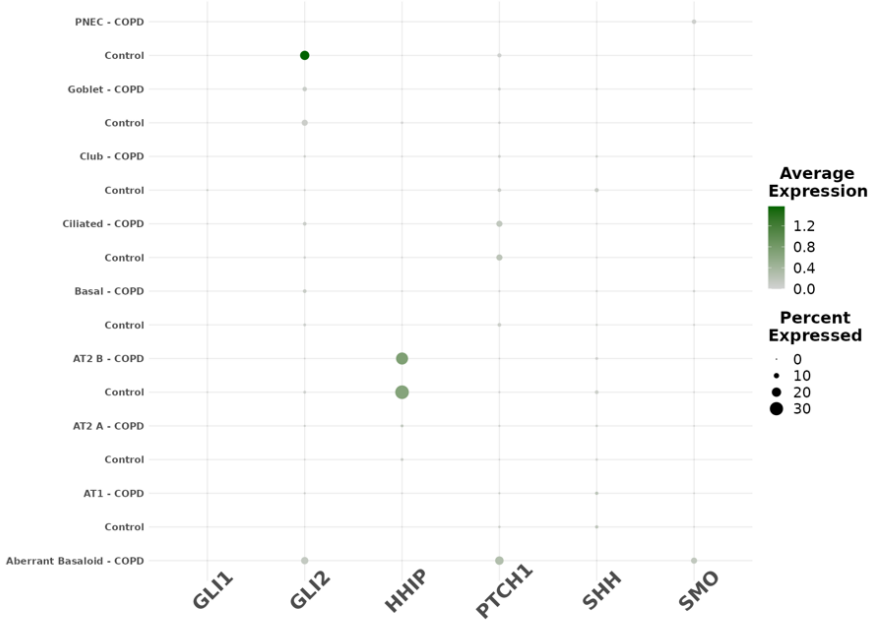

Figure 5.4. Expression of SHH signalling pathway genes across lung epithelial cells in COPD and control patient samples. Dot plot showing SHH pathway gene expression across epithelial cell types. Dot colour indicates average expression; dot size represents the percentage of cells expressing each gene.

5.2.2.2 *Observations in endothelial cells*

Next, I examined the expression of SHH pathway genes in endothelial cells (Figure. 5.5). Similar to epithelial cells, the endothelial subtypes investigated were identified in COPD and control samples and classified as part of the development of the COPD Cell Atlas (304). As with epithelial cells, endothelial cells were characterised by the expression of cell specific markers (304).

Overall *PTCH1* and *GLI2* were expressed the most across cell types compared to the other pathway genes. Notably, *PTCH1* expression was highest in VE Arterial cells from controls (large and dark dot on plot) and was expressed moderately in VE Arterial cells from COPD samples (Figure. 5.5). Expression of *PTCH1* was also high in control VE Venous cells and Lymphatic cells in both control and COPD samples. However expression of *PTCH1* in control VE Venous cells was higher than in COPD samples. *GLI2* on the other hand, was highly expressed in VE Capillary A cells of COPD patients compared to controls and also had a high expression in VE peribronchial cells of COPD patients. *GLI1, HHIP, SHH* and *SMO*, were expressed at low levels across the endothelial cell types, with minimal differences between control and COPD samples.

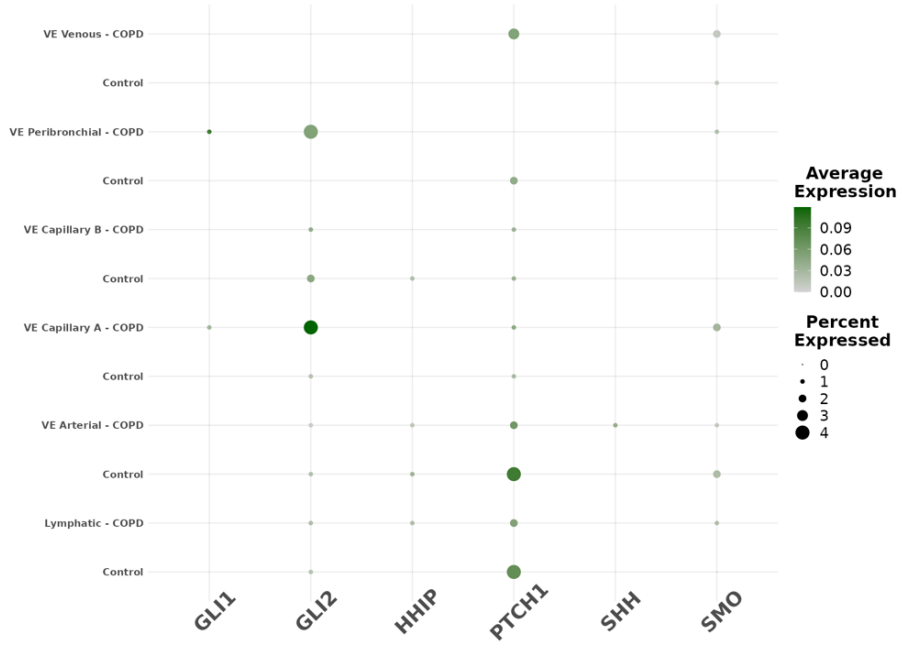

Figure 5.5. Expression of SHH signalling pathway genes across lung endothelial cells in COPD and control patient samples. Dot plot showing SHH pathway gene expression across epithelial cell types. Dot colour indicates average expression; dot size represents the percentage of cells expressing each gene.

5.2.2.3 *Observations in stromal cells*

Stromal cells were also identified during the development of the COPD Cell Atlas (304). After examining the expression of SHH pathway genes in epithelial and endothelial subtypes using the data output, I examined the expression of SHH pathway genes in stromal cells (Figure. 5.6). The stromal cells included in the COPD Cell Atlas were, smooth muscle cells (SMC), pericytes, mesothelial and fibroblast subtypes (CTHRC1^{+}, alveolar and adventitial).

GLI2 was the most prominently expressed gene across the stromal cells, while *PTCH1, GLI1, HHIP, SHH and SMO*, showed low expression. Notably, *GLI2* was expression was highest in the CTHRC1^{+} fibroblasts, in both control and COPD patients, the expression was slightly higher in controls compared to COPD samples as indicated by larger and darker dot on plot (Figure. 5.6). While, *PTCH1* was only expressed in collagen triple helix repeat containing 1^{+} (CTHRC1^{+}) fibroblasts of COPD samples and expression was moderate in comparison to expression observed for *GLI2.*

Expression of *GLI1, HHIP, SHH* and *SMO* were very low to negligible across all stromal cell types and differences between control and COPD samples were not substantial. *GLI2* was also moderately expressed in adventitial and alveolar fibroblasts in both control and COPD patient samples, with expression in control samples higher for both cell types.

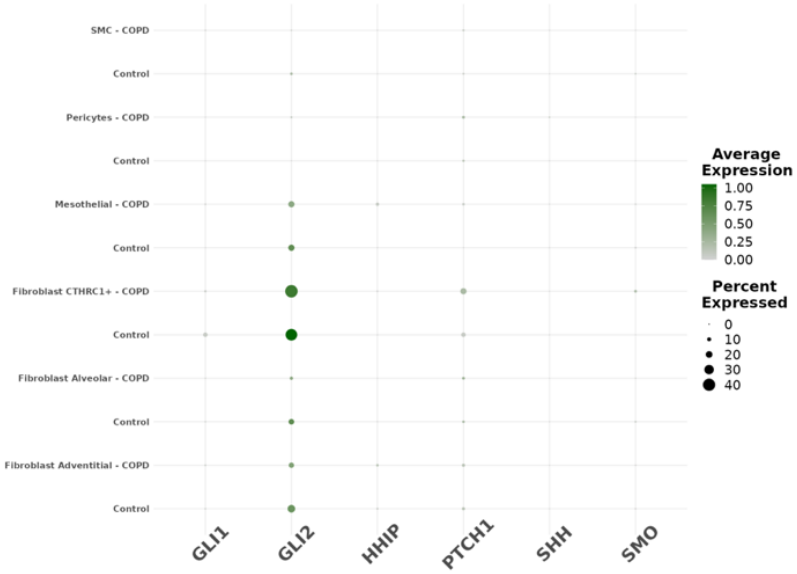

Figure 5.6. Expression of SHH signalling pathway genes across lung stromal cells in COPD and control patient samples. Dot plot showing SHH pathway gene expression across epithelial cell types. Dot colour indicates average expression; dot size represents the percentage of cells expressing each gene.

5.2.3 Establishing the AIR model using human PCLS (hAIR model)

As previously mentioned in methods section 2.3, adult human lung tissue samples were obtained from the Respiratory Biomedical Unit (BRU) Biobank at the Royal Brompton Hospital. Patient demographics for tissue samples used to generate human PCLS (hPCLS) were as shown in Table 5.2.

Table 5.2. Patient demographics and pulmonary function data for patient samples used to generate hPCLS

Gender	Age	Height	Weight	FEV1 (%)	FVC (%)	Smoking History
Female	70	168	64	114	128	Non- smoker
Female	78	167	70	98	No record	Ex-smoker (very limited information)
Male	64	174	96.3	3.41L (105%)	4.88L (116%)	Ex-smoker, started age 20, stopped age 37, 10cpd
Male	58	169	70	3.22L (106%)	4.58L (120.7%)	Ex-smoker, between age 24-54 yrs, 10 cpd
Female	71	175	74.5	2.31L (87.1%)	3.5L (111.2%)	Ex-smoker, stopped age 35 yrs, 1 pack/day
Male	72	185.5	86.2	2.82L (83%)	4.98L (110%)	Ex-smoker, stopped age 60, 20cpd
Female	76	158	62	1.82L (93%)	2.98L (117%)	Ex-smoker, between ages 16-40 yrs, 5 cpd
Male	74	167.6	95	1.78L (71%)	2.13L (65%)	Non-smoker
Male	58	167.6	82	3.13L (101%)	4.55L (116%)	Ex-smoker, between ages 14-58 yrs, 2 pack/year
Female	58	168	80.4	2.1L (78%)	3.1L (100%)	Ex-smoker, between ages 16-51 yrs, 30cpd
Male	77	174.9	81.1	2.67 (94%)	3.50 (92%)	Ex smoker, quit 25 years ago

The AIR model was originally established using mouse PCLS as a reproducible *ex vivo* model in which to investigate lung injury and repair (271, 276). To investigate the role of SHH signalling in human lung repair, as part of this project, the AIR model was successfully adapted to use human PCLS (hPCLS) (277).

hPCLS were generated as summarised in methods section 2.4.4 (Figure. 5.7), then an area of spatial acid injury was established by carefully placing a cloning cylinder coated with silicone grease onto PCLS to create a tight seal, ensuring isolation of the area within the cylinder from the surrounding lung tissue (Figure. 5.3). The area inside the cylinder was marked with an alcohol resistant marker to enable later identification of the injured region. 500 μl of SF-RPMI was added to the outside of the cylinder whilst the isolated area in the cylinder was injured by applying 100 μl of 0.1 M HCl in in 15 % w/v Pluronic gel for 1 min. The acid was immediately removed and the injured region was washed 5 times with 200 μl SF-RPMI to ensure complete removal of residual acid, after which the cloning cylinder was removed from the tissue. AIR-PCLS were subsequently transferred to a 24-well plate and cultured in SF-RPMI alone or SF-RPMI and Shh recombinant protein (0.1, 0.25 or 0.5 μg/mL) for 48 hr at 37°C prior to analysis.

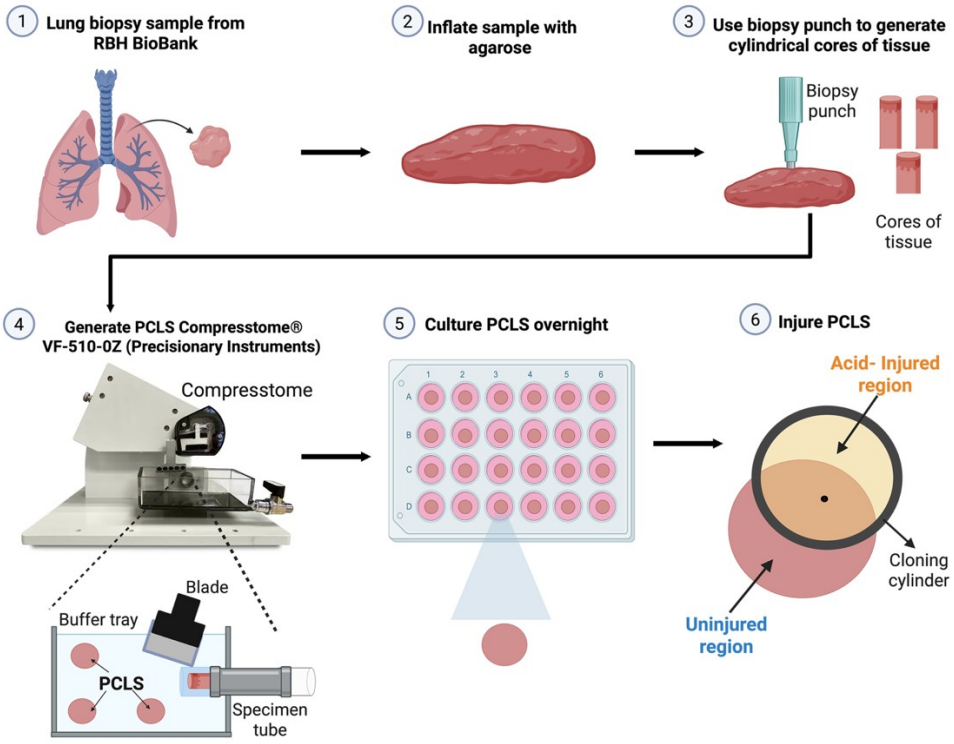

Figure 5.7. Generation of human Precision Cut Lung Slices (hPCLS) and the hAIR model.

Shows a schematic which outlines how PCLS are generated using human lung tissue samples and how the hAIR model is established by using a cloning cylinder to produce a spatially restricted area of injury. Figure generated using Biorender.

5.2.3.1 Investigating viability of hAIR-PCLS

To confirm the presence of a spatially restricted injury, hAIR-PCLS were stained using a live/dead viability kit, as outlined in methods section 2.6.2, which labels calcein positive live cells and ethidium homodimer-1 positive, dead cells (Figure. 5.8A). Calcein positive yellow staining, which is indicative of live cells was observed in control, uninjured PCLS (Figure. 5.8A(i)). Conversely, ethidium homodimer-1 positive, magenta staining, indicative of dead cells was observed in methanol treated PCLS (Figure. 5.8A(ii)). Images of hAIR-PCLS showed a visible difference between the uninjured region, which contained predominantly calcein positive (yellow staining), live cells and the injured region, which contained predominantly ethidium homodimer-1 positive (magenta staining), dead cells (Figure. 5.8A(iii), Figure. 5.8B). Furthermore, high magnification images confirmed that most cells in the uninjured region were live cells and the opposite was observed in the injured region. Despite this, some live cells were still observed in the injured region of hAIR-PCLS (Figure. 5.8A(iii), Figure. 5.8B).

MTT assays were also conducted to quantify the effect of acid injury on PCLS viability by comparing the metabolic activity of whole PCLS injured with 0.1M HCl to control, uninjured and whole methanol treated PCLS (Figure. 5.8C). A significantly reduced level of viability was found in methanol treated PCLS, in comparison to control, uninjured PCLS, confirming the efficacy of methanol as a cytotoxic agent (Figure. 5.8C, $P < 0.0001$). Similarly, PCLS injured with 0.1M HCl had a significantly reduced viability in comparison to control, uninjured PCLS (Figure. 5.8C, $p=0.0428$). Notably, the viability of PCLS treated with 0.1M HCl remained substantially higher than that of methanol treated PCLS (Figure. 5.8C, $p =0.0190$). This finding suggests that despite injury induced by HCl, a subset of cells within the PCLS retain metabolic function and viability. These findings were consistent with observations from live/dead staining, which also indicated the presence of live cells within the injured region of hAIR-PCLS.

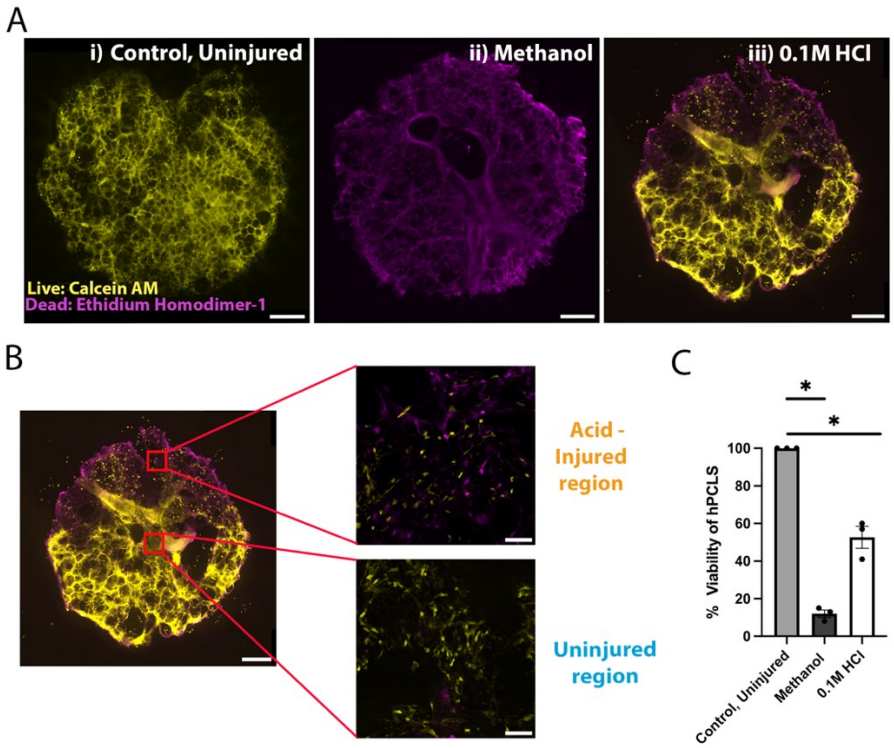

Figure 5.8. Investigating the viability of hAIR-PCLS.

(A) Whole slice PCLS images taken at 10 × magnification with a widefield microscope, showing live (Calcein AM, yellow) and dead (Ethidium Homodimer-1, magenta) cells in (i) control, uninjured, (ii) methanol and (iii) 0.1 M acid-injured slices (hAIR-PCLS) (n = 3) (B) Shows hAIR-PCLS with 0.1M acid injury and with regions of interest in the acid-injured region and uninjured region highlighted. Higher magnification images of acid-injured and uninjured region shown were taken at 40× using widefield microscopy. Scale bars: Widefield whole slice = 1000 µm, Higher magnification images (40×) = 50 µm. (C) A graphical summary of MTT assay data, showing a reduction in PCLS viability with the addition of 0.1M HCl and methanol treatment in comparison to control, uninjured PCLS (n = 3; Kruskal-Wallis test, Dunn's multiple comparisons test. *$p < 0.05$).

5.2.3.2 *The percentage of proSP-C$^+$ cells is increased in the acid-injured region of hAIR-PCLS*

As demonstrated in previous studies using mouse AIR-PCLS, alveolar repair in the hAIR model was assessed by visualising and quantifying alveolar markers of repair. After generation of hAIR-PCLS, slices were cultured for 48 hr, fixed and immunostained with anti-pro surfactant protein C (proSP-C) to track and quantify the ATII progenitor cell population. For each PCLS, proSP-C$^+$ cells were quantified in three separate fields of view in the uninjured region as well as in three separate fields of view within the acid-injured region of each hAIR-PCLS. This quantification was repeated for a minimum of three separate PCLS per group in each experiment (n=1). For control, uninjured PCLS (without acid injury) cells were quantified in three separate fields of view across the slice as described in methods chapter 2 section 2.13.1 (Figure. 5.9A). The proportion of progenitor cells was calculated relative to the total cell population, which was determined by counting DAPI-stained nuclei. The mean percentage of positive cells from each of the three technical replicates was calculated per experimental group for each experiment (biological replicate).

In control, uninjured hPCLS, the average percentage of proSP-C$^+$ cells was 4 % (Figure. 5.9B(iii-iv)), similar to the uninjured region of hAIR-PCLS, where the mean percentage of proSP-C$^+$ cells was 3 %. (Figure. 5.9B(v-vi), $p > 0.9999$). In contrast, the acid-injured region of hAIR-PCLS showed a significant increase in proSP-C$^+$ cells, with an average of 8 % proSP-C$^+$ cells (Figure. 5.9B(vii-viii)), which corresponds to a fold change of 2 (≈ 100 % increase). This was significantly higher than both the uninjured region of hAIR-PCLS ($p = 0.0065$) and control, uninjured hPCLS ($p=0.0487$). These findings are in agreement with previous results from mouse AIR-PCLS, which similarly demonstrated an increase in proSP-C$^+$ cells in the acid-injured region compared to the uninjured region and control, uninjured PCLS (271). The data presented in Figure. 5.9 is from 6 independent biological donors (N=6).

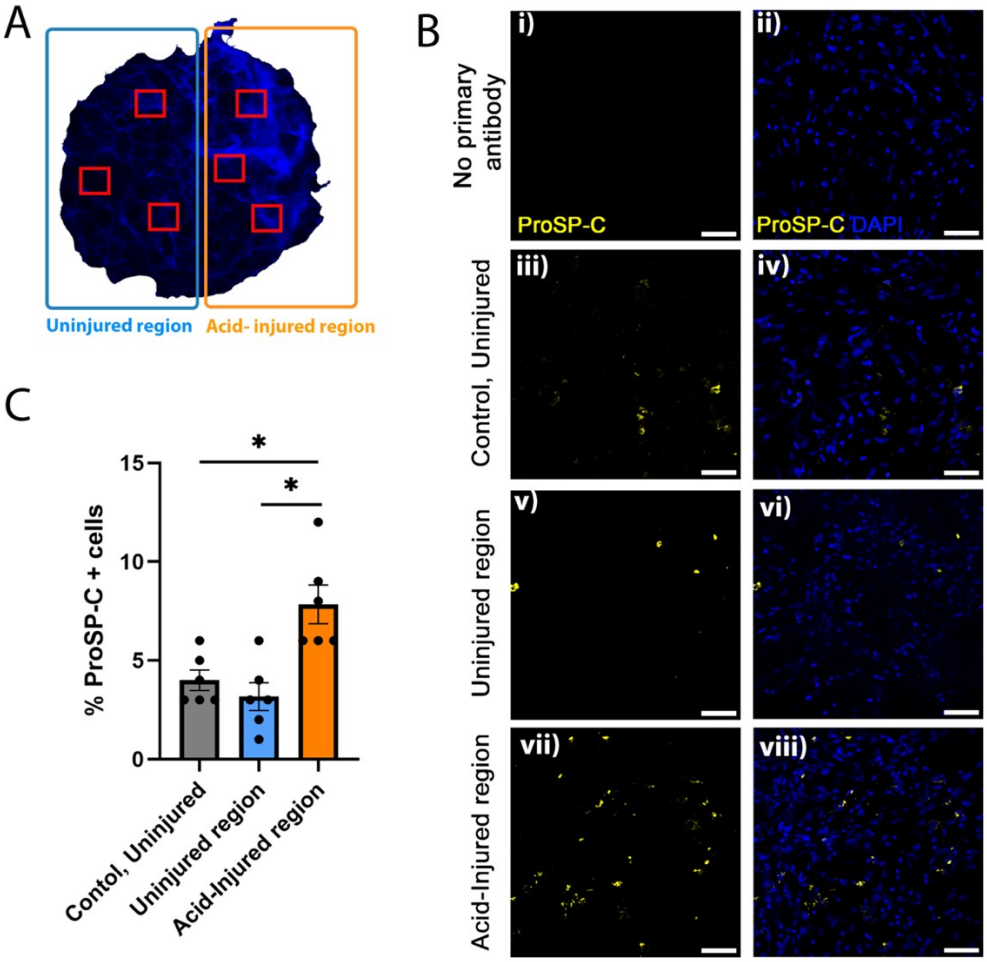

Figure 5.9. The percentage of proSP-C positive cells increase following acid-injury.
(A) Schematic showing the uninjured region (blue box) and acid-injured region (orange box) of hAIR- PCLS. (B) (i-ii) Shows no primary antibody staining for proSP-C in control, uninjured PCLS. (iii-iv) Immunofluorescence staining of control, uninjured PCLS with proSP-C (yellow) and DAPI (blue) (v-vi) Immunofluorescence staining of uninjured region of hAIR-PCLS and (vii-viii) Immunofluorescence staining of acid-injured region of hAIR-PCLS 48 hr post acid-injury. Widefield images taken at 40× magnification. Scale bars = 50 µm. (C) Quantification of proSP-C$^+$ cells in control, uninjured PCLS (grey bar) compared to the uninjured (blue bar) and acid-injured regions (orange bar) of hAIR-PCLS at 48 hr post-injury (n = 6; Kruskal-Wallis test with Dunn's multiple comparisons test, *p < 0.05).

5.2.3.3 injury does not increase cell proliferation in hAIR-PCLS

Following analysis of changes in the alveolar progenitor cell population, changes in cell proliferation were also investigated. To assess changes in proliferation in response to acid injury, hAIR-PCLS were immunostained with anti-ki67 antibody. As outlined in chapter 3 section 3.2.6.4, Ki67 is a well-established marker used to track cell proliferation. Similar to quantification of proSP-C$^+$ cells, the percentage of Ki67$^+$ cells were quantified in three distinct

fields of view within control, uninjured as well as in the uninjured and acid-injured regions of hAIR-PCLS (Figure. 5.10A). In control, uninjured hPCLS, the mean percentage of $Ki67^+$ cells was 1.2 % (Figure. 5.10(iii-iv)), while the mean percentage of $Ki67^+$ cells was 0.8 % in the uninjured region of hAIR-PCLS and 1 % in the acid-injured region. There was no significant difference in cell proliferation between any of these groups at 48hr post acid injury. Between the acid-injured and uninjured region of hAIR-PCLS ($p > 0.9999$) (Figure. 5.10). $Ki67^+$ cells in control, uninjured hPCLS was not significantly different from either the acid-injured region ($p > 0.9999$) or the uninjured region ($p = 0.8000$) of hAIR-PCLS. N=6 independent biological donors.

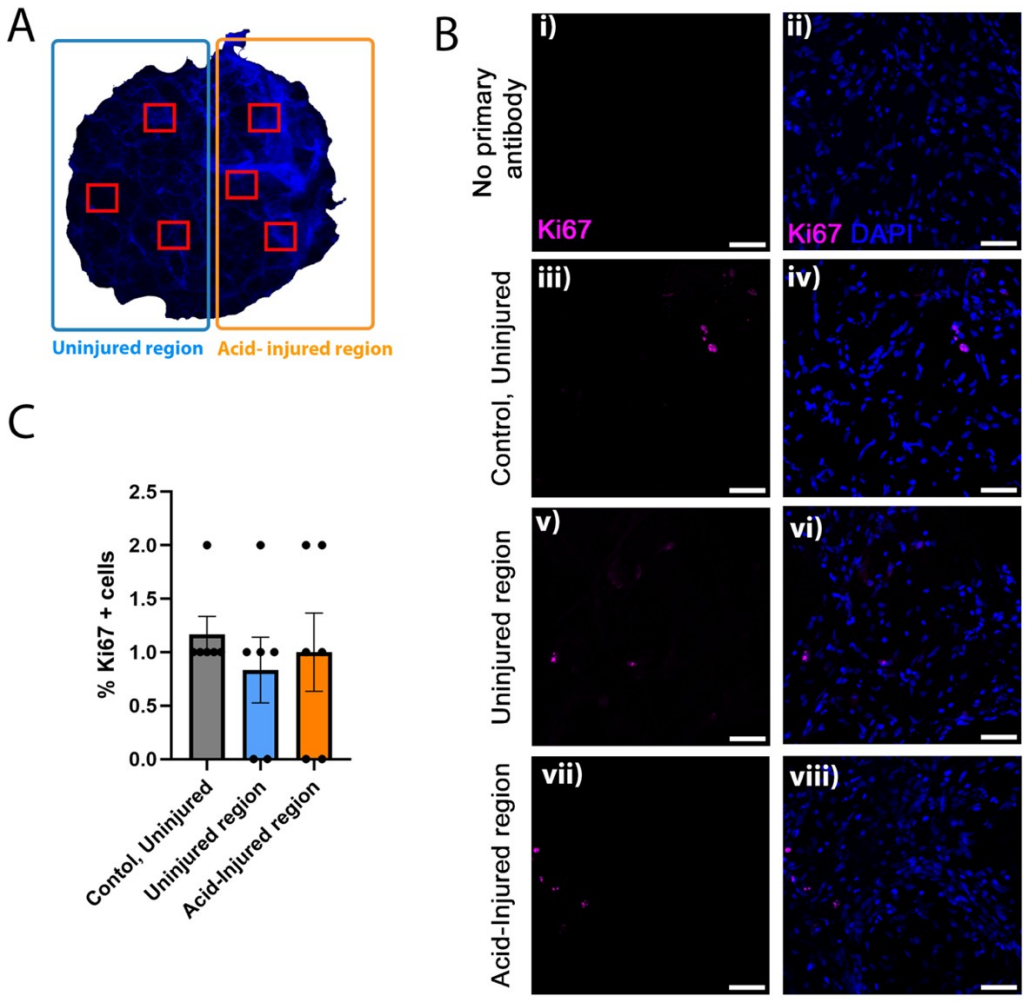

Figure 5.10. Cell proliferation remains unchanged following acid-injury.
A) Schematic showing the uninjured region (blue box) and acid-injured region (orange box) of hAIR- PCLS. (B) (i-ii) Shows no primary antibody staining in control, uninjured PCLS. (iii-iv) Immunofluorescence staining of control, uninjured PCLS with Ki67 (pink) and DAPI (blue) (v-vi) Immunofluorescence staining of uninjured region of hAIR-PCLS and (vii-viii) Immunofluorescence staining of acid-injured region of hAIR-PCLS 48 hr post acid-injury. Widefield images taken at 40× magnification. Scale bars = 50 µm. (C) Quantification of $Ki67^+$ cells in control, uninjured PCLS (grey bar) compared to the uninjured (blue bar) and acid-injured regions (orange bar) of hAIR-PCLS at 48 hours post-injury (n = 6; Kruskal-Wallis test with Dunn's multiple comparisons test, $*p < 0.05$).

5.2.3.4 HTII-280 expression increases in hAIR-PCLS following injury

To validate the findings from proSP-C$^+$ cell quantification in hAIR-PCLS, changes in the human specific ATII marker, HTII-280 (426) were quantified following acid injury. HTII-280 is an antibody that specifically recognises an antigen unique to the apical plasma membrane surface of human ATII cells (426). Consistent with previous applications of the antibody, immunostaining of hAIR-PCLS with anti-HTII-280 labelled a distinct population of cuboidal cells within the alveolar region (Figure. 5.11A-B). The mean percentage of HTII$^+$ cells in control, uninjured hPCLS was 2.3 % (Figure. 5.11B(i-ii)), while the mean percentage of HTII$^+$ cells in the uninjured region of hAIR-PCLS was 1.3 %. Similar to proSP-C cell population data (section 5.2.3.2) there was no statistically significant difference between control, uninjured hPCLS and the uninjured region of hAIR-PCLS (Figure. 5.11B(i-iv), Figure. 5.11C, p= 0.5710). Furthermore, in agreement to data from proSP-C$^+$ cell quantification, there was a significant increase in HTII$^+$ cells in the acid-injured region, which had a mean percentage of HTII$^+$ cells of 6 % compared to HTII$^+$ cells in the uninjured region of hAIR-PCLS, corresponding to a 4.62- fold change (≈ 362 % increase) (Figure. 5.11B (i-ii, v-vi), Figure. 5.11C, p= 0.0064). N=4 independent biological donors.

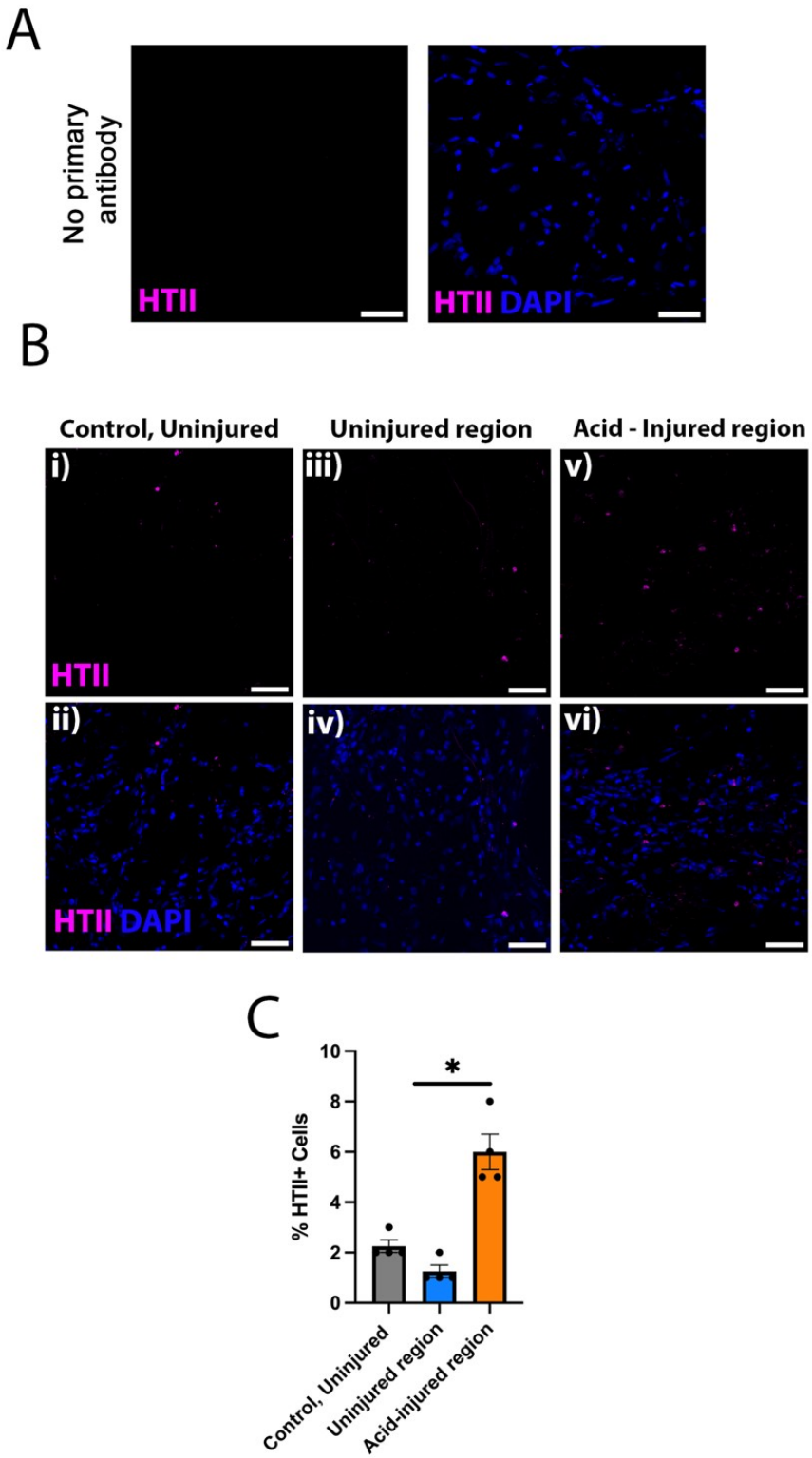

Figure 5.11. HTII-280 expression is increased in the acid-injured region of hAIR-PCLS.

(A) Shows no primary antibody staining for HTII-280 in control, uninjured PCLS. (B)(i-ii) Immunofluorescence staining for HTII-280 (pink) and DAPI (blue) in control, uninjured PCLS. (iii-iv) Immunofluorescence staining for HTII and DAPI in the uninjured region and (v-vi) acid-injured region of hAIR-PCLS 48 hr post acid-injury. Widefield images taken at 40× magnification. Scale bars = 50 µm. (C) Quantification of $HTII^{+}$ cells in control, uninjured PCLS (grey bar) compared to uninjured region (blue bar) and acid-injured region (orange bar) of hAIR-PCLS 48 hr post acid-injury (n = 4; Kruskal-Wallis test, Dunn's multiple comparisons test. *$p < 0.05$).

5.2.3.5 *The hAIR model also enables identification and tracking of lipofibroblasts and endothelial cells*

As previously outlined, lung repair and regeneration are complex multicellular processes (2, 3, 36, 37, 112). in addition to epithelial cells, other cell types such as fibroblasts and endothelial cells play crucial roles in repair and regeneration post injury(111, 112, 427-429). I immunostained control, uninjured and hAIR-PCLS with anti-ADRP (Figure. 5.12). As previously described in chapter 3 section 3.2.6.15, ADRP is a marker used to visualise lipofibroblasts. Interestingly, I observed an increase in ADRP^{+} cells in the acid-injured region of hAIR-PCLS in comparison to control, uninjured hPCLS and the uninjured region of hAIR-PCLS (Figure. 5.12B(i-ii, v-vi)).

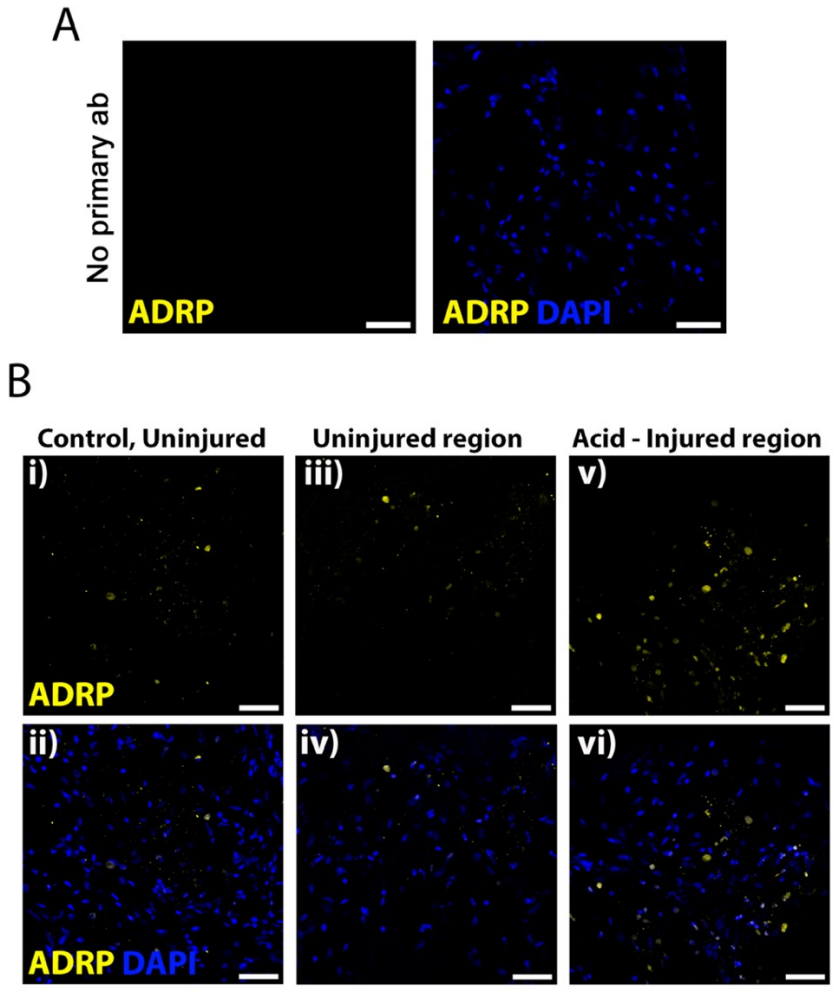

Figure 5.12. A trend toward increased lipofibroblasts in the acid-injured region of hAIR-PCLS.
(A) Shows no primary antibody staining for ADRP in control, uninjured PCLS. (B) (i-ii) Immunofluorescence staining for ADRP (yellow) and DAPI (blue) in control, uninjured PCLS. (iii-iv) Immunofluorescence staining for ADRP and DAPI in uninjured region and (v-vi) Immunofluorescence staining of ADRP and DAPI in acid-injured hAIR-PCLS 48 hr post acid-injury. Widefield images taken at 40× magnification, scale bar= 50 µm.

In addition, I immunostained control, uninjured hPCLS and hAIR-PCLS with anti-ETS related gene (ERG) (Figure. 5.13). ERG is a commonly used marker for endothelial cells (430, 431). In contrast to the ADRP cell population, I observed a reduction in ERG^{+} cells in the acid-injured region of hAIR-PCLS in comparison to both the uninjured region of hAIR-PCLS and in control, uninjured PCLS (Figure. 5.13B (i-vi)). Although quantitative analysis was not conducted for this cell type due to limited sample availability these finding provide a basis for further experimental investigation.

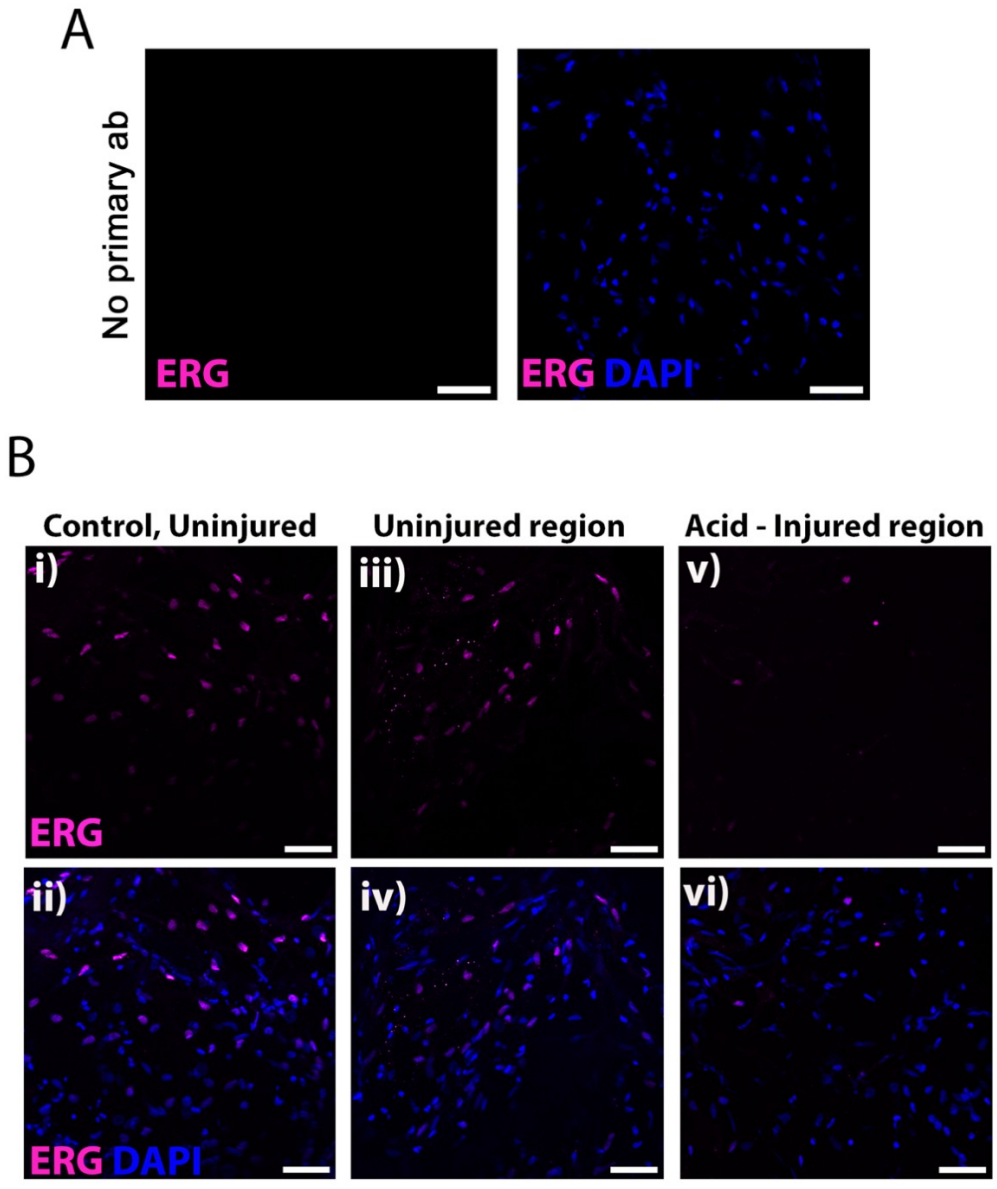

Figure 5.13. A trend toward reduced endothelial cells in the acid-injured region of hAIR-PCLS.
(A) Shows no primary antibody staining for ERG in control, uninjured PCLS. (B) (i-ii) Immunofluorescence staining for ERG (pink) and DAPI (blue) in control, uninjured PCLS. (iii-iv) Immunofluorescence staining for ERG and DAPI in uninjured region and (v-vi) Immunofluorescence staining of ERG and DAPI in acid-injured hAIR-PCLS 48 hr post acid-injury. Widefield images taken at 40× magnification, scale bar= 50 µm.

5.2.3.6 SHH treatment does not significantly affect PCLS viability

Having successfully established the hAIR model (277), I sought to determine whether Shh would affect lung repair. Based on findings from the mouse AIR-PCLS model presented in chapter 3, I focused on investigating potential changes in alveolar markers of repair (proSP-C and Ki67) following SHH treatment. The SHH pathway was stimulated by treatment with 0.1, 0.25 or 0.5 µg/mL Shh- N recombinant protein. As previously outlined (chapter 3, section 3.2.7.5), the selected concentrations of Shh were determined based on ED_{50}, which indicate the active range, along with supporting evidence from published literature(352).

If time had allowed, additional experiments would have been conducted to assess whether cyclopamine had an effect on the population of proSP-C cells and Ki67 cells in hAIR-PCLS, as was done for mouse AIR-PCLS in Chapter 3, but unfortunately there was insufficient time to conduct these experiments.

MTT assays were conducted to assess whether Shh affected PCLS viability, prior to treatment of hAIR-PCLS with Shh (Figure. 5.14). The metabolic activity of PCLS treated with 0.1, 0.25 or 0.5 µg/mL SHH was compared to that of control, uninjured and whole methanol treated PCLS.

PCLS treated with methanol to induce cell death had a viability of 17 %, which, as expected, was significantly lower compared to control, uninjured PCLS (Figure. 5.14, $p=0.0085$). Treatment with 0.1 µg/mL SHH resulted in a viability of 96 %, which was not significantly different from that of control, uninjured PCLS ($p > 0.9999$). Similarly, no statistically significant difference was observed between control uninjured PCLS and PCLS treated with 0.25 µg/mL SHH (viability of 87 %, $p=0.9057$) or PCLS treated with 0.5 µg/mL SHH (viability of 79 %, $p=0.1626$), though there was a small decrease in viability at these concentrations.

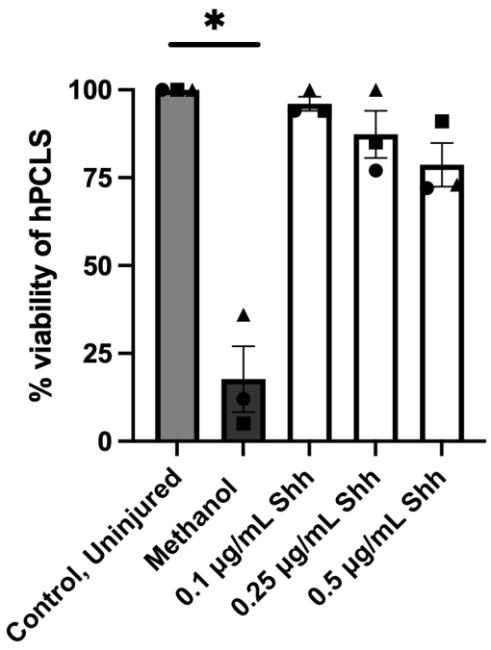

Figure 5.14. SHH treatment does not have a significant impact on hPCLS viability.
MTT assay demonstrating that SHH-N treatment does not lead to a significant reduction in PCLS viability compared to control-uninjured PCLS and methanol treated PCLS (n=3; Kruskal-Wallis test, Dunn's multiple comparisons test. *p < 0.05).

5.2.3.7 SHH treatment does not have a significant impact on the percentage proSP-C⁺ cells post acid injury

After assessing changes in the proSP-C⁺ cell population post injury in hAIR-PCLS without SHH treatment and confirming using MTT assays that Shh did not have any significant cytotoxic effect on PCLS in the absence of acid-injury, I assessed the effect of SHH treatment on the proSP-C⁺ cell population in hAIR-PCLS (Figure. 5.15). hAIR-PCLS were treated with 0.1, 0.25 or 0.5 µg/mL Shh- N recombinant protein, following the experimental plan established for mouse AIR-PCLS (chapter 3 section 3.2.7.3). 48hr after injury and SHH treatment, PCLS were fixed and immunostained with anti-prosurfactant protein-C(anti-proSP-C). Subsequently, imaging was conducted, for each PCLS and proSP-C⁺ cells were quantified as described in section 5.2.3.2. Untreated hAIR-PCLS were included as controls to assess changes in the progenitor cell population following injury without SHH treatment. As previously demonstrated in section 5.2.3.3 (Figure. 5.15B-C), acid injury leads to an increase in proSP-C⁺ cells in the acid-injured region of hAIR-PCLS compared to both the uninjured region of hAIR-PCLS and control,

uninjured PCLS (275). Consistent with these findings, I observed an increase in the percentage of proSP-C$^+$ cells in the acid-injured region of hAIR-PCLS, with a mean percentage of 9.7 %, compared to 2 % in the uninjured region ($p > 0.9999$) and 4.7 % in control, uninjured PCLS ($p=0.1266$) (Figure. 5.15). However, in this dataset only three replicates each from three independent biological donors were included due to limited sample availability, and findings did not reach statistical significance.

This pattern of increased proSP-C$^+$ cells in the acid-injured region of hAIR-PCLS compared to the uninjured region was consistently observed across all concentrations of SHH treatment. However, there were no significant changes in the percentage of proSP-C$^+$ cells in hAIR-PCLS treated with any of the 3 Shh concentrations.

In the uninjured region of hAIR-PCLS, treatment with 0.1 µg/mL SHH led to a 2.35-fold change (≈ 135 % increase) in proSP-C$^+$ cells in comparison to the uninjured region of untreated AIR-PCLS, however this not significant (mean = 4.7 %, Figure. 5.15A i, Figure. 5.15B, $p >0.9999$). Similarly, 0.25µg/mL SHH led to a 2.35-fold change (≈ 135 % increase) compared to the uninjured region of untreated AIR-PCLS (mean = 4.7 %, Figure. 8A ii, Figure. 8B, $p>0.9999$), while 0.5 µg/mL SHH resulted in a 3- fold change (≈ 200 % increase) (mean= 6 %, Figure. 8A v, Figure. 8B, $p>0.9999$). Although trends observed were not significant, the trend toward an increase in proSP-C$^+$ cells in the uninjured region of hAIR-PCLS with increasing concentrations of SHH treatment may indicate that SHH treatment could modulate the proSP-C cell population in the uninjured region.

In contrast, when the acid-injured region of untreated AIR-PCLS (mean percentage of proSP-C$^+$ cells of 9.7 %) was compared to the acid-injured region of AIR-PCLS treated with 0.1 µg/mL SHH there was a 0.79-fold change (≈ 21 % decrease) of proSP-C$^+$ cells (mean=7.7 %, Figure. 5.15A ii, Figure. 5.15B, $p >0.9999$), a 0.89- fold change (≈ 11 % decrease) with 0.25 µg/mL SHH treatment (mean= 8.6 %, Figure. 5.15A iv, Figure. 5.15B, $p >0.9999$) and a 0.82-fold change (≈ 17.5 % decrease) with 0.5 µg/mL SHH treatment (mean=8 %, Figure. 5.15A vi, Figure. 5.15B, $p >0.9999$). N=3 biological donors. Decreases observed in the percentage of proSP-C$^+$ cells in the acid-injured region of Shh treated hAIR-PCLS were modest but not statistically significant.

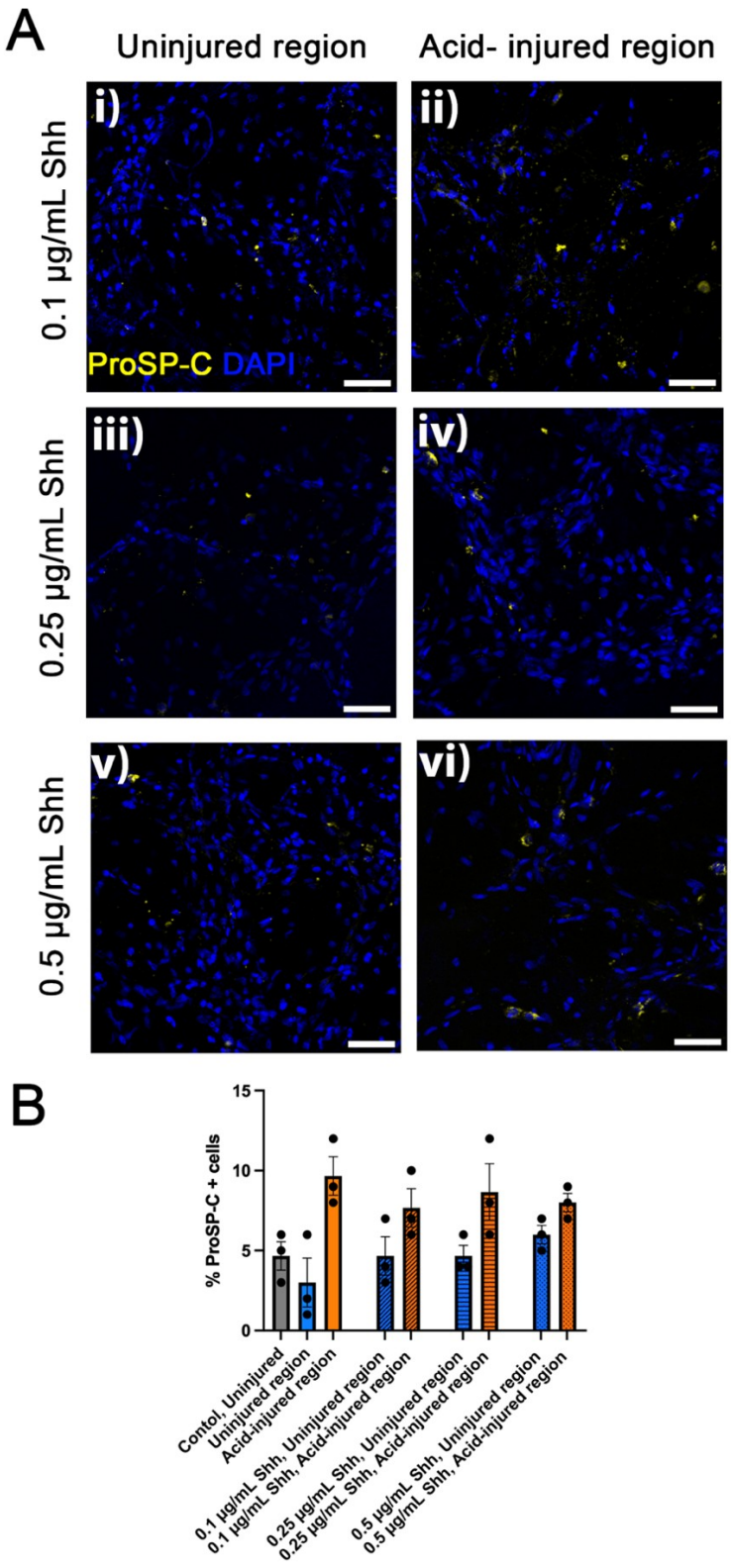

Figure 5.15. SHH treatment does not significantly effect proSP-C⁺ cell population in hAIR-PCLS.
(A)Immunofluorescence staining of uninjured region and acid-injured regions of hAIR-PCLS treated with Shh at concentrations of (i-ii) 0.1 µg/mL, (iii-iv) 0.25 µg/mL and (v-vi) 0.5 µg/mL. ProSP-C is shown in yellow and DAPI is shown in blue. Widefield images taken at 40× magnification. Scale bars = 50 µm. (B) Quantification of proSP-C⁺ cells in control, uninjured PCLS (grey bar) compared to the uninjured (blue bar) and acid-injured regions (orange bar) of hAIR-PCLS, as well as hAIR-PCLS treated with different concentrations of Shh at 48 hr post-injury (n = 3; Kruskal-Wallis test with Dunn's multiple comparisons test, *$p < 0.05$).

5.2.3.8 *SHH treatment does not appear to alter HTII⁺ cell population post injury*

Next, I investigated changes in the HTII⁺ cell population in hAIR-PCLS following SHH treatment (Figure. 5.16). Consistent with previous observations in hAIR-PCLS without SHH treatment, an increase in HTII⁺ cells was observed in the acid-injured regions of hAIR-PCLS across all concentrations of Shh (0.1, 0.25 or 0.5 µg/mL Shh) in comparison to uninjured regions. However, due to a limited number of biological replicates, quantitative analysis was not performed for this dataset. N=1 independent biological donor. This serves as preliminary data for further experimental investigations.

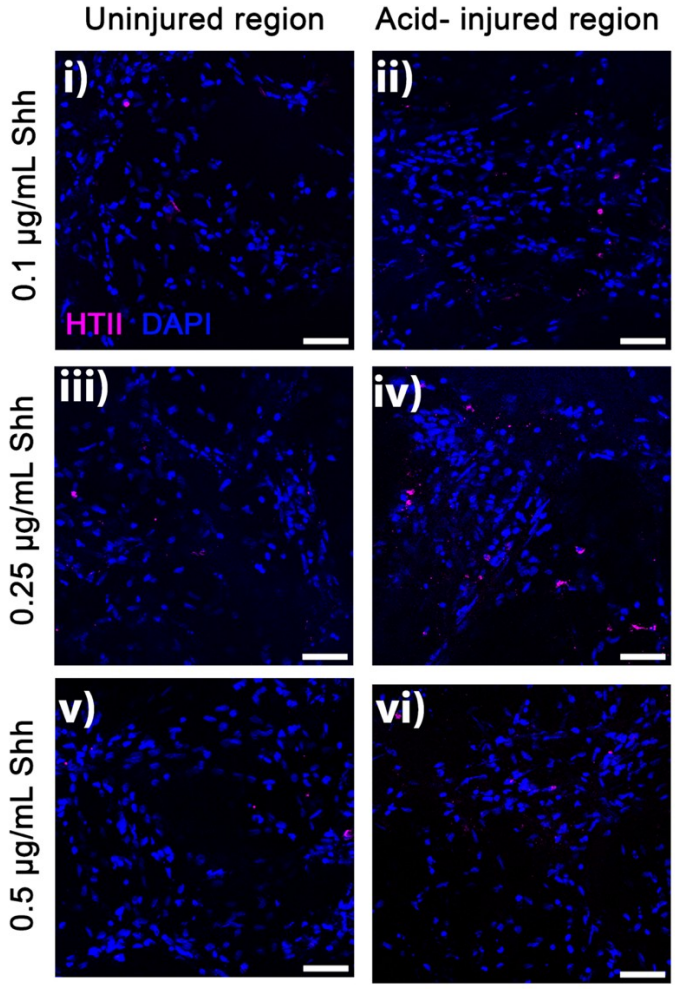

Figure 5.16. SHH treatment does not alter increased HTII-280 expression in acid-injured region of hAIR-PCLS.
Immunofluorescence staining of uninjured region and acid-injured regions of hAIR-PCLS treated with Shh at concentrations of (i-ii) 0.1 µg/mL, (iii-iv) 0.25 µg/mL and (v-vi) 0.5 µg/mL. HTII is shown in pink and DAPI is shown in blue. Widefield images taken at 40× magnification. Scale bars = 50 µm.

5.2.3.9 SHH treatment does not affect cell proliferation, post acid-injury

After assessing the effect of SHH treatment on the proSP-C$^+$ and HTII$^+$ cell population, I investigated the impact of SHH treatment on the percentage of proliferating cells in hAIR-PCLS (Figure. 5.17). 48 hr post injury, hAIR-PCLS treated with 0.1, 0.25 or 0.5 µg/mL SHH were fixed and immunostained with anti-ki67 before quantification as previously described (chapter 2 section 2.13.1). In this investigation, untreated hAIR-PCLS served as controls to assess changes in proliferating cells following injury in the absence of SHH treatment. Consistent with previous findings outlined in section 5.2.3.4 (Figure. 5.17B-C), I observed that 48 hr post injury, there was no significant difference in the percentage of Ki67$^+$ cells between the acid-injured region which had a mean of 1.3 % Ki67$^+$ cells and the uninjured region of hAIR-PCLS, which had a mean of 1 % Ki67$^+$ cells (Figure. 5.17B-C, $p > 0.9999$). Additionally, there was no significant difference in Ki67$^+$ cells between the acid-injured region (Figure. 5.9, $p > 0.9999$) or uninjured region (Figure. 5.17B-C, $p > 0.9999$) of hAIR-PCLS and control, uninjured PCLS which had a mean 1.3 % Ki67$^+$ cells.

SHH treatment did not lead to statistically significant changes in cell proliferation across any of the concentrations tested (0.1, 0.25 or 0.5 µg/mL Shh). These findings are similar to experiments were conducted using PCLS generated from mice, where SHH treatment did not lead to significant changes in cell proliferation across any of the concentrations of SHH in AIR-PCLS (Figure. 3.23). In the uninjured region of hAIR-PCLS, at all concentrations of SHH there was no difference in the mean percentage of Ki67$^+$ cells when compared to the uninjured region of untreated hAIR-PCLS (Figure. 5.17A(i, iii, v), Figure. 5.17B, $p > 0.9999$). All have a mean percentage of Ki67$^+$ cells of 1 %.

Similarly, in the acid-injured region, treatment with 0.1, 0.25 or 0.5 µg/mL SHH did not lead to a significant difference in Ki67$^+$ cells when compared to the acid-injured region of untreated hAIR-PCLS. The findings were also consistent with mouse AIR-PCLS experiments with SHH treatment (Figure. 3.23). The mean percentage of Ki67$^+$ cells in the acid-injured region of hAIR-PCLS treated with 0.1 or 0.25 µg/mL SHH was 0.7 % (Figure. 5.17A (ii, iv), Figure. 5.17B, $p > 0.9999$). While, the mean percentage of Ki67$^+$ cells in the acid-injured region of hAIR-PCLS treated with 0.5 µg/mL SHH was 1 % (Figure. 5.17A(vi), Figure. 5.17B, $p > 0.9999$).

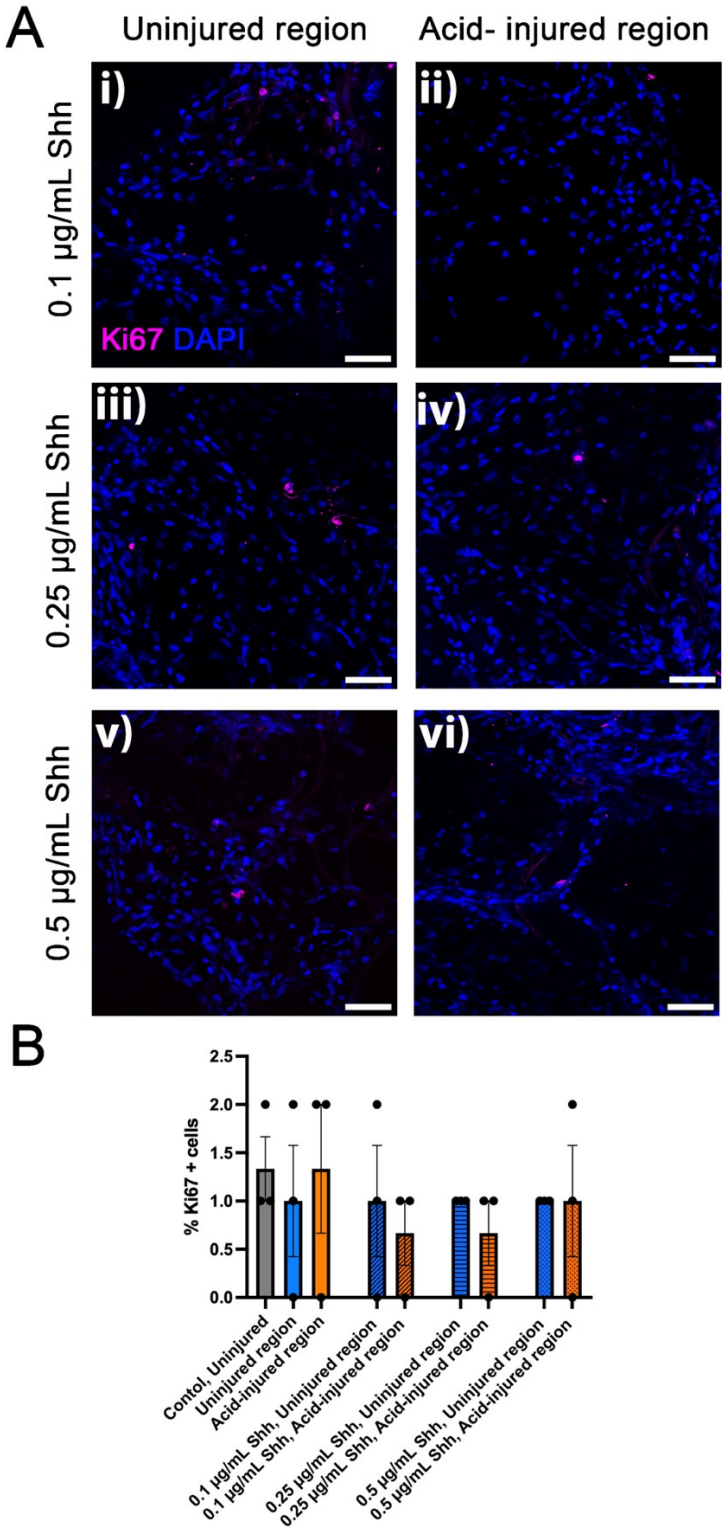

Figure 5.17. Shh treatment did not lead to changes in population of proliferating cells.

(A)Immunofluorescence staining of uninjured region and acid-injured regions of hAIR-PCLS treated with Shh at concentrations of (i-ii) 0.1 µg/mL, (iii-iv) 0.25 µg/mL and (v-vi) 0.5 µg/mL. Ki67 is shown in pink and DAPI is shown in blue. Widefield images taken at 40x magnification. Scale bars = 50 µm. (B) Quantification of $Ki67^{+}$ cells in control, uninjured PCLS (grey bar) compared to the uninjured (blue bar) and acid-injured regions (orange bar) of hAIR-PCLS, as well as hAIR-PCLS treated with different concentrations of Shh at 48 hr post-injury (n = 3; Kruskal-Wallis test with Dunn's multiple comparisons test, *$p < 0.05$).

5.2.3.10 SHH treatment is associated with a trend toward increased ADRP⁺ cells

When changes in the ADRP⁺ cell population were investigated in mouse AIR-PCLS following SHH treatment, I observed an increase in the ADRP⁺ cells as the concentration of Shh increased (Chapter 3, section 3.2.6.15, Figure. 3.32-3.33). Further to this, I observed that SHH treatment led to an increase in HLF wound closure (Figure. 4.10). These results indicate that SHH treatment plays an important role in fibroblast mediated repair post injury. To determine whether the same findings were recapitulated using human tissue, changes in the ADRP population following SHH treatment in hAIR-PCLS were also investigated (Figure. 5.18). As with previous markers investigated, hAIR-PCLS were fixed 48 hr post-injury following treatment with 0.1, 0.25 or 0.5 µg/mL SHH and were subsequently immunostained with anti-ADRP and the percentage of ADRP⁺ cells was quantified. The data presented is derived from a single biological replicate (one donor), with three PCLS analysed per experimental group (i.e. three technical replicates). Despite the limited sample size, quantification was performed to provide a preliminary assessment of potential changes in the ADRP⁺ cell population post injury and to determine the potential role of SHH treatment on lipofibroblasts in repair (Figure. 5.18). The aim of this was to build upon the findings outlined from chapters 3 and 4 on the role of the SHH signalling pathway in modulating the fibroblast cell population during repair post injury.

In untreated PCLS I observed that control, uninjured PCLS had a mean of 5.3 % ADRP⁺ cells. In comparison, the uninjured region of hAIR-PCLS had a lower mean of 2.3 %, corresponding to a 0.43- fold change (≈ 57 % decrease) compared to control, uninjured PCLS. The acid-injured region had a mean of 7.3 % (Figure. 5.18), corresponding to a 1.37-fold change (≈ 37.7 % increase) compared to control, uninjured PCLS. In the uninjured region of hAIR-PCLS, the differences observed at all concentrations were relatively low. Treatment with 0.1 µg/mL and 0.25 µg/mL resulted in a mean percentage of ADRP⁺ of 5 % (Figure. 5.18A (i, iii), Figure. 5.18B), while treatment with 0.5 µg/mL SHH led to a mean percentage of ADRP⁺ of 5.7 % (Figure. 5.18A(v), Figure. 5.18B). In the acid-injured region, SHH treatment did not lead to a consistent dose-dependent effect. Treatment with 0.1 µg/mL SHH led to a reduction in ADRP⁺, corresponding to a fold change of 0.51 (≈ 49.3 % decrease) compared to the acid-injured region of untreated hAIR-PCLS (mean= 3.7 %, Figure. 5.18A(ii), Figure. 5.18B). While in the

acid-injured region of hAIR-PCLS treated with 0.25 µg/mL SHH there was a 0.96-fold change (≈ 4 % decrease) (mean = 7 %, Figure. 5.18A(iv), Figure. 5.18B) and in hAIR-PCLS treated with 0.5 µg/mL SHH there was a 1.14-fold change (≈ 14.3 % increase) (mean = 8 %, Figure. 5.18A(vi), Figure. 5.18B). Whereas in mPCLS a concentration dependant increase in ADRP$^+$ was observed in both the uninjured and acid-injured regions of SHH treated AIR-PCLS compared to untreated AIR-PCLS (Figure. 3.32-3.33).

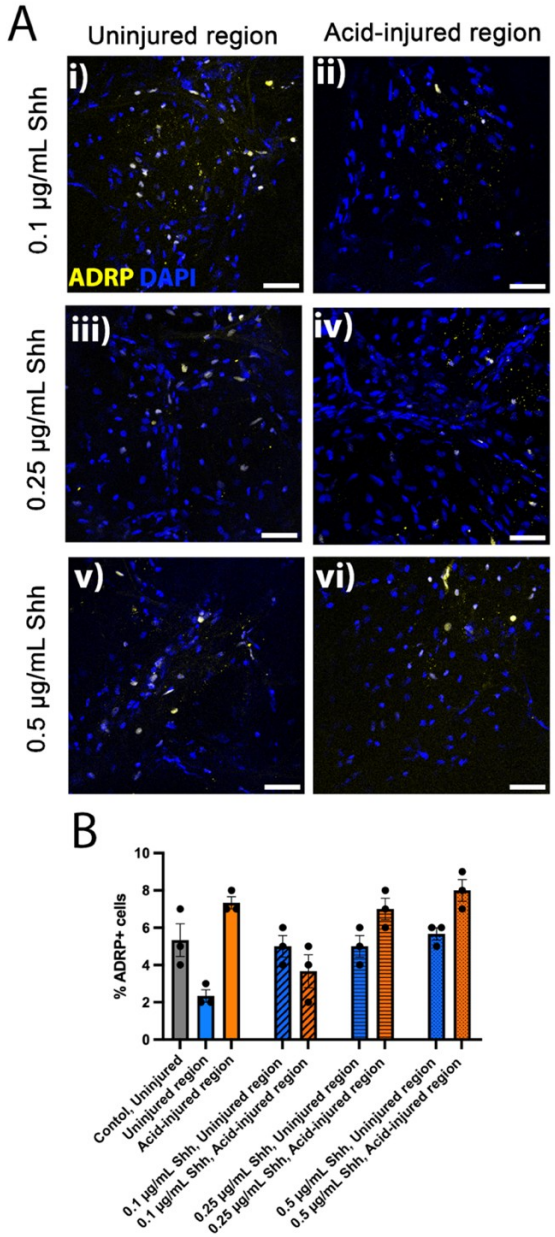

Figure 5.18. Investigating changes in the population of ADRP$^+$ cells following Shh treatment.

(A)Immunofluorescence staining of uninjured region and acid-injured regions of hAIR-PCLS treated with Shh at concentrations of (i-ii) 0.1 µg/mL, (iii-iv) 0.25 µg/mL and (v-vi) 0.5 µg/mL. ADRP is shown in yellow and DAPI is shown in blue. Widefield images taken at 40x magnification. Scale bars = 50 µm. (B) Quantification of ADRP$^+$ cells in control, uninjured PCLS (grey bar) compared to the uninjured (blue bar) and acid-injured regions (orange bar) of hAIR-PCLS, as well as hAIR-PCLS treated with different concentrations of Shh at 48 hr post-injury (n=1 biological replicate, 3 technical replicates are shown per experimental group investigated, statistics was not conducted due to insufficient sample availability).

5.3 Discussion

5.3.1 Gene expression profiling of SHH pathway in emphysematous and control lung tissue

SHH signalling has been shown to play a pivotal role in lung development, as well as in lung repair and/or regeneration(13, 181, 183, 184, 187, 314, 315). Therefore, changes in the expression of SHH signalling pathway components or dysregulation of the pathway itself, may serve as important biomarkers of disease or may contribute to the pathophysiology of lung diseases. In this study, I used qPCR to examine the relative expression of SHH pathway components in emphysema lung tissue compared to controls (Figure. 5.1-5.2). In addition to this, I investigated the expression of these genes across different lung cell types in the epithelial, endothelial and stromal cell compartments, using data from the COPD Cell Atlas developed by the Kaminski lab (Figure. 5.4-5.6) (304, 305).

Analysis of our qPCR data revealed an upregulation of key SHH pathway components in emphysematous lung tissue. Specifically, I demonstrated that *SHH* expression is upregulated in lung tissue samples from emphysema patients with a mean fold change of 1.41 (Figure. 5.2), this suggests an increase in pathway activation. This increase in ligand expression was observed along with an upregulation of the pathway receptor *PTCH1* which had a fold change of 1.38 and downstream transcription factors *GLI1 a*nd *GLI2* which had mean fold changes of 1.15 and 1.35, respectively. The upregulation of *PTCH1*, *GLI1* and *GLI2,* which are transcriptional targets of the SHH signalling pathway further highlight an increase in pathway activation in emphysema patient samples. Furthermore, upregulation of these genes highlighted that the upregulation of Shh was not limited to an increase in ligand availability but reflects pathway activation.

In the context of emphysema, which is characterised by destruction of alveoli and an impaired capacity for repair(414), reactivation of key developmental pathways like Shh suggests an attempt to initiate repair. However, persistent or dysregulated activation of SHH signalling could also contribute to disease pathology. Notably previous studies have observed an increase in Shh expression and activity in fibrosis(13, 181, 184, 185, 190, 314). I propose that

in disease pathology, the initial activation of Shh is protective, however further investigations will need to be conducted to determine whether sustained Shh activity in the diseased state is indicative of aberrant signalling.

Consistent with previous studies, our analysis also showed downregulation of *HHIP*, a known negative regulator of the SHH signalling pathway, in emphysematous tissue (68)(Figure. 5.2), with a mean fold change of 0.84. HHIP binds directly to the SHH ligand, modifying its structure and preventing its interaction with Ptch1, therefore preventing downstream signalling (171, 172, 416, 418). In the context of emphysema this reduced *HHIP* expression could contribute to a lack of pathway regulation, even in the absence of increased *SHH* ligand expression.

Our findings confirm previous studies, which found that *HHIP* expression is significantly reduced in samples from COPD patients compared to those from individuals with normal lung function(68). Additionally, both RNA and protein levels of HHIP have been shown to be markedly decreased in COPD lung tissue(68).This further validates the importance of our research investigating the role of SHH signalling in lung repair and regeneration. Furthermore, as previously outlined, several GWAS have identified that *HHIP* is associated with lung function (411-413). Further to this, our findings are particularly interesting and relevant, since *HHIP* has also been repeatedly identified in GWAS as a susceptibility gene for COPD (68, 304, 412-414, 432), specifically as a result of SNPs located upstream of the *HHIP* on chromosome 4q31(68, 304, 412-414, 432). Recent studies have also associated these SNPs to a reduction in distal enhancer activity, suggesting that this alteration may contribute to the observed associations with lung function and disease susceptibility(68, 432, 433). Animal studies further support this, as HHIP haploinsufficient mice exposed to cigarette smoke for 6 months exhibited more pronounced enlargement of airspaces, resembling emphysema, compared to wild type (WT) littermates exposed to cigarette smoke for the same period of time(432, 434). These findings further highlight that dysregulated *HHIP* expression contributes to disease susceptibility by reducing the ability to maintain lung homeostasis(432, 434). This reinforces the role of Hhip in modulating SHH pathway activity and highlights pathway dysregulation in the diseased state.

Despite this growing research, our understanding of how *HHIP* modulates repair at a cellular level remains limited. Our findings highlight the significant role of HHIP in lung disease, particularly in COPD, highlighting the importance of further investigating its impact on cellular processes within the lungs. Understanding whether HHIP influences mechanisms critical for lung repair or whether HHIP contributes to disease progression due to its inability to drive repair is important. Therefore it would be insightful to assess the effects of HHIP treatment on cellular migration and wound healing across various cell types, employing experimental approaches similar to those detailed in chapters 3 and 4. This will also build upon our understanding of the role of SHH in lung repair post injury.

It is important to note that, in addition to HHIP, GWAS have also identified genetic variants of *PTCH1* associated with COPD(317, 435). Moreover, a study has shown that PTCH1 protein is upregulated in the airway epithelium of COPD patients compared to control samples without COPD(317). This is in alignment with our finding that *PTCH1* gene expression is upregulated in emphysema patient samples. Interestingly, in contrast to Hhip, in the absence of the Shh ligand, Ptch1 inhibits downstream signalling by inhibiting Smo (171, 172, 174). Notably, the SHH pathway components identified as COPD susceptibility genes in GWAS, *PTCH1* and *HHIP* both function as pathway inhibitors. The opposing changes in regulation in COPD, with *PTCH1* being upregulated and *HHIP* being downregulated, suggests a disruption in pathway activation in COPD. Furthermore disruption to SHH signalling in this context may lead to aberrant repair.

To deepen our understanding of SHH pathway alterations in emphysema or COPD patients compared to control patients at the cellular level, I analysed the differential expression of pathway genes using the COPD Cell Atlas (Figure. 5.4-5.6), which is a database that provides scRNA-seq data from both healthy and COPD lungs (304, 305). This analysis revealed interesting cell specific expression patterns.

A high expression of *HHIP* was observed in $ATII_B$ epithelial cells in both COPD and control samples (Figure. 5.4). Indicating that HHIP expression supports alveolar epithelial homeostasis and is dysregulated. In addition to observing a high expression of *HHIP* in this ATII cell subpopulation, the researchers that developed the COPD Cell Atlas found high expression of

*SERPINA*1 and *SFTPD*, both of which has also been identified in GWAS studies as susceptibility genes for COPD(304, 436, 437). Interestingly the expression of *SHH* was negligible across all epithelial cell types (Figure. 5.4). This is concordant with gene expression data from our investigation assessing expression of SHH pathway components in different cell lines/types (Figure. 4.9) and suggests that while SHH is secreted by epithelial cells, synthesis and subsequent secretion may be directed by epithelial-mesenchymal interactions. Furthermore, COPD Cell Atlas data showed that *SMO* also exhibited negligible expression across epithelial cell types (Figure. 5.4). Therefore taken together this suggests that transcriptional regulation of the pathway ligand and the pathway signal transducer are regulated through paracrine interactions.

When I looked at expression levels in vascular endothelial cells (Figure. 5.5), *PTCH1* showed high expression in arterial and venous endothelial cells from controls, with reduced expression in COPD samples (Figure. 5.5). Further to this, I observed increased *GLI2* expression in capillary A and peribronchial endothelial cells of COPD lungs compared to controls (Figure. 5.5). Taken together differences in pathway expression in the vascular endothelium indicate that endothelial specific regulation of SHH signalling may be altered in disease which could also have an impact on angiogenesis and/or barrier integrity.

In stromal cells, *GLI2* was the most prominently expressed gene (Figure. 5.6), particularly in CTHRC1^{+} fibroblasts, where expression was higher in controls than in COPD samples. However, *PTCH1* was only expressed in CTHRC1^{+} fibroblasts of COPD samples at moderate levels (Figure. 5.6). CTHRC1^{+} fibroblasts have been associated with fibrosis and increased cell proliferation (438, 439)The expression level of the remaining SHH pathway genes (*GLI1, HHIP, SHH* and *SMO*), were negligible across stromal subtypes (Figure. 5.6). This suggests that stromal activation of the SHH pathway is limited but the modest upregulation of *PTCH1* observed in fibroblasts of COPD patients could reflect disease-specific fibroblast activation. However, this is unlikely since SHH pathway components have been demonstrated to be upregulated during fibrosis and the disease pathology of COPD and fibrosis exist on opposite spectrums of aberrant cellular remodelling (13, 37, 185, 190, 314).

While qPCR provides precise quantification of selected genes, it is limited to a small number of targets. For the purpose of this thesis qPCR provided us with useful insight about the expression of key SHH pathway components(440). However, to gain a more comprehensive understanding of the SHH pathway and changes in gene expression in normal versus emphysematous lung tissue, further investigations using RNA sequencing (RNA-seq) and/or microarray profiling could be conducted. Both techniques are high-throughput, allowing the examination of thousands of genes as well as potential to identify novel differentially expressed genes(440, 441). RNA-seq in particular can be used to detect transcripts present in low abundance, therefore offering deeper insight into gene expression changes(440, 441). Conducting these investigations will broaden our understanding of molecular mechanisms underlying emphysema and the role that the SHH pathway plays in this. Nevertheless, scRNA-seq analysis of COPD Cell Atlas data strengthened the interpretation of our findings.

Furthermore, in my analysis of emphysema and control patient samples, I was restricted to 6 age matched samples for each group due to tissue availability. Post-hoc sample size calculations further confirmed that to reach a higher effect I would need more samples (Figure. 5.3). The findings from my investigation are in agreement with previous research and GWAS studies demonstrating the association between SHH signalling and COPD (68, 304, 412, 414), therefore highlighting the potential of SHH as a therapeutic target. Further studies examining *SHH* expression within the context of lung injury could provide valuable insight into the role of SHH in pulmonary pathology and the mechanisms involved in SHH signalling dysregulation post injury. Future experimental investigations may involve inducing injury in whole PCLS and subsequently comparing gene expression between injured and uninjured PCLS to identify molecular differences and similarities.

5.3.2 Establishing and validating the hAIR model

The second half of this chapter focused on establishing the human AIR model (Figure. 5.7), using human lung tissue obtained from histologically normal biopsy samples. I successfully demonstrate that this model in which a spatially restricted region of human PCLS is injured

with acid, provides a more physiologically relevant and translatable platform for pre-clinal studies of lung injury and repair mechanisms. Consistent with findings from the previously established mouse AIR model (271), immunostaining for ATII progenitor cells using proSP-C demonstrated an increase in the number of proSP-C$^+$ cells in the acid-injured region of hAIR-PCLS 48 hr post injury (Figure. 5.9). Similar observations were made with a human specific marker for ATII progenitor cells, HTII-280, which also showed an increase in HTII$^+$ cells in the acid-injured region of hAIR-PCLS 48 hr post injury (Figure. 5.11). These findings corroborate data from the mouse AIR model (271) but also align with *in vivo* studies of lung repair (142, 385, 386), further highlighting the relevance and translational potential of the hAIR model for investigating alveolar repair and/or regeneration post injury(277). I also investigated whether the spatially restricted injury had an impact on proliferating cells but did not observe any significant changes (Figure. 5.1). Several factors may explain the lack of observable changes in proliferating cells, including timing of the analysis, it is possible that proliferation occurs before or after the 48 hr timepoint. Furthermore, it is possible that the increase in progenitor cells is driven by differentiation instead of proliferation. Interestingly, when cell proliferation was investigated using the mouse AIR model, proliferating cells were not observed after 24 hr but were observed 48 hr post injury(271). This suggests that there is some species-specific variability in the repair response, again highlighting the importance of physiologically relevant models.

5.3.3 Evaluating the impact of SHH treatment on epithelial markers of repair using the hAIR model

I employed the hAIR model to further investigate the role of SHH signalling in repair following acid-injury in hAIR-PCLS treated with SHH, I consistently observed an increase in proSP-C$^+$ cells within the acid-injured region compared to the uninjured region (Figure. 5.15). In contrast, results from the mouse AIR model, outlined in chapter 3, section 3.2.7.3, showed that the population of proSP-C$^+$ cells increased with 0.1 and 0.25 µg/mL SHH, but decreased with in 0.5 µg/mL SHH treatment in the acid-injured region compared to the uninjured region. Interestingly, when comparing the uninjured region of untreated and SHH treated hAIR-PCLS, I observed a trend that indicated a possible dose-dependent increase in proSP-C$^+$ cells, a trend that was not observed in the mouse.

AIR model. However, these findings were not significant. The lack of significant results is likely due to a lack of sufficient biological replicates. It is important to note that due to limited sample availability and time constraints, for investigations where hAIR PCLS were treated with SHH, I had 3 biological replicates which were from 3 individual donors. As demonstrated by the power analysis conducted in chapter 3, section (Figure. 3.27), a minimum of six biological replicates is required to detect an effect size of 80 %, the generally accepted threshold for interpretation of data. Therefore, increasing the number of biological replicates for future investigations would improve statistical power and would allow us to make more definitive conclusions about the impact of SHH signalling on alveolar markers of repair.

Furthermore, incorporating live-cell imaging to track and monitor changes in this cell population over time would provide useful insights into the regenerative process underlying alveolar repair, specifically in the context of SHH treatment. It has previously been demonstrated that time-lapse live imaging of PCLS can be successfully conducted using widefield microscopy(26, 442). In addition to integrating live imaging approaches to our investigations, future studies should focus on investigating the effect of SHH pathway inhibition in the hAIR model using the SHH pathway inhibitor cyclopamine, as was previously done with mouse AIR model. Based on gene expression studies which highlight changes in *HHIP* expression in emphysema and COPD patient samples compared to control samples, as well as GWAS studies that highlight the importance of HHIP in disease pathology (68, 304, 412, 414), it will also be important to assess whether HHIP treatment influences alveolar markers of repair. Furthermore, it would be important to determine the differences between the impact of HHIP, which is an endogenous inhibitor of the SHH signalling pathway (415-417) and cyclopamine which is a pharmacological agent that inhibits the pathway (351).

In addition to investigating differences in proSP-C$^+$ cells following SHH treatment, I investigated changes in HTII$^+$ cells (Figure. 5.16). Consistent with findings demonstrating increased proSP-C$^+$ cell populations in SHH treated hAIR-PCLS, our data similarly show an increase in HTII$^+$ cells across all SHH treatment concentrations (Figure 5.16). However, this data is preliminary and was only conducted with one biological replicate from one biological donor. Further replicates

need to be conducted before definitive conclusions about changes in HTII^{+} cells in SHH treated AIR-PCLS can be hAIR-PCLS.

5.3.4 Fibroblast and endothelial cell response to injury and SHH signalling in hAIR-PCLS

In addition to investigating epithelial progenitor cells and proliferating cells, I showed that the hAIR model can be effectively utilised to study a broad range of cell types involved in lung tissue repair(277). As previously emphasised, lung repair and/or regeneration is a complex, multicellular process requiring coordinated interactions among cellular populations(3, 11, 37, 102). In chapter 4 I showed that co-culturing alveolar epithelial cells (A549 cells) with human lung fibroblasts (HLF) led to increased cellular migration, following SHH treatment, compared with untreated controls, indicating that paracrine signalling between these two cell types plays a role in lung repair and regeneration. Highlighting the importance of investigating markers of repair across different cellular compartments within the alveolar niche. A key advantage of using PCLS to establish the hAIR model is that the native cellular composition and structure is maintained, making the model physiologically relevant for studying lung repair and regeneration and also enabling us to track cellular populations using relevant markers (238, 272, 273, 278). In chapter 3 I explored the impact of SHH treatment on fibroblast subtypes. Immunostaining for vimentin revealed a dose-dependent increase in the increase in the proportion of fibroblast staining in the acid-injured region of AIR-PCLS (sections 3.2.7.8-3.2.7.9). To further characterise fibroblast sub-populations, then I assessed whether Shh impacted sub-populations of fibroblasts, specifically myofibroblasts (Figure. 3.31, Figure. 3.34) and lipofibroblasts (Figure. 3.32-3.34). Notably, SHH treatment led to an increased proportion of α-SMA^{+} myofibroblasts in acid-injured regions of Shh treated AIR-PCLS, the proportion of lipofibroblasts was also elevated, lipofibroblasts were marked with ADRP staining (Figure. 3.32-3.33).

Building on these findings, in this current chapter I employed the hAIR model to investigate changes in the lipofibroblast population through ADRP immunostaining (Figure. 5.12 and Figure. 5.18). Due to time constraints toward the end of the project I could not investigate the changes in both fibroblast subpopulations (myofibroblast and lipofibroblast) using hAIR-

PCLS. Previous studies have demonstrated that SHH signalling promotes fibroblast differentiation into activated myofibroblasts, characterised by increased α-SMA and enhanced extracellular matrix proteins (181, 185, 314). Although the mechanisms that underlie this remain poorly understood, it is widely accepted that SHH plays an important role in the maintenance of myofibroblast(185, 188). I prioritised assessing changes in the lipofibroblast population, by staining for ADRP, due to the limited number of investigations examining the relationship between SHH signalling and lipofibroblasts. Furthermore, lipofibroblasts play an important role in alveolar homeostasis and regeneration, by secreting factors which support ATII differentiation into ATI cells and surfactant synthesis (94, 95, 101, 103)

In hAIR-PCLS without SHH treatment I observed a trend toward an increase in $ADRP^+$ cells in the acid-injured region of hAIR-PCLS in comparison to the uninjured region and control, uninjured PCLS (Figure. 5.12 and Figure. 5.18), however findings were not significant which is likely due to a lack of sufficient biological replicates. Despite this, these preliminary findings from hAIR-PCLS appear to be consistent with findings from the mouse AIR model (Figure. 3.32). Furthermore, when hAIR-PCLS were treated with SHH and changes in the $ADRP^+$ population were assessed, there appeared to be a trend towards an increase in $ADRP^+$ cells in the acid-injured region of hAIR-PCLS as the concentration of SHH treatment increased. Whereas in the uninjured region, changes appeared to be minimal across all concentrations of SHH treatment (Figure. 5.18).

In addition to this, I investigated endothelial cells with anti-ERG (Figure. 5.13). However, due to sample availability and time constraints this investigation was only performed once and I did not perform this investigation with Shh treated hAIR-PCLS. Nevertheless, the findings are informative and are a building point for further investigation.

5.4 Conclusion

In this chapter, I investigated the role of SHH signalling in the context of human lungs during homeostasis and repair. I validated previous studies demonstrating the association between Shh and COPD through gene expression analysis of control and emphysema patient samples. Additionally, I explored transcriptomic databases to characterise the differential expression profiles of the Shh ligand, pathway receptors, inhibitors and associated transcription factors across epithelial, endothelial and stromal cell types in both COPD and normal tissue samples.

Building upon the findings presented in chapters 3 and 4, I successfully established the hAIR model to investigate changes in markers of lung repair post injury. I demonstrate that the hAIR model is a versatile and reproducible ex *vivo* model of lung injury that can be used to investigate mechanisms of repair and can applied as a pre-clinical model for identifying therapeutic targets. Specifically, I employ the hAIR model to further investigate the role of SHH signalling in lung repair post injury.

Chapter 6

Final Discussion

6.1 Discussion

6.1.1 Summary of main findings and future directions

Alveolar repair and/or regeneration are complex processes that are coordinated by multicellular interactions between tissue compartments within the alveolar niche. Studies have shown that these interactions are orchestrated by a network of signalling pathways known to play key roles in development, including Wnt, RA and Hedgehog signalling. Despite growing research evidence, the precise mechanisms by which these pathways orchestrate repair remain poorly understood. This raises several key questions that need to be addressed, particularly if we are to develop successful regenerative medicine-based approaches to treat lung diseases; what are the molecular and cellular mechanisms that underlie the regulation of alveolar repair by developmental signalling pathways? How do each of these pathways affect intercellular interactions and how does this in turn co-ordinate repair in the alveolar niche? And, can these pathways be modulated to induce effective repair?

Therefore, this thesis aimed to investigate precisely how several key developmental signalling pathways regulate alveolar repair, following a step-wise experimental approach; 1) an initial screening approach was employed to identify and select one promising pathway with repair modulating effects, leading to the selection of the SHH signalling pathway for detailed investigation 2) defining the role of Shh in structural cells within the alveolar niche and 3) exploring the wider implications of SHH signalling in alveolar repair and disease.

6.1.2 Cell type specific responses to developmental signalling pathways

Our findings from initial screening of developmental pathways highlighted the heterogeneity of cellular responses within the alveolar niche. Alveolar repair is a complex, multicellular process, with distinct cell types responding differently to the same signalling cues(3, 11, 37, 102). Therefore, it has been challenging for researchers to define the precise role of individual pathways in the *in vivo* lung, where multiple signalling pathways act simultaneously and may interact and influence one another to regulate repair(3, 13, 102). For example, using monocultures of single cell-types, I have shown that while WNT5A supports epithelial

migration it does not have an impact on endothelial migration. On the other hand, RA enhanced endothelial migration but not epithelial migration. Interestingly, SHH impaired epithelial cell migration and an opposing trend was observed when epithelial cells were treated with the SHH pathway inhibitor, cyclopamine. However, I demonstrated that Shh had a significant impact on the fibroblast cell population. These findings provide interesting insight into how different developmental pathways affect repair of alveolar cell types in different ways. However*, in vivo*, the activity of signalling pathways is not isolated to single cell types of tissues, instead signalling pathways co-exist and drive development and repair by co-ordinating responses between cell/tissue types to provide a global effect on repair of the alveoli (11, 13), therefore future experimental investigations should focus on investigating interactions between pathways. For example, it would be interesting to investigate whether activation of one pathway stimulates the secretion of a ligand required to modulate the activity of another pathway. This will aid in our understanding of how signalling pathways collectively regulate alveolar repair.

The interplay between different pathways can be investigated using several different approaches. Since research has highlighted that SHH interacts with Wnt, TGF- β and FGF during development(8, 13, 28, 398), it would be particularly important to investigate the relationship between SHH and one of these pathways. For example using *in vitro* cell culture, cells can be co-treated with a pathway modulator (pathway antagonists or agonists) from the SHH signalling pathway and a second modulator from Wnt, TGF- β or FGF signalling pathways. Following this, changes in target gene expression, protein expression or protein activity can be measured to investigate whether pathways are activated or inhibited. Although I used qPCR to characterise changes in gene expression in this project, qPCR is not the only way that pathway activation or depletion can be assessed. It would be important to employ a wider range of approaches for future investigations to gain a more comprehensive understanding of the impact of these pathway interactions. immunostaining or immunohistochemistry can be employed to determine changes in the localisation of pathway components, which will allow us to determine changes in pathway activation or depletion. ELISA or Western blot can be used to measure protein expression.

Additionally, it would be important to investigate the relationship between SHH and one of these pathways in the context of injury and repair. For example *in vitro* wound healing assays can be adapted, so cells are co-treated with pathway modulators. This will allow us to investigate the impact of co-treatment on migration as well as gene or protein expression. Furthermore, the AIR or hAIR model can also be utilised to increase the complexity and physiological relevance of our investigations. AIR/hAIR-PCLS can be co-treated with pathway modulators and changes in different cellular populations can be tracked using relevant cell type specific markers. Following this, changes in the expression of localisation of cellular populations (determined using markers) can be used to infer whether pathway activation or depletion is occurring. As previously outlined the use of PCLS allows the investigation of cellular behaviour in a more physiologically and translationally relevant model (272, 273, 278)

Finally the interaction between SHH and one of these pathways can be investigated using the co-culture model that was established as part of this thesis, using A549 and HLFs. This provides a more physiologically relevant model to investigate intercellular interactions as well as crosstalk between pathways.

6.1.3 SHH signalling enhances fibroblast mediated repair

One of the most significant findings in this thesis is that Shh treatment induces wound repair in human fibroblast cultures. Using primary HLFs, I showed that exogenous Shh treatment significantly enhanced wound closure. Importantly, to our knowledge, this is the first study to demonstrate this effect using primary HLFs, this provides important insight into the mechanisms by which Shh influences alveolar repair. In addition to this, when I co-cultured epithelial and fibroblast cells, SHH treatment resulted in the increased migration of both cell types. This is particularly interesting, since SHH treatment did not have an effect on wound repair in epithelial monocultures. Highlighting that the response of cells to a particular ligand may be different in a more complex environment.

Beyond the observed increase in fibroblast cell migration, our data from *ex vivo* AIR-PCLS, demonstrated that Shh treatment increased the proportion of fibroblasts, specifically

myofibroblasts and lipofibroblasts in acid-injured regions. This suggests that Shh modulates fibroblast repair not only by enhancing migration but also potentially by driving fibroblast differentiation into functionally distinct subtypes. Myofibroblasts are key mediators of extracellular matrix deposition and tissue remodelling, which are essential processes for structural repair following alveolar injury (97, 359, 443). Lipofibroblasts, in contrast, support ATII cell differentiation and contribute to surfactant production by secreting factors that drive surfactant synthesis, highlighting their role in maintaining alveolar homeostasis(94, 101, 103, 104). Moreover, lipofibroblasts are thought to act as a reservoir of pro-repair factors, including RA(444-446), so this population of fibroblasts is particularly associated with repair (94, 101, 103, 104, 447). The ability of SHH to modulate both fibroblast migration and differentiation suggests that the SHH signalling pathway may play a role in multiple aspects of alveolar repair through fibroblast-mediated mechanisms.

However, SHH signalling, activation and expression has been associated with fibrosis across multiple organs including the lung, heart, kidney and skin(189, 448, 449). This raises an important question; does Shh activation occur as a consequence of this fibrosis or does Shh activation drive fibrotic tissue remodelling, or both? Distinguishing whether SHH pathway activation is a driver or a consequence of fibrosis is critical, as this will further enable us to determine whether SHH is a viable therapeutic target for preventing aberrant tissue repair or whether SHH is just a marker of ongoing injury. Future investigations should focus on addressing this. For example lineage tracing can be employed to determine whether SHH acts directly on fibroblasts to induce differentiation(450-452). To do this, genetically altered mice (such as Cre-lox reporter mice)(453), in which specific fibroblast subpopulations (myofibroblasts or lipofibroblast) are fluorescently tagged can be employed to determine whether fibroblast differentiate following exogenous SHH treatment in experimentally induced fibrosis (by bleomycin exposure or pro-fibrotic cytokine cocktail for example) and under baseline conditions (no fibrosis).

Lung tissue can be harvested from different mice at differing time points so potential temporal changes in fibroblast subpopulations can be assessed. PCLS can be generated from lung tissue to image and visualise changes in fibroblast subpopulations(454). Additionally, as an

alternative to imaging PCLS, lineage traced fibroblasts can be isolated and scRNA-seq can be utilised to characterise transcriptional states that are indicative of fibroblast differentiation(450, 451, 455). Furthermore Gli^{+} cells can also be traced, since Gli is a downstream transcriptional factor in the SHH pathway and has been and is expressed in fibroblasts, this will allow us to determine whether the pathway is activated(185). Kugler *et al.*,(185) employed a Gli1-CreER mouse model in their studies, to lineage trace Gli1 expressing cell, this could model could be employed for further comparisons between SHH activation in induced fibrosis versus induced COPD/emphysema phenotype in these mice.

6.1.4 Epithelial- mesenchymal crosstalk and Shh mediated repair

In addition to identifying that Shh treatment led to an increase in HLF wound closure in monoculture, in chapter 4 I observed that Shh treatment led to an increase in cell migration when HLF and A549 cells were co-cultured, despite having inhibitory effects on epithelial repair in monoculture. This highlights the importance of epithelial–mesenchymal crosstalk in shaping responsiveness to Shh and highlights that Shh mediated alveolar repair is context-dependent. Furthermore treating co-cultured cells with cyclopamine had no impact on wound closure.

However, co-culture wound healing assays were only assessed at two timepoints, t=0 hr and t=20 hr, which limits our understanding of cellular interactions and migratory behaviour of both cell types in between the beginning and end of the experiment. By only measuring the difference in migration at these two time points, critical migratory patterns and cell-cell interactions may have missed, as well as changes in speed of movement (rate of wound closure) that could have occurred within the 20-hr timeframe. For example, do fibroblasts move before epithelial cells and induce epithelial migration or vice versa? Incorporating time-lapse imaging in future co-culture studies would overcome this limitation and shed light on such additional aspects of cell biology by enabling us to monitor the behaviour of the cells over time. This approach would provide detailed insight into possible temporal trends in migration and epithelial–mesenchymal interactions, and potential reciprocal influences between cell types during Shh-mediated repair. Furthermore, time-lapse imaging could help

determine whether fibroblasts guide epithelial cells or vice versa, and/or whether coordinated migration emerges in response to Shh, therefore providing a more complete understanding of the contribution of Shh to alveolar repair.

6.1.5 Using 5E1 blocking antibody to study the role of Shh in alveolar repair

To strengthen the findings of this thesis and obtain greater knowledge about and how SHH signalling affects alveolar repair, it will be important to conduct additional experiments where SHH signalling is blocked. In chapters 3 and 4 of this thesis, I used cyclopamine which is a pharmacological agent that blocks SHH signalling by binding to Smo. However, an alternative method would be to employ the monoclonal Shh blocking antibody, 5E1, which binds directly to Shh preventing its interaction with ptch1 and therefore inhibiting downstream signalling (456-458).

A key advantage of using the 5E1 blocking antibody is that it inhibits SHH signalling and also allows for the visualisation of SHH itself, this enables the assessment of its presence and spatial distribution in cells (456-458). Therefore, in monoculture wound healing assays, cells can be treated with 5E1 alone or treated with 5E1 followed by SHH then live-cell imaging can be used to investigate the impact of blocking SHH signalling on wound healing and to track potential changes in the localisation of SHH in response to injury and treatment.

A similar approach can be employed using our co-culture model, where primary HLFs and A549 cells are co-cultured. By treating co-culture with 5E1 I could determine whether Shh is necessary for the increased migration that I observed in this assay. Similar to monocultures, co-cultured can be treated with 5E1 alone, or 5E1 followed by SHH, to assess whether the inhibitory effects of 5E1 can be reversed. The advantage of using 5E1 in the context of co-cultures is that 5E1 can be applied to block SHH signalling and live-cell time lapse imaging can be conducted to allow real-time observation of the Shh-dependent migration without the need for genetic manipulation of cells. This makes 5E1 particularly well-suited for integration with time-lapse imaging, application of 5E1 to block SHH signalling could reveal whether fibroblasts initiate migration, guide epithelial cells, or whether migration of both cell types

requires Shh-mediated paracrine signalling. Unlike genetic knockdown or knockout approaches such as genetically modified mice, which are permanent and may introduce compensatory effects(459, 460), antibody blockade is reversible and dose-dependent, allowing more precise temporal control over pathway inhibition. Therefore the impact of different concentrations of 5E1 on co-culture migration could also be assessed. Dose-response studies with 5E1 would also help establish whether there is a threshold of pathway inhibition required to disrupt cell migration of co-culture and potentially epithelial–mesenchymal crosstalk.

Beyond, *in vitro* studies, 5E1 could be incorporated into the ex vivo AIR or hAIR model to assess how blocking SHH affects markers of repair. Specifically, the AIR/hAIR model can be generated and AIR-PCLS or hAIR-PCLS can be treated with 5E1, and incubated for different time periods e.g. 12 hr, 24 hr and 48 hr. Following this, PCLS can be fixed and co-immunostained with markers of repair such as proSP-C and Ki67 as well as 5E1. Then PCLS can be visualised using imaging to determine the impact of blocking SHH with 5E1.

6.1.6 SHH pathway dysregulation in disease: the clinical implications of altered pathway activity

This thesis highlights a role for Shh in modulating fibroblast behaviour and epithelial-mesenchymal interactions during alveolar repair. However, in lung disease, activation of the SHH signalling pathway has been associated with both IPF and COPD (181). Reaffirming the question, is SHH detrimental or protective? Interestingly, although aberrant repair is seen in both IPF and COPD, the disease mechanisms are opposite, overactive repair occurs in IPF, while COPD is characterised by a lack of repair (37, 38, 461)

Moreover, a hallmark of IPF is fibroblast accumulation and persistent myofibroblast activation which leads to progressive scarring and damage of alveoli (19, 96, 99, 100, 185). The capacity of Shh to enhance fibroblast migration and influence differentiation into myofibroblasts and lipofibroblasts, as shown in this thesis, raises the possibility that excessive or prolonged pathway activity may tip the balance from adaptive repair to fibrosis.

A particularly interesting finding from this thesis was the consistently high expression of HHIP across endothelial cells and moderate to low expression in fibroblasts. HHIP is an endogenous inhibitor of Shh. Interestingly, a preliminary study has shown that increased expression of HHIP is observed in the early stage of fibrosis while lower levels are expressed in advanced fibrosis (462). While abnormal expression of *PTCH1, SMO* and *GLI1* has been observed in IPF lung tissue(181, 189). Furthermore, in Chapter 5 I show that *HHIP* is downregulated in COPD patient samples while *SHH, PTCH1, GLI1* and *GLI2* are upregulated. This aligns with GWAS which have shown that SNPs in HHIP are a major risk factor for COPD. I propose that this could be as a result of dysregulated epithelial-mesenchymal crosstalk, since I highlight the important role that SHH plays in mediating epithelial-mesenchymal interactions. Together, these findings suggest that reduced HHIP may impair the lung's ability to regulate Shh activity. I did not assess the levels of *HHIP* in IPF tissue samples, however it would be interesting to do this in the future and to compare findings with findings collected from COPD patient samples.

Furthermore, this suggests that the balance between pathway activation and inhibition may be a key determinant of whether SHH signalling supports regeneration or contributes to disease pathology. Specifically, in emphysema and COPD, downregulation of HHIP has been associated with disease susceptibility therefore may predispose individuals to aberrant SHH signalling, however, in fibrosis excessive pathway activation may drive myofibroblast accumulation. Further investigations into the regulation of HHIP in the alveolar niche, particularly during injury and repair, may therefore provide insight into mechanisms that lead to changes in Shh activity under physiological conditions.

These findings underscore both a clinical opportunity and a challenge for therapeutic targeting of Shh. It is evident that SHH signalling plays a critical role in both repair and disease pathology, but how can this be balanced? Pharmacological agents including vismodegib and sonidegib, which inhibit SHH signalling, specifically by blocking Smo activation, have already been licenced to treat cancers(463-466). Inhibition of SHH signalling is promising in fibrosis where the activity appears overactive, however, in COPD or emphysema, where HHIP is downregulated already downregulated, further inhibition could have a detrimental effect.

Therefore, therapeutic approaches should focus on restoring the balance of SHH signalling by targeting HHIP activity or selectively modulating SHH pathway transcription factors GLI1/GLI2.

Further to this, it would be important and interesting to utilise techniques such as Gene set variation analysis (GSVA) and/or Gene set enrichment analysis (GSEA) to investigate whether the gene expression patterns observed during this project are associated with specific pathways, which contribute to disease pathology(467-469). This would broaden our mechanistic knowledge and build upon findings towards the development of therapeutic approaches.

6.1.7 The AIR model and hAIR model as translational tools for lung repair studies

In this study I successfully established the human AIR model (hAIR model) (277), translating the previously developed mouse AIR model into a human system that is more physiologically relevant. The hAIR model uses human precision-cut lung slices (PCLS) in which a spatially restricted region is injured, allowing investigation of repair and regeneration. This *ex vivo* model retains the native cellular composition and architecture of the human lung, making it a versatile platform for studying alveolar repair mechanisms.

Importantly, the hAIR model enables a range of applications, including, assessing changes in epithelial, fibroblast and endothelial cell populations in response to injury, and evaluating the impact of signalling pathways such as SHH on repair, as demonstrated in chapter 5 of this thesis.

6.1.8 Study limitations

While this thesis provides important insights into the role of SHH signalling in alveolar repair, several limitations should be acknowledged. One major limitation is that the studies conducted primarily focused on structural cells, epithelial, endothelial and fibroblast cells, but the role of immune cells in lung regeneration was not investigated(107, 395). The immune response plays an important role in tissue repair. All models employed in this thesis lack a

functional immune compartment, and while PCLS retain tissue-resident macrophages, they do not have a circulatory system and therefore cannot recruit additional immune cells from the bloodstream, limiting the ability of PCLS to fully model the immune response(272, 273, 276-278). Therefore whilst the models used throughout this thesis provide insightful information, they do not fully recapitulate the interactions between structural cells and the immune system that occur *in vivo* during repair and/or regeneration.

Future studies incorporating *in vivo* models of lung injury and repair would be valuable to address this limitation and to enable us to gain a more comprehensive understanding of how SHH orchestrates alveolar repair in a physiologically relevant context.

6.1.9 Concluding remarks

The findings from this thesis highlight the potential role of SHH signalling in alveolar repair. More specifically, the data presented indicates that SHH is a key regulator of fibroblasts in the alveoli. By influencing fibroblast differentiation and function, SHH signalling could shape regenerative responses and limit maladaptive remodelling. Determining whether SHH acts as a driver of repair or whether SHH activation occurs as a consequence of injury remains a critical question. Understanding these mechanisms may inform the development of targeted strategies to enhance alveolar repair while regulating potential aberrant signalling.

Chapter 7

References

References

1. Societies FoIR. The Global Impact of Respiratory Disease 2nd ed. Sheffield: European Respiratory Society 2017.
2. Kotton DN, Morrisey EE. Lung regeneration: mechanisms, applications and emerging stem cell populations. Nature Medicine. 2014;20(8):822-832.
3. Hogan BL, Barkauskas CE, Chapman HA, Epstein JA, Jain R, Hsia CC, et al. Repair and regeneration of the respiratory system: complexity, plasticity, and mechanisms of lung stem cell function. Cell stem cell. 2014;15(2):123-138.
4. Akram KM, Patel N, Spiteri MA, Forsyth NR. Lung Regeneration: Endogenous and Exogenous Stem Cell Mediated Therapeutic Approaches. Int J Mol Sci. 2016;17(1).
5. Melo-Narváez MC, Stegmayr J, Wagner DE, Lehmann M. Lung regeneration: implications of the diseased niche and ageing. European Respiratory Review. 2020;29(157):200222.
6. Yusen RD, Edwards LB, Kucheryavaya AY, Benden C, Dipchand AI, Goldfarb SB, et al. The Registry of the International Society for Heart and Lung Transplantation: Thirty-second Official Adult Lung and Heart-Lung Transplantation Report—2015; Focus Theme: Early Graft Failure. The Journal of Heart and Lung Transplantation. 2015;34(10):1264-1277.
7. Christie JD, Raemdonck DV, Fisher AJ. Lung Transplantation. New England Journal of Medicine. 2024;391(19):1822-1836.
8. Warburton D, El-Hashash A, Carraro G, Tiozzo C, Sala F, Rogers O, et al. Lung organogenesis. Curr Top Dev Biol. 2010;90:73-158.
9. Ornitz DM, Yin Y. Signaling networks regulating development of the lower respiratory tract. Cold Spring Harb Perspect Biol. 2012;4(5).
10. Rackley CR, Stripp BR. Building and maintaining the epithelium of the lung. J Clin Invest. 2012;122(8):2724-2730.
11. Stabler CT, Morrisey EE. Developmental pathways in lung regeneration. Cell Tissue Res. 2017;367(3):677-685.
12. Nikolić MZ, Sun D, Rawlins EL. Human lung development: recent progress and new challenges. Development. 2018;145(16).
13. Chanda D, Otoupalova E, Smith SR, Volckaert T, De Langhe SP, Thannickal VJ. Developmental pathways in the pathogenesis of lung fibrosis. Mol Aspects Med. 2019;65:56-69.
14. Allen-Hyttinen J, Yung H, Nikolić MZ. Lung development. In: Nikolić M, Hogan BLM, editors. Lung Stem Cells in Development, Health and Disease (ERS Monograph). Sheffield: European Respiratory Society 2021. p. 1-16.
15. Burri PH. Fetal and postnatal development of the lung. Annu Rev Physiol. 1984;46:617-628.
16. Schittny JC. Development of the lung. Cell Tissue Res. 2017;367(3):427-444.
17. Burri PH. Development and Growth of the Human Lung. In: Terjung R, editor. Comprehensive Physiology. p. 1-46.
18. Meyerholz DK, Suarez CJ, Dintzis SM, Frevert CW. Respiratory System. In: Treuting P, Dintzis S, Montine KS, editors. Comparative Anatomy and Histology: A Mouse, Rat, and Human Atlas. 2nd ed. United Kingdom: Academic Press; 2018. p. 135-144.

19. Selman M, Pardo A, Kaminski N. Idiopathic Pulmonary Fibrosis: Aberrant Recapitulation of Developmental Programs? PLOS Medicine. 2008;5(3):e62.
20. Hodson EABWA. Development and growth of the airways. In: Hodson WA, editor. Lung Biology in Health and Disease Development of the Lung. 6. New York: Dekker; 1977. p. 3-35.
21. Caldeira I, Fernandes-Silva H, Machado-Costa D, Correia-Pinto J, Moura RS. Developmental Pathways Underlying Lung Development and Congenital Lung Disorders. Cells. 2021;10(11).
22. Koos BJ, Rajaee A, editors. Fetal Breathing Movements and Changes at Birth2014; New York, NY: Springer New York.
23. Wigglesworth JS, Desai R. IS FETAL RESPIRATORY FUNCTION A MAJOR DETERMINANT OF PERINATAL SURVIVAL? The Lancet. 1982;319(8266):264-267.
24. Rehman S, Bacha D. Embryology, Pulmonary. StatPearls. Treasure Island (FL)2022.
25. Negretti NM, Son Y, Crooke P, Plosa EJ, Benjamin JT, Jetter CS, et al. Epithelial outgrowth through mesenchymal rings drives lung alveologenesis. JCI Insight. 2025;10(4).
26. Akram KM, Yates LL, Mongey R, Rothery S, Gaboriau DCA, Sanderson J, et al. Live imaging of alveologenesis in precision-cut lung slices reveals dynamic epithelial cell behaviour. Nature Communications. 2019;10(1):1178.
27. Rodríguez-Castillo JA, Pérez DB, Ntokou A, Seeger W, Morty RE, Ahlbrecht K. Understanding alveolarization to induce lung regeneration. Respir Res. 2018;19(1):148.
28. Morrisey EE, Hogan BL. Preparing for the first breath: genetic and cellular mechanisms in lung development. Dev Cell. 2010;18(1):8-23.
29. Lumb AB. Chapter 1 - Functional Anatomy of the Respiratory Tract. In: Lumb AB, editor. Nunn's Applied Respiratory Physiology (Eighth Edition): Elsevier; 2017. p. 3-16.e11.
30. Weibel ER. Morphological basis of alveolar-capillary gas exchange. Physiol Rev. 1973;53(2):419-495.
31. Weibel ER, Gomez DM. Architecture of the human lung. Use of quantitative methods establishes fundamental relations between size and number of lung structures. Science. 1962;137(3530):577-585.
32. Irvin CG, Bates JHT. Measuring the lung function in the mouse: the challenge of size. Respiratory Research. 2003;4(1):1.
33. Rock JR, Randell SH, Hogan BLM. Airway basal stem cells: a perspective on their roles in epithelial homeostasis and remodeling. Disease Models & Mechanisms. 2010;3(9-10):545-556.
34. Mercer RR, Russell ML, Roggli VL, Crapo JD. Cell number and distribution in human and rat airways. Am J Respir Cell Mol Biol. 1994;10(6):613-624.
35. Dean CH, Snelgrove RJ. New Rules for Club Development: New Insights into Human Small Airway Epithelial Club Cell Ontogeny and Function. Am J Respir Crit Care Med. 2018;198(11):1355-1356.
36. Nikolić MZ, Hogan BLM. Lung Stem Cells in Development, Health and Disease2021.
37. Beers MF, Morrisey EE. The three R's of lung health and disease: repair, remodeling, and regeneration. J Clin Invest. 2011;121(6):2065-2073.
38. Dean CH, Lloyd CM. Lung Alveolar Repair: Not All Cells Are Equal. Trends Mol Med. 2017;23(10):871-873.
39. Sun X, Perl AK, Li R, Bell SM, Sajti E, Kalinichenko VV, et al. A census of the lung: CellCards from LungMAP. Dev Cell. 2022;57(1):112-145.e112.

40. Boers JE, Ambergen AW, Thunnissen FB. Number and proliferation of basal and parabasal cells in normal human airway epithelium. Am J Respir Crit Care Med. 1998;157(6 Pt 1):2000-2006.
41. Nakajima M, Kawanami O, Jin E, Ghazizadeh M, Honda M, Asano G, et al. Immunohistochemical and ultrastructural studies of basal cells, Clara cells and bronchiolar cuboidal cells in normal human airways. Pathol Int. 1998;48(12):944-953.
42. Rawlins EL, Okubo T, Xue Y, Brass DM, Auten RL, Hasegawa H, et al. The Role of Scgb1a1+ Clara Cells in the Long-Term Maintenance and Repair of Lung Airway, but Not Alveolar, Epithelium. Cell Stem Cell. 2009;4(6):525-534.
43. Evans MJ, Van Winkle LS, Fanucchi MV, Plopper CG. Cellular and molecular characteristics of basal cells in airway epithelium. Exp Lung Res. 2001;27(5):401-415.
44. Okuda K, Chen G, Subramani DB, Wolf M, Gilmore RC, Kato T, et al. Localization of Secretory Mucins MUC5AC and MUC5B in Normal/Healthy Human Airways. American Journal of Respiratory and Critical Care Medicine. 2019;199(6):715-727.
45. Rogers D. Airway goblet cells: responsive and adaptable front-line defenders. European Respiratory Journal.7(9):1690-1706.
46. Bansil R, Turner BS. The biology of mucus: Composition, synthesis and organization. Advanced Drug Delivery Reviews. 2018;124:3-15.
47. Tang MLK, Wilson JW, Stewart AG, Royce SG. Airway remodelling in asthma: Current understanding and implications for future therapies. Pharmacology & Therapeutics. 2006;112(2):474-488.
48. Pack RJ, Al-Ugaily LH, Morris G. The cells of the tracheobronchial epithelium of the mouse: a quantitative light and electron microscope study. J Anat. 1981;132(Pt 1):71-84.
49. Stripp BR, Reynolds SD. CLARA CELLS. In: Laurent GJ, Shapiro SD, editors. Encyclopedia of Respiratory Medicine. Oxford: Academic Press; 2006. p. 471-478.
50. Hong KU, Reynolds SD, Giangreco A, Hurley CM, Stripp BR. Clara cell secretory protein-expressing cells of the airway neuroepithelial body microenvironment include a label-retaining subset and are critical for epithelial renewal after progenitor cell depletion. Am J Respir Cell Mol Biol. 2001;24(6):671-681.
51. Watson Julie K, Rulands S, Wilkinson Adam C, Wuidart A, Ousset M, Van Keymeulen A, et al. Clonal Dynamics Reveal Two Distinct Populations of Basal Cells in Slow-Turnover Airway Epithelium. Cell Reports. 2015;12(1):90-101.
52. Rawlins EL, Hogan BL. Ciliated epithelial cell lifespan in the mouse trachea and lung. Am J Physiol Lung Cell Mol Physiol. 2008;295(1):L231-234.
53. Bustamante-Marin XM, Ostrowski LE. Cilia and Mucociliary Clearance. Cold Spring Harb Perspect Biol. 2017;9(4).
54. Roth D, Şahin AT, Ling F, Tepho N, Senger CN, Quiroz EJ, et al. Structure and function relationships of mucociliary clearance in human and rat airways. Nature Communications. 2025;16(1):2446.
55. Volckaert T, De Langhe S. Lung epithelial stem cells and their niches: Fgf10 takes center stage. Fibrogenesis & Tissue Repair. 2014;7(1):8.
56. Branchfield K, Nantie L, Verheyden JM, Sui P, Wienhold MD, Sun X. Pulmonary neuroendocrine cells function as airway sensors to control lung immune response. Science. 2016;351(6274):707-710.
57. Garg A, Sui P, Verheyden JM, Young LR, Sun X. Consider the lung as a sensory organ: A tip from pulmonary neuroendocrine cells. Curr Top Dev Biol. 2019;132:67-89.

58. Dash B, Kim E, Sun X. Neuroendocrine cells in lung development and disease. In: Nikolić M, Hogan BLM, editors. Lung Stem Cells in Development, Health and Disease (ERS Monograph). Sheffield: European Respiratory Society; 2021. p. 44-55.
59. Weibel ER. Lung morphometry: the link between structure and function. Cell and Tissue Research. 2017;367(3):413-426.
60. Knudsen L, Ochs M. The micromechanics of lung alveoli: structure and function of surfactant and tissue components. Histochem Cell Biol. 2018;150(6):661-676.
61. Hsia CC, Hyde DM, Weibel ER. Lung Structure and the Intrinsic Challenges of Gas Exchange. Compr Physiol. 2016;6(2):827-895.
62. Crapo JD, Barry BE, Gehr P, Bachofen M, Weibel ER. Cell number and cell characteristics of the normal human lung. Am Rev Respir Dis. 1982;126(2):332-337.
63. Berthiaume Y, Voisin G, Dagenais A. The alveolar type I cells: the new knight of the alveolus? J Physiol. 2006;572(Pt 3):609-610.
64. Weibel ER. On the tricks alveolar epithelial cells play to make a good lung. Am J Respir Crit Care Med. 2015;191(5):504-513.
65. Yang J, Hernandez BJ, Martinez Alanis D, Narvaez del Pilar O, Vila-Ellis L, Akiyama H, et al. The development and plasticity of alveolar type 1 cells. Development. 2016;143(1):54-65.
66. Herzog EL, Brody AR, Colby TV, Mason R, Williams MC. Knowns and Unknowns of the Alveolus. Proceedings of the American Thoracic Society. 2008;5(7):778-782.
67. DeFouw DO. Ultrastructural features of alveolar epithelial transport. Am Rev Respir Dis. 1983;127(5 Pt 2):S9-13.
68. Zhou X, Baron RM, Hardin M, Cho MH, Zielinski J, Hawrylkiewicz I, et al. Identification of a chronic obstructive pulmonary disease genetic determinant that regulates HHIP. Hum Mol Genet. 2012;21(6):1325-1335.
69. Chan M, Liu Y. Function of epithelial stem cell in the repair of alveolar injury. Stem Cell Research & Therapy. 2022;13(1):170.
70. Penkala IJ, Liberti DC, Pankin J, Sivakumar A, Kremp MM, Jayachandran S, et al. Age-dependent alveolar epithelial plasticity orchestrates lung homeostasis and regeneration. Cell Stem Cell. 2021;28(10):1775-1789.e1775.
71. Jain R, Barkauskas CE, Takeda N, Bowie EJ, Aghajanian H, Wang Q, et al. Plasticity of Hopx+ type I alveolar cells to regenerate type II cells in the lung. Nature Communications. 2015;6(1):6727.
72. Castranova V, Rabovsky J, Tucker JH, Miles PR. The alveolar type II epithelial cell: a multifunctional pneumocyte. Toxicol Appl Pharmacol. 1988;93(3):472-483.
73. Fehrenbach H. Alveolar epithelial type II cell: defender of the alveolus revisited. Respiratory Research. 2001;2(1):33.
74. Griese M. Pulmonary surfactant in health and human lung diseases: state of the art. Eur Respir J. 1999;13(6):1455-1476.
75. Veldhuizen EJA, Haagsman HP. Role of pulmonary surfactant components in surface film formation and dynamics. Biochimica et Biophysica Acta (BBA) - Biomembranes. 2000;1467(2):255-270.
76. Han S, Mallampalli RK. The Role of Surfactant in Lung Disease and Host Defense against Pulmonary Infections. Ann Am Thorac Soc. 2015;12(5):765-774.
77. Whitsett JA, Wert SE, Weaver TE. Alveolar surfactant homeostasis and the pathogenesis of pulmonary disease. Annu Rev Med. 2010;61:105-119.

78. Beers MF, Moodley Y. When Is an Alveolar Type 2 Cell an Alveolar Type 2 Cell? A Conundrum for Lung Stem Cell Biology and Regenerative Medicine. Am J Respir Cell Mol Biol. 2017;57(1):18-27.
79. Barkauskas CE, Cronce MJ, Rackley CR, Bowie EJ, Keene DR, Stripp BR, et al. Type 2 alveolar cells are stem cells in adult lung. The Journal of Clinical Investigation. 2013;123(7):3025-3036.
80. Desai TJ, Brownfield DG, Krasnow MA. Alveolar progenitor and stem cells in lung development, renewal and cancer. Nature. 2014;507(7491):190-194.
81. Marconett CN, Zhou B, Sunohara M, Pouldar TM, Wang H, Liu Y, et al. Cross-Species Transcriptome Profiling Identifies New Alveolar Epithelial Type I Cell-Specific Genes. Am J Respir Cell Mol Biol. 2017;56(3):310-321.
82. Liebler JM, Marconett CN, Juul N, Wang H, Liu Y, Flodby P, et al. Combinations of differentiation markers distinguish subpopulations of alveolar epithelial cells in adult lung. Am J Physiol Lung Cell Mol Physiol. 2016;310(2):L114-120.
83. Mammoto A, Mammoto T. Vascular Niche in Lung Alveolar Development, Homeostasis, and Regeneration. Front Bioeng Biotechnol. 2019;7:318.
84. Rafii S, Butler JM, Ding BS. Angiocrine functions of organ-specific endothelial cells. Nature. 2016;529(7586):316-325.
85. Stevens T, Phan S, Frid MG, Alvarez D, Herzog E, Stenmark KR. Lung vascular cell heterogeneity: endothelium, smooth muscle, and fibroblasts. Proc Am Thorac Soc. 2008;5(7):783-791.
86. Barron L, Gharib SA, Duffield JS. Lung Pericytes and Resident Fibroblasts: Busy Multitaskers. Am J Pathol. 2016;186(10):2519-2531.
87. Weibel E, Crystal R. Structural organization of the pulmonary interstitium. The lung. 1991;1:369-380.
88. Wijsman PC, van Smoorenburg LH, de Bruin DM, Annema JT, Kerstjens HAM, Mets OM, et al. Imaging the pulmonary extracellular matrix. Current Opinion in Physiology. 2021;22:100444.
89. Kapanci Y, Assimacopoulos A, Irle C, Zwahlen A, Gabbiani G. "Contractile interstitial cells" in pulmonary alveolar septa: a possible regulator of ventilation-perfusion ratio? Ultrastructural, immunofluorescence, and in vitro studies. J Cell Biol. 1974;60(2):375-392.
90. Hung CF, Wilson CL, Schnapp LM. Pericytes in the Lung. In: Birbrair A, editor. Pericyte Biology in Different Organs. Cham: Springer International Publishing; 2019. p. 41-58.
91. Kato K, Diéguez-Hurtado R, Park DY, Hong SP, Kato-Azuma S, Adams S, et al. Pulmonary pericytes regulate lung morphogenesis. Nat Commun. 2018;9(1):2448.
92. Armulik A, Abramsson A, Betsholtz C. Endothelial/Pericyte Interactions. Circulation Research. 2005;97(6):512-523.
93. Gerhardt H, Betsholtz C. Endothelial-pericyte interactions in angiogenesis. Cell Tissue Res. 2003;314(1):15-23.
94. McGowan SE, Torday JS. The pulmonary lipofibroblast (lipid interstitial cell) and its contributions to alveolar development. Annu Rev Physiol. 1997;59:43-62.
95. Ushakumary MG, Riccetti M, Perl A-KT. Resident Interstitial Lung Fibroblasts and their Role in Alveolar Stem Cell Niche Development, Homeostasis, Injury, and Regeneration. Stem Cells Translational Medicine. 2021;10(7):1021-1032.
96. Pakshir P, Noskovicova N, Lodyga M, Son DO, Schuster R, Goodwin A, et al. The myofibroblast at a glance. Journal of Cell Science. 2020;133(13).

97. Balestrini JL, Chaudhry S, Sarrazy V, Koehler A, Hinz B. The mechanical memory of lung myofibroblasts. Integrative Biology. 2012;4(4):410-421.
98. Zhang HY, Gharaee-Kermani M, Zhang K, Karmiol S, Phan SH. Lung fibroblast alpha-smooth muscle actin expression and contractile phenotype in bleomycin-induced pulmonary fibrosis. Am J Pathol. 1996;148(2):527-537.
99. Wynn TA. Integrating mechanisms of pulmonary fibrosis. J Exp Med. 2011;208(7):1339-1350.
100. Gabbiani G. The myofibroblast in wound healing and fibrocontractive diseases. The Journal of Pathology. 2003;200(4):500-503.
101. Torday JS, Rehan VK. On the evolution of the pulmonary alveolar lipofibroblast. Experimental Cell Research. 2016;340(2):215-219.
102. Hogan BLM, editor The Alveolar Stem Cell Niche of the Mammalian Lung2020; Singapore: Springer Singapore.
103. Ahlbrecht K, McGowan SE. In search of the elusive lipofibroblast in human lungs. Am J Physiol Lung Cell Mol Physiol. 2014;307(8):L605-608.
104. Schultz CJ, Torres E, Londos C, Torday JS. Role of adipocyte differentiation-related protein in surfactant phospholipid synthesis by type II cells. Am J Physiol Lung Cell Mol Physiol. 2002;283(2):L288-296.
105. Brasaemle DL, Barber T, Wolins NE, Serrero G, Blanchette-Mackie EJ, Londos C. Adipose differentiation-related protein is an ubiquitously expressed lipid storage droplet-associated protein. J Lipid Res. 1997;38(11):2249-2263.
106. Ardain A, Marakalala MJ, Leslie A. Tissue-resident innate immunity in the lung. Immunology. 2020;159(3):245-256.
107. Zazara DE, Belios I, Lücke J, Zhang T, Giannou AD. Tissue-resident immunity in the lung: a first-line defense at the environmental interface. Semin Immunopathol. 2022;44(6):827-854.
108. Tan SY, Krasnow MA. Developmental origin of lung macrophage diversity. Development. 2016;143(8):1318-1327.
109. Kopf M, Schneider C, Nobs SP. The development and function of lung-resident macrophages and dendritic cells. Nature Immunology. 2015;16(1):36-44.
110. Guilliams M, De Kleer I, Henri S, Post S, Vanhoutte L, De Prijck S, et al. Alveolar macrophages develop from fetal monocytes that differentiate into long-lived cells in the first week of life via GM-CSF. J Exp Med. 2013;210(10):1977-1992.
111. Basil MC, Alysandratos KD, Kotton DN, Morrisey EE. Lung repair and regeneration: Advanced models and insights into human disease. Cell Stem Cell. 2024;31(4):439-454.
112. Basil MC, Katzen J, Engler AE, Guo M, Herriges MJ, Kathiriya JJ, et al. The Cellular and Physiological Basis for Lung Repair and Regeneration: Past, Present, and Future. Cell Stem Cell. 2020;26(4):482-502.
113. Rawlins EL, Hogan BLM. Epithelial stem cells of the lung: privileged few or opportunities for many? Development. 2006;133(13):2455-2465.
114. Weissman IL, Anderson DJ, Gage F. Stem and progenitor cells: origins, phenotypes, lineage commitments, and transdifferentiations. Annu Rev Cell Dev Biol. 2001;17:387-403.
115. Blanpain C, Fuchs E. Plasticity of epithelial stem cells in tissue regeneration. Science. 2014;344(6189):1242281.
116. Tata PR, Mou H, Pardo-Saganta A, Zhao R, Prabhu M, Law BM, et al. Dedifferentiation of committed epithelial cells into stem cells in vivo. Nature. 2013;503(7475):218-223.

117. Tata PR, Rajagopal J. Plasticity in the lung: making and breaking cell identity. Development. 2017;144(5):755-766.
118. Lin B, Sun J, Mou H, Rajagopal J. Adult mouse and human airway epithelial basal stem cells. In: Nikolić M, Hogan BLM, editors. Lung Stem Cells in Development, Health and Disease (ERS Monograph). Sheffield: European Respiratory Society; 2021. p. 56-69.
119. Rawlins EL, Okubo T, Que J, Xue Y, Clark C, Luo X, et al. Epithelial stem/progenitor cells in lung postnatal growth, maintenance, and repair. Cold Spring Harb Symp Quant Biol. 2008;73:291-295.
120. Donne ML, Lechner AJ, Rock JR. Evidence for lung epithelial stem cell niches. BMC Developmental Biology. 2015;15(1):32.
121. Heijink IH, ten Hacken NHT. Stem/Progenitor Cell Populations Resident in the Lung and the Role of Stromal Support in Their Maintenance and Differentiation. In: Burgess JK, Heijink IH, editors. Stem Cell-Based Therapy for Lung Disease. Cham: Springer International Publishing; 2019. p. 15-34.
122. Rock JR, Onaitis MW, Rawlins EL, Lu Y, Clark CP, Xue Y, et al. Basal cells as stem cells of the mouse trachea and human airway epithelium. Proceedings of the National Academy of Sciences. 2009;106(31):12771-12775.
123. Hong KU, Reynolds SD, Watkins S, Fuchs E, Stripp BR. Basal cells are a multipotent progenitor capable of renewing the bronchial epithelium. Am J Pathol. 2004;164(2):577-588.
124. Borok Z, Whitsett JA, Bitterman PB, Thannickal VJ, Kotton DN, Reynolds SD, et al. Cell plasticity in lung injury and repair: report from an NHLBI workshop, April 19-20, 2010. Proc Am Thorac Soc. 2011;8(3):215-222.
125. Hong KU, Reynolds SD, Watkins S, Fuchs E, Stripp BR. In vivo differentiation potential of tracheal basal cells: evidence for multipotent and unipotent subpopulations. American Journal of Physiology-Lung Cellular and Molecular Physiology. 2004;286(4):L643-L649.
126. Montoro DT, Haber AL, Biton M, Vinarsky V, Lin B, Birket SE, et al. A revised airway epithelial hierarchy includes CFTR-expressing ionocytes. Nature. 2018;560(7718):319-324.
127. Plasschaert LW, Žilionis R, Choo-Wing R, Savova V, Knehr J, Roma G, et al. A single-cell atlas of the airway epithelium reveals the CFTR-rich pulmonary ionocyte. Nature. 2018;560(7718):377-381.
128. Mori M, Mahoney JE, Stupnikov MR, Paez-Cortez JR, Szymaniak AD, Varelas X, et al. Notch3-Jagged signaling controls the pool of undifferentiated airway progenitors. Development. 2015;142(2):258-267.
129. Morimoto M, Nishinakamura R, Saga Y, Kopan R. Different assemblies of Notch receptors coordinate the distribution of the major bronchial Clara, ciliated and neuroendocrine cells. Development. 2012;139(23):4365-4373.
130. Rock JR, Gao X, Xue Y, Randell SH, Kong YY, Hogan BL. Notch-dependent differentiation of adult airway basal stem cells. Cell Stem Cell. 2011;8(6):639-648.
131. Gomi K, Arbelaez V, Crystal RG, Walters MS. Activation of NOTCH1 or NOTCH3 Signaling Skews Human Airway Basal Cell Differentiation toward a Secretory Pathway. PLOS ONE. 2015;10(2):e0116507.
132. Evans MJ, Cabral-Anderson LJ, Freeman G. Role of the Clara cell in renewal of the bronchiolar epithelium. Lab Invest. 1978;38(6):648-653.
133. Dabrowska C, Li J, Mulay A, Carraro G, Gupta M, Kim CF, et al. Adult mouse intralobar airway stem cells. In: Nikolić M, Hogan BLM, editors. Lung Stem Cells in Development, Health and Disease (ERS Monograph). Sheffield: European Respiratory Society; 2021. p. 84–98.

134. Plopper CG, Suverkropp C, Morin D, Nishio S, Buckpitt A. Relationship of cytochrome P-450 activity to Clara cell cytotoxicity. I. Histopathologic comparison of the respiratory tract of mice, rats and hamsters after parenteral administration of naphthalene. J Pharmacol Exp Ther. 1992;261(1):353-363.
135. Giangreco A, Reynolds SD, Stripp BR. Terminal Bronchioles Harbor a Unique Airway Stem Cell Population That Localizes to the Bronchoalveolar Duct Junction. The American Journal of Pathology. 2002;161(1):173-182.
136. Boyd MR, Statham CN, Longo NS. The pulmonary clara cell as a target for toxic chemicals requiring metabolic activation; studies with carbon tetrachloride. J Pharmacol Exp Ther. 1980;212(1):109-114.
137. Basil MC, Morrisey EE. BASC-ing in the glow: bronchioalveolar stem cells get their place in the lung. Embo j. 2019;38(12).
138. Kim CF, Jackson EL, Woolfenden AE, Lawrence S, Babar I, Vogel S, et al. Identification of bronchioalveolar stem cells in normal lung and lung cancer. Cell. 2005;121(6):823-835.
139. Guha A, Vasconcelos M, Cai Y, Yoneda M, Hinds A, Qian J, et al. Neuroepithelial body microenvironment is a niche for a distinct subset of Clara-like precursors in the developing airways. Proceedings of the National Academy of Sciences. 2012;109(31):12592-12597.
140. Guha A, Deshpande A, Jain A, Sebastiani P, Cardoso WV. Uroplakin 3a(+) Cells Are a Distinctive Population of Epithelial Progenitors that Contribute to Airway Maintenance and Post-injury Repair. Cell Rep. 2017;19(2):246-254.
141. Toth A, Zhao B, Zacharias WJ. Alveolar epithelial stem cells in homeostasis and repair. In: Nikolić M, Hogan BLM, editors. Lung Stem Cells in Development, Health and Disease (ERS Monograph). Sheffield: European Respiratory Society; 2021. p. 122-133.
142. Evans MJ, Johnson LV, Stephens RJ, Freeman G. Cell renewal in the lungs of rats exposed to low levels of ozone. Experimental and Molecular Pathology. 1976;24(1):70-83.
143. Evans MJ, Bils RF. Identification of Cells Labeled with Tritiated Thymidine in the Pulmonary Alveolar Walls of the Mouse. American Review of Respiratory Disease. 1969;100(3):372-378.
144. Evans MJ, Cabral LJ, Stephens RJ, Freeman G. Renewal of alveolar epithelium in the rat following exposure to NO2. Am J Pathol. 1973;70(2):175-198.
145. Kapanci Y, Weibel ER, Kaplan HP, Robinson FR. Pathogenesis and reversibility of the pulmonary lesions of oxygen toxicity in monkeys. II. Ultrastructural and morphometric studies. Lab Invest. 1969;20(1):101-118.
146. Kawada H, Shannon JM, Mason RJ. Improved maintenance of adult rat alveolar type II cell differentiation in vitro: effect of hydrocortisone and cyclic AMP. Biochim Biophys Acta. 1988;972(2):152-166.
147. Mason RJ, Dobbs LG. Synthesis of phosphatidylcholine and phosphatidylglycerol by alveolar type II cells in primary culture. J Biol Chem. 1980;255(11):5101-5107.
148. Chapman HA, Li X, Alexander JP, Brumwell A, Lorizio W, Tan K, et al. Integrin α6β4 identifies an adult distal lung epithelial population with regenerative potential in mice. J Clin Invest. 2011;121(7):2855-2862.
149. Fukada A, Enomoto Y, Horiguchi R, Aoshima Y, Meguro S, Kawasaki H, et al. Integrin α8 is a useful cell surface marker of alveolar lipofibroblasts. Respiratory Research. 2025;26(1):14.

150. Nabhan AN, Brownfield DG, Harbury PB, Krasnow MA, Desai TJ. Single-cell Wnt signaling niches maintain stemness of alveolar type 2 cells. Science. 2018;359(6380):1118-1123.
151. Zepp JA, Zacharias WJ, Frank DB, Cavanaugh CA, Zhou S, Morley MP, et al. Distinct Mesenchymal Lineages and Niches Promote Epithelial Self-Renewal and Myofibrogenesis in the Lung. Cell. 2017;170(6):1134-1148.e1110.
152. Gonzalez RF, Allen L, Dobbs LG. Rat alveolar type I cells proliferate, express OCT-4, and exhibit phenotypic plasticity in vitro. Am J Physiol Lung Cell Mol Physiol. 2009;297(6):L1045-1055.
153. Gurtner GC, Werner S, Barrandon Y, Longaker MT. Wound repair and regeneration. Nature. 2008;453(7193):314-321.
154. Sahebjami H, Vassallo CL. Effects of Starvation and Refeeding on Lung Mechanics and Morphometry. American Review of Respiratory Disease. 1979;119(3):443-451.
155. Massaro D, Massaro GD, Baras A, Hoffman EP, Clerch LB. Calorie-related rapid onset of alveolar loss, regeneration, and changes in mouse lung gene expression. American Journal of Physiology-Lung Cellular and Molecular Physiology. 2004;286(5):L896-L906.
156. Coxson HO, Chan IH, Mayo JR, Hlynsky J, Nakano Y, Birmingham CL. Early emphysema in patients with anorexia nervosa. Am J Respir Crit Care Med. 2004;170(7):748-752.
157. Cook VJ, Coxson HO, Mason AG, Bai TR. Bullae, Bronchiectasis and Nutritional Emphysema in Severe Anorexia Nervosa. Canadian Respiratory Journal. 2001;8(5):873632.
158. Butler JP, Loring SH, Patz S, Tsuda A, Yablonskiy DA, Mentzer SJ. Evidence for Adult Lung Growth in Humans. New England Journal of Medicine. 2012;367(3):244-247.
159. Buhain WJ, Brody JS. Compensatory growth of the lung following pneumonectomy. J Appl Physiol. 1973;35(6):898-902.
160. Thane K, Ingenito EP, Hoffman AM. Lung regeneration and translational implications of the postpneumonectomy model. Transl Res. 2014;163(4):363-376.
161. Danopoulos S, Shiosaki J, Al Alam D. FGF Signaling in Lung Development and Disease: Human Versus Mouse. Frontiers in Genetics. 2019;10.
162. Yang L, Zhou F, Zheng D, Wang D, Li X, Zhao C, et al. FGF/FGFR signaling: From lung development to respiratory diseases. Cytokine & Growth Factor Reviews. 2021;62:94-104.
163. Guzy RD, Stoilov I, Elton TJ, Mecham RP, Ornitz DM. Fibroblast growth factor 2 is required for epithelial recovery, but not for pulmonary fibrosis, in response to bleomycin. Am J Respir Cell Mol Biol. 2015;52(1):116-128.
164. Xie Y, Su N, Yang J, Tan Q, Huang S, Jin M, et al. FGF/FGFR signaling in health and disease. Signal Transduction and Targeted Therapy. 2020;5(1):181.
165. Serra R, Pelton RW, Moses HL. TGFβ1 inhibits branching morphogenesis and N-myc expression in lung bud organ cultures. Development. 1994;120(8):2153-2161.
166. Bragg AD, Moses HL, Serra R. Signaling to the epithelium is not sufficient to mediate all of the effects of transforming growth factor β and bone morphogenetic protein 4 on murine embryonic lung development. Mechanisms of Development. 2001;109(1):13-26.
167. Shi W, Zhao J, Anderson KD, Warburton D. Gremlin negatively modulates BMP-4 induction of embryonic mouse lung branching morphogenesis. American Journal of Physiology-Lung Cellular and Molecular Physiology. 2001;280(5):L1030-L1039.
168. Saito A, Horie M, Nagase T. TGF-β Signaling in Lung Health and Disease. Int J Mol Sci. 2018;19(8).

169. Akhurst RJ, Hata A. Targeting the TGFβ signalling pathway in disease. Nature Reviews Drug Discovery. 2012;11(10):790-811.
170. Thannickal VJ, Horowitz JC. Evolving concepts of apoptosis in idiopathic pulmonary fibrosis. Proc Am Thorac Soc. 2006;3(4):350-356.
171. Carballo GB, Honorato JR, de Lopes GPF, Spohr TCLdSe. A highlight on Sonic hedgehog pathway. Cell Communication and Signaling. 2018;16(1):11.
172. Choudhry Z, Rikani AA, Choudhry AM, Tariq S, Zakaria F, Asghar MW, et al. Sonic hedgehog signalling pathway: a complex network. Ann Neurosci. 2014;21(1):28-31.
173. Briscoe J, Thérond PP. The mechanisms of Hedgehog signalling and its roles in development and disease. Nat Rev Mol Cell Biol. 2013;14(7):416-429.
174. Villavicencio EH, Walterhouse DO, Iannaccone PM. The sonic hedgehog-patched-gli pathway in human development and disease. Am J Hum Genet. 2000;67(5):1047-1054.
175. Porter JA, von Kessler DP, Ekker SC, Young KE, Lee JJ, Moses K, et al. The product of hedgehog autoproteolytic cleavage active in local and long-range signalling. Nature. 1995;374(6520):363-366.
176. Bumcrot DA, Takada R, McMahon AP. Proteolytic processing yields two secreted forms of sonic hedgehog. Mol Cell Biol. 1995;15(4):2294-2303.
177. Hammerschmidt M, Brook A, McMahon AP. The world according to hedgehog. Trends in Genetics. 1997;13(1):14-21.
178. Zeng X, Goetz JA, Suber LM, Scott WJ, Jr., Schreiner CM, Robbins DJ. A freely diffusible form of Sonic hedgehog mediates long-range signalling. Nature. 2001;411(6838):716-720.
179. Burke R, Nellen D, Bellotto M, Hafen E, Senti KA, Dickson BJ, et al. Dispatched, a novel sterol-sensing domain protein dedicated to the release of cholesterol-modified hedgehog from signaling cells. Cell. 1999;99(7):803-815.
180. Fernandes-Silva H, Correia-Pinto J, Moura RS. Canonical Sonic Hedgehog Signaling in Early Lung Development. J Dev Biol. 2017;5(1).
181. Kugler MC, Joyner AL, Loomis CA, Munger JS. Sonic hedgehog signaling in the lung. From development to disease. Am J Respir Cell Mol Biol. 2015;52(1):1-13.
182. Miller LA, Wert SE, Clark JC, Xu Y, Perl AK, Whitsett JA. Role of Sonic hedgehog in patterning of tracheal-bronchial cartilage and the peripheral lung. Dev Dyn. 2004;231(1):57-71.
183. Pepicelli CV, Lewis PM, McMahon AP. Sonic hedgehog regulates branching morphogenesis in the mammalian lung. Current Biology. 1998;8(19):1083-1086.
184. Wang C, Cassandras M, Peng T. The Role of Hedgehog Signaling in Adult Lung Regeneration and Maintenance. Journal of developmental biology. 2019;7(3):14.
185. Kugler MC, Loomis CA, Zhao Z, Cushman JC, Liu L, Munger JS. Sonic Hedgehog Signaling Regulates Myofibroblast Function during Alveolar Septum Formation in Murine Postnatal Lung. Am J Respir Cell Mol Biol. 2017;57(3):280-293.
186. Peng T, Frank DB, Kadzik RS, Morley MP, Rathi KS, Wang T, et al. Hedgehog actively maintains adult lung quiescence and regulates repair and regeneration. Nature. 2015;526(7574):578-582.
187. Liu L, Kugler MC, Loomis CA, Samdani R, Zhao Z, Chen GJ, et al. Hedgehog Signaling in Neonatal and Adult Lung. American Journal of Respiratory Cell and Molecular Biology. 2013;48(6):703-710.
188. Cao H, Chen X, Hou J, Wang C, Xiang Z, Shen Y, et al. The Shh/Gli signaling cascade regulates myofibroblastic activation of lung-resident mesenchymal stem cells via the

modulation of Wnt10a expression during pulmonary fibrogenesis. Laboratory Investigation. 2020;100(3):363-377.
189. Bolaños AL, Milla CM, Lira JC, Ramírez R, Checa M, Barrera L, et al. Role of Sonic Hedgehog in idiopathic pulmonary fibrosis. Am J Physiol Lung Cell Mol Physiol. 2012;303(11):L978-990.
190. Froidure A, Marchal-Duval E, Homps-Legrand M, Ghanem M, Justet A, Crestani B, et al. Chaotic activation of developmental signalling pathways drives idiopathic pulmonary fibrosis. European Respiratory Review. 2020;29(158):190140.
191. Yeung B, Yu J, Yang X. Roles of the Hippo pathway in lung development and tumorigenesis. International Journal of Cancer. 2016;138(3):533-539.
192. Tang W, Li M, Yangzhong X, Zhang X, Zu A, Hou Y, et al. Hippo signaling pathway and respiratory diseases. Cell Death Discovery. 2022;8(1):213.
193. Zhao B, Li L, Lei Q, Guan KL. The Hippo-YAP pathway in organ size control and tumorigenesis: an updated version. Genes Dev. 2010;24(9):862-874.
194. Kizawa R, Araya J, Fujita Y. Divergent roles of the Hippo pathway in the pathogenesis of idiopathic pulmonary fibrosis: tissue homeostasis and fibrosis. Inflammation and Regeneration. 2023;43(1):45.
195. Isago H, Mitani A, Mikami Y, Horie M, Urushiyama H, Hamamoto R, et al. Epithelial Expression of YAP and TAZ Is Sequentially Required in Lung Development. American Journal of Respiratory Cell and Molecular Biology. 2020;62(2):256-266.
196. Noguchi S, Saito A, Nagase T. YAP/TAZ Signaling as a Molecular Link between Fibrosis and Cancer. Int J Mol Sci. 2018;19(11).
197. Fu M, Hu Y, Lan T, Guan K-L, Luo T, Luo M. The Hippo signalling pathway and its implications in human health and diseases. Signal Transduction and Targeted Therapy. 2022;7(1):376.
198. Kiyokawa H, Morimoto M. Notch signaling in the mammalian respiratory system, specifically the trachea and lungs, in development, homeostasis, regeneration, and disease. Dev Growth Differ. 2020;62(1):67-79.
199. Alhashem Z, Feldner-Busztin D, Revell C, Alvarez-Garcillan Portillo M, Camargo-Sosa K, Richardson J, et al. Notch controls the cell cycle to define leader versus follower identities during collective cell migration. Elife. 2022;11.
200. Tsao PN, Matsuoka C, Wei SC, Sato A, Sato S, Hasegawa K, et al. Epithelial Notch signaling regulates lung alveolar morphogenesis and airway epithelial integrity. Proc Natl Acad Sci U S A. 2016;113(29):8242-8247.
201. Zepp JA, Morrisey EE. Cellular crosstalk in the development and regeneration of the respiratory system. Nature Reviews Molecular Cell Biology. 2019;20(9):551-566.
202. Papaioannou AI, Kostikas K, Kollia P, Gourgoulianis KI. Clinical implications for Vascular Endothelial Growth Factor in the lung: friend or foe? Respiratory Research. 2006;7(1):128.
203. Voelkel NF, Vandivier RW, Tuder RM. Vascular endothelial growth factor in the lung. American Journal of Physiology-Lung Cellular and Molecular Physiology. 2006;290(2):L209-L221.
204. Bhatt AJ, Pryhuber GS, Huyck H, Watkins RH, Metlay LA, Maniscalco WM. Disrupted pulmonary vasculature and decreased vascular endothelial growth factor, Flt-1, and TIE-2 in human infants dying with bronchopulmonary dysplasia. Am J Respir Crit Care Med. 2001;164(10 Pt 1):1971-1980.

205. Medford ARL, Millar AB. Vascular endothelial growth factor (VEGF) in acute lung injury (ALI) and acute respiratory distress syndrome (ARDS): paradox or paradigm? Thorax. 2006;61(7):621-626.
206. Jakkula M, Cras TDL, Gebb S, Hirth KP, Tuder RM, Voelkel NF, et al. Inhibition of angiogenesis decreases alveolarization in the developing rat lung. American Journal of Physiology-Lung Cellular and Molecular Physiology. 2000;279(3):L600-L607.
207. Sakurai MK, Lee S, Arsenault DA, Nose V, Wilson JM, Heymach JV, et al. Vascular endothelial growth factor accelerates compensatory lung growth after unilateral pneumonectomy. Am J Physiol Lung Cell Mol Physiol. 2007;292(3):L742-747.
208. Kunig AM, Balasubramaniam V, Markham NE, Morgan D, Montgomery G, Grover TR, et al. Recombinant human VEGF treatment enhances alveolarization after hyperoxic lung injury in neonatal rats. Am J Physiol Lung Cell Mol Physiol. 2005;289(4):L529-535.
209. Yun EJ, Lorizio W, Seedorf G, Abman SH, Vu TH. VEGF and endothelium-derived retinoic acid regulate lung vascular and alveolar development. Am J Physiol Lung Cell Mol Physiol. 2016;310(4):L287-298.
210. Nilsson M, Heymach JV. Vascular Endothelial Growth Factor (VEGF) Pathway. Journal of Thoracic Oncology. 2006;1(8):768-770.
211. Pongracz JE, Stockley RA. Wnt signalling in lung development and diseases. Respir Res. 2006;7(1):15.
212. Königshoff M, Eickelberg O. WNT signaling in lung disease: a failure or a regeneration signal? Am J Respir Cell Mol Biol. 2010;42(1):21-31.
213. Skronska-Wasek W, Gosens R, Königshoff M, Baarsma HA. WNT receptor signalling in lung physiology and pathology. Pharmacol Ther. 2018;187:150-166.
214. Aros CJ, Pantoja CJ, Gomperts BN. Wnt signaling in lung development, regeneration, and disease progression. Commun Biol. 2021;4(1):601.
215. Nusse R. Wnt signaling. Cold Spring Harbor perspectives in biology. 2012;4(5):a011163.
216. Niehrs C. The complex world of WNT receptor signalling. Nature reviews Molecular cell biology. 2012;13(12):767-779.
217. Wiese KE, Nusse R, van Amerongen R. Wnt signalling: conquering complexity. Development. 2018;145(12).
218. Rogers S, Scholpp S, editors. Vertebrate Wnt5a–at the crossroads of cellular signalling. Seminars in Cell & Developmental Biology; 2022: Elsevier.
219. Kim SY, McTeague D, Cheong S-S, Hind M, Dean CH. Deciphering the impacts of modulating the Wnt-planar cell polarity (PCP) pathway on alveolar repair. Frontiers in Cell and Developmental Biology. 2024;Volume 12 - 2024.
220. Li C, Hu L, Xiao J, Chen H, Li JT, Bellusci S, et al. Wnt5a regulates Shh and Fgf10 signaling during lung development. Dev Biol. 2005;287(1):86-97.
221. Davey CF, Moens CB. Planar cell polarity in moving cells: think globally, act locally. Development. 2017;144(2):187-200.
222. Henderson DJ, Long DA, Dean CH. Planar cell polarity in organ formation. Curr Opin Cell Biol. 2018;55:96-103.
223. Li C, Bellusci S, Borok Z, Minoo P. Non-canonical WNT signalling in the lung. J Biochem. 2015;158(5):355-365.
224. Aros CJ, Pantoja CJ, Gomperts BN. Wnt signaling in lung development, regeneration, and disease progression. Communications Biology. 2021;4(1):601.

225. Rhinn M, Dollé P. Retinoic acid signalling during development. Development. 2012;139(5):843-858.
226. McGowan SE. Retinoids and pulmonary alveolar regeneration: Rationale and therapeutic challenges. Drug Discovery Today: Disease Mechanisms. 2006;3(1):77-84.
227. Fernandes-Silva H, Araújo-Silva H, Correia-Pinto J, Moura RS. Retinoic Acid: A Key Regulator of Lung Development. Biomolecules. 2020;10(1).
228. Desai TJ, Malpel S, Flentke GR, Smith SM, Cardoso WV. Retinoic acid selectively regulates Fgf10 expression and maintains cell identity in the prospective lung field of the developing foregut. Dev Biol. 2004;273(2):402-415.
229. Wolbach SB, Howe PR. EPITHELIAL REPAIR IN RECOVERY FROM VITAMIN A DEFICIENCY : AN EXPERIMENTAL STUDY. J Exp Med. 1933;57(3):511-526.
230. Desai TJ, Chen F, Lü J, Qian J, Niederreither K, Dollé P, et al. Distinct roles for retinoic acid receptors alpha and beta in early lung morphogenesis. Dev Biol. 2006;291(1):12-24.
231. Hustead VA, Gutcher GR, Anderson SA, Zachman RD. Relationship of vitamin A (retinol) status to lung disease in the preterm infant. J Pediatr. 1984;105(4):610-615.
232. Verma RP, McCulloch KM, Worrell L, Vidyasagar D. Vitamin A deficiency and severe bronchopulmonary dysplasia in very low birthweight infants. Am J Perinatol. 1996;13(7):389-393.
233. Checkley W, West KP, Jr., Wise RA, Baldwin MR, Wu L, LeClerq SC, et al. Maternal vitamin A supplementation and lung function in offspring. N Engl J Med. 2010;362(19):1784-1794.
234. Massaro GD, Massaro D. Retinoic acid treatment abrogates elastase-induced pulmonary emphysema in rats. Nat Med. 1997;3(6):675-677.
235. Cunningham TJ, Duester G. Mechanisms of retinoic acid signalling and its roles in organ and limb development. Nature Reviews Molecular Cell Biology. 2015;16(2):110-123.
236. Nizamoglu M, Joglekar MM, Almeida CR, Larsson Callerfelt AK, Dupin I, Guenat OT, et al. Innovative three-dimensional models for understanding mechanisms underlying lung diseases: powerful tools for translational research. Eur Respir Rev. 2023;32(169).
237. Miller AJ, Spence JR. In Vitro Models to Study Human Lung Development, Disease and Homeostasis. Physiology (Bethesda). 2017;32(3):246-260.
238. Dean CH, Cheong S-S. Simple Models of Lung Development. In: Magin CM, editor. Engineering Translational Models of Lung Homeostasis and Disease. Cham: Springer International Publishing; 2023. p. 17-28.
239. da Silva ACG, Valadares MC. The Application of New Approach Methodologies in Respiratory Disease Research: Their Role in Improving Translational Medicine from Bench to Bedside. Alternatives to Laboratory Animals. 2023;51(3):161-174.
240. Lam T, Quach HT, Hall L, Abou Chakra M, Wong AP. A multidisciplinary approach towards modeling of a virtual human lung. npj Systems Biology and Applications. 2025;11(1):38.
241. Vis MAM, Ito K, Hofmann S. Impact of Culture Medium on Cellular Interactions in in vitro Co-culture Systems. Frontiers in Bioengineering and Biotechnology. 2020;Volume 8 - 2020.
242. Bogdanowicz DR, Lu HH. Multifunction co-culture model for evaluating cell-cell interactions. Methods Mol Biol. 2014;1202:29-36.
243. Boyden S. The chemotactic effect of mixtures of antibody and antigen on polymorphonuclear leucocytes. J Exp Med. 1962;115(3):453-466.

244. Justus CR, Leffler N, Ruiz-Echevarria M, Yang LV. In vitro cell migration and invasion assays. J Vis Exp. 2014(88).
245. Ashby WJ, Zijlstra A. Established and novel methods of interrogating two-dimensional cell migration. Integr Biol (Camb). 2012;4(11):1338-1350.
246. Ibidi. ibidi Application Guide: Wound Healing and
Migration Assays. 1 ed. GmbH i, editor. Germany2019. 1-10 p.
247. Dichtl S, Posch* W, Wilflingseder D. The breathtaking world of human respiratory in vitro models: Investigating lung diseases and infections in 3D models, organoids, and lung-on-chip. European Journal of Immunology. 2024;54(3):2250356.
248. Francis I, Shrestha J, Paudel KR, Hansbro PM, Warkiani ME, Saha SC. Recent advances in lung-on-a-chip models. Drug Discovery Today. 2022;27(9):2593-2602.
249. Whitcutt MJ, Adler KB, Wu R. A biphasic chamber system for maintaining polarity of differentiation of cultured respiratory tract epithelial cells. In Vitro Cell Dev Biol. 1988;24(5):420-428.
250. Tan Q, Choi KM, Sicard D, Tschumperlin DJ. Human airway organoid engineering as a step toward lung regeneration and disease modeling. Biomaterials. 2017;113:118-132.
251. Nadkarni RR, Abed S, Draper JS. Organoids as a model system for studying human lung development and disease. Biochemical and Biophysical Research Communications. 2016;473(3):675-682.
252. Barkauskas CE, Chung MI, Fioret B, Gao X, Katsura H, Hogan BL. Lung organoids: current uses and future promise. Development. 2017;144(6):986-997.
253. McGowan SE. Extracellular matrix and the regulation of lung development and repair. Faseb j. 1992;6(11):2895-2904.
254. Wilkinson DC, Alva-Ornelas JA, Sucre JM, Vijayaraj P, Durra A, Richardson W, et al. Development of a Three-Dimensional Bioengineering Technology to Generate Lung Tissue for Personalized Disease Modeling. Stem Cells Transl Med. 2017;6(2):622-633.
255. Bonnans C, Chou J, Werb Z. Remodelling the extracellular matrix in development and disease. Nat Rev Mol Cell Biol. 2014;15(12):786-801.
256. Andrade CF, Wong AP, Waddell TK, Keshavjee S, Liu M. Cell-based tissue engineering for lung regeneration. Am J Physiol Lung Cell Mol Physiol. 2007;292(2):L510-518.
257. Prakash YS, Tschumperlin DJ, Stenmark KR. Coming to terms with tissue engineering and regenerative medicine in the lung. Am J Physiol Lung Cell Mol Physiol. 2015;309(7):L625-638.
258. Gilpin SE, Ott HC. Using nature's platform to engineer bio-artificial lungs. Ann Am Thorac Soc. 2015;12 Suppl 1:S45-49.
259. Gilpin SE, Charest JM, Ren X, Ott HC. Bioengineering Lungs for Transplantation. Thorac Surg Clin. 2016;26(2):163-171.
260. Shrestha J, Razavi Bazaz S, Aboulkheyr Es H, Yaghobian Azari D, Thierry B, Ebrahimi Warkiani M, et al. Lung-on-a-chip: the future of respiratory disease models and pharmacological studies. Critical Reviews in Biotechnology. 2020;40(2):213-230.
261. Huh D, Matthews BD, Mammoto A, Montoya-Zavala M, Hsin HY, Ingber DE. Reconstituting Organ-Level Lung Functions on a Chip. Science. 2010;328(5986):1662-1668.
262. Gkatzis K, Taghizadeh S, Huh D, Stainier DYR, Bellusci S. Use of three-dimensional organoids and lung-on-a-chip methods to study lung development, regeneration and disease. European Respiratory Journal. 2018;52(5):1800876.

263. Bonniaud P, Fabre A, Frossard N, Guignabert C, Inman M, Kuebler WM, et al. Optimising experimental research in respiratory diseases: an ERS statement. European Respiratory Journal. 2018;51(5):1702133.
264. García-García MJ. A History of Mouse Genetics: From Fancy Mice to Mutations in Every Gene. In: Liu A, editor. Animal Models of Human Birth Defects. Singapore: Springer Singapore; 2020. p. 1-38.
265. Skarnes WC, Rosen B, West AP, Koutsourakis M, Bushell W, Iyer V, et al. A conditional knockout resource for the genome-wide study of mouse gene function. Nature. 2011;474(7351):337-342.
266. Russell WMS, Burch RL, Hume CW. The principles of humane experimental technique: Methuen London; 1959.
267. Directive E. 63/EU of the European Parliament and of the Council of 22 September 2010 on the protection of animals used for scientific purposes. Off J Eur Union. 2010;276:33-79.
268. Behrsing HP, Amin K, Allen D, Hughes J, Obermok M, Patel V. The Development of an Animal Product-free, Precision-cut Lung Slice Cryopreservation and Post-thaw Culture Method. Alternatives to Laboratory Animals. 2025;53(3):138-153.
269. Liu G, Betts C, Cunoosamy DM, Åberg PM, Hornberg JJ, Sivars KB, et al. Use of precision cut lung slices as a translational model for the study of lung biology. Respiratory Research. 2019;20(1):162.
270. Sanderson MJ. Exploring lung physiology in health and disease with lung slices. Pulmonary Pharmacology & Therapeutics. 2011;24(5):452-465.
271. Kim SY, Mongey R, Wang P, Rothery S, Gaboriau DCA, Hind M, et al. The acid injury and repair (AIR) model: A novel ex-vivo tool to understand lung repair. Biomaterials. 2021;267:120480.
272. Koziol-White C, Gebski E, Cao G, Panettieri RA. Precision cut lung slices: an integrated ex vivo model for studying lung physiology, pharmacology, disease pathogenesis and drug discovery. Respiratory Research. 2024;25(1):231.
273. Dean C, Königshoff M. Three-dimensional tissue-based models for translational lung stem cell research: precision-cut lung slices. In: Nikolić MZ, Hogan BLM, editors. Lung Stem Cells in Development, Health and Disease (ERS Monograph). Sheffield: European Respiratory Society; 2021. p. 222-231.
274. Dandurand RJ, Wang CG, Phillips NC, Eidelman DH. Responsiveness of individual airways to methacholine in adult rat lung explants. J Appl Physiol (1985). 1993;75(1):364-372.
275. Alsafadi HN, Uhl FE, Pineda RH, Bailey KE, Rojas M, Wagner DE, et al. Applications and Approaches for Three-Dimensional Precision-Cut Lung Slices. Disease Modeling and Drug Discovery. Am J Respir Cell Mol Biol. 2020;62(6):681-691.
276. Kim SY, Mongey R, Griffiths M, Hind M, Dean CH. An Ex Vivo Acid Injury and Repair (AIR) Model Using Precision-Cut Lung Slices to Understand Lung Injury and Repair. Curr Protoc Mouse Biol. 2020;10(4):e85.
277. Bankole E, Wong CW, Kim S, Hind M, Dean CH. A human PCLS model of lung injury and repair for discovery and pharmaceutical research. Respiratory Research. 2025;26(1):237.
278. Lehmann M, Krishnan R, Sucre J, Kulkarni HS, Pineda RH, Anderson C, et al. Precision-Cut Lung Slices: Emerging Tools for Preclinical and Translational Lung Research: An Official

American Thoracic Society Workshop Report. American Journal of Respiratory Cell and Molecular Biology. 2025;72(1):16-31.
279. Tigges J, Eggerbauer F, Worek F, Thiermann H, Rauen U, Wille T. Optimization of long-term cold storage of rat precision-cut lung slices with a tissue preservation solution. American Journal of Physiology-Lung Cellular and Molecular Physiology. 2021;321(6):L1023-L1035.
280. Patel VS, Amin K, Wahab A, Marimoutou M, Ukishima L, Alvarez J, et al. Cryopreserved human precision-cut lung slices provide an immune competent pulmonary test system for “on-demand” use and long-term cultures. Toxicological Sciences. 2023;191(2):253-265.
281. Soto Veliz D, Lin K-L, Sahlgren C. Organ-on-a-chip technologies for biomedical research and drug development: A focus on the vasculature. Smart Medicine. 2023;2(1):e20220030.
282. Mosmann T. Rapid colorimetric assay for cellular growth and survival: application to proliferation and cytotoxicity assays. J Immunol Methods. 1983;65(1-2):55-63.
283. Riss TL, Moravec RA, Niles AL, Duellman S, Benink HA, Worzella TJ, et al. Cell Viability Assays. In: Markossian S, Grossman A, Brimacombe K, Arkin M, Auld D, Austin CP, et al., editors. Assay Guidance Manual. Bethesda (MD)2004.
284. Lichtenfels R, Biddison WE, Schulz H, Vogt AB, Martin R. CARE-LASS (calcein-release-assay), an improved fluorescence-based test system to measure cytotoxic T lymphocyte activity. Journal of Immunological Methods. 1994;172(2):227-239.
285. Liminga G, Jonsson B, Nygren P, Larsson R. On the mechanism underlying calcein-induced cytotoxicity. European Journal of Pharmacology. 1999;383(3):321-329.
286. Uggeri J, Gatti R, Belletti S, Scandroglio R, Corradini R, Rotoli BM, et al. Calcein-AM is a detector of intracellular oxidative activity. Histochemistry and Cell Biology. 2000;122(5):499-505.
287. Gaugain B, Barbet J, Capelle N, Roques BP, Le Pecq JB, Le Bret M. DNA bifunctional intercalators. 2. Fluorescence properties and DNA binding interaction of an ethidium homodimer and an acridine ethidium heterodimer. Appendix: Numerical solution of McGhee and von Hippel equations for competing ligands. Biochemistry. 1978;17(24):5078-5088.
288. Cregan SP. Detection of Cell Death in Neuronal Cultures. In: Doering LC, editor. Protocols for Neural Cell Culture: Fourth Edition. Totowa, NJ: Humana Press; 2010. p. 343-351.
289. Legesse FB, Chernavskaia O, Heuke S, Bocklitz T, Meyer T, Popp J, et al. Seamless stitching of tile scan microscope images. J Microsc. 2015;258(3):223-232.
290. Giard DJ, Aaronson SA, Todaro GJ, Arnstein P, Kersey JH, Dosik H, et al. In Vitro Cultivation of Human Tumors: Establishment of Cell Lines Derived From a Series of Solid Tumors2. JNCI: Journal of the National Cancer Institute. 1973;51(5):1417-1423.
291. Lieber M, Todaro G, Smith B, Szakal A, Nelson-Rees W. A continuous tumor-cell line from a human lung carcinoma with properties of type II alveolar epithelial cells. International Journal of Cancer. 1976;17(1):62-70.
292. Nichols WW, Buynak EB, Bradt C, Hill R, Aronson M, Jarrell BE, et al. Cytogenetic evaluation of human endothelial cell cultures. J Cell Physiol. 1987;132(3):453-462.
293. Krump-Konvalinkova V, Bittinger F, Unger RE, Peters K, Lehr HA, Kirkpatrick CJ. Generation of human pulmonary microvascular endothelial cell lines. Lab Invest. 2001;81(12):1717-1727.

294. Witherden IR, Tetley TD. Isolation and Culture of Human Alveolar Type II Pneumocytes. In: Rogers DF, Donnelly LE, editors. Human Airway Inflammation: Sampling Techniques and Analytical Protocols. Totowa, NJ: Humana Press; 2001. p. 137-146.
295. Desjardins PR, Conklin DS. Microvolume quantitation of nucleic acids. Curr Protoc Mol Biol. 2011;Appendix 3:3j.
296. Cole K, Levine BS. Ultraviolet-Visible Spectrophotometry. In: Levine BS, Kerrigan S, editors. Principles of Forensic Toxicology. Cham: Springer International Publishing; 2020. p. 127-134.
297. Wilfinger WW, Mackey K, Chomczynski P. Effect of pH and ionic strength on the spectrophotometric assessment of nucleic acid purity. Biotechniques. 1997;22(3):474-476, 478-481.
298. Desjardins P, Conklin D. NanoDrop microvolume quantitation of nucleic acids. J Vis Exp. 2010(45).
299. Walker JE, Oliver JC, Stewart AM, Beh ST, Arce RA, Glass MJ, et al. Measuring Up: A Comparison of TapeStation 4200 and Bioanalyzer 2100 as Measurement Tools for RNA Quality in Postmortem Human Brain Samples. Int J Mol Sci. 2023;24(18).
300. Schroeder A, Mueller O, Stocker S, Salowsky R, Leiber M, Gassmann M, et al. The RIN: an RNA integrity number for assigning integrity values to RNA measurements. BMC Molecular Biology. 2006;7(1):3.
301. Zhan C, Zhang Y, Ma J, Wang L, Jiang W, Shi Y, et al. Identification of reference genes for qRT-PCR in human lung squamous-cell carcinoma by RNA-Seq. Acta Biochimica et Biophysica Sinica. 2014;46(4):330-337.
302. Yin R, Tian F, Frankenberger B, de Angelis MH, Stoeger T. Selection and evaluation of stable housekeeping genes for gene expression normalization in carbon nanoparticle-induced acute pulmonary inflammation in mice. Biochemical and Biophysical Research Communications. 2010;399(4):531-536.
303. Liu DW, Chen ST, Liu HP. Choice of endogenous control for gene expression in nonsmall cell lung cancer. European Respiratory Journal.26(6):1002-1008.
304. Sauler M, McDonough JE, Adams TS, Kothapalli N, Barnthaler T, Werder RB, et al. Characterization of the COPD alveolar niche using single-cell RNA sequencing. Nature Communications. 2022;13(1):494.
305. Raredon MSB, Adams TS, Suhail Y, Schupp JC, Poli S, Neumark N, et al. Single-cell connectomic analysis of adult mammalian lungs. Sci Adv. 2019;5(12):eaaw3851.
306. Wansleeben C, Barkauskas CE, Rock JR, Hogan BLM. Stem cells of the adult lung: their development and role in homeostasis, regeneration, and disease. WIREs Developmental Biology. 2013;2(1):131-148.
307. Kim J, Koo BK, Knoblich JA. Human organoids: model systems for human biology and medicine. Nat Rev Mol Cell Biol. 2020;21(10):571-584.
308. Hiemstra PS, Tetley TD, Janes SM. Airway and alveolar epithelial cells in culture. European Respiratory Journal. 2019;54(5):1900742.
309. Rutting S, Chapman DG, Farah CS, Thamrin C. Lung heterogeneity as a predictor for disease severity and response to therapy. Current Opinion in Physiology. 2021;22:100446.
310. Wolpert L, Tickle, C., Martinez Arias, A., Lawrence, P.A., Locke, J. Principles of development. Sixth edition. ed. Oxford, United Kingdom ; New York, NY: Oxford University Press; 2019. xxiv, 741 pages p.

311. Barresi MJF, Gilbert SF. Developmental biology. Thirteenth edition. ed. New York, NY: Oxford University Press; 2024. 1 volume (unpaged) p.
312. Page MJ, McKenzie JE, Bossuyt PM, Boutron I, Hoffmann TC, Mulrow CD, et al. The PRISMA 2020 statement: an updated guideline for reporting systematic reviews. Syst Rev. 2021;10(1):89.
313. Chen X, Jin Y, Hou X, Liu F, Wang Y. Sonic Hedgehog Signaling: Evidence for Its Protective Role in Endotoxin Induced Acute Lung Injury in Mouse Model. PLOS ONE. 2015;10(11):e0140886.
314. Hu B, Liu J, Wu Z, Liu T, Ullenbruch MR, Ding L, et al. Reemergence of hedgehog mediates epithelial-mesenchymal crosstalk in pulmonary fibrosis. American journal of respiratory cell and molecular biology. 2015;52(4):418-428.
315. Zhang M, Wang H, Teng H, Shi J, Zhang Y. Expression of SHH signaling pathway components in the developing human lung. Histochemistry and Cell Biology. 2010;134(4):327-335.
316. Belgacemi R, Luczka E, Ancel J, Diabasana Z, Perotin JM, Germain A, et al. Airway epithelial cell differentiation relies on deficient Hedgehog signalling in COPD. EBioMedicine. 2020;51:102572.
317. Tam A, Hughes M, McNagny KM, Obeidat M, Hackett TL, Leung JM, et al. Hedgehog signaling in the airway epithelium of patients with chronic obstructive pulmonary disease. Scientific Reports. 2019;9(1):3353.
318. Belgacemi R, Danopoulos S, Deutsch G, Glass I, Dormoy V, Bellusci S, et al. Hedgehog Signaling Pathway Orchestrates Human Lung Branching Morphogenesis. Int J Mol Sci. 2022;23(9).
319. Maden M, Hind M. Retinoic acid, a regeneration-inducing molecule. Developmental Dynamics. 2003;226(2):237-244.
320. Maden M, Hind M. Retinoic acid in alveolar development, maintenance and regeneration. Philos Trans R Soc Lond B Biol Sci. 2004;359(1445):799-808.
321. Malpel S, Mendelsohn C, Cardoso WV. Regulation of retinoic acid signaling during lung morphogenesis. Development. 2000;127(14):3057-3067.
322. Massaro GD, Massaro D. Retinoic acid treatment partially rescues failed septation in rats and in mice. Am J Physiol Lung Cell Mol Physiol. 2000;278(5):L955-960.
323. Ng-Blichfeldt JP, Alçada J, Montero MA, Dean CH, Griesenbach U, Griffiths MJ, et al. Deficient retinoid-driven angiogenesis may contribute to failure of adult human lung regeneration in emphysema. Thorax. 2017;72(6):510-521.
324. Schuger L, Varani J, Mitra R, Jr., Gilbride K. Retinoic acid stimulates mouse lung development by a mechanism involving epithelial-mesenchymal interaction and regulation of epidermal growth factor receptors. Dev Biol. 1993;159(2):462-473.
325. Belloni PN, Garvin L, Mao CP, Bailey-Healy I, Leaffer D. Effects of all-trans-retinoic acid in promoting alveolar repair. Chest. 2000;117(5 Suppl 1):235s-241s.
326. Kaza AK, Kron IL, Kern JA, Long SM, Fiser SM, Nguyen RP, et al. Retinoic acid enhances lung growth after pneumonectomy. Ann Thorac Surg. 2001;71(5):1645-1650.
327. Zhang Y, Goss AM, Cohen ED, Kadzik R, Lepore JJ, Muthukumaraswamy K, et al. A Gata6-Wnt pathway required for epithelial stem cell development and airway regeneration. Nat Genet. 2008;40(7):862-870.

328. Witze ES, Litman ES, Argast GM, Moon RT, Ahn NG. Wnt5a Control of Cell Polarity and Directional Movement by Polarized Redistribution of Adhesion Receptors. Science. 2008;320(5874):365-369.
329. Hu Y, Ciminieri C, Hu Q, Lehmann M, Königshoff M, Gosens R. WNT Signalling in Lung Physiology and Pathology. Handb Exp Pharmacol. 2021;269:305-336.
330. Poobalasingam T, Yates LL, Walker SA, Pereira M, Gross NY, Ali A, et al. Heterozygous Vangl2(Looptail) mice reveal novel roles for the planar cell polarity pathway in adult lung homeostasis and repair. Dis Model Mech. 2017;10(4):409-423.
331. Cheong SS, Akram KM, Matellan C, Kim SY, Gaboriau DCA, Hind M, et al. The Planar Polarity Component VANGL2 Is a Key Regulator of Mechanosignaling. Front Cell Dev Biol. 2020;8:577201.
332. Hussain M, Xu C, Lu M, Wu X, Tang L, Wu X. Wnt/β-catenin signaling links embryonic lung development and asthmatic airway remodeling. Biochim Biophys Acta Mol Basis Dis. 2017;1863(12):3226-3242.
333. Portas L, Pereira M, Shaheen SO, Wyss AB, London SJ, Burney PGJ, et al. Lung Development Genes and Adult Lung Function. Am J Respir Crit Care Med. 2020;202(6):853-865.
334. Jenei V, Sherwood V, Howlin J, Linnskog R, Säfholm A, Axelsson L, et al. A t-butyloxycarbonyl-modified Wnt5a-derived hexapeptide functions as a potent antagonist of Wnt5a-dependent melanoma cell invasion. Proc Natl Acad Sci U S A. 2009;106(46):19473-19478.
335. Curis E, Nepost C, Grillault Laroche D, Courtin C, Laplanche J-L, Etain B, et al. Selecting reference genes in RT-qPCR based on equivalence tests: a network based approach. Scientific Reports. 2019;9(1):16231.
336. Bustin SA, Benes V, Garson JA, Hellemans J, Huggett J, Kubista M, et al. The MIQE guidelines: minimum information for publication of quantitative real-time PCR experiments. Clin Chem. 2009;55(4):611-622.
337. Yuan JS, Reed A, Chen F, Stewart CN, Jr. Statistical analysis of real-time PCR data. BMC Bioinformatics. 2006;7:85.
338. Mane VP, Heuer MA, Hillyer P, Navarro MB, Rabin RL. Systematic method for determining an ideal housekeeping gene for real-time PCR analysis. J Biomol Tech. 2008;19(5):342-347.
339. Livak KJ, Schmittgen TD. Analysis of relative gene expression data using real-time quantitative PCR and the 2(-Delta Delta C(T)) Method. Methods. 2001;25(4):402-408.
340. Duester G. Retinoic acid synthesis and signaling during early organogenesis. Cell. 2008;134(6):921-931.
341. West RM. Best practice in statistics: The use of log transformation. Ann Clin Biochem. 2022;59(3):162-165.
342. Curran-Everett D. Explorations in statistics: the log transformation. Advances in Physiology Education. 2018;42(2):343-347.
343. Warburton D, Perin L, Defilippo R, Bellusci S, Shi W, Driscoll B. Stem/progenitor cells in lung development, injury repair, and regeneration. Proc Am Thorac Soc. 2008;5(6):703-706.
344. Franz CM, Jones GE, Ridley AJ. Cell migration in development and disease. Dev Cell. 2002;2(2):153-158.

345. Todaro GJ, Lazar GK, Green H. The initiation of cell division in a contact-inhibited mammalian cell line. J Cell Physiol. 1965;66(3):325-333.
346. Rodriguez LG, Wu X, Guan J-L. Wound-Healing Assay. In: Guan J-L, editor. Cell Migration: Developmental Methods and Protocols. Totowa, NJ: Humana Press; 2005. p. 23-29.
347. Cooper JR, Abdullatif MB, Burnett EC, Kempsell KE, Conforti F, Tolley H, et al. Long Term Culture of the A549 Cancer Cell Line Promotes Multilamellar Body Formation and Differentiation towards an Alveolar Type II Pneumocyte Phenotype. PLoS One. 2016;11(10):e0164438.
348. Chary A, Groff K, Stucki AO, Contal S, Stoffels C, Cambier S, et al. Maximizing the relevance and reproducibility of A549 cell culture using FBS-free media. Toxicology in Vitro. 2022;83:105423.
349. Moura RS, Carvalho-Correia E, daMota P, Correia-Pinto J. Canonical Wnt Signaling Activity in Early Stages of Chick Lung Development. PLOS ONE. 2014;9(12):e112388.
350. Chen J, Tang J, Nie M, Li Y, Wurfel MM, Meyer NJ, et al. WNT9A Affects Late-Onset Acute Respiratory Distress Syndrome and 28-Day Survival: Evidence from a Three-Step Multiomics Study. American Journal of Respiratory Cell and Molecular Biology. 2023;69(2):220-229.
351. Incardona JP, Gaffield W, Kapur RP, Roelink H. The teratogenic Veratrum alkaloid cyclopamine inhibits sonic hedgehog signal transduction. Development. 1998;125(18):3553-3562.
352. Nakamura T, Aikawa T, Iwamoto-Enomoto M, Iwamoto M, Higuchi Y, Pacifici M, et al. Induction of osteogenic differentiation by hedgehog proteins. Biochem Biophys Res Commun. 1997;237(2):465-469.
353. Bellusci S, Furuta Y, Rush MG, Henderson R, Winnier G, Hogan BLM. Involvement of Sonic hedgehog (Shh) in mouse embryonic lung growth and morphogenesis. Development. 1997;124(1):53-63.
354. Ostrowska-Podhorodecka Z, Ding I, Norouzi M, McCulloch CA. Impact of Vimentin on Regulation of Cell Signaling and Matrix Remodeling. Frontiers in Cell and Developmental Biology. 2022;10.
355. Chao CM, Moiseenko A, Zimmer KP, Bellusci S. Alveologenesis: key cellular players and fibroblast growth factor 10 signaling. Mol Cell Pediatr. 2016;3(1):17.
356. Gauthier V, Kyriazi M, Nefla M, Pucino V, Raza K, Buckley CD, et al. Fibroblast heterogeneity: Keystone of tissue homeostasis and pathology in inflammation and ageing. Frontiers in Immunology. 2023;14.
357. Plikus MV, Wang X, Sinha S, Forte E, Thompson SM, Herzog EL, et al. Fibroblasts: Origins, definitions, and functions in health and disease. Cell. 2021;184(15):3852-3872.
358. Cigna N, Farrokhi Moshai E, Brayer S, Marchal-Somme J, Wémeau-Stervinou L, Fabre A, et al. The Hedgehog System Machinery Controls Transforming Growth Factor-β-Dependent Myofibroblastic Differentiation in Humans: Involvement in Idiopathic Pulmonary Fibrosis. The American Journal of Pathology. 2012;181(6):2126-2137.
359. Tai Y, Woods EL, Dally J, Kong D, Steadman R, Moseley R, et al. Myofibroblasts: Function, Formation, and Scope of Molecular Therapies for Skin Fibrosis. Biomolecules. 2021;11(8).

360. Ho H-YH, Susman MW, Bikoff JB, Ryu YK, Jonas AM, Hu L, et al. Wnt5a–Ror–Dishevelled signaling constitutes a core developmental pathway that controls tissue morphogenesis. Proceedings of the National Academy of Sciences. 2012;109(11):4044-4051.
361. Kumawat K, Gosens R. WNT-5A: signaling and functions in health and disease. Cell Mol Life Sci. 2016;73(3):567-587.
362. Yang D-H, Yoon J-Y, Lee S-H, Bryja V, Andersson ER, Arenas E, et al. Wnt5a Is Required for Endothelial Differentiation of Embryonic Stem Cells and Vascularization via Pathways Involving Both Wnt/β-Catenin and Protein Kinase Cα. Circulation Research. 2009;104(3):372-379.
363. Cornett B, Snowball J, Varisco BM, Lang R, Whitsett J, Sinner D. Wntless is required for peripheral lung differentiation and pulmonary vascular development. Dev Biol. 2013;379(1):38-52.
364. Chalak M, Hesaraki M, Mirbahari SN, Yeganeh M, Abdi S, Rajabi S, et al. Cell Immortality: In Vitro Effective Techniques to Achieve and Investigate Its Applications and Challenges. Life (Basel). 2024;14(3).
365. Tsikis ST, Hirsch TI, Fligor SC, Quigley M, Puder M. Targeting the lung endothelial niche to promote angiogenesis and regeneration: A review of applications. Front Mol Biosci. 2022;9:1093369.
366. Iismaa SE, Kaidonis X, Nicks AM, Bogush N, Kikuchi K, Naqvi N, et al. Comparative regenerative mechanisms across different mammalian tissues. npj Regenerative Medicine. 2018;3(1):6.
367. Serdar CC, Cihan M, Yücel D, Serdar MA. Sample size, power and effect size revisited: simplified and practical approaches in pre-clinical, clinical and laboratory studies. Biochem Med (Zagreb). 2021;31(1):010502.
368. Mutsaers SE, Bishop JE, McGrouther G, Laurent GJ. Mechanisms of tissue repair: from wound healing to fibrosis. Int J Biochem Cell Biol. 1997;29(1):5-17.
369. Moshai EF, Wémeau-Stervinou L, Cigna N, Brayer S, Sommé JM, Crestani B, et al. Targeting the Hedgehog–Glioma-Associated Oncogene Homolog Pathway Inhibits Bleomycin-Induced Lung Fibrosis in Mice. American Journal of Respiratory Cell and Molecular Biology. 2014;51(1):11-25.
370. Lyu H, Warren R, Gao S, Klinkhammer K, Yuan T, Zhang JS, et al. Niche-mediated repair of airways is directed in an occupant-dependent manner. Cell Rep. 2022;41(12):111863.
371. Miller L-AD, Wert SE, Whitsett JA. Immunolocalization of Sonic Hedgehog (Shh) in Developing Mouse Lung. Journal of Histochemistry & Cytochemistry. 2001;49(12):1593-1603.
372. McCulley D, Wienhold M, Sun X. The pulmonary mesenchyme directs lung development. Current Opinion in Genetics & Development. 2015;32:98-105.
373. Volckaert T, De Langhe SP. Wnt and FGF mediated epithelial-mesenchymal crosstalk during lung development. Dev Dyn. 2015;244(3):342-366.
374. Lebeche D, Malpel S, Cardoso WV. Fibroblast growth factor interactions in the developing lung. Mechanisms of Development. 1999;86(1):125-136.
375. Theveneau E, Mayor R. Collective cell migration of epithelial and mesenchymal cells. Cell Mol Life Sci. 2013;70(19):3481-3492.
376. Tschumperlin DJ. Fibroblasts and the ground they walk on. Physiology (Bethesda). 2013;28(6):380-390.

377. Menz A, Gorbokon N, Viehweger F, Lennartz M, Hube-Magg C, Hornsteiner L, et al. Pan-keratin Immunostaining in Human Tumors: A Tissue Microarray Study of 15,940 Tumors. Int J Surg Pathol. 2023;31(6):927-938.
378. Yuan K, Shamskhou EA, Orcholski ME, Nathan A, Reddy S, Honda H, et al. Loss of Endothelium-Derived Wnt5a Is Associated With Reduced Pericyte Recruitment and Small Vessel Loss in Pulmonary Arterial Hypertension. Circulation. 2019;139(14):1710-1724.
379. Kumar S, West DC, Ager A. Heterogeneity in endothelial cells from large vessels and microvessels. Differentiation. 1987;36(1):57-70.
380. Turner RR, Beckstead JH, Warnke RA, Wood GS. Endothelial cell phenotypic diversity. In situ demonstration of immunologic and enzymatic heterogeneity that correlates with specific morphologic subtypes. Am J Clin Pathol. 1987;87(5):569-575.
381. Aird WC. Phenotypic heterogeneity of the endothelium: I. Structure, function, and mechanisms. Circ Res. 2007;100(2):158-173.
382. Aird WC. Phenotypic Heterogeneity of the Endothelium II: Representative Vascular Beds. Circulation Research. 2007;100(2):174-190.
383. Wang D, Chen Z, Wai Kan Yeung A, Atanasov AG. Differences between common endothelial cell models (primary human aortic endothelial cells and EA.hy926 cells) revealed through transcriptomics, bioinformatics, and functional analysis. Current Research in Biotechnology. 2021;3:135-145.
384. Liao H, He H, Chen Y, Zeng F, Huang J, Wu L, et al. Effects of long-term serial cell passaging on cell spreading, migration, and cell-surface ultrastructures of cultured vascular endothelial cells. Cytotechnology. 2014;66(2):229-238.
385. Salybekov AA, Salybekova AK, Pola R, Asahara T. Sonic Hedgehog Signaling Pathway in Endothelial Progenitor Cell Biology for Vascular Medicine. Int J Mol Sci. 2018;19(10).
386. Kusano KF, Pola R, Murayama T, Curry C, Kawamoto A, Iwakura A, et al. Sonic hedgehog myocardial gene therapy: tissue repair through transient reconstitution of embryonic signaling. Nature Medicine. 2005;11(11):1197-1204.
387. Pola R, Ling LE, Silver M, Corbley MJ, Kearney M, Blake Pepinsky R, et al. The morphogen Sonic hedgehog is an indirect angiogenic agent upregulating two families of angiogenic growth factors. Nature Medicine. 2001;7(6):706-711.
388. Renault MA, Roncalli J, Tongers J, Thorne T, Klyachko E, Misener S, et al. Sonic hedgehog induces angiogenesis via Rho kinase-dependent signaling in endothelial cells. J Mol Cell Cardiol. 2010;49(3):490-498.
389. Chinchilla P, Xiao L, Kazanietz MG, Riobo NA. Hedgehog proteins activate pro-angiogenic responses in endothelial cells through non-canonical signaling pathways. Cell Cycle. 2010;9(3):570-579.
390. Alvarez JI, Dodelet-Devillers A, Kebir H, Ifergan I, Fabre PJ, Terouz S, et al. The Hedgehog pathway promotes blood-brain barrier integrity and CNS immune quiescence. Science. 2011;334(6063):1727-1731.
391. Yoshikura H, Hirokawa Y. Endogenous C-type virus of a mouse cell line and its defectiveness. J Virol. 1974;13(6):1319-1325.
392. Li X, Bi Z, Liu S, Gao S, Cui Y, Huang K, et al. Antifibrotic Mechanism of Cinobufagin in Bleomycin-Induced Pulmonary Fibrosis in Mice. Frontiers in Pharmacology. 2019;Volume 10 - 2019.

393. Bermudez O, Hennen E, Koch I, Lindner M, Eickelberg O. Gli1 mediates lung cancer cell proliferation and Sonic Hedgehog-dependent mesenchymal cell activation. PLoS One. 2013;8(5):e63226.
394. Liang J, Huang G, Liu X, Zhang X, Rabata A, Liu N, et al. Lipid Deficiency Contributes to Impaired Alveolar Progenitor Cell Function in Aging and Idiopathic Pulmonary Fibrosis. Am J Respir Cell Mol Biol. 2024;71(2):242-253.
395. Beppu AK, Zhao J, Yao C, Carraro G, Israely E, Coelho AL, et al. Epithelial plasticity and innate immune activation promote lung tissue remodeling following respiratory viral infection. Nature Communications. 2023;14(1):5814.
396. Hay RJ, Williams CD, Macy ML, Lavappa KS. Cultured cell lines for research on pulmonary physiology available through the American type culture collection. Am Rev Respir Dis. 1982;125(2):222-232.
397. Swain RJ, Kemp SJ, Goldstraw P, Tetley TD, Stevens MM. Assessment of cell line models of primary human cells by Raman spectral phenotyping. Biophys J. 2010;98(8):1703-1711.
398. Herriges M, Morrisey EE. Lung development: orchestrating the generation and regeneration of a complex organ. Development. 2014;141(3):502-513.
399. Prager-Khoutorsky M, Lichtenstein A, Krishnan R, Rajendran K, Mayo A, Kam Z, et al. Fibroblast polarization is a matrix-rigidity-dependent process controlled by focal adhesion mechanosensing. Nature Cell Biology. 2011;13(12):1457-1465.
400. Assémat E, Bazellières E, Pallesi-Pocachard E, Le Bivic A, Massey-Harroche D. Polarity complex proteins. Biochim Biophys Acta. 2008;1778(3):614-630.
401. Noble PW, Albera C, Bradford WZ, Costabel U, Glassberg MK, Kardatzke D, et al. Pirfenidone in patients with idiopathic pulmonary fibrosis (CAPACITY): two randomised trials. The Lancet. 2011;377(9779):1760-1769.
402. King TE, Bradford WZ, Castro-Bernardini S, Fagan EA, Glaspole I, Glassberg MK, et al. A Phase 3 Trial of Pirfenidone in Patients with Idiopathic Pulmonary Fibrosis. New England Journal of Medicine. 2014;370(22):2083-2092.
403. Richeldi L, Bois RMd, Raghu G, Azuma A, Brown KK, Costabel U, et al. Efficacy and Safety of Nintedanib in Idiopathic Pulmonary Fibrosis. New England Journal of Medicine. 2014;370(22):2071-2082.
404. Raghu G, Rochwerg B, Zhang Y, Garcia CA, Azuma A, Behr J, et al. An Official ATS/ERS/JRS/ALAT Clinical Practice Guideline: Treatment of Idiopathic Pulmonary Fibrosis. An Update of the 2011 Clinical Practice Guideline. Am J Respir Crit Care Med. 2015;192(2):e3-19.
405. Rosenfeld M, Wainwright CE, Higgins M, Wang LT, McKee C, Campbell D, et al. Ivacaftor treatment of cystic fibrosis in children aged 12 to <24 months and with a CFTR gating mutation (ARRIVAL): a phase 3 single-arm study. Lancet Respir Med. 2018;6(7):545-553.
406. Ramsey BW, Davies J, McElvaney NG, Tullis E, Bell SC, Dřevínek P, et al. A CFTR potentiator in patients with cystic fibrosis and the G551D mutation. N Engl J Med. 2011;365(18):1663-1672.
407. Wainwright CE, Elborn JS, Ramsey BW. Lumacaftor-Ivacaftor in Patients with Cystic Fibrosis Homozygous for Phe508del CFTR. N Engl J Med. 2015;373(18):1783-1784.

408. Taylor-Cousar JL, Munck A, McKone EF, van der Ent CK, Moeller A, Simard C, et al. Tezacaftor-Ivacaftor in Patients with Cystic Fibrosis Homozygous for Phe508del. N Engl J Med. 2017;377(21):2013-2023.
409. Okiyoneda T, Veit G, Dekkers JF, Bagdany M, Soya N, Xu H, et al. Mechanism-based corrector combination restores ΔF508-CFTR folding and function. Nat Chem Biol. 2013;9(7):444-454.
410. Fitch PM, Wakelin SJ, Lowrey JA, Wallace WAH, Howie SEM. Shh Expression in Pulmonary Injury and Disease. Hedgehog-Gli Signaling in Human Disease. Boston, MA: Springer US; 2006. p. 119-128.
411. Repapi E, Sayers I, Wain LV, Burton PR, Johnson T, Obeidat Me, et al. Genome-wide association study identifies five loci associated with lung function. Nature Genetics. 2010;42(1):36-44.
412. Hobbs BD, de Jong K, Lamontagne M, Bossé Y, Shrine N, Artigas MS, et al. Genetic loci associated with chronic obstructive pulmonary disease overlap with loci for lung function and pulmonary fibrosis. Nature Genetics. 2017;49(3):426-432.
413. Wilk JB, Chen T-h, Gottlieb DJ, Walter RE, Nagle MW, Brandler BJ, et al. A Genome-Wide Association Study of Pulmonary Function Measures in the Framingham Heart Study. PLOS Genetics. 2009;5(3):e1000429.
414. Golpon HA, Coldren CD, Zamora MR, Cosgrove GP, Moore MD, Tuder RM, et al. Emphysema lung tissue gene expression profiling. Am J Respir Cell Mol Biol. 2004;31(6):595-600.
415. Chuang P-T, McMahon AP. Vertebrate Hedgehog signalling modulated by induction of a Hedgehog-binding protein. Nature. 1999;397(6720):617-621.
416. Bosanac I, Maun HR, Scales SJ, Wen X, Lingel A, Bazan JF, et al. The structure of SHH in complex with HHIP reveals a recognition role for the Shh pseudo active site in signaling. Nat Struct Mol Biol. 2009;16(7):691-697.
417. Griffiths SC, Schwab RA, El Omari K, Bishop B, Iverson EJ, Malinauskas T, et al. Hedgehog-Interacting Protein is a multimodal antagonist of Hedgehog signalling. Nature Communications. 2021;12(1):7171.
418. Chuang PT, Kawcak T, McMahon AP. Feedback control of mammalian Hedgehog signaling by the Hedgehog-binding protein, Hip1, modulates Fgf signaling during branching morphogenesis of the lung. Genes Dev. 2003;17(3):342-347.
419. Administration USFaD. FDA Announces Plan to Phase Out Animal Testing Requirement for Monoclonal Antibodies and Other Drugs: FDA; 2025 [Available from: https://www.fda.gov/news-events/press-announcements/fda-announces-plan-phase-out-animal-testing-requirement-monoclonal-antibodies-and-other-drugs?utm_source=chatgpt.com.
420. Party L. Change - Labour Party Manifesto 2024 London: Labour Party; 2024 [Available from: https://labour.org.uk/wp-content/uploads/2024/06/Change-Labour-Party-Manifesto-2024-large-print.pdf.
421. Meyer KB, Wilbrey-Clark A, Nawijn M, Teichmann SA. The Human Lung Cell Atlas: a transformational resource for cells of the respiratory system. In: Nikolić MZ, Hogan BLM, editors. Lung Stem Cells in Development, Health and Disease (ERS Monograph. Sheffield: European Respiratory Societ; 2021. p. 158-174.

422. Sikkema L, Ramírez-Suástegui C, Strobl DC, Gillett TE, Zappia L, Madissoon E, et al. An integrated cell atlas of the lung in health and disease. Nature Medicine. 2023;29(6):1563-1577.
423. Adams TS, Schupp JC, Poli S, Ayaub EA, Neumark N, Ahangari F, et al. Single-cell RNA-seq reveals ectopic and aberrant lung-resident cell populations in idiopathic pulmonary fibrosis. Science Advances. 2020;6(28):eaba1983.
424. Unterman A, Sumida TS, Nouri N, Yan X, Zhao AY, Gasque V, et al. Single-cell multi-omics reveals dyssynchrony of the innate and adaptive immune system in progressive COVID-19. Nature Communications. 2022;13(1):440.
425. Cohen J. Statistical power analysis for the behavioral sciences: routledge; 2013.
426. Gonzalez RF, Allen L, Gonzales L, Ballard PL, Dobbs LG. HTII-280, a biomarker specific to the apical plasma membrane of human lung alveolar type II cells. J Histochem Cytochem. 2010;58(10):891-901.
427. McGowan S. Understanding the developmental pathways pulmonary fibroblasts may follow during alveolar regeneration. Cell Tissue Res. 2017;367(3):707-719.
428. Zhang K, Yao E, Aung T, Chuang PT. The alveolus: Our current knowledge of how the gas exchange unit of the lung is constructed and repaired. Curr Top Dev Biol. 2024;159:59-129.
429. Kotton DN, Morrisey EE. Lung regeneration: mechanisms, applications and emerging stem cell populations. Nat Med. 2014;20(8):822-832.
430. Hewett PW, Nishi K, Daft EL, Clifford Murray J. Selective expression of erg isoforms in human endothelial cells. Int J Biochem Cell Biol. 2001;33(4):347-355.
431. Nikolova-Krstevski V, Yuan L, Le Bras A, Vijayaraj P, Kondo M, Gebauer I, et al. ERG is required for the differentiation of embryonic stem cells along the endothelial lineage. BMC Dev Biol. 2009;9:72.
432. Werder RB, Zhou X, Cho MH, Wilson AA. Breathing new life into the study of COPD with genes identified from genome-wide association studies. European Respiratory Review. 2024;33(172):240019.
433. Guo F, Zhang L, Yu Y, Gong L, Tao S, Werder RB, et al. Identification of a distal enhancer regulating hedgehog interacting protein gene in human lung epithelial cells. EBioMedicine. 2024;101:105026.
434. Lao T, Glass K, Qiu W, Polverino F, Gupta K, Morrow J, et al. Haploinsufficiency of Hedgehog interacting protein causes increased emphysema induced by cigarette smoke through network rewiring. Genome Medicine. 2015;7(1):12.
435. Hiemstra P, Wu X, Khedoe P, Gosens R. The role of altered stem cell function in airway and alveolar repair and remodelling in COPD. 2021. p. 322-339.
436. Alam S, Li Z, Atkinson C, Jonigk D, Janciauskiene S, Mahadeva R. Z α1-antitrypsin confers a proinflammatory phenotype that contributes to chronic obstructive pulmonary disease. Am J Respir Crit Care Med. 2014;189(8):909-931.
437. Wert SE, Yoshida M, LeVine AM, Ikegami M, Jones T, Ross GF, et al. Increased metalloproteinase activity, oxidant production, and emphysema in surfactant protein D gene-inactivated mice. Proc Natl Acad Sci U S A. 2000;97(11):5972-5977.
438. Li E, Cheung HC, Ma S. CTHRC1+ fibroblasts and SPP1+ macrophages synergistically contribute to pro-tumorigenic tumor microenvironment in pancreatic ductal adenocarcinoma. Scientific Reports. 2024;14(1):17412.

439. Lingampally A, Truchi M, Mauduit O, Delcroix V, Vasquez-Pacheco E, Gautier-Isola M, et al. Evidence for a lipofibroblast-to-Cthrc1+ myofibroblast reversible switch during the development and resolution of lung fibrosis in young mice. European Respiratory Journal. 2025;65(2):2300482.
440. Nonis A, De Nardi B, Nonis A. Choosing between RT-qPCR and RNA-seq: a back-of-the-envelope estimate towards the definition of the break-even-point. Analytical and Bioanalytical Chemistry. 2014;406(15):3533-3536.
441. Devonshire AS, Sanders R, Wilkes TM, Taylor MS, Foy CA, Huggett JF. Application of next generation qPCR and sequencing platforms to mRNA biomarker analysis. Methods. 2013;59(1):89-100.
442. Akram KM, Yates LL, Mongey R, Rothery S, Gaboriau DCA, Sanderson J, et al. Time-lapse Imaging of Alveologenesis in Mouse Precision-cut Lung Slices. Bio Protoc. 2019;9(20):e3403.
443. Klingberg F, Hinz B, White ES. The myofibroblast matrix: implications for tissue repair and fibrosis. J Pathol. 2013;229(2):298-309.
444. McGowan SE. The lipofibroblast: more than a lipid-storage depot. American Journal of Physiology-Lung Cellular and Molecular Physiology. 2019;316(5):L869-L871.
445. McGowan SE, Doro MM, Jackson SK. Endogenous retinoids increase perinatal elastin gene expression in rat lung fibroblasts and fetal explants. Am J Physiol. 1997;273(2 Pt 1):L410-416.
446. McGowan SE, Harvey CS, Jackson SK. Retinoids, retinoic acid receptors, and cytoplasmic retinoid binding proteins in perinatal rat lung fibroblasts. Am J Physiol. 1995;269(4 Pt 1):L463-472.
447. El Agha E, Bellusci S. Evidence for the involvement of lipofibroblasts, airway smooth muscle cells and FGF10 signalling in lung repair. In: Nikolić MZ, Hogan BLM, editors. Lung Stem Cells in Development, Health and Disease (ERS Monograph). Sheffield: European Respiratory Society; 2021. p. 99-113.
448. Gu D, Soepriatna AH, Zhang W, Li J, Zhao J, Zhang X, et al. Activation of the Hedgehog signaling pathway leads to fibrosis in aortic valves. Cell & Bioscience. 2023;13(1):43.
449. Kramann R. Hedgehog Gli signalling in kidney fibrosis. Nephrology Dialysis Transplantation. 2016;31(12):1989-1995.
450. Short S, García-Tejera R, Schumacher LJ, Coutu DL. Next generation lineage tracing and its applications to unravel development. npj Systems Biology and Applications. 2025;11(1):60.
451. Burgess DJ. Tracing cell-lineage histories. Nature Reviews Genetics. 2018;19(6):327-327.
452. Gabbutt C, Wright NA, Baker AM, Shibata D, Graham TA. Lineage tracing in human tissues. J Pathol. 2022;257(4):501-512.
453. Rawlins EL, Perl A-K. The a“MAZE”ing World of Lung-Specific Transgenic Mice. American Journal of Respiratory Cell and Molecular Biology. 2012;46(3):269-282.
454. Stegmayr J, Wagner DE. The dawn of the omics era in human precision-cut lung slices. European Respiratory Journal. 2021;58(1):2100203.
455. Wagner DE, Klein AM. Lineage tracing meets single-cell omics: opportunities and challenges. Nature Reviews Genetics. 2020;21(7):410-427.

456. Maun HR, Wen X, Lingel A, de Sauvage FJ, Lazarus RA, Scales SJ, et al. Hedgehog pathway antagonist 5E1 binds hedgehog at the pseudo-active site. J Biol Chem. 2010;285(34):26570-26580.
457. Ericson J, Morton S, Kawakami A, Roelink H, Jessell TM. Two critical periods of Sonic Hedgehog signaling required for the specification of motor neuron identity. Cell. 1996;87(4):661-673.
458. Constable S, Long AB, Floyd KA, Schurmans S, Caspary T. The ciliary phosphatidylinositol phosphatase Inpp5e plays positive and negative regulatory roles in Shh signaling. Development. 2020;147(3).
459. Zimmer AM, Pan YK, Chandrapalan T, Kwong RWM, Perry SF. Loss-of-function approaches in comparative physiology: is there a future for knockdown experiments in the era of genome editing? Journal of Experimental Biology. 2019;222(7).
460. El-Brolosy MA, Stainier DYR. Genetic compensation: A phenomenon in search of mechanisms. PLoS Genet. 2017;13(7):e1006780.
461. Chilosi M, Poletti V, Rossi A. The pathogenesis of COPD and IPF: distinct horns of the same devil? Respir Res. 2012;13(1):3.
462. Kugler M, Yie T-A, Chang M, Li Y-H, Lin Z, Segal L, et al. The Role of Hedgehog-Interaction Protein (HHIP) in Pulmonary Fibrosis. C28 MORE THAN MEET THE EYE: NOVEL INSIGHTS IN IPF PATHOGENESIS: American Thoracic Society; 2024. p. A5187-A5187.
463. Carpenter RL, Ray H. Safety and Tolerability of Sonic Hedgehog Pathway Inhibitors in Cancer. Drug Saf. 2019;42(2):263-279.
464. Robarge KD, Brunton SA, Castanedo GM, Cui Y, Dina MS, Goldsmith R, et al. GDC-0449-a potent inhibitor of the hedgehog pathway. Bioorg Med Chem Lett. 2009;19(19):5576-5581.
465. Proctor AE, Thompson LA, O'Bryant CL. Vismodegib: an inhibitor of the Hedgehog signaling pathway in the treatment of basal cell carcinoma. Ann Pharmacother. 2014;48(1):99-106.
466. Pan S, Wu X, Jiang J, Gao W, Wan Y, Cheng D, et al. Discovery of NVP-LDE225, a Potent and Selective Smoothened Antagonist. ACS Med Chem Lett. 2010;1(3):130-134.
467. Hänzelmann S, Castelo R, Guinney J. GSVA: gene set variation analysis for microarray and RNA-seq data. BMC Bioinformatics. 2013;14:7.
468. Ferreira MR, Santos GA, Biagi CA, Silva Junior WA, Zambuzzi WF. GSVA score reveals molecular signatures from transcriptomes for biomaterials comparison. J Biomed Mater Res A. 2021;109(6):1004-1014.
469. Subramanian A, Tamayo P, Mootha VK, Mukherjee S, Ebert BL, Gillette MA, et al. Gene set enrichment analysis: a knowledge-based approach for interpreting genome-wide expression profiles. Proc Natl Acad Sci U S A. 2005;102(43):15545-15550.